Mass Transfer Analysis of Transdermal Drug Delivery Using Microneedles

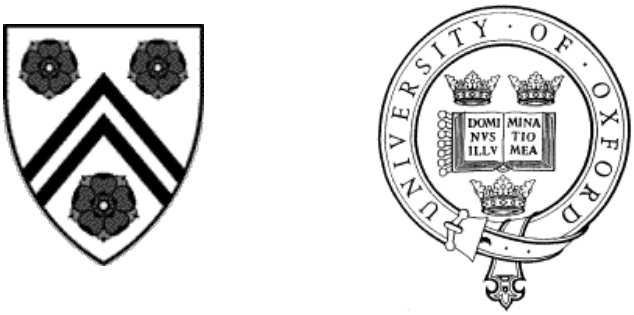

By

Barrak Al-Qallaf

A thesis submitted for the degree of
Doctor of Philosophy

New College
University of Oxford
Oxford

Michaelmas Term 2009

Abstract

Microneedle is a promising technique for delivering high molecular weight drugs across skin. The microneedles can offer a number of benefits over other drug delivery methods. For example, the drugs only diffuse over a short distance before reaching the blood circulation which enhances the absorption of drugs by the tissue. However, the drug transport behaviour in skin is affected by a complex interplay of many parameters (e.g., microneedle geometries, permeability across skin, etc).

In this thesis, many aspects of the microneedle field were examined. A mathematical model for drug transport from microneedle systems into skin was developed. Issues such as microneedle penetration, surface area of the microneedle arrays, etc. were investigated. This work helped us to focus into optimizing the design of microneedles by developing an in-house algorithm to enhance the performance of transdermal drug delivery using microneedles. Following the development of this algorithm, the influence of skin thickness with its classification (i.e., age group, race, etc.) on drug permeability across skin was studied. Attention was then given to determine the effective permeability (P_{eff}) and the effective skin thickness (H_{eff}) for various solid microneedle models. The outcome of this research allowed us to study the influence of microneedle dimensions on the drug concentration in blood (C_b). Furthermore, the 'pattern' (shape) of the microneedles array (i.e., square or rectangular) and the 'distribution' (arrangement) of the microneedles inside an array (i.e., triangular or diamond) were investigated to identify the optimum microneedle models. Finally, the effect of skin metabolism on both the patch (without microneedles) and the microneedle arrays on drug intake were examined.

Acknowledgment

I would like to express my sincere gratefulness to my co-supervisors, sponsor and family.

I would like to thank my co-advisor, Dr DB Das, for his valuable guidance, support and patience during my study. He shaped my interest as a researcher and taught me the essential skills. He afforded me the opportunity of knowing and exploring the world of pharmacology and tissue engineering. I learned how to apply the basic principles of chemical engineering into the biological sciences. I am enjoying discovering the real meaning of 'Transdermal Drug Delivery' and being able to create significant ideas with the freedom to explore new things.

I would also like to thank my co-supervisor, Prof ZF Cui, for his constant precious advice. He helped me on numerous occasions and gave me important suggestions and recommendations during my study. Prof Cui leads mostly through different case studies that were most useful and relevant to my research. His reputation as an expert in Tissue Engineering is well deserved.

I would like to thank Prof. Kakuji Tojo and Dr D Mori of Kyushu Institute of Technology, Japan, for their assistance in setting up the simulation software "SKIN-CAD". My thanks also go to the Kuwaiti government and, especially, to the Ministry of Interior who provided me with a scholarship to pursue my DPhil study at Oxford.

Last but not least, I would like to thank my parents and wife who supported me all the time and, encouraged me to continue and complete this work.

Table of Contents

Contents **Page**

Nomenclature

Symbol	Description	Units
A	Surface area of the microneedle arrays	L^2
c	Dimensionless constant	-
C	Drug concentration	M/L^3
C_a	Drug concentration at the coated surface area	M/L^3
C_b	Drug concentration in blood	M/L^3
$C_{b,ss}$	Steady state drug concentration in blood	M/L^3
CD	Microneedle drug coating depth	L
C_s	Skin surface concentration	M/L^3
C_{sc}	Drug concentration in stratum corneum	M/L^3
C_t	Drug concentration in tissue	M/L^3
C_{vs}	Drug concentration in viable skin	M/L^3
C_1	Drug concentration at the tip of microneedle	M/L^3
C_2	Drug concentration at the bottom of epidermis	M/L^3
D	Diffusion coefficient	L^2/t
dQ/dt	Permeation rate of drug through the skin	M/L^2t
D_{sc}	Diffusion coefficient in stratum corneum	L^2/t
D_{vs}	Diffusion coefficient in viable skin	L^2/t
f	Fractional area of skin covered by microneedle	-
g	Optimization function	-
h	Skin thickness (i.e., distance to blood vessel)	L
H	Thickness of the skin after microneedles have been inserted	L
h_e	Effective skin thickness after hollow microneedles have been inserted	L
H_{eff}	Effective skin thickness after solid microneedles have been inserted	L
h_{sc}	Thickness of stratum corneum	L
h_{vs}	Thickness of viable skin	L
J	Flux of drug across the skin	M/L^2t
J_{ss}	Steady state diffusive flux	M/L^2t
K	Optimized permeability across skin	L/t
K_e	Elimination rate constant	1/t
K_m	First order metabolic rate constant	1/t
$K_{sc/vs}$	Stratum corneum/viable skin partition coefficient	-
K_{12}	Transfer rate constant from the central compartment to the tissue compartment	1/t
K_{21}	Transfer rate constant from the tissue compartment to the central compartment	1/t
L	Microneedle penetration depth	L
L_h	Length of a hole in skin	L
L_m	Microneedle length	L
L_u	Uncoated microneedle length	L
m	Number of microneedles per column	-
n	Number of microneedles per row	-

Symbol	Description	Units
N	Total number of microneedles for a given patch	-
N_t	Optimum total number of microneedles	-
P	Permeability across skin	L/t
P_{sc}	Permeability of stratum corneum	L/t
P_t	Microneedle pitch (i.e., centre-to-centre spacing)	L
P_{tm}	Pitch of a given pattern per column	L
P_{tn}	Pitch of a given pattern per row	L
P_{vs}	Permeability of viable skin	L/t
R	Microneedle radius	L
R_D	Ratio of diffusion coefficient in the viable skin and stratum corneum	-
R_p	Ratio of permeability with microneedles to the permeability of normal skin	-
R_s	Skin resistance	t/L
S_a	Surface area of the delivery system	L^2
t	Time	t
T	Microneedle thickness	L
t_a	Duration of application of the microneedle arrays	t
t_m	Duration of medication	t
V_b	Volume of distribution in skin	L^3
V_t	Volume of distribution in tissue	L^3
x	Distance in a given skin layer	L
X	Total distance for a given row/column	L
Y	Dimensionless constant	-
z	Unknown power	-
α	Aspect ratio of the pitch over microneedle radius	-
ε	Ratio of annular gap width to the radius of microneedle	-
θ_{pt}	Angle of a given pitch	-
ϕ	Unknown function	-

List of Tables

List of Figures

List of Publications from this DPhil Research

List of Publications:

A. Journals:

1. Al-Qallaf, B., Das, D.B., Mori, D., Cui, Z.F. (2009) Transdermal drug delivery by microneedles: Does skin metabolism matter?. International Journal of Chemical Reactor Engineering. (submitted).

2. Al-Qallaf, B., Das, D.B., Davidson, A. (2009) Transdermal drug delivery by coated microneedles: Geometry effects on drug concentration in blood. Asia-Pacific Journal of Chemical Engineering, doi:10.1002/apj.353 (in press).

3. Al-Qallaf, B., Das, D.B. (2009) Optimizing microneedle arrays to increase skin permeability for transdermal drug delivery. Annals of the New York Academy of Sciences, 1161, 83-94.

4. Al-Qallaf, B., Das, D.B. (2009) Optimizing microneedle arrays for transdermal drug Delivery: Extension to non-square distribution of microneedles. Journal of Drug Targeting, 17(2), 108-122.

5. Al-Qallaf, B., Das, D.B. (2008) Optimization of square microneedle arrays for increasing drug permeability in skin. Chemical Engineering Science, 63, 2523-2535.

6. Davidson, A., Al-Qallaf, B., Das, D.B. (2008) Transdermal drug

delivery by coated microneedles: geometry effects on effective skin thickness and drug permeability. Chemical Engineering Research and Design, 86, 1996-1206.

7. Al-Qallaf, B., Das, D.B., Mori, D., Cui, Z.F. (2007) Modelling transdermal delivery of high molecular weight drugs from microneedle systems. Philosophical Transactions of the Royal Society A. 365, 2951–2967.

B. Conferences:

1. Olatunji, O., Das, D.B., Al-Qallaf, B. (2009) Simulation based optimization of microneedle geometry to improve drug permeability in skin. ISC2009, The European Multidisciplinary Society for Modelling and Simulation Technology, June 1st-3rd 2009, Loughborough, United Kingdom.

2. Al-Qallaf, B., Das, D.B. (2008) Modeling microneedles systems for predicting effective skin permeability of high molecular weight of human growth hormone. 14th UKICRS, Predicting Drug Delivery: Opportunities and challenges, January 23rd 2008, Hertfordshire, UK.

3. Al-Qallaf, B., Das, D.B. (2007) Optimizing microneedle arrays to increase skin permeability for transdermal drug delivery. ITP2007, Interdisciplinary Transport Phenomena V: Fluid, Thermal, Biological, Materials and Space Sciences, October 12th-19th 2007, Bansko, Bulgaria.

4. Al-Qallaf B., Das, D.B. (2006) Modelling percutaneous absorption of toxic chemicals in skin tissue. 2nd international conference "Strategies in Tissue Engineering", May 31st-June 2nd 2006, Wuerzburg, Germany.

C. Abstract Published in Journals:

1. Al-Qallaf, B., Das, D.B. (2006) Modelling percutaneous absorption of toxic chemicals in skin tissue. Cytotherapy. 8(supplement 2), 71.

2. Al-Qallaf, B., Das, D.B. (2007) Modelling transdermal delivery of high molecular weight drugs from microneedle systems. Tissue Engineering. 13(7), 1728-1729.

CHAPTER 1

Introduction

1.1 The problem definition

Although transdermal drug delivery has been used for about three decades, the range of therapeutics that is administered this way is limited by the barrier function of the stratum corneum (the top layer of skin). The skin is the largest and structurally most heterogeneous organ of the human body. It acts as a barrier organ against foreign substances, e.g., environmentally hazardous chemicals and drugs. The outer layer "stratum corneum" is the rate limiting barrier of the skin. Over the past few years, a number of different approaches have been proposed to enhance transdermal delivery of high molecular weight drugs, e.g., ultrasound, iontophoresis, chemical enhancers, microneedles, etc. The newest technology among them is the application microneedles systems - a method borrowed from microelectronics industry.

Microneedle arrays can be used to inject drugs directly below the stratum corneum of skin and, therefore, they increase the transdermal drug transport (Henry et. al, 1998; McAllister et. al, 2000). The first microneedle arrays were fabricated in 1998 by Henry et al. (1998). This technique combines hypodermic needles and patches for transdermal drug delivery. Among other advantages, the microneedles are envisaged to provide a method for efficient and painless drug delivery in skin. Since it was first developed, there has been substantial interests in this method with an increasing number of activities aimed at developing various microneedle arrays for pharmaceutical applications using different materials e.g., metals, glass, polymers, etc. However, the development of the optimal microneedle design for transdermal drug delivery in skin requires an understanding of the transport mechanisms for the drugs in skin and the relationships of the microneedle design with the drug transport behaviour. For example, one of the issues that should be taken into the consideration is to

optimise the distribution of the microneedles and their impacts on the drug transport in skin. Therefore, many relevant factors should be examined, e.g., the length of the microneedle, the radius of the microneedles, the number of the microneedles, etc. The aim of this thesis is to analyse the mass transfer of drug delivery process by using microneedles with a view to optimise the microneedle system design.

1.2 Objective of the research

The overall objective of this thesis is to develop a mathematical framework to improve the design and performance of the microneedle arrays as a transdermal drug delivery technique through a thorough mathematical analysis. In order to achieve this we need to understand the transport and kinetics of drug delivery, optimise the design of the microneedle systems, quantify the apparent skin permeability to drugs, etc. The core to all these is the mathematical model on the drug mass transfer process, which links all the design parameters of the microneedle systems, skin properties, drug molecular characteristics, to the drug release kinetics.

There are many important factors that should be considered when designing any microneedle. The skin-specific factors such as skin thickness have a huge effect in the penetration of these microneedles. In addition, optimizing the geometry of the microneedles has so far remained a challenge for lack of systematic analyses of the effects of various parameters on the drug distribution in skin. To address these issues, the following specific objectives have been formulated in this study:

- To identify the significance of various factors that influence the drug delivery while designing microneedle arrays by using various analysis such as parametric and scaling.

- To optimize the microneedle geometry to obtain their most effective performance based on numerical simulations.
- To determine the effects of different skin parameters, e.g., thickness based on age, race, sex or anatomical region, etc, and, hence enhance their applicability to wider range of cases.
- To evaluate the effective permeability and skin thickness for a range of microneedle shapes and dimensions in order to identify the most efficient geometry.
- To compare different patches such as square, rectangular, etc to identify the optimum design.
- To investigate the influence of skin metabolism in order to examine the importance of considering skin metabolism during the drug injection using microneedles.

1.3 Thesis outline

This thesis is composed of eight chapters with additional sections devoted to references. A literature review is presented in Chapter 2 to discuss various important issues including the structure of the skin along with the transdermal drug delivery methods, the microneedle systems, the implications of using different geometries in designing microneedles and mathematical modelling of transdermal drug delivery using microneedles. In addition, some suggestions on how to develop modelling strategy based on these models to improve the process of drug delivery using microneedles are given.

Chapter 3 presents a mathematical model on the drug transport in skin and demonstrates a sensitivity study of the hollow microneedle arrays. The outcome of this research provides an understanding of the various factors that should be taken into the consideration for designing the microneedle arrays. This model developed here is expanded further in Chapter 5.

Chapter 4 describes a numerical modelling of drug transport from a microneedle array. The geometry effects of various types of solid microneedles are presented. The model can be used to evaluate the effective skin thickness and permeability for a variety of needles. Furthermore, the influence of the microneedle dimensions of various solid microneedles on drug concentration in blood has also been examined.

Chapter 5 provides quantitative evaluations of parameters influencing the drug concentration in blood. The parameters considered in this work have been used to generalize their effects through the development of scaling relationships. This has been done by carrying out a dimensional analysis using Buckingham's π theorem.

Chapter 6 summarizes an optimization framework for transdermal delivery of high molecular weight drug from microneedle. Optimizing these microneedles is envisaged to have a significant impact in the fabrication industry involving any new needle systems to achieve the desired results in the application of various pharmaceutical studies. An analysis considering both the pattern and distribution of different microneedles will help to decide what the best microneedle to be used. In practice, knowing the best design among various microneedle models will make the use of this microneedle more applicable in the future and more widely available.

Chapter 7 explores the importance of considering skin metabolism on drug delivery using microneedles. To address this issue, numerical simulations have been carried out for both transdermal patch and microneedle arrays.

The conclusions and future research including an overall discussion on the impact of our results are given in Chapter 8.

CHAPTER 2

Literature Review

2.1 Drug delivery

Over the past decade, various routes have been chosen to administer drugs into the body such as oral, nasal, transdermal, rectal, pulmonary, etc. Drug delivery via the parenteral route, either by intravenous or intramuscular injection is particularly common. Injection by hypodermic needle has been the gold standard for drug delivery for over a century (Hallow et al., 2008; McAllister et al., 2003), but it has a number of disadvantages associated with it. Hypodermic needles often cause pain, transmit pathogens through needle re-use, need avoidance of the same puncture site (i.e., different points along a vein) and require medical expertise to complete the injection process (Haq et al., 2009; Stachowiak et al., 2009; Gill and Prausnitz, 2007; Diehl et al., 2001). Oral delivery has a disadvantage associated with the degradation, first pass metabolism and may be susceptible to poor absorption (Sonaje et al., 2009; Stoeber and Liepmann, 2000) and hence have a low bioavailability (Nomeir et al., 2009; Cross and Roberts, 2004). In addition, most of these routes exhibit more enzymatic activity (Lee, 1988) as compared to the transdermal route (Tauber, 1987).

On the other hand, transdermal drug delivery is painless, user-friendly and offer an advantage by increasing the bioavailability of the drug delivered (Lanke et al., 2009; Amsden and Goosen, 1995). The chemical engineers have the potential to develop various techniques of drug delivery (Lad, 2007). This is because they have the ability to understand the drug transport by performing the basic principles of chemical engineering (Lad, 2007). This involves mass transfer, thermodynamics, chemical reaction engineering, chemical kinetics, etc (Amsden and Goosen, 1995). In particular, chemical engineers have the knowledge to propose

different mathematical models by studying the factors that influence the drug transport to improve and hence enhance the drug delivery process (Amsden and Goosen, 1995).

2.1.1 Transdermal drug delivery

This is an alternative to pills and injections of methods of drug delivery which operates by transporting the drug into the human body across the skin. Most of the drugs that cannot be taken as pills will use injections (hypodermic needle). As mentioned previously, the problems arise in using hypodermic needle and oral delivery lead to inventions and development of new transdermal drug delivery methods including use of the patch. The first transdermal patch was developed in 1979 as a treatment for motion sickness (Prausnitz et al., 2004; Tojo, 1987). Since then, patches have been used in applications such as hormonal therapy, pain relief and as aid to smoking cessation (Baksu et al., 2009; Gass et al., 2009; Nicholson, 2009; Prausnitz et al., 2004). The transdermal patches have the ability to eliminate the problems associated with the oral delivery and hypodermic needle. Furthermore, these transdermal patches offer another advantages such as administrating drug at a constant rate for a longer time, avoiding first pass metabolism, bypassing gastrointestinal tract, etc. (Farahmand and Maibach, 2009; Shufelt and Braunstein, 2009; Sujith and Lane, 2009). These patches usually have a drug reservoir that can maintain a steady drug flow up to about one week (Farahmand and Maibach, 2009; Wokovich et al., 2009; Prausnitz et al., 2004). Although these patches have proven to be very successful, they still depend on the structure of the drug e.g., the size, charge and even some physiochemical properties (Coulman et al., 2009; Naik et al., 2000). This is due to the barrier function of the skin represented by the outer layer, stratum corneum, which generally allows diffusion of only small solutes (<500 Da) with the ability of being oil soluble (Farahmand and Maibach, 2009; Vecchia and Bunge, 2003; Schaefer and Redelmeier, 1996).

To solve these problems, methods have been developed to more effectively drive drugs across the stratum corneum which includes chemical enhancers (Golla et al., 2009; William and Barry, 2004) or physical enhancer techniques such as iontophoresis and ultrasound (Nair et al., 2009; Barry, 2001; Mitragotri et al., 2000; Roberts et al., 1997). However, the high cost, complexity and the difficulty to deal with these methods at home pose problems for the users (Koutsonanos et al., 2009; Power and McCormack, 2008; Howard et al., 1997). A new approach that combines the concepts of delivery of the drug by patches and the injections has been receiving significant attention in the field of the transdermal drug delivery. Arrays of needles of microns in dimensions, called microneedles, have been fabricated for transdermal drug transport (Jiang et al., 2009; Prausnitz, 2004; Reed and Lye, 2004; McAllister et al., 2000). These microneedles have been shown experimentally to increase the drug permeability across skin by orders of magnitude in vitro for a range of drugs varying in molecular size (Coulman et al., 2009; Park et al., 2008; Chabri et al., 2004; McAllister et al., 2003; Henry et al., 1998). The microneedle arrays penetrate the stratum corneum to reach the viable epidermis to deliver the drugs (Koutsonanos et al., 2009). A comparison between all the transdermal drug delivery approaches has been studied as shown in table 2.1. This shows the usefulness of using the microneedles as a promising method for transdermal drug delivery.

Table 2.1- Comparison of approaches used for transdermal drug delivery; √≡limited, √√≡moderate and √√√≡good (Prausnitz et. al., 2004).

Delivery method	**Increased transport**	**Sustained delivery**	**No pain/ irritation**	**Low cost/ complexity**
Hypodermic needle	√√√	√√	√	√√√
Chemical enhancers	√	√√√	√√	√√√
Iontophoresis	√√	√√√	√√√	√
Electroporation	√√	√√√	√√	√
Ultrasound	√√	√√√	√√√	√
Microneedle	√√	√√√	√√√	√
Jet injection	√√√	√	√	√
Thermal poration	√√	√√√	√√√	√

2.2 Microneedle technique

The concept behind microneedles was suggested in the 1970's (Banks et al., 2008) but it was not until the 1990's that their utility was demonstrated experimentally (Roxhed et al., 2007). This was mainly thanks to the advances in the microelectronics industry that allowed the production of micron-scale structures. The first needles to be reported in literature were created by Hashmi et al. (1995) to increase molecular and genetic material uptake in cells. The first study to determine whether microneedles could be used to increase drug permeability across skin was conducted by Henry et al. (1998). They found that calcein (a model drug) permeability across skin could be increased by over 3 orders of magnitude in vitro. Microneedles have been shown to deliver high molecular weight drugs, DNA, proteins and vaccine (Lee et al., 2008; Pearton et al., 2007; Reed and Lye, 2004). In addition to this, it was found that the use of microneedles is painless (Haq et al., 2009; Shirkhanzadeh, 2005; Sivamani et al., 2005; Miyano et al., 2005; Kaushik et al., 2001) and does not damage the tissue as the short micro-projections were not long enough to stimulate the nerve endings in the deeper tissue of the skin (Jiang et al., 2007; McAllister et al., 2000). Furthermore, microneedles have many advantages such as it can be used for some problems arising with the oral delivery (e.g., unpleasant odour) (Lad, 2007), easy to use without any expertise (Koutsonanos et al., 2009), could be used for blood extraction (Chakraborty and Tsuchiya, 2008), no need for regular dosage (Lad, 2007), safely to employ without any infection (Arora et al., 2008; Widera et al., 2006; Matriano et al., 2002), no possibility of bleeding (Alarcon et al., 2007; Dean et al., 2005; Mikszta et al., 2005), enhancing the absorption of drugs (Aziz and Majlis 2006; Aggarwal and Johnston, 2004), etc. Since these promising early results, developing microneedles suitable for pharmaceutical applications has been an active area of research. These microneedles are available as both solid (coated) and hollow microneedles made of various materials as discussed below. The microneedles can also vary according to their tip shape, e.g., volcano like, micro-hypodermis and snake-fang design (Mukerjee et al.,

2004) or the overall shape, e.g., pyramidal, spiked, candle-like and spear-shaped structure (Davidson et al., 2008; Shikida et al., 2004). Till date, four methods of transdermal delivery mediated by microneedles have been attempted (Gill and Prausnitz, 2007):

(i) Applying an array of microneedles to first permeabilize the skin before using a traditional transdermal patch.

(ii) Coating the microneedles with a drug containing film before inserting into the skin.

(iii) Creating the microneedles from a polymeric material that contains the drug. The drug is then released in a controlled manner after insertion into the skin.

(iv) Injection through hollow microneedles.

The first three methods utilise solid microneedles and the last method relies on a liquid drug formulation being injected through hollow microneedles. Hollow microneedles have generally received less attention to date as they are inherently weak structurally and have practical problems such as the insertion of microneedle into skin (Wang et al., 2006).

2.2.1 Solid microneedles

The solid microneedle was first fabricated to increase gene transfection (Hashmi et al., 1995). After this work was published, the concept of applying the solid microneedle for the use of transdermal drug delivery has also appeared. For example, solid microneedle has been successfully used for vaccine injection to prevent influenza (Koutsonanos et al., 2009). Many solid microneedles have been developed for a variety of different drugs both in vitro and in vivo. These solid microneedles are easier to fabricate, have better mechanical strength and sharper tips as compared to hollow microneedles (Roxhed et al., 2008; Jiang, 2006) which might result in higher drug transport (Verbaan et al., 2008). Furthermore, coated microneedles

with a solid drug may provide an advantage by increasing their long-term stability (Gill and Prausnitz, 2007).

2.2.1.1 Silicon microneedles

When microneedles first began to be used in transdermal drug delivery (Henry et al., 1998), they were made out of silicon. Therefore, solid silicon microneedles have been widely used for the transdermal drug delivery studies (Donnelly et al., 2009; Haq et al., 2009; Izumi and Aoyagi, 2007). However, silicon is expensive and brittle which breaks easily during the penetration across skin (Chen et al., 2008). Henry et al. (1998) used the silicon to fabricate the microneedles and realized that calcein can be delivered and that permeability across skin was increased when using this technique.

Figure 2.1-Image of solid microneedles used for the transdermal drug delivery (Henry et al., 1998).

Another study using the same microneedles concluded that permeability across skin was also increased when using these microneedles to deliver insulin and bovine serum albumin (McAllister, 2000). As shown in Figure 2.1, the microneedles are in a 20 by 20 array and each microneedle has a base of 80 µm and a height of 150 µm with a tip radius of 1 µm.

For example, silicon microneedles which were inserted into mice skin for gene delivery have a length of 50-200 µm with a square tip as shown in Figure 2.2 (Mikszta et al., 2002). In another gene delivery, solid silicon microneedles have been used across human skin in vitro (Chabri et al., 2004).

Figure 2.2-Solid silicon microneedles array used for gene delivery in mice skin (Mikszta et al., 2002).

2.2.1.2 Polymer microneedles

As mentioned previously, silicon is brittle and this led to the use of other materials. Polymer has been developed as an alternative because it is a cheaper and stronger material which could reduce tissue damage (Fernandez et al., 2009). In spite of these advantages, polymer increases the bluntness of the microneedle tip due to the low modulus and yield strength of polymer (Davis, 2003). On the other hand, polymer microneedles have a main limitation with its mechanical properties by which could cause needle failure during the penetration across skin (Park et al., 2007). This is because microneedle failure force depends on the mechanical properties of the polymer (Park et al., 2007; Park et al., 2005). Different kinds of polymer microneedles have been designed to increase permeability across skin as discussed below.

2.2.1.2.1 Bevelled microneedles

Bevelled tip microneedles have been fabricated using biodegradable polymers (Park, 2004). Poly-glycolic acid (PGA) was chosen as the main material of this microneedle because it is relatively inexpensive and believed to be mechanically strong (Ambrose and Clanto, 2004). For example, these microneedles were arranged in an array of 20 needles in each raw with a centre-to-centre spacing of 1400 μm by 6 columns with a centre-to-centre spacing of 400 μm. In total, there were 120 needles in this array. The array has an area of 9 × 9mm as shown in Figure 2.3.

Figure 2.3-Bevelled solid microneedles made of polymer (Park, 2004).

2.2.1.2.2 Tapered microneedles

Tapered microneedles have been fabricated with Poly-glycolic acid (PGA). For example, Park et al. (2005) proposed an array consisted of 200 needles with a height of 1500 µm, base diameter of 200 µm and tip diameter of 20 µm as shown in Figure 2.4.

Figure 2.4-Tapered solid microneedles made of Poly-glycolic acid (PGA) (Park et al., 2005; Park et al., 2004).

In addition, tapered microneedles have been fabricated with biocompatible polycarbonate with various microneedle densities (Oh et al., 2008) as shown in Figure 2.5. In another study, Park et al. (2006) demonstrated that calcein as a model drug was delivered successfully when using both bevelled and tapered microneedles. On the other hand, Park et al. (2007) concluded that tapered microneedles could solve the problem that arises with the polymer microneedles as discussed previously in section 2.2.1.2. In contrast, Kolli and Banga (2008) demonstrated that solid maltose microneedle could be a promising technique to replace the biodegradable polymer. This is because maltose microneedles dissolve within minutes as compared to the biodegradable polymer which remains in the skin for period of time (Kolli and Banga, 2008).

Figure 2.5-Tapered solid microneedles made of biocompatible polycarbonate (Oh et al., 2008).

2.2.1.3 Metal microneedles

Metal is the third material which is used to manufacture microneedles. It is mechanically strong and relatively cheap to produce. The main components of this type of patches are either stainless steel (Bal et al., 2008; Martanto et al., 2004) or titanium (Fernandez et al., 2009; Parker et al., 2007).

Figure 2.6- Metal microneedles array (Macroflux) (Matriano et al., 2002) on the left, another Macroflux patch with different dimensions on the right (Cormier et al., 2004).

The microinjection arrays (Macroflux) are coated with medical drugs. For example, this array consists of 190 needles per cm^2 over an area of 1 or 2 cm^2 with a length of 330 μm (Matriano et al., 2002), while another design of this patch has 321 microneedles per cm^2 over 2 cm^2 with a measured length of 200 μm, a thickness of 35 μm and a width of 170 μm (Cormier et al., 2004). They are shown in Figure 2.6.

2.2.2 Hollow microneedles

Less attention has been given to hollow microneedles for the drug delivery. This is because hollow microneedles are harder to use since they are weaker than solid microneedles requiring care in terms of needle design and insertion method (Davis et al., 2004). The main purpose of this type was to deliver drugs through the bore at the needle tip. This reduces the sharpness of needle tip which affect the penetration of this needle into skin. These issues have been resolved recently through development of a new microneedle design and insertion method (Roxhed et al., 2008; Roxhed et al., 2007; Wang et al., 2006; Griss and Stemme, 2003). However, one of the main advantages of hollow microneedle is that it offers continuous infusion through the skin (Roxhed et al., 2008).

2.2.2.1 Silicon microneedles

Hollow microneedles made of silicon (Matteucci et al., 2009; Shibata et al., 2009) have been studied and designed to enhance the transdermal delivery by e.g., increasing permeability across skin. Silicon has been generally used in microelectronic industry with wide manufacturing experience (Park et al., 2005). Despite this advantage, it is a high-priced, not biocompatible and breakable material (Verbaan et al., 2007; Park et al. 2005; Runyan and Bean, 1990). The first design of this was a tapered needle in which there were 8 needles in each array and with a height of 200 μm and a lumen diameter of 40 μm (Stoeber and Liepmann, 2000). Another type was the bevelled needle in which the length was 350 μm, the diameter of the tip was 70 μm, while the base was 250μm and the distance from the needle tip to the centre of the hole was 40μm (Gardeniers et al., 2003) as shown in Figure 2.7.

Figure 2.7- Left: Tapered microneedles to deliver dye into chicken thigh (Stoeber and Liepmann, 2000), Right: bevelled microneedles (Gardeniers et al., 2003).

2.2.2.2 Polymer microneedles

Polymer microneedles have been less widely used (Stupar and Pisano, 2001). Nevertheless, it is a cheap and biocompatible material (Park et al., 2005) with a lower melting temperature than silicon (Zhou et al., 2009). Furthermore, it may improve the deformation of a material substance because of the polymer viscoelasticity (Park et al., 2005; Ratner et al., 1996).

Figure 2.8-Hollow polymer microneedles (Moon and Lee, 2003).

The polymer microneedles are fabricated from, SU-8 (Fernandez et al., 2009), PMMA (polymethylmethacrylate) (Moon and Lee, 2003), etc. For example, polymer microneedle array consists of 120 needles per cm^2 with a height of 900 μm and a measured base of 470μm and 750 μm centre-to-centre spacing (Moon and Lee, 2003) as shown in Figure 2.8.

2.2.2.3 Metal microneedles

As mentioned previously, metal is a cheap, strong and biocompatible material (Verbaan et al., 2007; Braybrook, 1997). In particular, it has been commonly used in hollow microneedles which require structural strength (Park et al., 2005; Davis et al., 2004). However, there has been a concern about its safety usage if the needles during the insertion break inside the skin (Park et al., 2007). The hollow metal microneedles have been fabricated by using various metals such as nickel (Kim and Lee, 2007), nickel-iron metal (McAllister, 2000), etc.

Figure 2.9-Hollow metal microneedles on the left (McAllister, 2000), Tapered hollow metal microneedles on the right (Davis, 2003).

These microneedles were arranged in a 20 by 20 array, with a height of 150 µm, base of 80 µm, tip radius of 10 µm with a wall thickness of 3 µm and centre-to-centre spacing of 150 µm (McAllister, 2000). The needle bore has a conical shape with an approximate base of 145 µm which decreases to reach the top of the tip with an approximate radius of 5 µm. An alternative way of fabricating hollow metal microneedles was designed (Davis, 2003). These microneedles have a height of 500 µm, tip diameter of 75 µm, base diameter of 300 µm with a wall thickness of 10 µm. This array was arranged in 4 by 4 of a total of 16 microneedles with a centre-to-centre spacing of 600 µm as shown in Figure 2.9.

2.3 Skin structure

The skin is the largest and the most heterogeneous organ of the body. It has an area of almost 1.73 m^2 in average for any human adult (Goyal et al., 2007; Panchagnula, 1997). Skin has many functions such as protection against the dangerous rays of sun, prevention of water loss, controlling the temperature, etc. (Goyal et al., 2007; Membrino, 2002; Suhonen et al., 1999; Holbrook, 1994). The skin (Figure 2.10) consists of three main tissue layers: the epidermis, dermis and hypodermis (subcutaneous tissue).

This image is not available in ORA due to copyright reasons

Figure 2.10 –The structure of the skin (http://www.pharmpress.com)

2.3.1 Epidermis

The epidermis is divided into four layers, which are the stratum corneum, stratum granulosum, stratum spinosum and stratum basale. The last three layers are mostly called viable epidermis with thickness of approximately 20-100 µm (Matteucci et al., 2008; Schaefer and Redelmeier, 1996). The first layer, stratum corneum (10-20 µm), is one of the most important layers. This layer has been considered for a long time as the main barrier for any solute diffusing through the skin (Banks et al., 2008; Kalia and Guy, 2001; Ghanem et al., 1992; Kim et al., 1992; Bommannan et al., 1990; Michaels et al., 1975; Scheuplein and Blank,

1971; Scheuplein, 1967; Scheuplein, 1965; Blank, 1964; Rein, 1924). The structure and the relative thickness of each of these layers of the epidermis are shown in Figure 2.11.

Figure 2.11-The relative thickness of different layers of the epidermis (Schaefer and Redelmeier, 1996).

2.3.2 Dermis

The dermis is a flexible and very elastic layer with a typical thickness of 1.5-3 mm (Lambert and Laurent, 2008), while the maximum thickness is on the back with a thickness of ~ 4 mm (Rushmer et al., 1966). Blood and lymphatic vessels exist within this layer. This implies that the lymphatic flow plays a role for the clearance of large molecules (Cross and Roberts, 1993). The dermis contains capillaries, sweat glands, hair follicles and nerves (Lambert and Laurent, 2008).

2.4 Skin thickness

Skin thickness has been shown as a critical factor on the absorption process (van de Sandt et al., 2004). Therefore, it is very important to consider the variation of skin thickness which could affect the natural behaviour of skin barrier and hence influence the drug delivery. There are different factors that should be taken into consideration. These factors play important roles in the transportation of any solute released from the drug delivery systems, and therefore influence the rate of drug delivery through the human skin as discussed below. Skin thickness can vary according to age, anatomical region, race and sex (Lee and Hwang, 2002) as discussed below.

2.4.1 Age

The skin structures of infants, children, and adults differ hugely, and this may affect the solute diffusion process. Seidenari et al. (2000) investigated the skin thickness of both adults and children at various anatomical sites as shown in Table 2.2. This study showed that the skin thickness for a given anatomical region is quite different between adults and children. For example, the variation of skin thickness between adults (i.e., aged 25-40 years) and children (i.e., aged 2-13 years) in forehead has the highest value. The variation of skin thickness can be increases when comparing the previous age groups of adults with children aged 2-3 years. Moreover, the results show that as the age grows, the skin thickness increases (Seidenari et al., 2000). The relationship between skin thickness and age has been more thoroughly studied for adulthood. However, skin thickness was found to be inversely proportional with age (Whitmore and Sago, 2000) as confirmed with other studies (Whitmore and Levine, 1998; Shuster et al., 1975; Shuster and Bottoms, 1963). The same inverse relationship was obtained between the body mass index (i.e. weight in Kg divided by height in meter square) and the skin thickness. However, Gniadecka and Jemec (1998) found that the relationship between skin thickness and age is related to the anatomical site. In particular, there was a proportional relationship between skin thickness and age in axial skin (i.e., buttock and forehead). On the

other hand, in extremity skin (i.e., ankle, dorsal forearm, ventral forearm), there was an inverse relationship between skin thickness and age (Gniadecka and Jemec, 1998). Moreover, Diridollou et al. (2001) evaluated skin thickness of both males and females aged between six months and ninety years. The result showed that there was a fluctuation in the trend of skin thickness for different age groups. For example, the thickness of the skin increases until a person reaches the age of 20 which then remains almost constant between the ages 20-60 until it subsequently starts to decrease. For women, this is most likely to be in her 50s (Diridollou et al., 2001). On the other hand, this observation was different for other authors who believed that the thickness decreased when a person reaches the age range of 20-30 years old (Gniadecka and Jemec, 1998; Takema et al., 1994; Tan et al., 1982). There is also a strong evidence of the change in the function and the structure of the human skin as human age (Fenske and Lober, 1986). This can be more clearly seen by comparing the morphological differences between the normal (complete) skins in adults with that of a neonate (incomplete) skin in infants. There are fears associated with the incompleteness of the development of the skin barrier of the neonate.

Table 2.2- The skin thickness of various age groups in mm (Seidenari et. al., 2000).

Age(years) / Location	25-40	2-13	2-3	4-10	11-13
Forehead	1.99±0.34	1.43±0.43	1.18±0.22	1.50±0.49	1.56±0.36
Cheek	1.84±0.27	1.22±0.21	1.15±0.12	1.20±0.22	1.38±0.20
Upper abdomen	2.01±0.32	1.38±0.27	1.28±0.1.21	1.34±0.32	1.63±0.33
Interscapular region	2.34±0.26	1.70±0.41	1.48±0.26	1.72±0.73	1.97±0.31
Volar forearm	1.30±0.24	1.01±0.16	0.98±0.10	0.98±0.17	1.12±0.14
Dorsal forearm	1.45±0.24	1.21±0.17	1.18±0.12	1.18±0.17	1.34±0.17
Elbow crease	0.98±0.10	0.89±0.14	0.86±0.10	0.89±0.17	0.95±0.09
Lower leg	1.49±0.23	1.27±0.20	1.23±0.14	1.23±0.21	1.42±0.18

2.4.2 Anatomical site

The structure of the skin varies to some degree over different anatomical locations. Skin thickness in terms of anatomical region has been considered to be one of the most important factors that influence the percutaneous absorption (Korinth et al., 2005; Poet and McDougal,

2002; Wilkinson and Williams, 2002; Lundh et al., 1997; Environmental protection agency, 1992; Ritschel and Hussain, 1988; Scheuplein, 1978; Blank and Scheuplein, 1969; Tregear, 1966). Some authors have compared skin thickness in different regions of the body on a range of ages (Bloom and Fawcett, 1975; Barker, 1951). For example, Artz et al. (1979) proved that the ratio of epidermis to dermis varies considerably from one anatomical region to another as shown in Table 2.3.

Table 2.3- The average thickness of Epidermis/Dermis in Microns (Artz et al., 1979).

Age / Location	0-5	11-15	16-20	26-30	46-50	66-70
Medial thigh	35/583	84/576	50/1020	44/1151	48/1006	40/911
Lateral thigh	35/684	83/638	52/111	70/1084	59/1256	36/851
Posterior thigh	56/863	86/156	74/1278	61/1151	58/1100	38/1076
Medial leg	37/695	69/913	53/957	43/1371	55/1029	43/1188
Lateral leg	55/565	80/913	60/1093	58/1103	64/831	48/812
Posterior leg	33/519	77/536	70/1404	63/1371	58/1017	36/768
Anterior abdomen	32/692	51/1020	40/1470	41/1551	40/1457	31/1075
Anterior thorax	42/698	55/655	44/1362	34/1275	42/1320	32/1363
Back	32/503	67/1102	58/1876	75/2159	53/1699	44/2242
Medial arm	41/510	59/558	41/857	45/1275	46/950	32/770
Lateral arm	33/682	57/806	52/1137	55/1263	41/1004	40/1038
Back forearm	53/935	N/A	55/1071	N/A	41/920	37/852
Lateral forearm	36/669	79/551	52/950	52/1012	57/899	42/666

Lee and Hwang (2002) observed a significant variation in skin thickness between different anatomical regions of both epidermis and dermis. The results show that the skin thickness of epidermis and dermis ranged from 31 μm to 637 μm and from 469 μm to 1,942 μm, respectively. Lee and Hwang (2002) found reasonable differences in skin thickness of both epidermis and dermis between proximal and distal parts for a given extremity. The thickness of dermis was also investigated and shows a substantial relationship between the age and the anatomical site but no general correlation was observed between them (Gniadecka and Jemec, 1998). This observation agreed with other authors who found an increase in skin thickness in the dermis (Gniadecka et al., 1994; Hoffmann et al., 1994; Richard et al., 1994; De Rigal et al., 1989). This study shows the importance of the final factor which is the anatomical region

for any comparison of skin thickness. Wester and Maibach (1989) examined the permeability of different regional skin and concluded that the thickness of the stratum corneum does not affect permeability. There was a variation in the absorption of the drug from one site to another with similar thickness of the stratum corneum, while in the area with different thickness of stratum corneum, the amount of drug absorbed was similar. This implies that the permeability of skin is not a function of the stratum corneum thickness for different anatomical sites in the human skin. Furthermore, there was some variation of the permeability across skin in terms of anatomical location in which the highest values were in forehead, while the lowest where in arm (Rougier et al., 1987). In contrast, other researchers have observed that the most permeable body site were in the scrotum while, the lowest tissue was determined in the foot due to the thickness of the epidermis (Feldmann and Maibach, 1967).

2.4.3 Race

The variation of skin thickness in terms of ethnicity has been considered as an important issue in drug absorption (Johnson, 1997). There is a discussion in the literature on defining the meaning of ethnicity and race. According to Rawlings (2006) ethnicity describes a certain group having the same culture and languages, whereas, race refers to a group of people that have similar genes. A comparison has been done between the thickness of the Korean skin with another race (Caucasian) which shows that the thickness of the epidermis is lower in Caucasian than in Koreans (Lee and Hwang, 2002) as shown in Table 2.4.

It should be mentioned that in most of studies, scientist consider the Chinese as the Asian race and the African American as the Black race (Johnson, 1997). The skin thickness of black women has been measured and compared with white women's skin thickness (Whitmore and Sago, 2000).

Table 2.4-Skin thickness of epidermis for various races in microns (Lee and Hwang, 1979).

Race / Location	Caucasian		Korean
	Southwood (1955)	Artz et al. (1979)	Lee and Hwang (2002)
Chest	44	39	98
Back	66	62	76
Abdomen	41	40	79
Medial arm	42	44	69
Lateral arm	50	49	83
Medial forearm	52	48	74
Lateral Forearm	55	53	102
Medial thigh	54	47	87
Lateral thigh	57	60	94
Posterior thigh	57	64	102
Medial leg	55	50	91
Lateral leg	58	60	109
Posterior leg	58	63	129

The results show that the skin thickness of white women was approximately higher (i.e., doubled) as compared to black women. In contrast, Abrams et al. (1995) notice that the absorption of calcium in black girls was higher than in white girls.

2.4.4 Sex

Thickness of skin based on sex has varied values and is a further factor to be taken into account in comparisons. In the literature, different studies compared the skin thickness between males and females. Lee and Hwang (2002) found that Korean women have thinner skin than Korean men in almost 12 anatomical regions.

These differences were similar to those between Caucasian males and females (Rudolph et al., 1980; Artz et al., 1979; Southwood, 1955). Although the variations of different anatomical sites according to sex are very complex, there are some general rules in the literature to illustrate them in a ranked order as shown in Table 2.5 (Lee and Hwang, 2002). The soles and penises are shown to have the highest and lowest epidermis thickness, respectively comparing to the other tissues when evaluating the skin thickness of males. On the other hand, for the measurement of the epidermis thickness in females, the palm and eyelid were the thickest and

thinnest, respectively than the other tissues (Lee and Hwang, 2002). Another study shows that the skin thickness of males on the volar forearm is approximately 5.2% higher than in females (Diridollou et al., 2001). This observation is similar to those cited in other published studies (Seidenari et al., 1994; Escoffier et al., 1980).

Table 2.5-Skin thickness of epidermis with respect to sex in microns (Lee and Hwang, 2002).

Sex / Rank	Male		Female	
	Location	thickness	location	thickness
1	Sole	792.8	Palm	647.4
2	Palm	557.3	Sole	478.1
3	Dorsum of hand	246.8	Dorsum of foot	175.3
4	Dorsum of foot	180.1	Dorsum of hand	132.2
5	Buttock	147.8	Buttock	127.5
6	Posterior leg	124.4	Posterior leg	116.2
7	Cheek	115.4	Lateral leg	111.1
8	Lateral forearm	112.7	Chest	101.0
9	Lateral thigh	110.7	Lateral forearm	97.1
10	Lateral leg	109.5	Lateral thigh	92.6
11	Medial thigh	103.7	Neck (anterior)	91.9
12	Lateral arm	101.2	Forehead	90.4
13	Medial leg	100.6	Medial thigh	89.3
14	Forehead	95.9	Posterior thigh	88.1
15	Posterior thigh	92.4	Cheek	85.0
16	Neck (anterior)	89.3	Chin	81.5
17	Chest	88.1	Medial forearm	80.3
18	Back	88.1	Abdomen	79.9
19	Axilla	85.8	Medial leg	78.3
20	Chin	84.4	Lateral arm	72.5
21	Abdomen	80.4	Inguinal r.	72.1
22	Supraclavicular r.	76.3	Medial arm	65.5
23	Inguinal r.	73.7	Postauricular r.	63.5
24	Medial arm	72.8	Supraclavicular r.	63.1
25	Postauricular r.	69.3	Back	59.6
26	Medial forearm	67.8	Axilla	54.6
27	Eyelid	57.7	Eyelid	49.9
28	Penis	31.2	Penis	n/a

2.5 Mathematical models of drug transport

Mathematical models based on pharmacokinetics or diffusion approaches have been applied most widely (Goyal et al., 2007). The pharmacokinetics models are based on one or multi compartments (Goyal et al., 2007; McCarley and Bunge, 2001; Reddy et al., 1998; Guy et al.,

1982) which describe the drug concentration profile in the blood (Tojo, 2005). In particular, these models have the ability to quantify the pharmacokinetics processes such as absorption, distribution, metabolism, etc. On the other hand, the diffusion models which describe the rate of drug permeation across the skin (Tojo, 2005) obey Fick's law of diffusion (Naegel et al., 2008; Goyal et al., 2007; Barbero and Frasch, 2005; George et al., 2004; Kubota et al., 2002). More specifically, the prediction of these models are based on knowing the model parameters e.g., diffusion and partition coefficients (Naegel et al., 2008; Tojo, 2005). Some researchers proposed the diffusion models as one-layer model (mono-layer model) based on the assumption that the skin is homogenous (He et al., 2005; Tojo, 2005; Hashida et al., 1988; Okamoto et al., 1988; Foreman and Kelly, 1976). However, it is more realistic to consider the skin as two-layer model (bi-layer model) (He et al., 2005). Therefore, other researchers defined that these two layers represent the stratum corneum and the viable skin (He et al., 2005; Tojo, 2005; Yamashita et al., 1994; Okamoto et al., 1989; Tojo et al., 1987).

Figure 2.12-The pathways of drug transport through the skin: (a) Paracellular, (b) Transcellular and (c) transappendageal (Amsden and Goosen, 1995).

As well known, the drug diffuses through the skin via three main routes which are the paracellular or intercellular (i.e., through spaces between cells) pathway, transcellular (i.e., through cells) pathway and transappendageal (i.e., through hair follicles and sweat glands)

pathway as shown in Figure 2.12 (Goyal et al., 2007; Amsden and Goosen, 1995; Williams and Barry, 1992).

2.5.1 Mathematical models of transdermal drug delivery

As discussed previously, different approaches have been developed to enhance the transdermal drug delivery process such as iontophoresis, ultrasound. As a result, a variety of mathematical models have been proposed to provide a quantitative analysis and hence to determine the important parameters affecting the drug transport through the skin. For example, a mathematical model has been presented to analyze the iontophoretic transdermal drug delivery system using three model drugs with different molecular weights (Fan et al., 2008). In addition, a general mathematical model has been developed to predict drug transport of iontophoretic transdermal delivery (Tojo, 2005). This model has the ability to determine the influences of different factors on both the skin permeation and blood concentration profile of a given drug if iontophoresis has been applied (Tojo, 2005). Furthermore, a theoretical model which describes the transdermal drug delivery using ultrasound has also been developed (Joshi and Raje, 2002). This model can predict the drug concentration in blood delivered transdermally by using ultrasound. The influence of skin electroporation has been investigated by performing a numerical study (Becker and Kuznetsov, 2008; Pavšelj and Miklavčič, 2008).

2.5.2 Mathematical models of transdermal delivery by microneedles

Throughout the literature, several works have been conducted to assessment of safety and efficacy of the microneedles. The major purpose of these studies was to predict the bending force, evaluate the microneedle strength, calculate the buckling force, etc.

2.5.2.1 Mathematical models to determine the mechanical properties of microneedles

Aggarwal and Johnston (2004) investigated the influence of various hollow microneedles shapes (i.e., square, rectangular and circular) on bending force and buckling force to obtain the optimal design. The result shows that the circular microneedle has the maximum bending force as compared to both square and rectangular microneedles. Moreover, the bucking force reaches its highest value for both circular and rectangular microneedles. Therefore, the circular microneedle can withstand more force as compared to both square and rectangular microneedle. The effect of the microneedle length has also been studied. However, the number of microneedles has not been linked with both the bending force and the buckling force. This may change the insertion force needed to penetrate the skin with a large number of microneedles (Roxhed, 2007). An optimization approach has been proposed by Vasquez and Pelesko (2005) to maximize the buckling force. The result indicates that the buckling force is higher as compared with the previous work done by Aggarwal and Johnston (2004). However, the permeability across skin has not been linked with the insertion force. Once the microneedles are inserted into skin, this will lead to a huge deformation of the skin (Roxhed, 2007). As a result, this will damage the skin and hence influence (Roxhed et al., 2007) or even reduce the permeability across skin (Roxhed, 2007). In another study, a theoretical model has been presented by measuring experimentally both the fracture force and penetration (insertion) force for solid and hollow microneedles (Davis et al., 2004). The result suggests that there is a linear relationship between the penetration force and the full cross sectional area of the microneedles, whereas no relationship has been observed between the penetration force and the wall thickness. According to Davis et al. (2004), the full cross sectional area of microneedles was only a function the microneedle tip radius. This limits the feasibility of predicting the insertion force since the centre-to-centre spacing between the microneedles has not been considered. On the other hand, the fracture force decreases by decreasing wall thickness, wall angle and tip radius. Consequently, the highest safety margin (i.e., the ratio of

fracture force to penetration force) occurs when microneedle has small tip radius and large wall thickness. However, the experiments were performed on human skin for various ages of Caucasian males. As mentioned previously, the skin thickness could vary according to different factors such as sex, anatomical sites, etc. and consequently this could influence the prediction of the insertion force (Roxhed, 2007). The critical buckling load has been theoretically studied and numerically simulated for various microneedles geometries (Lee et al., 2008; Park et al., 2007; Parker et al., 2007; Ji et al., 2006; Paik et al., 2004).

2.5.2.2 Mathematical models to determine the microneedle flow rate

The volumetric flow rate of hollow microneedles has been measured by adopting the Hagen-Poiseuille equation (Haider et al., 2001). A relationship has been observed between the pressure drop, microneedle radius, number of microneedles and flow rate, whereas the flow rate does not depend on the microneedle centre-to-centre spacing. Nevertheless, the variation of skin thickness (Lee and Hwang, 2002) has not been discussed. In another work, the liquid flow rate of hollow microneedle has been determined by applying Bernoulli equation (Stoeber and Liepmann, 2005). The experimental results agreed well with the theoretical model which shows that Bernoulli equation is a useful model to describe the liquid flow through the microneedle lumen (Stoeber and Liepmann, 2005). However, this model has failed to study the influence of the number of microneedles on the flow rate. For example, for a larger number of microneedles, the delivery rate is lower as compared to smaller number of microneedles (Roxhed, 2007). As a consequence the flow rate may affect the flow resistance in the bores of microneedles (Griss and Stemme, 2003).

2.5.2.3 Mathematical models to determine the permeability across skin

It is important to know the factors that affect permeability across skin when applying microneedle arrays which could have significant impact on transdermal drug delivery. To

date, different methods have been proposed to predict permeability across the stratum corneum which are mostly applicable for low molecular weight compounds. Wilschut et al. (1995) reviewed these models for predicting permeability across skin of transdermal delivery of low molecular weight drugs. In these approaches, the stratum corneum is assumed to be the rate limiting layer and the resistance of the drug transport provided by the viable skin is ignored (McCarley and Bunge, 2001). In the present context, the resistance of the stratum corneum is overcome by insertion of the microneedle and the rate limiting barrier of skin is the viable skin. Consequently, most of these approaches are not directly applicable. It must be pointed out that a number of attempts have been already made to evaluate permeability across skin when using microneedle arrays. Wu et al. (2006) obtained a relationship between the number of bores and permeability across skin using macroneedles instead of microneedles. They also found a relationship between molecular weight of macromolecules and permeability across skin for hairless rat's skin. Another relationship between permeability across skin and high molecular weight compounds was observed for hairless rat skin (Wu et al., 2007). However, both of these attempts used animal skin and not human skin. Also, these approaches did not consider the geometry of microneedles (e.g., number of microneedle, microneedle radius, etc) while evaluating permeability across skin. Wu et al. (2006) used macroneedles instead of microneedles and obtained a relationship between the number of bores and permeability across skin. They also found a relationship between permeability across skin and molecular weight of macromolecules across an animal skin.

It is apparent from the above literature that optimizing the dimensions of the microneedle arrays is important to enhance the solute diffusion across skin. Recently, there have been many investigations on optimizing different parameters for transdermal drug delivery. Wilke and Morrissey (2007) optimized mask shape of microneedles for three different shapes. They concluded that the square mask shape has is the optimum shape instead of diamond and

circular shape. Khumpuang et al. (2007) determined the optimum location for various microneedle holes locations. The microneedle tip radius has also been optimized to improve the tip sharpness (Teo et al., 2006). With drug delivery methods, it is therefore logical to expect the optimum values of drug permeability depending on the dimensions of the microneedles. In general, the main aim of drug delivery optimization is to deliver a small quantity of a given drug in an effective manner (i.e. microneedles) to avoid any problems such as the possibility of damaging the liver or low drug absorption (Perennes et al., 2006). However, other questions have appeared recently while using these microneedles, e.g., how to reduce the sizes of holes produced by microneedles so that transport of bacteria and other foreign particles can be minimized (Meidan and Michniak, 2004).

In addition, Lv et al. (2006) have showed the insulin distribution profiles across skin by proposing a theoretical model. They studied both the transient and spatial distribution in the skin tissue as well as in the drug solution. However, they have not considered the implications of the geometry of various microneedle models. For example, the transdermal drug delivery is constrained by the surface area of the microneedles (Gill and Prausnitz, 2007). Teo el al. (2005) concluded that the radius of microneedles is a critical parameter when designing microneedles. In addition, the performance of the transdermal drug delivery process has been improved by increasing the number of microneedles (Stoeber and Liepmann, 2005). A theoretical in vitro approach appeared in the literature that describes the permeability of the skin when microneedles are inserted and removed (McAllister et al., 2003). The calculations of this theoretical model agreed well with their experimental data with an accuracy of 95% (McAllister et al., 2003). From the first investigation, one can conclude that the permeability across skin increases by decreasing the surface area of the microneedles and increasing both the number of microneedles and the microneedle radius. This lead to include another physical parameter which is the centre-to-centre spacing in order to increase the permeability across

skin and hence obtain the optimum microneedle design for a given range of microneedle dimensions. Furthermore, this theoretical model could be improved by considering the influence of the skin thickness variation as mentioned previously. Another mathematical model has been presented to determine the dosing rate needed for a given transdermal patch (Banks et al., 2008). This has been done by computing the surface area of the patch, permeability across skin and the solubility of the drug (Banks et al., 2008). However, this model has some limitation such as studying the influence of microneedle geometries. For example, the thickness of microneedles has been considered as an important parameter since it is related to the length of microneedle and hence its strength (Rajaraman and Henderson, 2005). In addition controlling the depth of penetration has a significant limitation when using the microneedles of different geometries (Matriano et al., 2002). In this study, the analytical solution has not been explored as explained below. It has been shown that the analytical solution can solve simple geometries under certain boundary conditions (Kalia and Guy, 2001). For example, the analytical solution was not obtained for complex geometries such as microneedles and hence, a numerical simulation has been carried out to compare the experimental results of transdermal drug delivery using microneedles (Zahn, 2001). On the other hand, numerical methods are widely available (O'Riordan and Shishkin et al., 2008) and they are powerful tools for modeling complex geometry (e.g., Kalia and Guy, 2001). These methods could closely resemble an experimental study (Kalia and Guy, 2001; Crank, 1979) and hence, to fit the experimental data for a given situation that is difficult to solve by analytical solution (Simon et al., 2006). For example, finite element solutions are capable of calculating both the diffusion in 3D (Davis, 2003) and the drug concentration profile in combination with microneedle geometry. Altogether, the numerical methods are more broadly applicable and have the ability to solve complex geometry as compared to analytical solutions.

2.6 Summary

Oral delivery (e.g. pills) has been considered as the most appropriate method of drug administration for decades. Most of the drugs that cannot be taken by oral delivery have traditionally used injections by hypodermic needles. However, the hypodermic injections have many disadvantages, such as the presence of pain, the appearance of having infections and the requirement for medical expertise to complete the injection process (Park et al., 2005). These problems have therefore led to inventions and development of new methods of drug delivery. Transdermal drug delivery is an alternative route of drug administration to pills and injections. This method operates by delivering drugs into the human body across the skin using a patch. The transdermal patches have the ability to eliminate the problems mentioned above. They usually contain a drug reservoir that can maintain a steady drug flow up to about one week (Prausnitz et al., 2004). Although these patches have proven to be very successful, they depend on the characteristics of the drug, e.g. the size, charge and even some physiochemical properties (Naik et al., 2000). This is due to the barrier function of the skin represented by the outer layer, the stratum corneum, which generally allows diffusion of only small molecular weight solutes (less than 500 Da) with the ability to allow penetration of certain oil-soluble solutes (Shah, 2003). To circumvent this diffusion limitation, methods have been developed to more effectively deliver drugs across the stratum corneum, including chemical enhancers (Williams and Barry, 2004) or physical enhancer techniques, e.g. iontophoresis (Kalia et al., 2004) and ultrasound (Prausnitz et al., 2004). However, the high cost, complexity and the difficulty in dealing with these methods at home pose problems for potential users. In addition to the methods mentioned previously, the transdermal drug delivery can also be enhanced through the use of microneedles (Kim and Lee, 2007). Arranged into an array, these are micron-scale projections that penetrate through the stratum corneum, creating a superficial pathway through which drugs can reach the deeper levels of the skin. They are available as solid or hollow microneedles made of glass (Martanto et al.,

2006), silicon (Wilke and Morrissey, 2007), polymer (Sammoura et al., 2007; Park et al., 2007), metal (Kim and Lee, 2007; Parker et al., 2007), etc.

The skin thickness can be a function of age, anatomical site, sex and race (Lee and Hwang, 2002). If the skin thickness has been changed while maintaining the same length of microneedles, then there will be a change the transdermal drug delivery process. This shows the necessity of evaluating the influence of skin thickness on drug permeation in skin.

Although different mathematical models have been proposed in recent year, their feasibility in relating both the permeability across skin and drug concentration have not been thoroughly investigated. Recently, there has been an interest to investigate the influence of different variables related to the microneedles to reach optimum microneedle design and hence, improve the transdermal drug delivery using microneedle arrays. However, the permeability across skin while using microneedle arrays has yet to be fully studied. In some cases, microneedles which were developed based on certain criteria (e.g., dimensions of the microneedles) have to be related to other criteria (e.g., drug permeability in skin, skin thickness, etc.). Therefore, in order to determine the optimum design of the microneedle arrays, the effect of different factors (e.g., number of microneedles, surface area of the patch, etc.) along with permeability across skin and drug concentration in blood by using microneedles should be determined accurately. In order to numerically solve these developed theoretical models, different numerical techniques have been adopted such as finite difference method, finite element method, etc.

CHAPTER 3

Parametric Study of Hollow Microneedles

3.1 Introduction

Although different microneedle designs have been fabricated, not all of them have paid attention to the drug concentration in blood. Different approaches have been proposed to evaluate the influences of different parameters on the drug delivery process. For example, Lv et al. (2006) proposed a theoretical model to determine the influence of injection velocity, blood perfusion rate and tissue porosity on the transdermal drug delivery process by using microneedles. Teo et al. (2006) outlined different key parameters (e.g. sharpness, materials of microneedles, etc) that may affect the design of microneedles. There have been some discussions on how to determine the length of microneedle while designing these microneedle arrays. This is because the length is an important factor on determining whether the arrays touch the nerve endings and cause pains or not. Shikida et al. (2006) defined the length to be longer than 50 μm but shorter than 200 μm. Stoeber and Liepmann (2005) pointed out that the length of the microneedle must be longer than 100 μm. These differences of the microneedle length show the importance to determine the influence of the length of the microneedle in transdermal drug delivery with respect of obtaining the optimum concentration of drugs in blood.

In general, a parametric analysis implies a study to observe the effects on a range of dependent variables by changing the independent variables. In this thesis, a parametric study has been conducted to quantify and examine the effects of various dependent parameters that may influence the transdermal drug delivery using microneedles. This is done by identifying as many factors as possible that may influence the drug concentration in blood. The outcomes

of this parametric study then allow us to focus on certain important parameters in order to optimize them which would enhance the transdermal drug delivery process.

Following the above discussions, the major focus in this chapter is to investigate the influences of a variety of variables related to the hollow microneedles and their impacts on the drug transport in skin. Many relevant factors have been considered, including the length of the microneedle, the duration of application, the size of the patch, etc. Subsequently, we aim to determine the influence of microneedles on drug concentration in blood during a drug delivery process. For our purpose, a mathematical framework has been developed and numerical simulations have been carried out which describe the pharmacokinetics of human growth hormone (hGH) penetrated into skin using hollow microneedle array. The study presented in this chapter is expected to be useful in identifying the most important parameters for the transdermal drug delivery using microneedles. The hollow microneedle has been chosen in this study since it does not need any further investigation to determine the effective skin thickness (h_e). This is because the effective skin thickness is simply the distance between the tip of microneedle to the blood vessels. However, this is not the case in solid microneedle since the effective skin thickness represents the path length from the coated surface area of the microneedles to the blood vessels. In addition, the effective skin thickness of solid microneedles (H_{eff}) depends on microneedle geometry as discussed in Chapter 4.

3.2 Modelling strategy

SKIN-CAD® has been adopted to study the human growth hormone concentration in blood and determine its relation to different microneedles and skin tissue parameters. The developed mathematical framework represents the phenomena of transdermal human growth hormone delivery across skin using hollow microneedles which contain a reservoir of drug on top. As shown in Figure 3.1, the resistance of the stratum corneum is overcome by insertion of the

microneedle and the rate limiting barrier of skin is the viable skin. The human growth hormone concentration at the interface between the skin tissue and needle edge is defined to be the same as the human growth hormone concentration in the reservoir (Al-Qallaf et al., 2007). The back diffusion of the drugs from needle edge towards the stratum corneum is ignored because their diffusion coefficient in the stratum corneum is estimated to be too small (i.e., 10^{-17} cm^2/s for human growth hormone, MW=22000; Tojo, 2005). The drug administered by using hollow microneedles diffuses across skin obeying Fick's second law until it reaches blood vessels. This transport behaviour is controlled by different parameters such as diffusion coefficient, thickness of viable epidermis, length of microneedle, etc. In our case, we want to be able to predict the concentration of human growth hormone in blood (C_b) at given time from the time of drug injection. The human growth hormone permeated through the skin is absorbed into the bloodstream (blood compartment) and the body pharmacokinetics follows one-compartment model which depicts the body as a simple homogeneous compartment (Xu and Weisel, 2005). The one-compartment model is used because it is assumed that the drugs distribute rapidly between blood and tissue (short distribution half-life) (Shiflet and Shiflet, 2006).

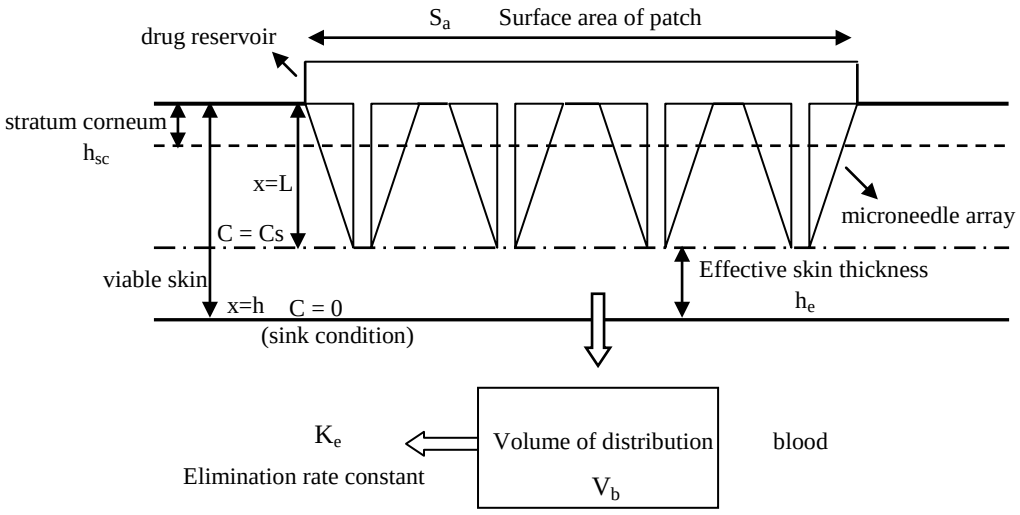

Figure 3.1- Schematic diagram for transdermal drug delivery of hollow microneedle array where back diffusion of drugs into stratum corneum is ignored.

3.3 Governing equation for drug transport

The human growth hormone movement in skin tissue is expressed by Fick's second law as:

$$\frac{\partial C}{\partial t} = D\frac{\partial^2 C}{\partial x^2} \tag{3.01}$$

Where C is the concentration, D is the diffusion coefficient, t is time and x is the distance in a given skin layer. The initial boundary condition for solving equation (3.01) is given by the following equation, where the initial human growth hormone concentration in skin is set to zero:

$$C = 0 \quad \text{at} \quad L < x < h \; (t = 0) \tag{3.02}$$

The assumption of no back diffusion of the human growth hormone is given as:

$$-\frac{dC}{dx} = 0 \quad \text{at} \quad t > 0 \tag{3.03}$$

The negative sign indicates that the back diffusion is from the bottom (tip of the microneedle) towards the top of the microneedle itself.

At the tip of the microneedle, the human growth hormone concentration is:

$$C = C_s \quad \text{at} \quad x = L \quad (0 < t \leq t_a) \tag{3.04}$$

At the bottom of the skin, the concentration of the human growth hormone is:

$$C = 0 \quad \text{at} \quad x = h \quad (0 < t) \tag{3.05}$$

Where, C_s is the human growth hormone concentration at the tip of microneedle, L is the microneedle penetration depth, t_a is the duration of application of the microneedles array and h is the skin thickness (i.e., distance to blood vessel). At x = h the concentration of the human growth hormone is assumed to be zero (sink condition), as the hGH has been up taken by dermal circulation (100% absorbed). We imposed a perfect sink condition (i.e., complete absorption of drug) at x = h because the concentration gradient is very low and for this reason it has been approximated to be zero (Lv et al., 2006). In addition, this assumption is consistent with the findings from previous experimental studies. For example, Kiptoo et al. (2006)

assumed sink condition during their experiment to enhance the transdermal delivery of 6-β-naltrexol. The concentration difference between the donor and receiver compartment was approximated by the drug concentration in the donor compartment (Kiptoo et al. 2006). This agreed well with the assumption presented by Sartorelli (1998), where the permeability across skin equal to the flux divided by the concentration difference. The concentration difference was also approximated to the concentration applied due to sink condition of the body. In another study, sink condition occurs once the drug has been taken up by blood stream when drug reaches the epidermis-dermis junction (Kielhorn et al. 2005). The sink condition was applied once the molecules of drug reached the capillaries when diffusing across skin (Bosman, 1996). In addition, the permeability (Oh et al., 2008) and insulin distribution (Lv et al., 2006) across skin for the transdermal drug delivery using microneedles have been determined by assuming sink condition at the receptor side.

3.4 Governing equation for hGH concentration in blood

In our approach, the hGH concentration in blood after imposing the transdermal delivery using hollow microneedles is given by one-compartmental pharmacokinetic model (Tojo, 2005; Al-Qallaf et al., 2007):

$$V_b \frac{dC_b}{dt} = \left(\frac{dQ}{dt}\right) S_a - K_e C_b V_b \qquad (3.06)$$

Where, K_e is the elimination rate constant from the blood compartment, dQ/dt is the penetration rate of hGH through the skin, S_a is the surface area of the delivery system (i.e., patch of microneedles), V_b is the volume of distribution in the blood, C_b is the hGH concentration in the blood.

The rate of hGH permeation and the cumulative amount of hGH permeated per unit area of skin are given by equations (3.07) and (3.08), respectively (Al-Qallaf et al., 2007; Tojo, 2005):

$$\left(\frac{dQ}{dt}\right) = -D\left(\frac{dC}{dx}\right)_{x=h} \tag{3.07}$$

$$Q = \int_0^t \left(\frac{dQ}{dt}\right) dt = \int_0^t \left(-D\frac{dC}{dx}\right)_{x=h} dt \tag{3.08}$$

3.5 Method of solution

The governing equations (3.01-3.08) were implemented and solved using the software, SKIN-CAD® (Biocom Systems, 2006). After penetrating across the skin, the drug molecules diffuse into the systemic blood circulation and then take part in the human body pharmacokinetics. The in-built pharmacokinetics models within SKIN-CAD® help to determine the transport of the drug when it leaves or goes through the body.

3.6 Results and discussions

We begin our discussion by demonstrating the utility of microneedle systems for transdermal drug delivery. For this purpose, we compare this technique with a common drug delivery such as a patch, which does not contain any microneedles.

Table 3.1- The values of model parameters used in this work for analysis the blood concentration of Fentanyl penetrated through the skin with and without microneedle array patch, and hGH penetrated through the skin by the microneedle arrays (Tojo, 2005).

	Drug	
Parameters	Fentanyl	hGH
Duration for medication (calculation): t_m (hour)	8	8
Duration of microneedles application: t_d (hour)	4	4
Surface area of microneedles array: S_a (cm^2)	2	2
Thickness of stratum corneum: h_{sc} (cm)	0.002	-
Distance to blood vessel: h (cm)	0.02	0.0125
Effective skin thickness: h_e (cm)	0.012	variable
Stratum corneum/viable skin partition coefficient: $K_{sc/vs}$ (-)		
Diffusion Coefficient in stratum corneum: D_{sc} (cm^2/s)	9.75×10^{-11}	-
Diffusion Coefficient in viable skin: D_{vs} (cm^2/s)	9.75×10^{-8}	5×10^{-10}
Volume of distribution: V_b(mL)	731000	100
Elimination rate constant: K_e (s^{-1})	2.840×10^{-5}	1.16×10^{-3}
Skin surface concentration: C_s (μg/ml)	15800	4000
Penetration depth: L (cm)	0.01	variable

To make a logical comparison, the molecular weight of the candidate drug is chosen to be low as this overcomes the problem of the permeability across skin. Fentanyl (MW=336.5) is a good candidate for this comparison. The input parameters are shown in Table 3.1. It must be pointed out that in case of the transdermal patch, Fentanyl is released on top of stratum corneum. Figure 3.2 shows the difference between Fentanyl delivery with and without using the microneedle system.

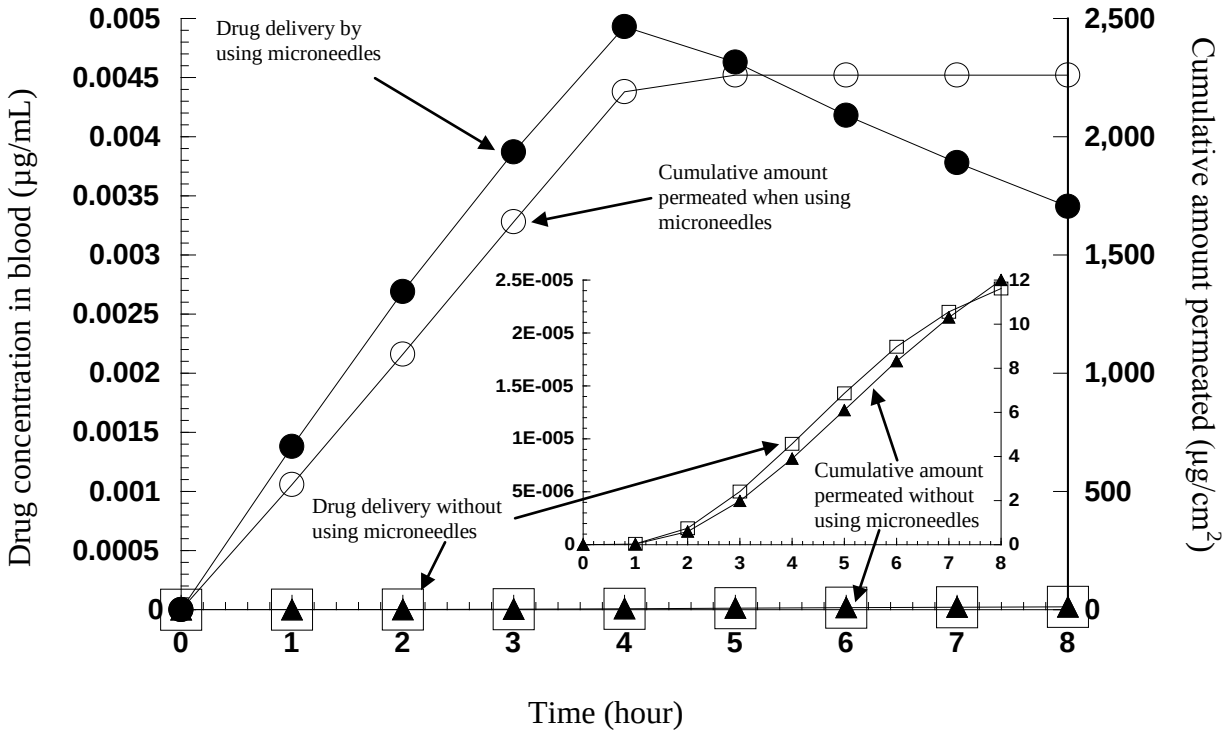

Figure 3.2- Effect of fentanyl delivery in skin with/without microneedle array for the input parameters in Table 3.1.

The results show clearly that the microneedle array enhances the transdermal drug delivery as the drug concentration and cumulative amount permeated are higher in this case. This is because the stratum corneum generally permits transport of fentanyl which reduces the amount of drug permeated. On the other hand, microneedles penetrate the stratum corneum to reach the viable epidermis which increase the amount of drug permeated. The drug concentration in blood decreases after 4 hours because the duration of application is defined to be 4 hours. Unless otherwise mentioned, in all our subsequent simulations in this chapter,

we use hGH (MW=22000) as a model drug for microneedle systems. Injection of hGH has many benefits such as improving kidney function, improving skin quality (e.g., eliminating of wrinkles), increasing bone density, etc. (Rudman et al., 1990). Model parameters for our simulations are shown in Table 3.1. In Figure 3.3 we show the drug distribution profile of hGH across skin. This describes how the drug diffuses from the tip of the microneedle until it reaches the blood stream across a given skin thickness. The steady state human growth hormone concentration occurs approximately at a period of time between 1 to 4 hours and decreases gradually afterward towards the blood/tissue interface. This is because the duration of application is defined to be 4 hours.

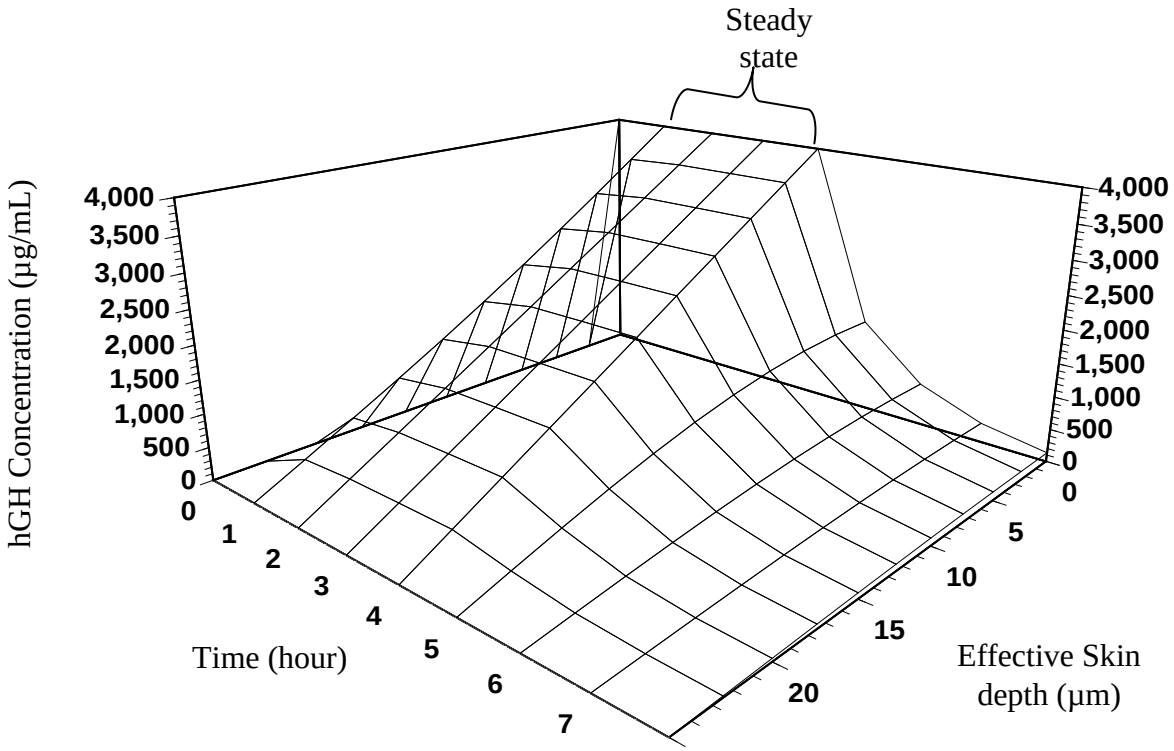

Figure 3.3- Transient drug distribution profile in skin for human growth hormone (hGH) (L= 0.01 cm; all the remaining parameters are as shown in Table 3.1)

3.6.1 Effects of duration of transdermal drug application and penetration depth

The insertion of microneedles has a significant ability to increase the permeability of the skin. For example, the permeability of calcein as a model drug was determined for different durations by Henry et al. (1998). By comparing two different intervals, one for 10 second and

the other for 1 hour, the permeability was shown to increase by two fold for an hour insertion (Henry et al., 1998). This means that the duration of drug application is an important factor to be considered while designing microneedle arrays. Figure 3.4 shows the effects of the duration of application ranging from 4 to 6 hours for various penetration depths of microneedle and patch surface area of 2 cm^2. The steady state human growth hormone concentration in blood ($C_{b,ss}$) does not change that much as there is a constant plateau concentration of ≈ 0.023 µg/ml in case penetration depth L=0.011 cm. However, the time duration within which the drug is active in skin varies depending on the duration of application. As expected, the results indicate that the blood human growth hormone concentration increases as the penetration depth increases and the duration of steady state blood human growth hormone concentration increases, as the duration of application increases.

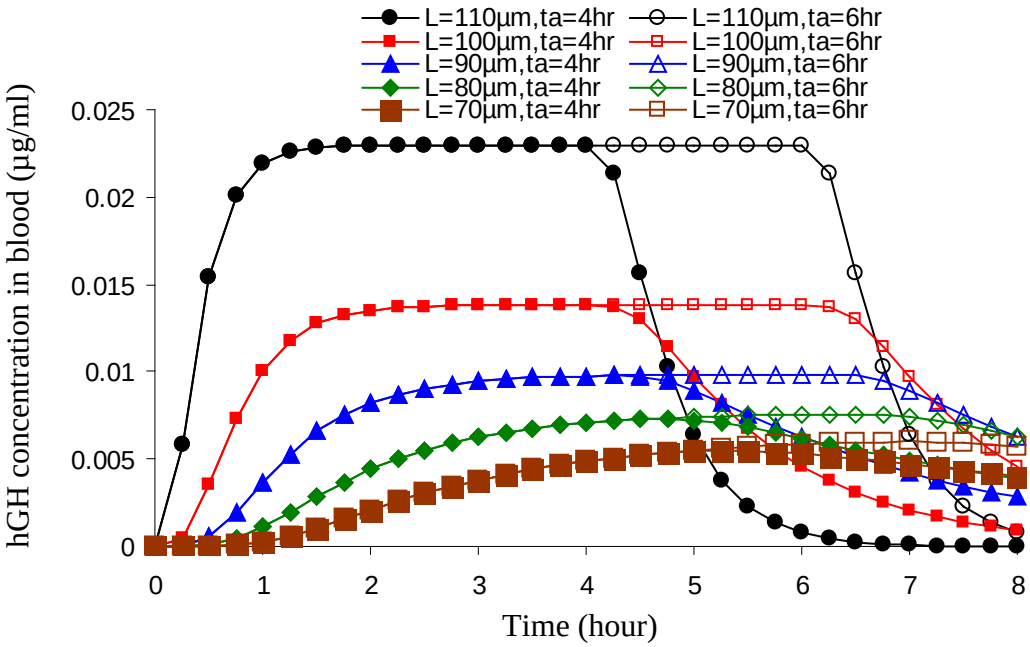

Figure 3.4-Influence of transdermal delivery of hGH for different penetration depths of microneedle and duration of application (t_a) for the input parameters in Table 3.1.

The diffusion of drugs across human skin through the use of microneedle systems is also related to the penetration depth of the microneedles (L). This means that the lengths should be chosen so that they are not too short to be ineffective and not too long to touch the nerves

ending embedded in the dermis. If the microneedles are too long, they contact the nerves ending and cause pain. Therefore, the amount of pain is also related to the microneedle lengths. The skin thickness chosen in our simulations represents the effective diffusion length from the needle tip to dermal circulation when the microneedles system is applied (Figure 3.1). In other words, it is the distance from the microneedle tip to blood vessels. This has been calculated by knowing the difference between the distance from the skin surface to dermal circulation and the length of the microneedles. In the results presented in Figure 3.4, the penetration depth of the microneedles is 0.01 cm and the distance from skin surface to dermal circulation is 0.0125 cm. This means that the effective diffusion length of the drug across the skin is 0.0025 cm.

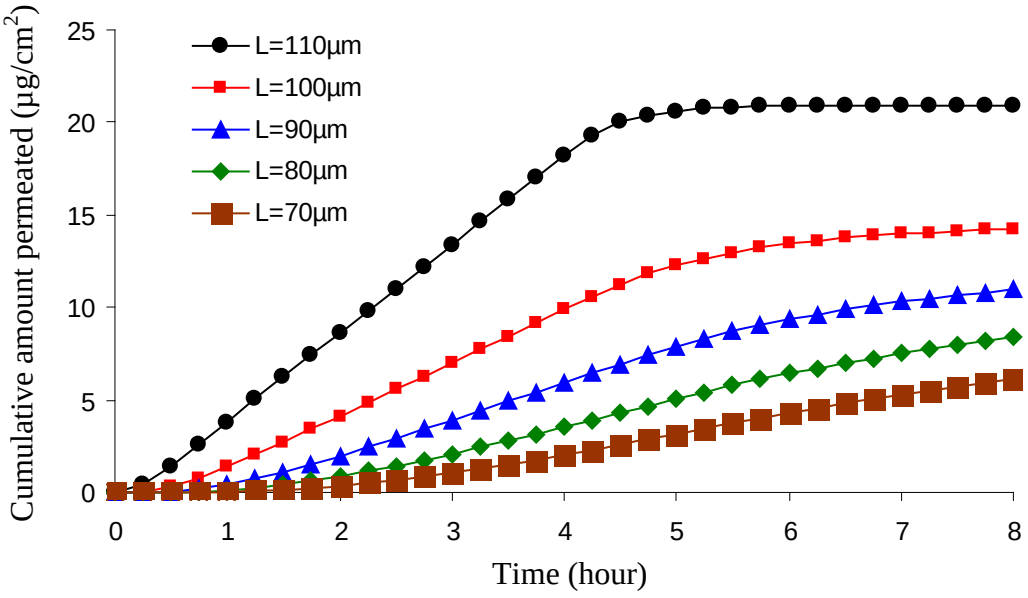

Figure 3.5-Cumulative amount of hGH permeated into blood per unit area of skin with various penetration depths of microneedles for the input parameters in Table 3.1.

The duration of application is either 4 or 6 hours and the surface area of the patch is 2 cm^2. By increasing the penetration depth of the microneedles from 0.01 cm to 0.011 cm, the effective diffusion length of human growth hormone is reduced to 0.0015 cm which enhances the drug concentration in blood. On the other hand, decreasing the penetration depth of the microneedles to 0.009 cm, the effective diffusion length is increased to 0.0035 cm which

drops the blood human growth hormone concentration. In the cases we considered, the steady state blood hGH concentration varies between 0.005-0.023 µg/ml. Figure 3.5 shows the cumulative amount permeated per unit area of skin for hGH with different microneedle penetration depths, which represents equation (3.08). As expected, the cumulative amount permeated of hGH increases as the penetration depth increases. This is because the effective diffusion length is decreased by increasing the penetration depth of microneedles.

3.6.2 Effects of patch surface area of microneedle

Since the first fabrication of the microneedles for drug delivery, there have been many different sizes of the microneedles surface areas. Some of them are relatively small with a surface area of 0.09 cm^2 (Kaushik et al., 2001) while others have larger area up to of 0.56 cm^2 (Wu et al., 2007). For the purpose of this chapter, we have carried out simulations to synthesise the effects of the size of the patch on drug delivery, as shown in Figure 3.6. The surface area represents the perpendicular area of the direction of the drug diffusion for a patch with a uniform area. Therefore, $(dQ/dt)S_a$ in equation (3.08) represents the drug penetration rate into blood that passes an area inclined perpendicularly to the direction of diffusion per unit time.

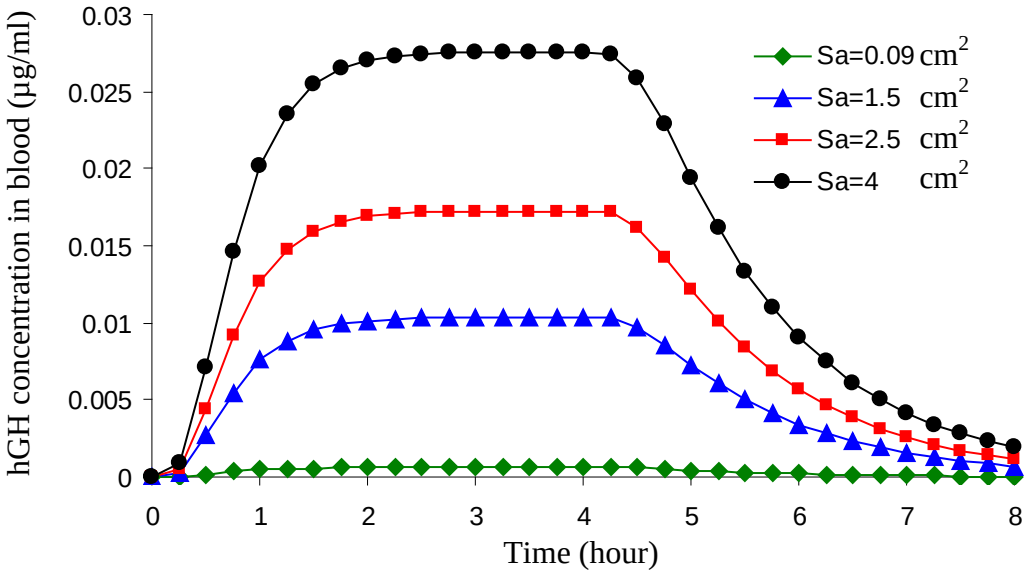

Figure 3.6-Influence of transdermal delivery of hGH for various sizes of patch for the input parameters in Table 3.1.

In Figure 3.6, the duration of application is 4 hours while the size of the patch varies from 0.09 cm^2 to 4 cm^2. We can see that the steady state blood hGH concentration ($C_{b,ss}$) varies between 0.0006 and 0.027 µg/ml and there is a steady-state concentration (the plateau) after certain duration of application.

By increasing the size of the patch, the hGH concentration in blood is increased. This implies that there is a proportional relationship between the size of the array (S_a) and the blood hGH concentration. This relationship must be taken into consideration while designing microneedle array systems in practice. However, no differences have been observed for the cumulative amount permeated per unit area of skin for insulin with different patch size (data not shown). This is because the effective skin thickness of hollow microneedle (h_e) has not been changed in all cases.

3.6.3 Effects of skin thickness

The distance from the skin surface to dermal circulation represents the skin thickness. This can be a function of age, anatomical region, race and sex (Lee and Hwang, 2002). If we change the skin thickness while maintaining the same penetration depth of the microneedles, then there will be a change in effective diffusion length and hence, hGH concentration in blood. The implications of changing skin thickness while keeping a constant penetration depth of the microneedle are shown in Figure 3.7. By reducing the skin thickness, the effective skin thickness is also reduced which enhances the hGH concentration in blood. The difference in hGH concentration in blood shows the necessity of considering the variation of skin thickness when applying microneedle arrays into human skin for drug delivery. This means that the diffusion of drugs across human skin through the use of microneedles is also related to the skin thickness (h).

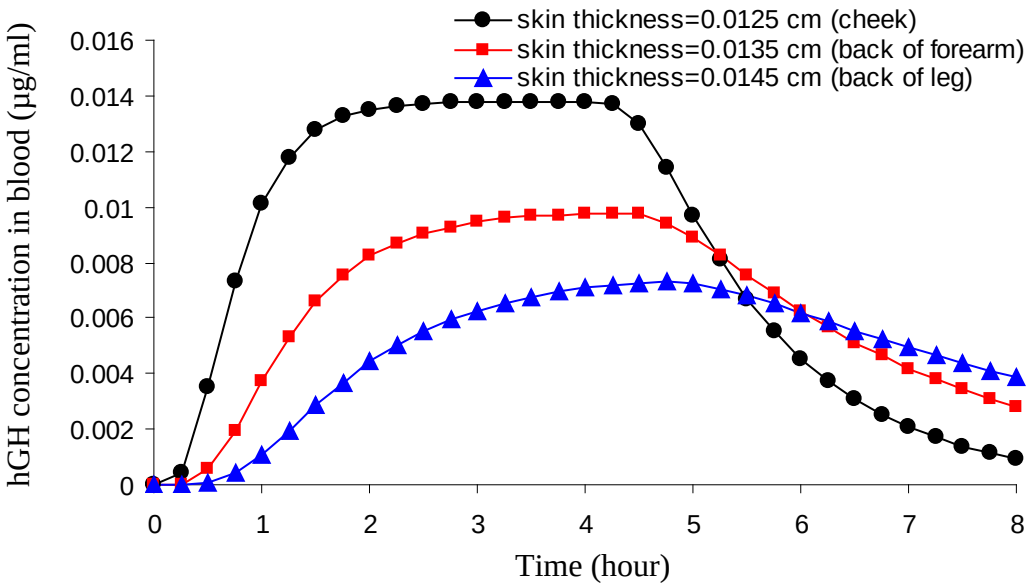

Figure 3.7-Influence of transdermal delivery of hGH for various skin thicknesses for the input parameters in Table 3.1.

3.6.4 Effects of pharmacokinetics variables

To evaluate the effects of both the elimination rate constant (K_e) and the volume of distribution (V_b) on the blood drug concentration, different values were chosen as shown in Figure 3.8. These reflect the influences of different pharmacokinetic of K_e and V_b variables on blood fentanyl concentration after applying microneedle arrays. We chose fentanyl as a model drug, as experimental values of V_b and K_e are available (Gupta et al., 1992). As expected, the fentanyl concentration in blood varies for different cases depending on the given input parameters. In all cases, the fentanyl concentration in blood decreases after 24 hours because the duration of application is defined to be 24 hours. The slow decrease of fentanyl concentration in blood following the removal of the microneedle systems is mainly due to the drug molecules dissolved in the skin at 24 hours (Tojo, 2005). Although these profiles have different distribution, it shows that pharmacokinetic variables have an effect on delivery using microneedles. As a result, the pharmacokinetic variables are important on defining the drug concentration in blood. This simulation is useful to predict the quantitative influence of pharmacokinetic variables on blood drug concentration.

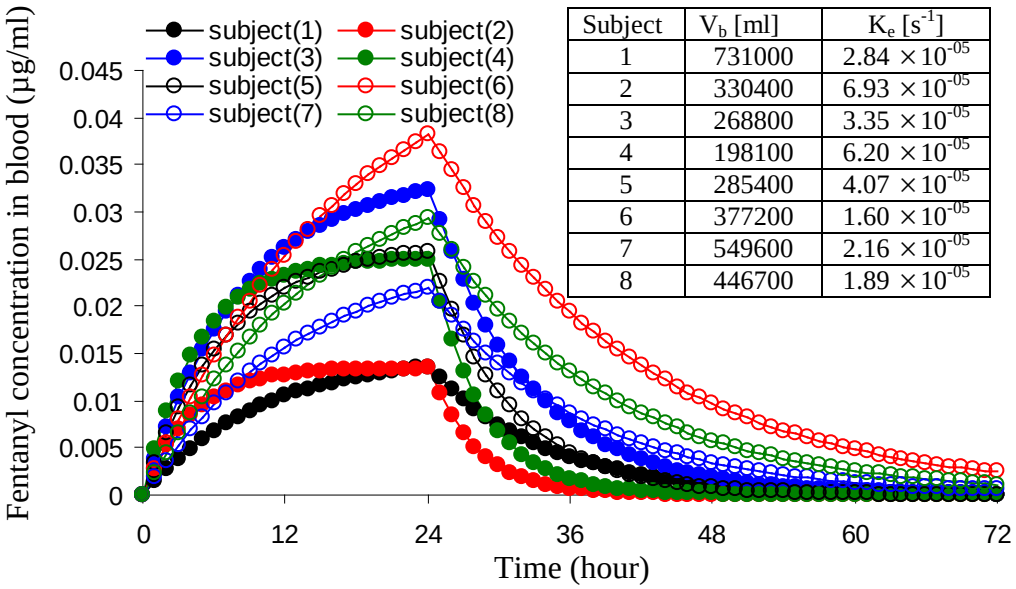

Subject	V_b [ml]	K_e [s^{-1}]
1	731000	2.84×10^{-05}
2	330400	6.93×10^{-05}
3	268800	3.35×10^{-05}
4	198100	6.20×10^{-05}
5	285400	4.07×10^{-05}
6	377200	1.60×10^{-05}
7	549600	2.16×10^{-05}
8	446700	1.89×10^{-05}

Figure 3.8-Effect of different pharmacokinetics parameters (Gupta et al., 1992) on fentanyl concentration in blood using hollow microneedles for condition (1-8) as shown above (total calculation length (t_m) = 72 hours, duration of application (t_a) = 24 hours, and all the remaining parameters are the same as shown in Table 3.1.

3.7 Summary

A parametric analysis for transdermal delivery of high molecular weight drug (i.e., human growth hormone) from hollow microneedles has been presented. The simulations have allowed us to identify the significance of various factors that influence the drug delivery while designing microneedle arrays. It has been found that there are different parameters that must be considered in designing and hence, optimizing any microneedle systems. These may include, e.g., the penetration depth of the microneedle, duration of the application, surface area of the array system, etc. These suggest that for the design of a microneedle system, evaluating various transport parameters as well as physical dimensions of the system enhances the efficiency of transdermal drug delivery techniques.

CHAPTER 4

Effects of Various Parameters Defining Different Geometries of Microneedles on Effective Skin Thickness and Drug Permeability

4.1 Introduction

Motivated by the previous results in Chapter 3, the effective skin thickness for solid microneedles has been determined in this chapter. Recently, there has been an interest to investigate the influences of a variety of variables related to the microneedles to reach the optimum microneedle design and hence, improve the transdermal drug delivery when using microneedle arrays. Many relevant factors have been considered to formulate an optimized microneedle array, including the mask shape of the microneedle (Wilke and Morrissey, 2007), location of the microneedle hole (Khumpuang et al., 2007), the microneedle tip radius (Teo et al., 2006), etc. However, most of these studies made their decision based on different criteria such as microneedle insertion, but not permeability across skin, although permeability has been considered as a key factor that determines the efficiency of transdermal drug delivery process (Wilke et al., 2006). In addition, the radius of the microneedle and the centre-to-centre spacing between the microneedles are important parameters in designing any patch and hence, they need to be considered in the simulations. In the following simulations, the driving force for drug transport is the concentration gradient as they move from locations of higher concentration towards the locations of lower concentration. In each layer inside the skin it is assumed that the permeation through these layers occurs by Fickian diffusion, and then the steady-state flux for a given compound is assumed (Park et al., 2005; Tregear, 1966).

Since drugs are limited by the barrier function of the skin, a certain time is needed to reach the steady state. At short time duration when the transport behaviour is not steady state, Fick's second law can be used. This means that the rate of change in concentration with respect to

time for any compound diffusing at a point is proportional to the rate of change in concentration gradient at this point. The permeation profile of a drug diffusing across the skin that describes the change of state from the non steady-state to the steady-state is shown in Figure 4.1.

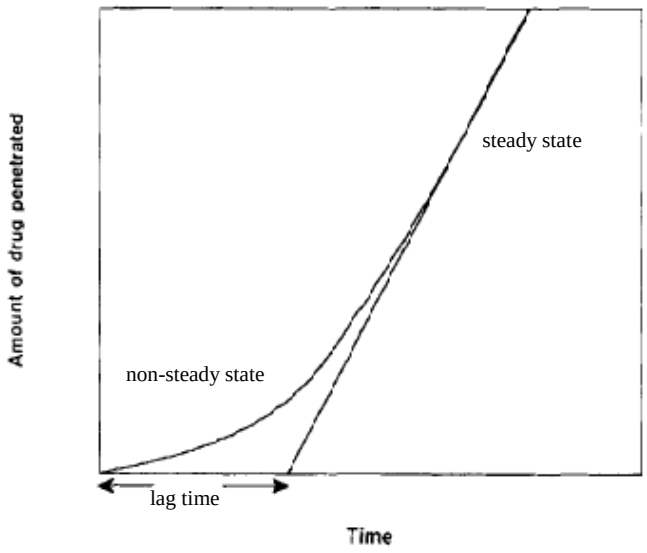

Figure 4.1-Permeation profile of drug following Fick's Law across skin (Amsden and Goosen, 1995).

Applying these fundamental concepts, it should be possible to determine the concentration distribution of a drug inside the skin for microneedle array system provided the required parameters are available. This will help us to know the best design of any microneedles array. For example, the tip radius of the microneedles should match the centre-to-centre spacing. If the tip radius is too big and the centre-to-centre spacing is too small then the concentration could be overdosing and that might lead to some side effect for the patient. On the other hand, if the tip radius is too small and the spacing centre is too far, then this will make the concentration too low and will not reach the desired dose for the proposed cure. This is why the design of the microneedle must be very accurate, having the qualification and the ability to deliver the drug across the skin in the appropriate way with the optimum design.

This chapter aims to quantify the influence of various geometrical parameters (e.g., microneedle thickness, coating depth, etc) associated with different microneedle shapes of coated drugs on the effective permeability across skin with a view to identify the most effective geometry of the microneedles. The ratio (R_P) of drug permeability with microneedles to the permeability of normal skin (i.e., without microneedle arrays) has also been determined. This has been done to obtain more information for designing microneedle arrays since that little quantitative research has been presented for determining permeability across skin using microneedles (Wu et al., 2006). This ratio helps to assess the ability of increasing permeability across skin using microneedles. This parameters seems to be useful to compare various microneedles models, and hence, to achieve the optimum geometry.

4.2 Modelling strategy

For the purpose of this study, a commercial package (i.e., FEMLAB®) has been used to study the drug transport of solid microneedles. This study has been focused on the so-called "coat and poke" approach (Prausnitz, 2004) as shown in Figure 4.2.

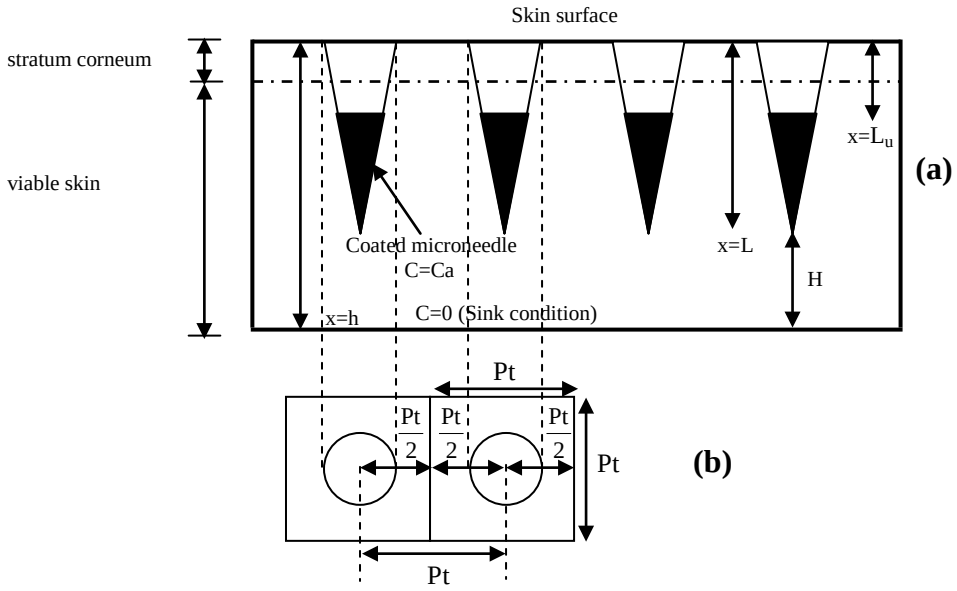

Figure 4.2- Schematic of coated microneedles for transdermal drug delivery: (a) side view, (b) top view. L_u is the uncoated microneedle length, L is the microneedle penetration depth, h is the skin thickness and H is the thickness of the skin after microneedles have been inserted, i.e., the distance between micro-needle tip and the blood micro-circulation.

4.2.1 Model assumptions

For the purpose of this chapter, the following assumptions are made (Davidson et al. 2008):

(1) The concentration of the drug (C) in the blood remains low throughout, and so the blood is considered to act as a sink, i.e. C = 0 for all time (t).

(2) Skin binding is assumed to be negligible in the viable skin.

(3) Drug metabolism is assumed to be negligible in the viable skin.

(4) All drug molecules that diffuse through the viable skin are taken up by the blood circulation.

(5) The diffusion is occurring in an isotropic media.

(6) The rate limiting step is diffusion through the viable skin.

The first assumption can be considered to be realistic as drugs coating are generally many orders of magnitude greater than the drug plasma concentration. Skin binding involves drug molecules becoming bound to active sites on macromolecules, which can cause a reduction of the diffusion coefficient to an 'effective value' that is a function of drug concentration (Tojo, 2005). Drug binding tends to be prevalent in the stratum corneum rather than the viable skin, so ignoring it is a reasonable approximation.

Metabolism by the living cells in the viable skin however can lead to an appreciable decrease in the systemic delivery of the drug (Tojo, 2005). To our best knowledge, there is no data to quantify the effect of skin metabolism on various drugs, particularly for those drugs that have not typically been used in transdermal delivery before. For simplicity, the metabolism of drugs in the viable skin is ignored.

The fourth assumption defines that 100% of the drug molecules that diffuse into the area of skin occupied by the blood circulation (taken to be 200 μm deep) are absorbed into the blood. This is a common assumption and is considered realistic (see, e.g., Tojo, 1987).

The diffusion is defined to occur in an isotropic media in consistence with previous work on transdermal drug delivery using microneedles (Lv et al., 2006; Davis, 2003; McAllister et al., 2003).

The final assumption defines that the rate at which the drug dissolves into the tissue fluids and the rate at which it is absorbed by the blood is rapid compared to the rate at which it diffuses through the viable skin. This is a fair approximation, as the coating should be a mainly dry-film and will quickly dissolve into the skin's tissues (i.e., within 20 seconds) according to Gill and Prausnitz (2007). Drug molecules should also be quickly absorbed into the blood, especially in vivo (Tojo, 1987).

4.2.2 Governing equations for drug transport in skin

For solid microneedles coated by a dry-film of drug molecules, the rate-limiting step is the transport of drugs through the viable epidermis. Drug molecules dissolve in the interstitial fluids of the skin and diffuse towards the blood circulation in the dermis. It is assumed that absorption by the blood is rapid compared to permeation through the skin (Tojo, 1987).

In order to determine the effective permeability across skin, and hence, the effective skin thickness, Fick's first law has been adopted:

$$J = -D\frac{dC}{dx} \qquad (4.01)$$

Where J is the flux of drug through the skin, D is the diffusion coefficient of drugs in skin, C is the concentration of diffusing drug and $\frac{dC}{dx}$ is the concentration gradient. The negative sign means that the flux is toward the direction of decreasing concentration.

At steady state (i.e. $\frac{dC}{dt} = 0$) it can be defined that,

$$\frac{dC}{dx} = \text{constant} = \frac{C_2 - C_1}{H} \tag{4.02}$$

Here, H is the thickness of the skin after microneedles have been inserted, C_2 is drug concentration at the bottom of epidermis layer and C_1 is drug concentration at the tip of microneedles. Now, combining Fick's first law (equation 4.01) with equation (4.02), we obtain an expression for steady state diffusive flux J_{ss} as follows:

$$J_{ss} = -\frac{D}{H}(C_2 - C_1) \tag{4.03}$$

$$J_{ss} = -P(C_2 - C_1) \tag{4.04}$$

Where P is the drug permeability in skin. When C_2 is defined to be zero (i.e., sink condition) J_{ss} is given by:

$$J_{ss} = PC_1 \tag{4.05}$$

For coated microneedles, the drug permeability is increased by bypassing the stratum corneum. This leaves the drug to diffuse across the viable skin (which consists of the viable epidermis and dermis) into the blood circulation. Assuming steady state transport across skin (Park et al., 2005), the effective permeability P_{eff} of the skin when coated microneedles are being used is calculated by:

$$P_{eff} = \frac{D_{vs}}{H_{eff}} \tag{4.06}$$

Where D_{vs} is the diffusion coefficient of the drug in the viable skin which is assumed to be constant (i.e., the diffusion coefficients in the viable epidermis and dermis are of the same magnitude) (Tojo, 1987) and H_{eff} is the effective thickness of the skin after microneedles have been inserted. Therefore, H_{eff} is a function of purely of microneedle geometry. It must be pointed out that the effective skin thickness of solid microneedles (H_{eff}) is different that the effective skin thickness of hollow microneedles (h_e). As mentioned in Chapter 3, the effective

skin thickness of hollow microneedles is simply the distance between the microneedle tip to blood circulation. However, this is not the case in solid microneedle where the effective skin thickness is the distance between the coated areas of microneedle to blood circulation which consequently depends on the microneedle geometry as shown in this chapter.

4.2.3 Skin permeability (without microneedle arrays)

In order to understand the utility of microneedles, the permeability across skin without microneedles has been calculated. Therefore, the effective permeability of a drug due to microneedles has been compared with its permeability through normal skin that has its stratum corneum intact. By considering the skin to act as a bilayer membrane (Tojo, 1987), the permeability of intact skin is found by reciprocal addition of the permeability of the two layers, the stratum corneum and viable skin as follows:

$$R_s = \frac{1}{P_{skin}} = \frac{1}{P_{sc}} + \frac{1}{P_{vs}} \tag{4.07}$$

$$P = \frac{D_{sc} \times D_{vs}}{D_{sc} \times h_{vs} + D_{vs} \times h_{sc}} \tag{4.08}$$

Where R_s is the skin resistance, P is permeability across skin, D_{sc} and D_{vs} are diffusion coefficients of stratum corneum and viable skin, respectively while h_{sc} and h_{vs} are thicknesses of stratum corneum and viable skin, respectively. The resistance implies the inverse of permeability.

The ratio (R_P) of permeability with microneedles to the permeability of normal skin is given by dividing equation (4.06) by equation (4.08) as follows:

$$R_p = \frac{h_{vs} + R_D \times h_{sc}}{H_{eff}} \tag{4.09}$$

Where, R_D is the ratio of diffusion coefficients in the viable skin and stratum corneum. This value is typically 500 – 10,000 (Tojo, 1987).

4.3 Method of solution

Drug diffusion from coated microneedles is modelled in 3D using FEMLAB®, a piece of scientific modelling software from Comsol (Comsol, 2005). It allows equation-based multiphysics modelling in an interactive environment. Free-form partial differential equations can be set up or particular physics applications can be chosen, in this case diffusion. 3D geometry of the microneedles can then be drawn and the diffusion of drug molecules analysed in transient or steady state. This is done by performing finite element analysis on the domain of interest. The domain is discretised into a mesh of small 3D elements, usually tetrahedrons. Our results show that the mesh is accurate enough, so that refining it did not significantly change the results. Boundary conditions and subdomains parameters are set and the PDE's that characterise the physics of the domain are discretised and solved in FEMLAB®.

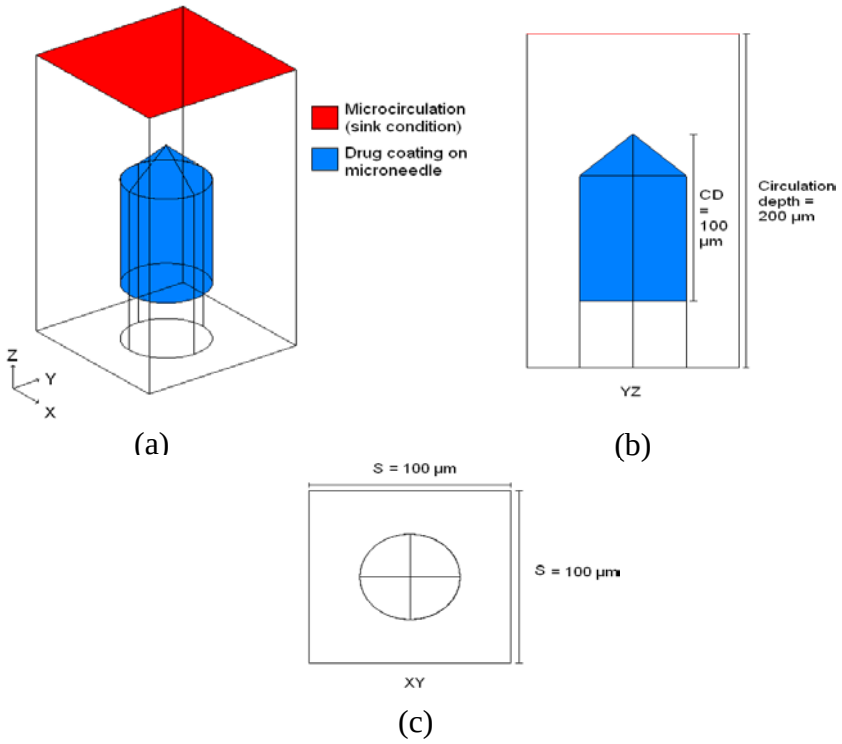

Figure 4.3- A schematic model for modelling diffusion from a microneedle through the skin: (a) 3D view, (b) side view and (c) top view. CD is the coating depth of drug on the microneedle and S is the width and length of the square element of skin.

In order to model the diffusion process from the coated microneedles into the skin, the diffusion model was used in FEMLAB® along with their dimension for microneedle model A as shown in Figure 4.3. CD is the coating depth of drug on the microneedle (i.e., the distance from the tip that is coated by the drug film). As an example, this is 100 μm, as seen in literature (Widera et al. 2006). S is the width and length of the square element of skin. It also represents the centre-to-centre spacing of the microneedles, assuming they are in a square pattern. As an example, this distance was 100 μm. The distance to the blood circulation from the skin surface has been reported as 200 μm (Tojo, 1987) and so that is used here.

The skin is modelled as a single subdomain with an isotropic diffusion coefficient (D). It was found that having a layer to represent the stratum corneum did not significantly affect the results and so it is not included in the model for simplicity. The blood is assumed to act as a sink for the drug and so this boundary condition is set (concentration is set to zero on this boundary).

The boundary conditions for the drug concentration at the surface of the coated microneedle are,

$$C = C_a \quad \text{at} \quad L_u < z < L \quad \text{for } t > 0 \tag{4.10}$$

On the other hand, the boundary condition for the drug concentration at the bottom of the epidermis layer is,

$$C = 0 \quad \text{at} \quad z = h \quad \text{for } t > 0 \tag{4.11}$$

Where C_a is the drug concentration at the surface of the coated drug, L_u is the uncoated microneedle length, L is the microneedle penetration depth, h is the skin thickness (i.e. equal to 200 μm), z is the distance in a given skin layer and t is time.

We calculate the steady state diffusive flux of drug through the blood interface assuming the concentration of drug on the needle is constant. It allows the calculation of effective skin thickness H_{eff}, which is purely dependent on microneedle geometry. In our approach, H_{eff} is calculated using the following method. The flux term determined from the simulations is integrated over the blood circulation boundary and then divided by the boundary area to give an average steady state flux, J_{ss}. By rearranging the steady state of Fick's first law, the following expression is found:

$$H_{eff} = \frac{D_{vs} \times C_a}{J_{ss}} \tag{4.12}$$

Where C_a is the drug concentration at the surface area of the coated drug and H_{eff} can then be used to calculate the effective permeability across skin P_{eff} in equation (4.06). It is assumed that the drug concentration at the surface area of the coated drug is 1% (w/v), which is 1 g/100 ml. This is a typical value from the work by Gill and Prausnitz (2007). This value was kept the same in all cases.

4.4 Microneedles types

For the purpose of this work, six microneedle shapes have been chosen, as shown in Table 4.1 and Figures 4.4-4.8. The shapes have been chosen according to what have been seen in literature, although the exact dimensions are not necessarily the same.

Table 4.1. The design parameters of each microneedle type (Davidson et al., 2008).

Type	Penetration depth (µm)	Diameter or Width (µm)	Microneedle thickness (µm)	Center-to-center spacing (µm)	Coating depth (µm)
A	140	50	N/A	100	100
B	140	50(at base)	N/A	100	100
C	140	50	N/A	100	100
D	140	50	35	100	100
E	140	30(shaft) and 60(tip)	35	100	100
F	140	50	35	100	100

Figure 4.4- Microneedle type: (A) was fabricated by Xie et al. (2005) and (B) was fabricated by Henry et al. (1998).

Microneedle type A consists of a cylindrical shaft with a cone tip. Needles of this form have been constructed by Xie et al. (2005). The design dimensions are shown in Figure 4.4(A). Whenever the dimensions are varied, the tip angle is maintained at 45°. Microneedle type B is a cone shape. An example of this type of needle can be seen in Figure 4.4(B), fabricated by Henry et al. (1998). As the geometry is varied, the tip angle is maintained at 79.9°.

Figure 4.5- Microneedle type (C) was proposed by McAllister et al. (2003).

Microneedle type C is a cylinder with a bevelled tip. An example of such a microneedle is shown in Figure 4.5, fabricated by McAllister et al. (2003). The design dimensions are also shown. As the geometry is varied, the bevel angle of 45° is maintained.

Figure 4.6- Microneedle type (D) was fabricated by Gill and Prausnitz (2007).

Microneedle type D is shown in Figure 4.6 with its design dimensions, along with an example of this type of needle from Gill and Prausnitz (2007). The tip angle is maintained at 45°.

Figure 4.7- Microneedle type (E) was fabricated by Gill and Prausnitz (2007).

Microneedle type E is an ‘arrow-head’ type needle manufactured by Gill and Prausnitz (2007) as shown in Figure 4.7. The arrow-head length and tip angle of 53.1° is maintained as the microneedle geometry is varied.

Figure 4.8- Microneedle type (F) was fabricated by Martanto et al. (2004).

Microneedle type F is a triangular type microneedle proposed by Martanto et al. (2004) as shown in Figure 4.8. The tip angle is maintained at 79.9° as the geometry is varied.

4.5 Results and discussions

In the present chapter, the following geometrical parameters of the microneedles were varied: depth of penetration, diameter (microneedle types A and C), thickness (microneedle types D and E), coating depth, centre-to-centre spacing. In addition, hexagonal symmetrical elements were designed for microneedle types A and B to compare with the case of square elements. Skin is wrinkled and has various surface features such as hairs. In addition to the visco-elasticity of the skin, this means that microneedles will not penetrate to their full length (McAllister et al., 2003). In general, microneedles longer than 100 μm should be used to ensure that they penetrate beyond the stratum corneum (Stoeber and Liepmann, 2005). As the blood circulation is located ~200 μm beneath the skin's surface in general, the microneedles should be shorter than this to prevent any chance of bleeding. For these reasons, the microneedles in the model are varied between 100-180 μm. The microneedle diameter ranges from 30-70 μm and the thicknesses between 25-75 μm. The diameter of microneedle model B

was not varied as the tip angle of 79.9° must be maintained and a change in diameter would not be possible without a change in penetration depth. Coating depth ranges between 40-120 µm and centre-to-centre spacing ranges between 75 – 200 µm. These ranges have been chosen based upon typical values seen in literature.

4.5.1 Effects of microneedle density

Microneedle density (i.e., number of needles per unit area) has been shown to be an important parameter that should be taken into account (Matteucci et al., 2008; Shikida et al., 2006). The needle density varies from one design to another. Some researchers have used a low needle density, e.g., 144 needle/cm^2 (Wilke and Morrissey, 2007). Others have used a high needle density, e.g., 640 needle/cm^2 (Stoeber and Liepmann, 2005). In general, the number of microneedles are related to the surface area of the array either per 1 or 2 cm^2 (Cormier et al., 2004; Matriano, et al., 2002). Morrissey et al. (2005) demonstrated that the insertion force depends on the needle density. Widera et al. (2006) investigated the influence of needle density on the immune response for both low (i.e., 140 needle/cm^2) and high (657 needle/cm^2) needle densities. The results show that the immune response does not depend on the density of microneedles. Verbaan et al. (2008) revealed no significant differences between various needle densities (i.e., 16,36 and 81 needle/cm^2). This finding agreed well with another study conducted by Wu et al. (2006). However, the drug permeation rate has been increased by increasing the density of microneedles (Donnelly et al., 2009; Li et al., 2009; Oh et al., 2008).

Following the above discussion, we have addressed the implication of changing the needle density of microneedles. As an example, we present the results for microneedle type D (Figure 4.6). By symmetry, it is possible to model a whole array of microneedles by modelling only a single microneedle. For instance, it can be shown that the permeability across skin of drug from one microneedle is represented by a given number of microneedles

in the array provided that the microneedle geometries are the same in both cases. For example, an array of twenty five microneedles can be represented by the modelling a single microneedle, due to symmetry as shown in Figure 4.9. This is convenient as the geometry of the problem becomes considerably simpler. 3D modelling of complex geometry requires greater computer processing power and takes longer simulation time.

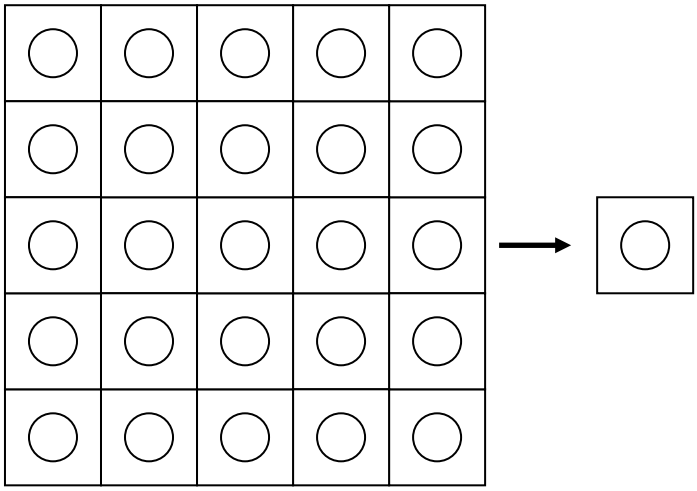

Figure 4.9- A top view of an array of 25 microneedles which can be represented by the modelling of a single microneedle due to symmetry.

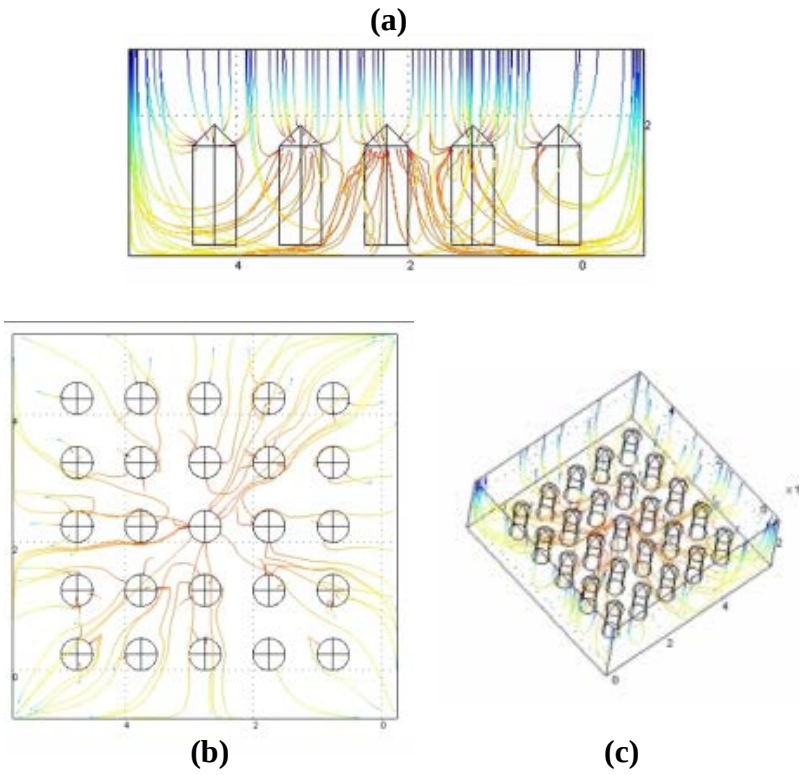

Figure 4.10- A schematic diffusion model of microneedle type D with 25 needles: (a) side view, (b) top view and (c) 3D view.

In order to validate this claim, we have simulated microneedle type D by considering twenty five needles as shown in Figure 4.10 and compared it with one needle.

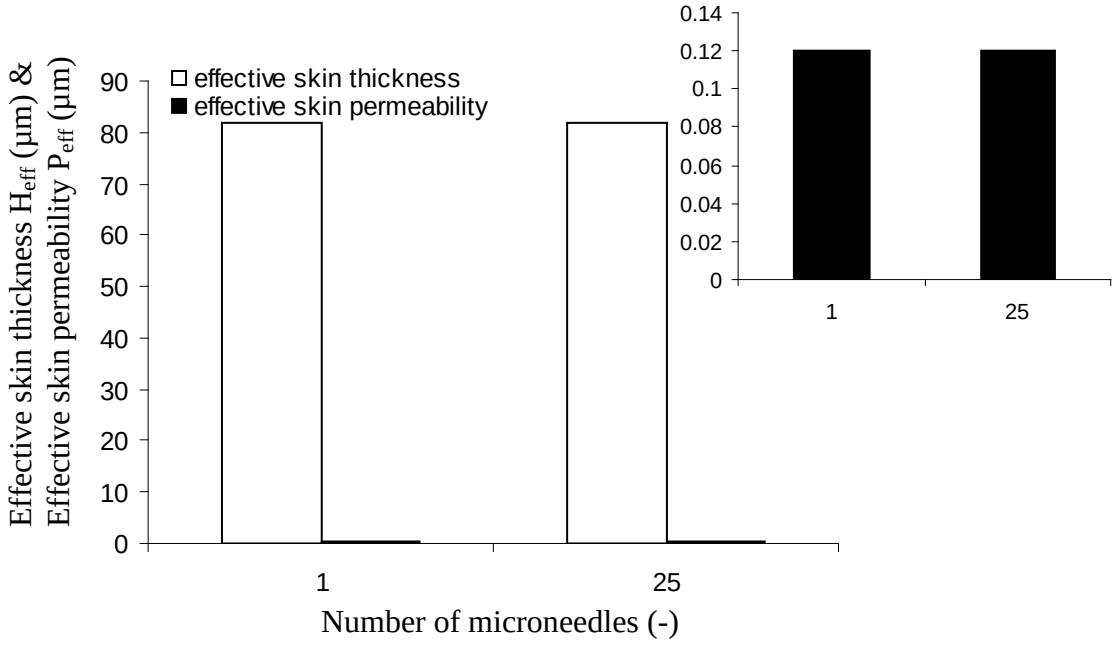

Figure 4.11- Influence of the changing numbers of microneedles for microneedles type D, coated with insulin, on effective skin thickness H_{eff} (blank markers) and effective permeability across skin P_{eff} (solid markers).

As shown in Figure 4.11, the effective permeability across skin (P_{eff}) is the same for both one needle and twenty five needles. The similarity of the effective skin thickness in both cases is due to the symmetry in the diffusion model. In other words, in both cases the microneedle geometries are identical. Therefore, this supports our claim that modelling one microneedle could represent a given number of microneedles (i.e., 25 needles) and hence the simulations in the following sections have been done by modelling one microneedle for various microneedle types.

4.5.2 Effects of microneedle interactions

During the injection of microneedles, the drug molecules are assumed to move through an isotropic media which is consistent with many previous works (e.g., Davis, 2003). However, the molecules could potentially diffuse around the spacing among microneedles and surrounding skin (McAllister et al., 2003). Haider et al. (2001) concluded that the flow performance of hollow microneedles was independent of the centre-to-centre spacing, implying that any effects of the interactions of the microneedles are insignificant. In all the simulations carried out in this research, the centre-to-centre spacing was large enough to possibly avoid any microneedle interaction (i.e., ranged between 75 to 200 µm). This agreed well with the theoretical model presented by McAllister et al. (2003) where the permeability across the skin has been predicted as a function of both the surface area of microneedle arrays and number of microneedles. This theoretical model agreed well with their experimental study.

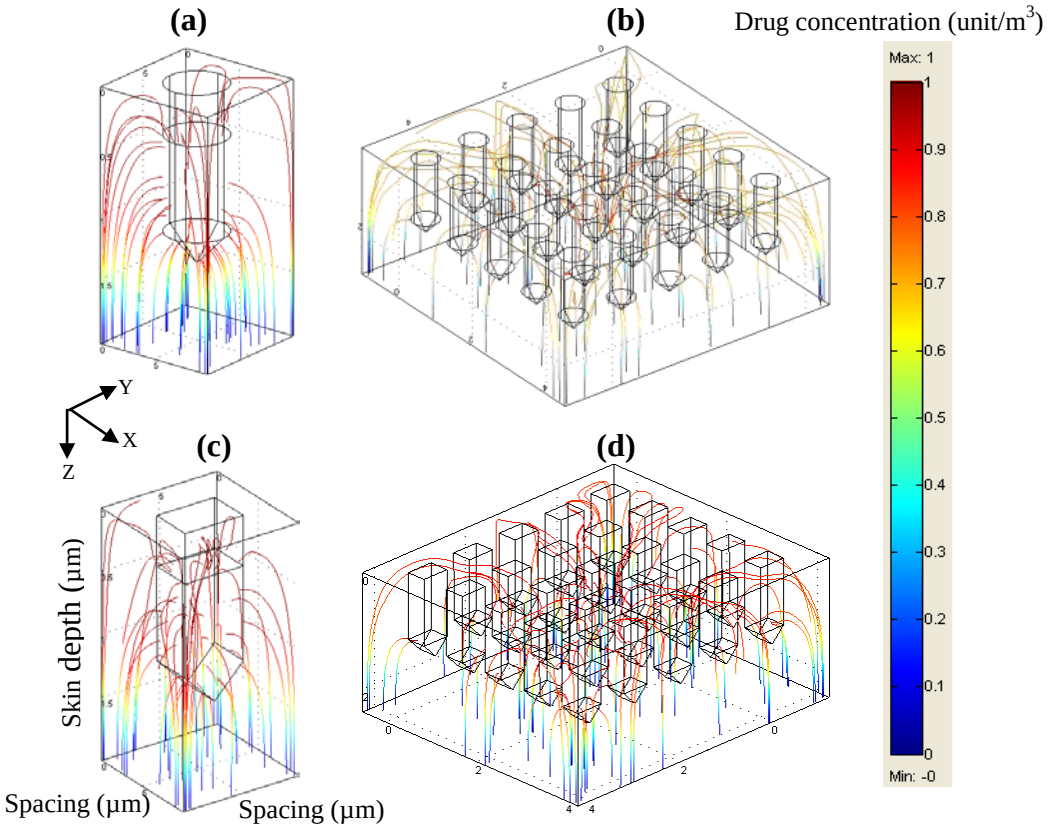

Figure 4.12- A schematic diffusion model in 3D of microneedle: (a) type A with 1 microneedle, (b) type A with 25 microneedles, (c) type D with 1 microneedle, (d) type D with 25 microneedles.

Figure 4.12 shows the effects of microneedles interactions for microneedle types A and D for one microneedle and twenty five microneedles in 3D. This has been done to observe microneedles interactions for a given number of microneedles (i.e., 25 microneedles) in 3D and to explore how these interactions affect the drug permeability behaviour. To further examine the influence of microneedles interaction, the effective skin thickness and the insulin concentration in blood have been determined for all microneedle types for both one microneedle and twenty five microneedles as shown in Figures 4.13 and 4.14, respectively.

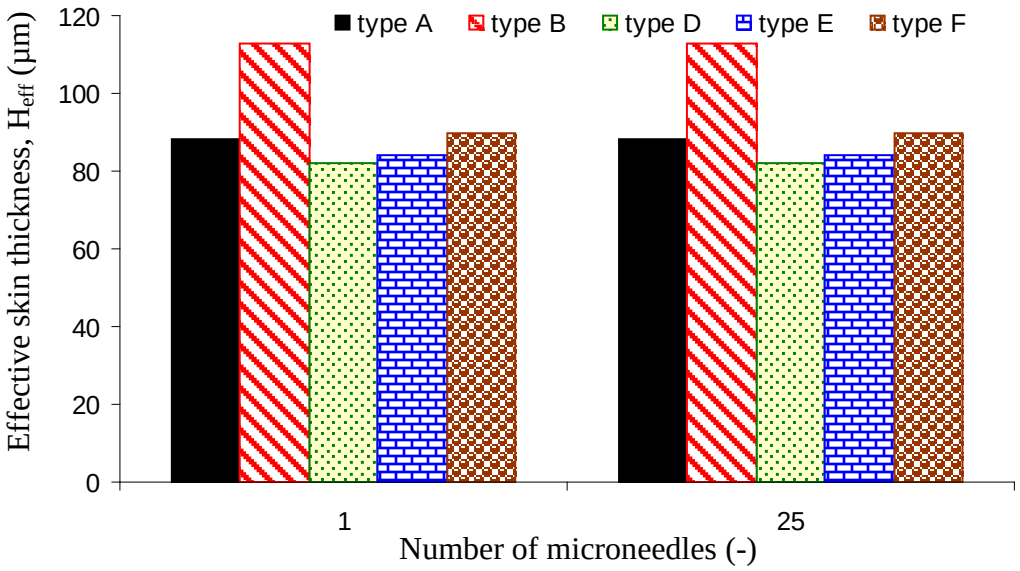

Figure 4.13- Influence of the changing the number of microneedles for various microneedle types coated with insulin on effective skin thickness H_{eff}.

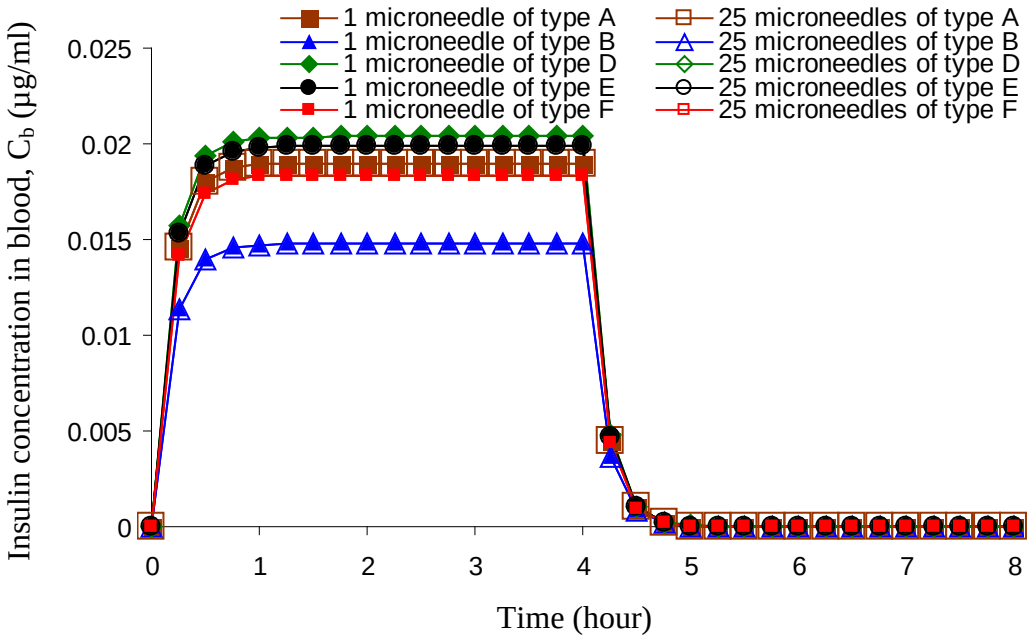

Figure 4.14- Influence of the changing the number of microneedles for various microneedle types on insulin concentration in blood C_b.

The result shows the interaction between microneedles without any differences in the values of both the effective skin thickness and insulin concentration in blood. The procedures for calculating insulin concentration are discussed in Chapter 5 and are outside the scope of discussion in this chapter.

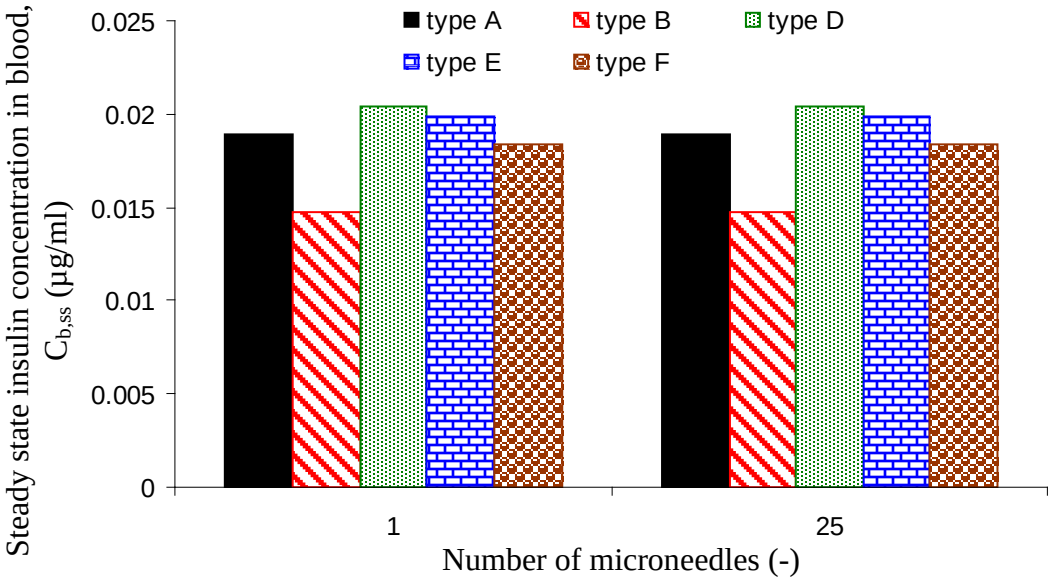

Figure 4.15- Influence of the changing the number of microneedles for various microneedle types on steady state insulin concentration in blood $C_{b,ss}$.

Moreover, Figure 4.15 shows the influence of microneedles interaction for all microneedle types for both one microneedle and twenty five microneedles on the steady state insulin concentration in blood. As expected, the steady state insulin concentrations in blood for all microneedle types for both cases were similar.

In addition, the effective skin thickness and the steady state insulin concentration have been determined for microneedle type D with various centre-to-centre spacing of both one microneedle and twenty five microneedles as shown in Figures 4.16 and 4.17, respectively. As mentioned previously, the centre-to-centre spacing also represents the width and length of the square element of skin as shown in Figure 4.2(b). Therefore, the centre-to-centre spacing of one microneedle has been varied by simply changing the dimensions of the square element

of skin. As expected, the effective skin thickness and steady state insulin concentration have a similar value in a given centre-to-centre spacing for both one microneedle and twenty five microneedles. Altogether, the simulations show that the microneedles interaction has been taken into our consideration with no differences in both the one microneedle model and twenty five microneedles.

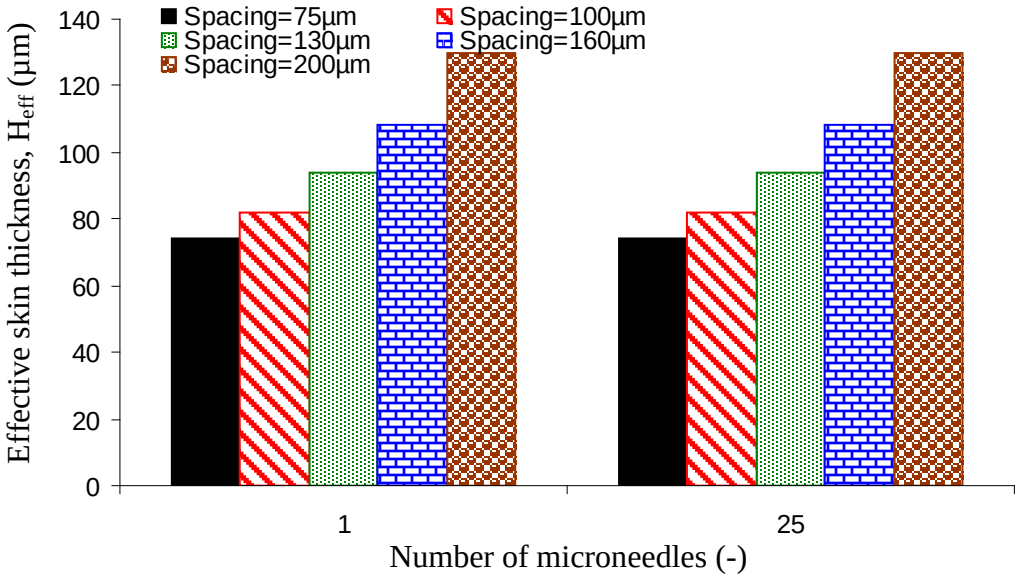

Figure 4.16- Influence of the changing the number of microneedles for various centre-to-centre spacing of microneedle type D coated with insulin on effective skin thickness H_{eff}.

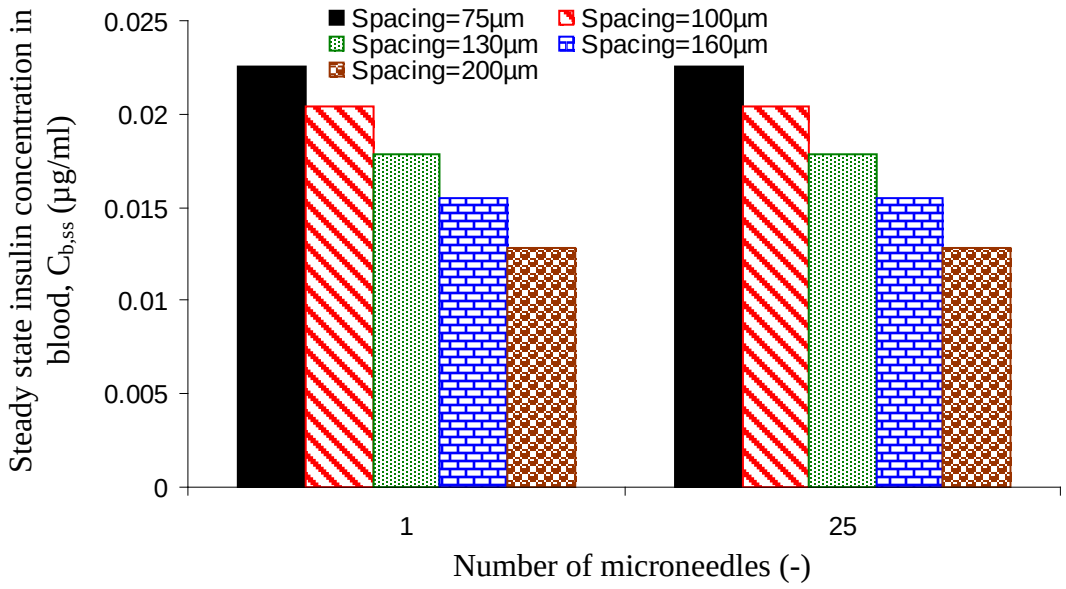

Figure 4.17- Influence of the changing the number of microneedles for various centre-to-centre spacing of microneedle type D on steady state insulin concentration in blood $C_{b,ss}$.

4.5.3 Effects of depth of penetration

The ability of controlling the depth of penetration has a significant limitation when using the microneedles of different geometries (Matriano et al., 2002). It is therefore important to relate microneedle dimensions to the penetration depth which then influence the performance of the microneedles for drug delivery process (Teo et al., 2005). Widera et al. (2006) showed that coated microneedles with different drug doses did not decrease the penetration depth for a given microneedle length. However, the depth of penetration decreased with increased microneedles length for a given dose (Widera et al., 2006). In contrast, Cormier et al. (2004) compared the penetration depth for both coated and uncoated microneedles. In their study, they found a significant reduction in penetration depth for coated microneedles.

To address this issue in a systematic manner, the depth of microneedle penetration was varied for all types of microneedle to calculate the effective skin thickness H_{eff} and effective permeability across skin P_{eff} of insulin as a model drug ($D_{vs}=1\times10^{-10}\,m^2/s$; Lv et al., 2006).

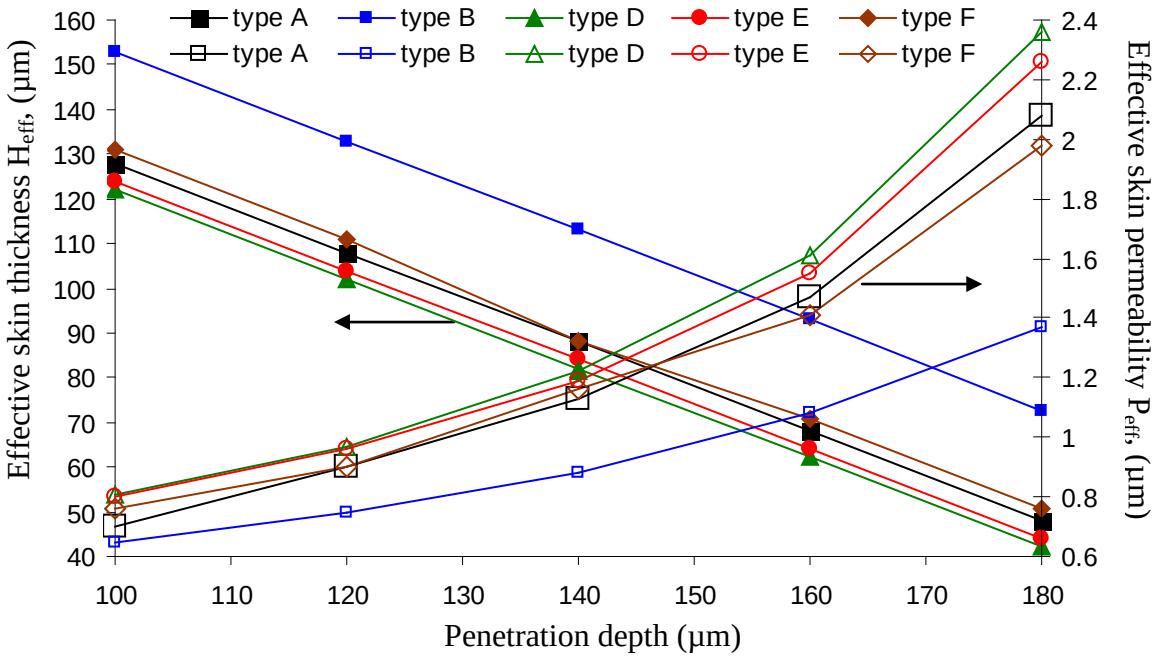

Figure 4.18- Influence of the changing penetration depth of various microneedles types, coated with insulin, on effective skin thickness H_{eff} (solid markers) and effective permeability across skin P_{eff} (blank markers).

Microneedle length in our model represents the depth to which the microneedle penetrates the skin, and as such, does not directly represent the physical length of the microneedle. Besides depth of penetration, the design dimensions in Table 4.1 are used in all of the microneedle types and the results are shown in Figure 4.18.

There is an obvious linear relationship between H_{eff} and microneedle penetration depth for all the models. The data points for both microneedles types A and C are indistinguishable due to the similarity in their geometry. For this reason, the data for microneedle type C is not plotted. The linear result is a consequence of the fact that the average diffusion path length becomes shorter in proportion to the depth of penetration. For a given length, the effective permeability across skin is maximum for microneedle type D and minimum for microneedle type B. The geometry of microneedle type D is such that its tip has a relatively large surface area and thus presents a larger amount of drug closer to the blood circulation. This reduces the effective skin thickness and increases the effective permeability across skin. Altogether, the result indicates that by increasing the penetration depth of microneedle, the effective skin thickness decreases and the effective permeability across skin increases.

4.5.4 Effects of microneedle diameter

Rajaraman and Henderson (2005) argued that the microneedle diameter depends on the materials used for fabrication. The experimental results conducted by Stoeber and Liepmann (2005) illustrated that microneedle diameter depends on the maximum microneedle density (i.e., number of microneedles per unit area). The force needed to cause microneedle failure during piercing through skin increases by increasing microneedle diameter (Park et al., 2007). These results were consistent with the simulations presented by Haider et al. (2001) where the insertion force requirements increased with increasing microneedle diameter. Teo et al. (2005) demonstrated that increasing microneedle diameter improved transdermal drug transport.

Microneedles tend to buckle for a given diameter by increasing microneedles length but of the same diameter at pressure less than that needed to penetrate the stratum corneum (Mukerjee et al., 2004). Microneedles with larger diameter provide higher mechanical stability than that with a smaller diameter (Ovsianikov and Chichkov, 2007). Khumpuang et al. (2005) fabricated microneedle arrays with a microneedle diameter of 40 µm to prevent any problems of blood clogging due to the diameter of white blood cells (i.e., approximately more than 20 µm).

Following the above discussions, we investigated the influence of various microneedle diameters on both the effective skin thickness and effective permeability across skin for various geometries. Figure 4.19 was obtained when the diameters of microneedles type A and type C were varied. Besides diameter, the other dimensions are design values (penetration depth = 140 µm, coating depth = 100 µm, microneedle spacing = 100 µm).

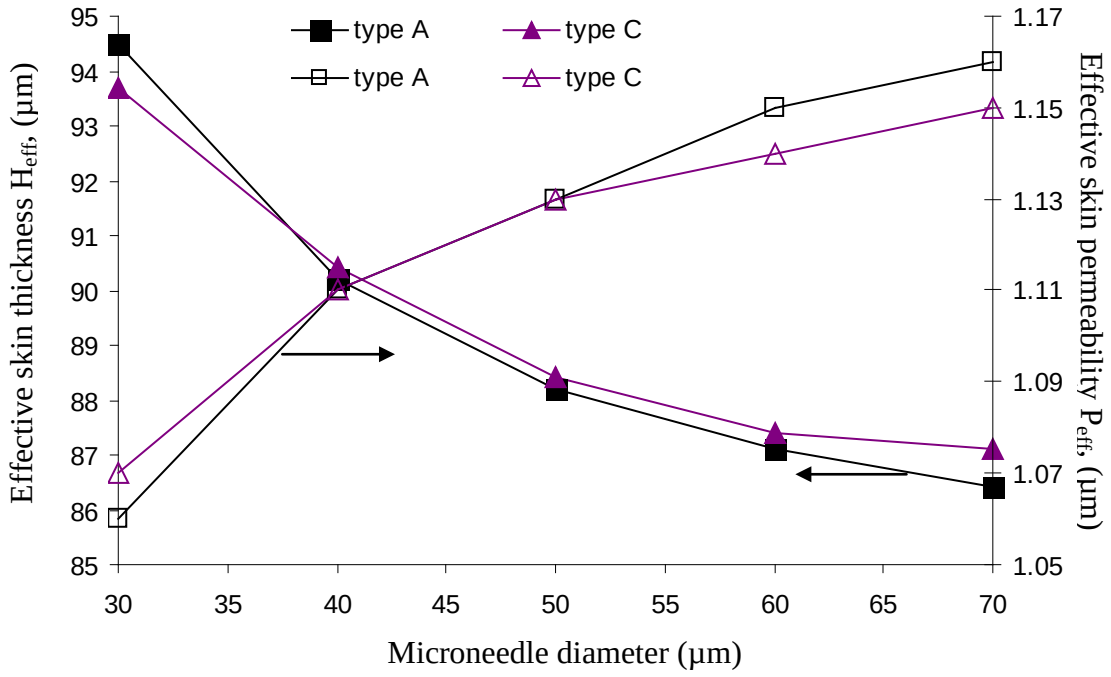

Figure 4.19- Influence of the microneedle diameter of insulin coated microneedles types on the effective skin thickness H_{eff} (solid markers) and effective permeability across skin P_{eff} (blank markers).

It can be seen in Figure 4.19 that by increasing the diameter, the effective skin thickness is decreased, increasing the effective permeability across skin. However, over the range of diameters tested, the effective skin thickness only changed by less than 10%, indicating the effective skin thickness is not a strong function of the diameter. As the diameter is increased, the diffusion paths from the microneedle to the corners of the blood circulation interface are reduced. This is responsible for decreasing effective skin thickness and increasing effective permeability across skin. Diameter may be more important in increasing the available surface area for drug coating on the microneedle. Effective permeability across skin appears to tend to a constant value as diameter is increased. For a given diameter, there is little difference in the effective permeability across skin when either microneedle is considered. This is presumably due to the similarity of geometry in the two models. However, the effective permeability across skin is maximum for microneedle type A and minimum for microneedle type C. To sum up, changing the microneedle diameter has a lower influence on both the effective skin thickness and permeability as compared to changing the penetration depth of microneedle.

4.5.5 Effects of microneedle thickness

The thickness of microneedle has been considered as an important parameter, since it is related to the length of microneedles and hence its strength (Rajaraman and Henderson, 2005). Davis et al. (2004) found that the force of microneedle fracture depends on the microneedle thickness. They noticed that the margin of safety (i.e., ratio between microneedle fracture and skin insertion force) reached its highest value with large microneedle thickness.

To determine the effects of this parameter, the thickness of microneedle types D-F was varied and the results are shown in Figure 4.20. Design dimensions were used in Table 4.1. The results indicate that by increasing the thickness of these microneedles, effective skin thickness will decrease and permeability will increase. For a given microneedle thickness, the effective

permeability across skin is maximum for microneedle type D and minimum for microneedle type F. The range of effective skin thickness is quite small for each microneedle (13-15%) when compared to the range that was obtained by varying length (>60%).

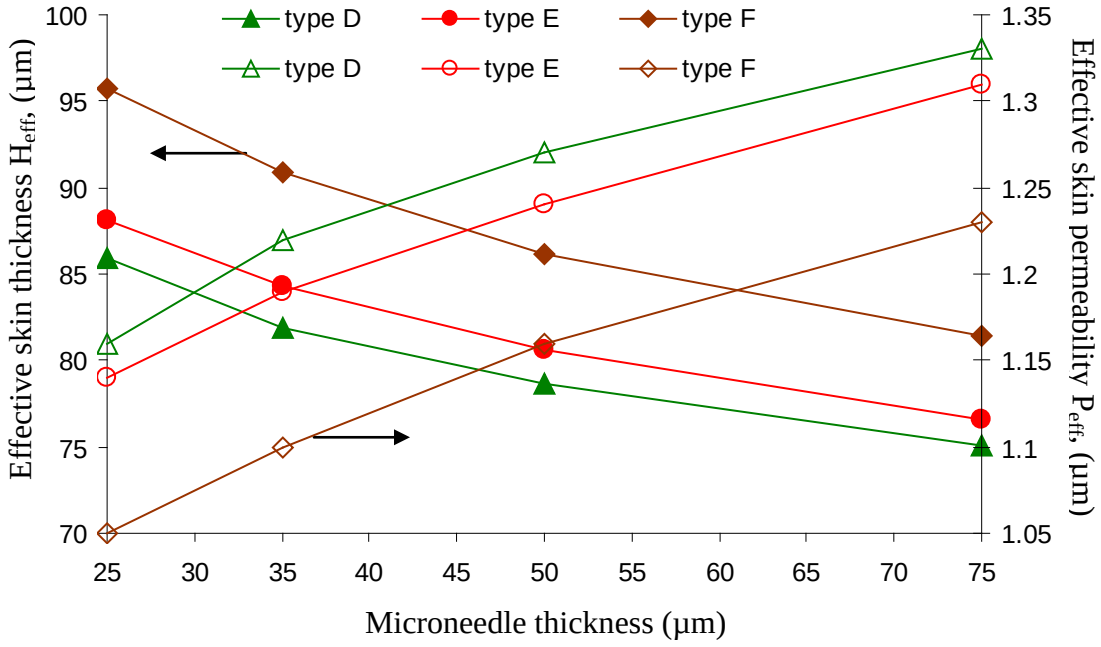

Figure 4.20- Influence of microneedle thickness of insulin coated microneedles types on effective skin thickness H_{eff} (solid markers) and effective permeability across skin P_{eff} (blank markers).

This indicates effective skin thickness is a relatively weak function of thickness, like diameter. Unlike in the case of diameter though, effective permeability across skin appears to be a linear function of thickness. The mechanism by which permeability is increased is probably due to the shortening of diffusion paths from the microneedle to the corners of the blood circulation interface in the skin diffusion model. Overall, changing the microneedle thickness has a lower influence on both the effective skin thickness and permeability across skin as compared to changing the penetration depth of microneedle but has a higher influence as compared to changing the microneedle diameter. In all cases of microneedle thickness, the range of both the effective skin thickness and permeability is quite small.

4.5.6 Effects of microneedle drug coating depth

Gill and Prausnitz (2007) examined the ability of controlling the microneedle length by varying the coverage coating percentage of the microneedle length. However, they did not study the influence of this variation on permeability across skin. Widera et al. (2006) studied the effect of changing the coating dose for four microneedle array designs. They found that both the length and density of microneedles did not influence the total amount of drug delivered into the skin. The amount delivered of ovalbumin as a model protein increased as a result of increasing the coating concentration of ovalbumin (Matriano et al., 2002). However, decreasing the coating dose would improve the drug delivery efficiency (Cormier et al., 2004).

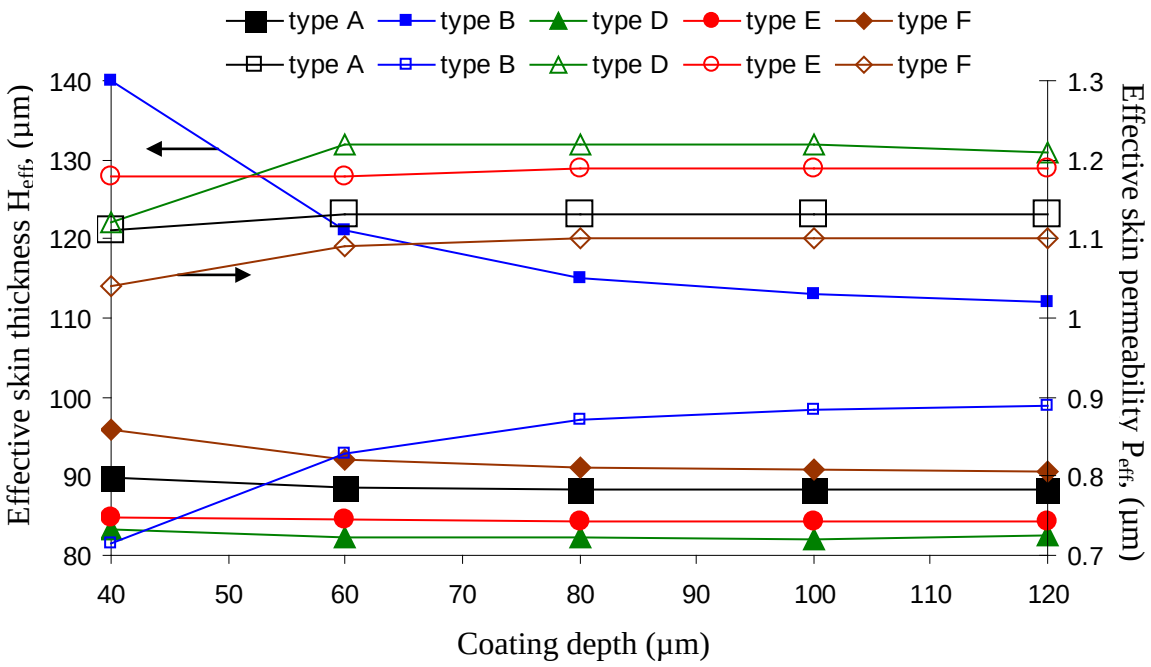

Figure 4.21- Influence of microneedle coating depth of insulin for various microneedles types on effective skin thickness H_{eff} (solid markers) and effective permeability across skin P_{eff} (blank markers).

In this study, the depth of drug coating was varied on all microneedles (with otherwise design dimensions), between 40 to 120 µm. The effect on effective skin thickness and permeability are shown in Figure 4.21. For a given coating depth, the effective permeability across skin is maximum for microneedle type D and minimum for microneedle type B. For all cases, except

microneedle type B, effective skin thickness and permeability across skin are very weak functions of the coating depth of the drug film on the microneedle. As mentioned before, microneedle type A and microneedle type C were found to be indistinguishable so microneedle type C is not plotted. Beyond 60-80 μm it seems that effective skin thickness and effective permeability across skin become independent of coating depth. It is difficult to explain why coating depth appears to be more important in determining effective permeability across skin for microneedle B than the other types. In general, the results show that coating depth has the lowest influence on both the effective skin thickness and permeability as compared to previous parameters.

4.5.7 Effects of microneedle spacing

As expected, the centre-to-centre distance between two adjacent microneedles is an important factor for fabricating microneedles (Choi et al., 2006). The insertion force of microneedles depends on microneedles spacing (Parker et al., 2007). This accords well where the insertion force of microneedles depends on microneedles spacing as well as microneedle length (Davis et al., 2004). They suggest that the insertion force depends also on the number of microneedles as long as the spacing is wide enough. Increasing the centre-to-centre spacing improves the transdermal drug delivery efficiency of coated microneedles (Gill and Prausnitz, 2007). Haider et al. (2001) also demonstrated this by increasing microneedle spacing which reduced penetration force. While the previous studies attempted to determine effects of microneedle spacing on the force of insertion, it is not clear how the spacing influences the effective permeability across skin and thickness.

To address this issue in this work, the centre-to-centre spacing was varied between 75-200 μm for all the microneedle types (with design dimensions). From Figure 4.22, it appears that an exponential relationship exists between microneedle spacing and both effective skin thickness

and effective permeability across skin. When each series of data is fitted to an exponential trend line, the R^2 value is greater than 0.99, indicating a strong agreement.

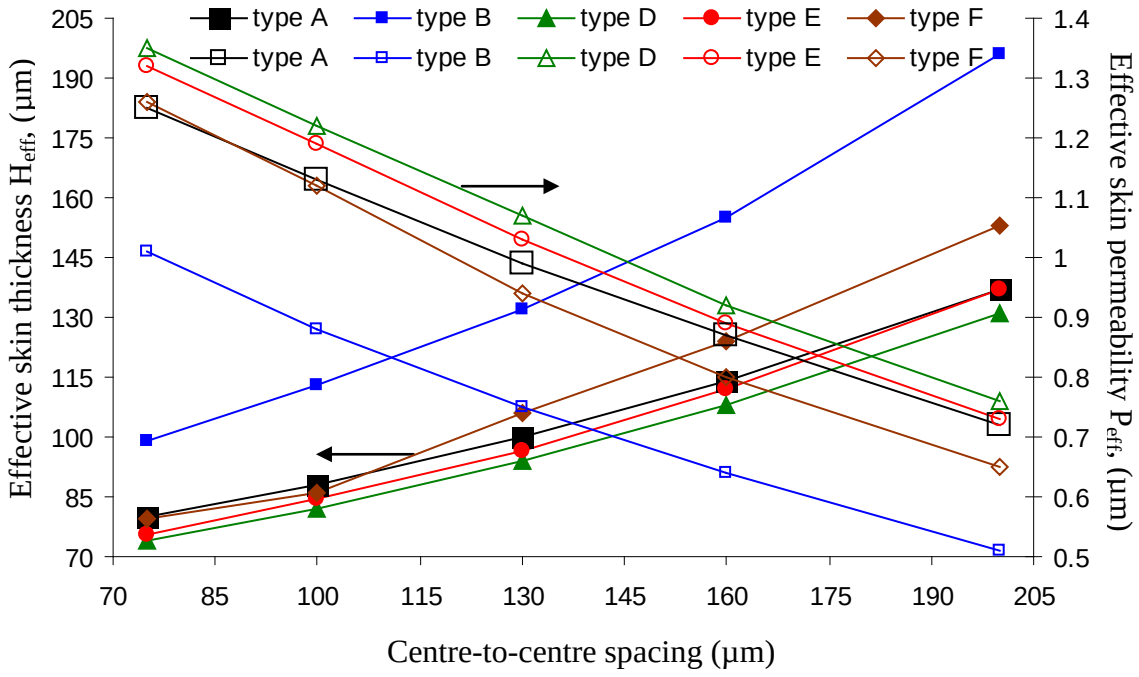

Figure 4.22- Influence of insulin coated microneedle spacing on the effective skin thickness H_{eff} (solid markers) and effective permeability across skin P_{eff} (blank markers).

As centre-to-centre spacing increases, the surface area of the blood circulation interface (where the sink condition exists) in each square symmetrical element of the microneedle array also increases. The diffusion paths from the microneedle surfaces in the centre of the element to the corners of the blood circulation interface become longer as the area of the interface increases. This is responsible for the increase in effective skin thickness and hence the decrease in effective permeability across skin. For a given centre-to-centre spacing, the effective permeability across skin is maximum for microneedle type D and minimum for microneedle type B. As stated before, the data for microneedle type C was indistinguishable from microneedle type A and so was not plotted. Altogether, the range of effective skin thickness is relatively large for each microneedle (>42%) when compared to the range that was obtained by varying all the previous parameters except the penetration depth. This indicates effective skin thickness is a relatively strong function of centre-to-centre spacing.

4.5.8 Square or hexagonal microneedle array pattern

Since the first fabrication of microneedles, different microneedles array patterns have been proposed such as square (Hsu et al., 2007), hexagonal (Widera et al., 2006), etc. However, the shape of the pattern does not represent the shape of microneedle cross section (Rodriguez et al., 2005). In this work, it was determined whether arranging the microneedles into a hexagonal pattern affected the effective permeability of skin. This was done by using hexagonal shaped elements in the skin diffusion model instead of square ones. Therefore, the demonstration has been done for microneedle types A and D. Figure 4.23 indicates that for a given centre-to-centre spacing, effective permeability across skin is slightly greater (2-5%) when a hexagonal array pattern is used over a square pattern.

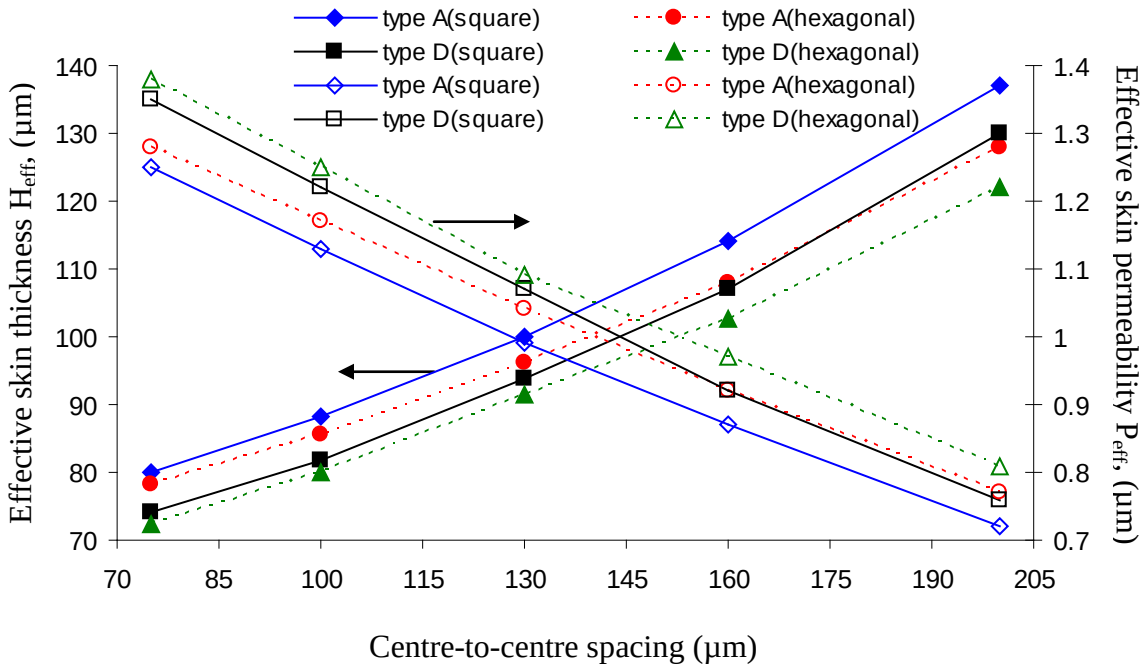

Figure 4.23- Comparison of the effects of insulin coated microneedle spacing for types A and D for square and hexagonal microneedle patterns on effective skin thickness H_{eff} (solid markers) and effective permeability across skin P_{eff} (blank markers).

As mentioned previously, the relation between effective skin thickness and effective permeability across skin with microneedle spacing is an exponential increasing and decaying, respectively. For a given centre-to-centre microneedle spacing, the area of the blood circulation interface is greater for square elements. As a result, the diffusion paths are then

longer which results in a greater effective skin thickness. Overall, there is not much difference between the performance of the square and hexagonal patterns since the square pattern has almost the same influence as the hexagonal pattern.

4.5.9 Effects of increase in skin permeability relative to untreated skin

Microneedle arrays have been considered as an intelligent drug delivery devices (Tao and Desai, 2003). Over the past few years, a variety of methods have been proposed to determine the skin permeation of drugs caused by microneedles. Wu et al. (2006) used macroneedles instead of microneedles and determined permeability through treated skin by macroneedles. Wu et al. (2007) compared permeability of high molecular compounds through treated skin by microneedle before and after applying the iontophoresis. This has been done by evaluating permeability factor (i.e., ratio of flux through fresh intact skin over flux post-iontophoresis). However, as far as the authors know, no theoretical effort had ever been done for evaluating the relative permeability across skin to quantify the changes before and after applying the microneedles across skin. For that reason, we determine the ratio of permeability with microneedles and permeability of normal skin (R_P) which is a function of H_{eff}, the effective skin thickness and R_D, the ratio of diffusion coefficients in the viable skin and stratum corneum. As mentioned previously, the value of R_D varies between 500 -10,000 (Tojo, 1987). The thickness of stratum corneum and viable skin were assumed to be 20 μm and 180 μm, respectively. This has been assumed since that the distance to the blood circulation from the skin surface has been reported as 200 μm (Tojo, 1987).

Figure 4.24 shows how R_P varies as a function of H_{eff} for particular values of R_D. The range of H_{eff} corresponds to the range calculated in the previous section. The permeability of skin is increased by around 3 orders of magnitude compared to normal untreated skin (i.e., R_p ranges from 63 – 6673). This result is consistent with literature, which states that microneedles can

improve permeability across skin by over 1000 times when left in place (Henry et al., 1998). For a given effective skin thickness, the relative permeability is maximum for R_D = 10000 and minimum for R_D = 500. The result shows clearly that the microneedle arrays enhance the transdermal drug delivery as the permeability across skin with microneedles is higher when compared with the permeability across skin without microneedles.

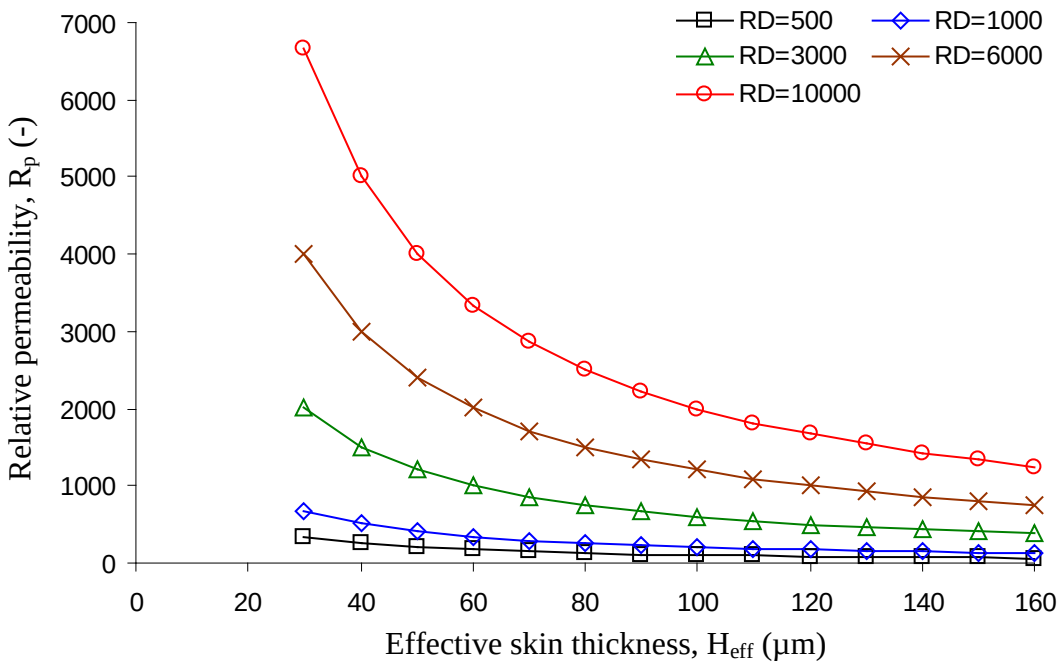

Figure 4.24- The relative permeability of treated skin to untreated skin (R_p) as a function of the ratio of diffusion coefficients in the viable skin and stratum corneum (R_D) and the effective skin thickness (H_{eff}). Rp (-) is the ratio of drug permeability with microneedles to the permeability of normal skin (i.e., without microneedles).

4.6 Summary

The work in this chapter addresses the use of microneedles coated with a drug solution film. In particular, to identify how the geometries of various microneedles affect the drug permeability in skin. Effective permeability across skin has been calculated for a range of microneedle shapes and dimensions in order to identify the most efficient geometry. To calculate effective permeability (P_{eff}), the effective skin thickness (H_{eff}) has been calculated. These are then plotted for insulin as a model drug to see how various microneedle parameters

affect the profiles of both H_{eff} and P_{eff}. It has been found that the depth of penetration from the microneedle array was the most important factor in determining P_{eff}, followed by the microneedle spacing. Other parameters such as microneedle diameter and coating depth are less significant.

CHAPTER 5
Numerical Modelling of Drug Concentration in Blood

5.1 Introduction

As discussed previously in Chapter 2, solid microneedles have generally received more attention as compared to hollow microneedles. According to Gill and Prausnitz (2007), coated microneedles could potentially provide an alternative means to systemically deliver drugs in a bolus form. It has been noted that the drug coating should be localised on the microneedle surface rather than the array base. Even though coating the base of the array could increase the dosage, it has been found that the drug is poorly delivered from the array base and instead most drugs are delivered from the tips of the microneedles (Gill and Prausnitz, 2007). For example, when the model antigen 'ovalbumin' was coated onto the tips of a microneedle array its delivery efficiency was increased by 48-58% (Widera et al., 2006) compared to 4-14% when the whole array was coated (Matriano et al., 2002). The coating should adhere well to the microneedles in order to avoid deposition of the drug on the skin's surface during insertion. This will increase delivery efficiency and is also beneficial from safety perspective (Widera et al., 2006). This study describes a model for coated microneedles, the so-called "coat and poke" approach (Prausnitz, 2004).

Martanto et al. (2004) studied whether permeability across skin to insulin can be enhanced by using a microneedle array while insulin solution is applied topically in a so-called "poke with patch" method (Prausnitz, 2004). Solid microneedles coated with insulin have been applied to diabetic hairless rats where the decrease in blood glucose levels was significantly greater than in the control case when microneedles were not used (Martanto et al., 2004). The initial concentration of the drug decreases over time to an ineffectual stage once the drug penetrates into human skin. Therefore, to reach an effective blood concentration, the therapeutic efficacy of drug should be improved by increasing drug administration (Santini et al., 2000). Kolli and

Banga (2008) show that the plasma drug concentration reaches its maximum when using microneedles as compared to passive delivery.

Motivated with the results obtained in Chapters 3 and 4, we seek to further study the effects of several geometrical parameters (e.g., microneedle thickness, coating thickness, etc.) on the insulin blood concentration profile. Consequently, a dimensional analysis has been carried out using Buckingham's π theorem to determine the functional dependence of blood drug concentration on various parameters. For our purpose, a mathematical framework has been developed and numerical simulations have been carried out which describe the pharmacokinetics of insulin penetrated into skin from using microneedle array. It is rare to find a study that has systematically addressed how the microneedle array design parameters influence drug blood concentration profiles from a computational point of view. This work is envisaged to determine the steady state insulin concentration in the blood for various microneedle types, and hence identify the optimum design, if any, for the transdermal drug delivery of insulin.

5.2 Dimensional analysis

As discussed before, a number of variables influence the process of drug delivery by using microneedles. However, in most practical cases, the main variable of interest is the steady state drug concentration in blood ($C_{b,ss}$) and its dependency on other variables. To address this issue, a scaling relationship is obtained by using dimensional analysis. The dimensionless groups obtained in this can describe drug transport behaviour to a very good accuracy, as discussed later. Following the procedures of Buckingham π theorem (Buckingham, 1914), it can be shown that:

$$\frac{C_{b,ss}}{Cs} = \phi\left[\frac{S_a}{L^2}, \frac{h}{L}, \frac{V_b}{L^3}, \frac{L^2 K_e}{D}, \frac{T}{L}, \frac{CD}{L}, \frac{P_t}{L}\right] \tag{5.01}$$

Where, ϕ is an unknown function. This unknown function that appears in the dimensional analysis may need different approach in order to identify its value. Although equation (5.01) provides the relationship of the dimensionless steady state blood concentration $C_{b,ss}/C_s$ with other individual dimensionless groups, in reality however the combined effects of all groups are more relevant for drug transport in skin. To address this issue, all groups have been combined by multiplication or division to form a new dimensionless group. Then, the power law form is applied to convert the dimensionless groups, which are related to each other, with an unknown function as follows (Yahya and Manning, 2004):

$$\frac{C_{b,ss}}{C_s} = Y\left[\frac{S_a \times L^3 \times K_e \times T \times P_t}{V_b \times h \times D \times CD}\right]^z \qquad (5.02)$$

Where, Y is a dimensionless constant and z is an unknown power. Ordinary regression is applied to determine the above dimensionless constant and the unknown power (Smith et al., 1992).

5.3 Modelling strategy

A schematic diagram of the developed mathematical framework for insulin transport across the skin via a microneedle array is illustrated in Figure 5.1. Solid microneedle arrays are coated by an aqueous solution of insulin molecules which bypass the stratum corneum (Davidson et al., 2008). Insulin molecules diffuse across viable epidermis until they reach the epidermal-dermal junction where they are absorbed by the blood circulation. In the figure L_u is the length of the uncoated microneedles, L is the penetration depth of microneedles, H is the thickness of the skin after microneedles have been inserted (i.e., the distance between the tip of the microneedle and the blood circulation), h is the epidermis thickness and Pt is the microneedle centre-to-centre spacing. Insulin pharmacokinetics is described by a one compartment model (i.e. blood compartment) with first order elimination kinetics (Tojo, 1987).

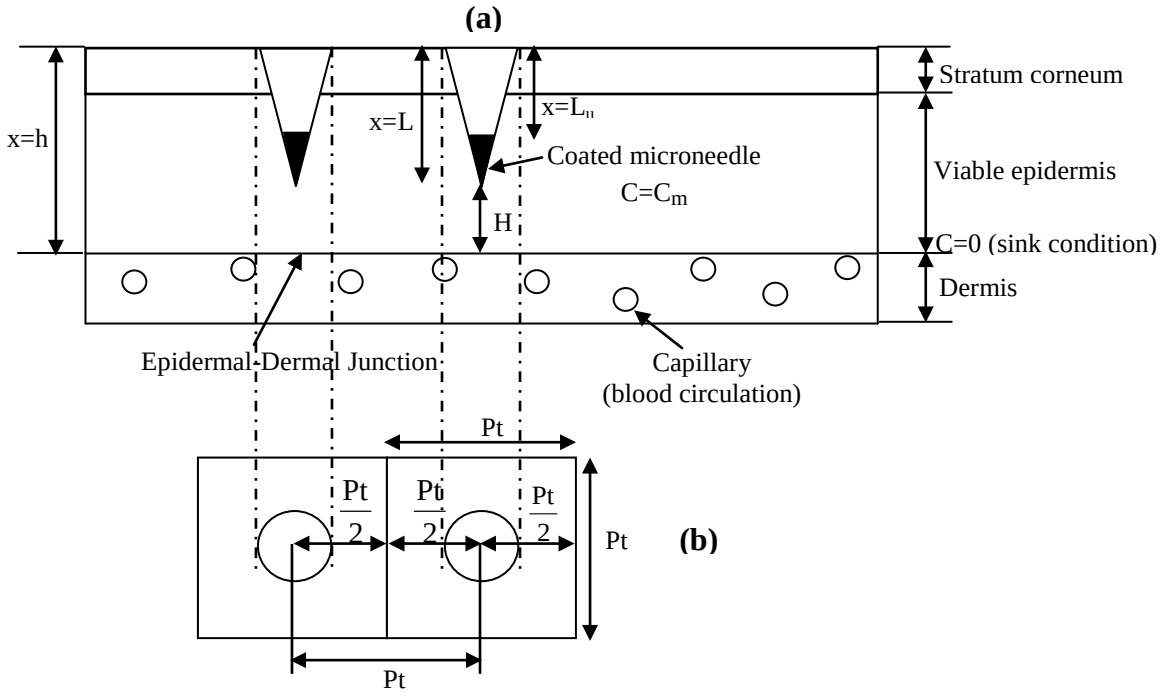

Figure 5.1- Schematic of coated microneedles for transdermal insulin delivery: (a) side view, (b) top view. H is the thickness of the skin after microneedles have been inserted (i.e., the distance between the tip of the microneedle and the blood circulation), h is the skin thickness, L is the penetration depth of microneedles, L_u is the length of the uncoated microneedles and Pt is the centre-to-centre spacing.

To model the diffusion process from the coated microneedles into the skin and determine the effects of geometry, six microneedles shapes have been selected as shown in Figure 5.2. These shapes have been chosen based on what has been reported in the literature, though they are not all drawn to scale (Davidson et al., 2008). These shapes are the same as discussed previously in Chapter 4.

In this section, the model assumptions in the mathematical framework will be presented. Then, the governing equations of both the diffusive flux and drug concentration in blood along with their initial and boundary conditions will be given and explained in detail.

Figure 5.2- The six microneedle types used in this study adopted from Davidson et al. (2008).

5.3.1 Model assumptions

When considering the delivery of insulin from the microneedles through the skin, the same assumptions included in chapter 4 were taken in our consideration. However, these assumptions may be briefly explained as below.

The stratum corneum is mainly impermeable to insulin due to the intercellular lipid layers (Sadrzadeh et al., 2007). The partition coefficient on the boundary between the viable epidermis and dermis has been assumed to be equal one since both layers (i.e., viable epidermis and dermis) consist mainly of water (Ranade, 1991). Drug partition in the skin was not considered during an intracutaneous injection as the diffusion coefficient was considered more important than the partition coefficient (Yoshida et al., 2008). McAllister et al. (2003) develop a theoretical model to determine the permeability across skin of various macromolecules, including insulin, when using microneedles. The permeability was a function of the microneedle dimensions, skin thickness and drug diffusivity and the partition coefficient was not considered. The results agreed well with their experimental data.

As mentioned before, microneedles have been shown to be a promising technique for achieving effective drug delivery to the blood stream (Yang and Zahn, 2004). The drug is absorbed almost completely by the blood vessels once the drug diffuses across the viable

epidermis (Tojo, 1987; Zesch and Schaefer, 1975). In another study, it has been shown that almost 97% of the drug is taken up by the blood stream (Tojo, 2005). Furthermore, the blood glucose levels in diabetic hairless rats has been reduced by 80% when using an array of solid microneedles and an insulin solution placed in contact with the skin (Martanto et al., 2004). The drop in blood glucose levels due to insulin delivery from microneedles was found to be comparable to that from a hypodermic injection of 0.05-0.5 U insulin (μU/mL = 0.0417 μg/L). These results indicate that microneedles can successfully deliver drugs such as insulin *in vivo* and the majority of the insulin is absorbed by the blood circulation. Ito et al. (2006) concluded that insulin administered through microneedles was well absorbed by the blood stream.

5.3.2 Governing equations for diffusive flux from coated microneedles

The movement of insulin across the viable skin is represented by Fick's second law of diffusion (equation 3.01). In order to solve this equation, the Dirichlet type boundary conditions have been imposed (equations 4.10 and 4.11). Under the above assumptions, the steady state flux of insulin is applied (equation 4.05). In our case, we have previously defined the effective skin thickness H_{eff} of the skin after solid microneedles have been inserted as a function of microneedle geometry (equation 4.12) (Davidson et al., 2008).

Diffusion of insulin in the skin from the coated microneedles has been also modelled in 3D using FEMLAB®. The flux term determined from the simulations has been integrated over the blood circulation boundary and then divided by the boundary area (i.e. 100μm x 100μm $=1\times10^{-8}$ m^2) to give an average steady state flux. This value has been used to calculate the effective skin thickness (H_{eff}) as discussed in Chapter 4. This result has been used in the governing equations of blood insulin concentration as will be discussed in the following section.

5.3.3 Governing equations for insulin concentration in blood

For the purpose of this work, the insulin concentration in blood after imposing the transdermal drug delivery is given by a one-compartmental pharmacokinetic model (Al-Qallaf et al., 2007; Tojo, 2005):

$$V_b \frac{dC_b}{dt} = \left(\frac{dQ}{dt}\right)_e S_a - K_e C_b V_b \tag{5.03}$$

Where, K_e is the elimination rate constant from the blood compartment, dQ/dt is the effective penetration rate of insulin through the skin, S_a is the surface area of the delivery system (i.e., patch of microneedles), V_b is the volume of distribution in the blood, C_b is the insulin concentration in the blood.

The rate of insulin permeation and the cumulative amount of insulin permeated per unit area of skin are given by equations (5.04) and (5.05), respectively (Al-Qallaf et al., 2007; Tojo, 2005):

$$\left(\frac{dQ}{dt}\right)_e = -D\left(\frac{dC}{dx}\right)_{x=h} \tag{5.04}$$

$$Q = \int_0^t \left(\frac{dQ}{dt}\right)_e dt = \int_0^t \left(-D\frac{dC}{dx}\right)_{x=h} dt \tag{5.05}$$

The distance to the blood circulation from the skin surface has been reported as 200 μm (Tojo, 1987), which is used here as well. The viable skin is modelled as a single domain with a single isotropic diffusion coefficient. The width and length of the square element of skin represents the centre-to-centre spacing of the microneedles, assuming they are in a square pattern as shown in Figure 5.1. The spacing has been assumed to be 100 μm, leading to an

area for a square element of skin equal to 1×10^{-8} m^2. The governing equations have been solved by applying the SKIN-CAD® software, (Biocom system, 2006).

This one-compartment model, the simplest pharmacokinetic model, mimics the drug transport behaviour in this case. One assumption that is being made for the above model is that the drug distribution and concentration equilibrium occur rapidly (Xu and Weisel, 2005). It is therefore adequate to describe the pharmacokinetics of drugs that minimally distribute into the body's tissue (van Rossum, 1977). As mentioned earlier, the one-compartment model has been used in this study where we apply the values for the volume of distribution (V_b) and the elimination rate constant (K_e) obtained from literature for insulin. The one-compartment model with steady state values provides a good approximation, especially for those drugs that distribute and reach steady state quickly. Moreover, the one-compartment model is more appropriate for a drug when using transdermal drug delivery (e.g., hypodermic injection, microneedle arrays) than for an oral delivery (e.g., pill), which takes time to dissolve, absorb, and distribute into the system (Shiflet and Shiflet, 2006). Therefore, it is sufficient for the purpose of this work, i.e., to determine the effects of microneedle geometry with insulin as a model drug.

5.4 Results and discussions

In the following simulations, the concentration of insulin in blood has been calculated using equation (5.03). The input parameters of both the design dimensions and the ranges used of various microneedle types for these simulations are shown in Table 5.1. Unless otherwise stated, microneedle type D has been used as an example for all the numerical simulations associated with the variations of the microneedle geometries. Injection of insulin has many benefits such as lowering the blood glucose levels in the treatment of diabetes (Davis et al., 2005), reducing the infarct size and hence improving the diagnosis of the patient once the stroke occurred (Capes et al., 2001), etc. In fact, insulin has been adopted as a model drug in

many studies for transdermal drug delivery using microneedles (Nordquist et al., 2007; Davis et al., 2005; Prausnitz, 2004).

Table 5.1- The input of model parameters used in this work for analysing the blood concentration of insulin permeated through the skin by using microneedle arrays.

	Insulin	
Parameters	Type D	Ranges
Duration for medication (calculation): t_m (hour)	8[a]	-
Duration of microneedles application: t_d (hour)	4[a]	-
Surface area of microneedles array: S_a (cm^2)	0.8[b,c]	[l]0.04-0.81[b,c]
Distance to blood vessel: h (cm)	0.02[a,d]	0.016-0.024
Effective skin thickness: H_{eff} (cm)	0.00819[e]	variable[e]
Diffusion Coefficient in viable skin: D_{vs} (cm^2/s)	[f,g]1×10^{-6}	-
Volume of distribution: V_b(L)	12[h,i]	12[h,i]-21[m]
Elimination rate constant: K_e (h^{-1})	6[h,j]	0.46[m]-6[h,j]
Skin surface concentration: C_s (μg/ml)	4170[k]	-
Penetration depth: L (cm)	0.014[e]	0.01[e]-0.018[e]
Microneedle thickness: T (cm)	0.0035[e]	0.0025[e]-0.0075[e]
Microneedle centre-to-centre spacing: Pt (cm)	0.01[e]	0.0075[e]-0.02[e]
Coating depth: CD (cm)	0.01[e]	0.004[e]-0.01[e]

[a]Al-Qallaf et al., 2007; [b]Park et al., 2005; [c]Al-Qallaf and Das, 2008; [d]Tojo, 2005; [e]Davidson et al., 2008; [f]McAllister et al., 2003; [g]Lv et al., 2006; [h]Søeborg et al., 2009; [i]Kraegen and Chisholm, 1984; [j]Hansen, 2004; [k]Martanto et al., 2004; [l]Teo et al., 2005; [m]Van Rossum, 1977.

5.4.1 Validation of the developed approach

We start our discussion by validating the simulations carried out in this mathematical framework. This has been done by comparing the numerical results with the experimental work by Martanto et al. (2004) as shown in Figure 5.3. It should be noted that only two points were taken in the experimental results. The results show that the simulation results compare adequately with the experimental results. It must be pointed out that the results are for cases when the microneedles have been inserted into diabetic hairless rat. Therefore, an animal skin has been used because of the difficulties of using human skin for various reasons such as ethical consideration (Sartorelli et al., 2000). However, a review has been presented to compare various skins including human and animal skins (Godin and Touitou, 2007). In this study, the authors have concluded that mammal skin is a reasonable model to study transdermal delivery in humans (Godin and Touitou, 2007). In brief, less remarkable

differences have been observed between the experimental results and the numerical results (2-16%). Therefore, the level of agreement is quite good.

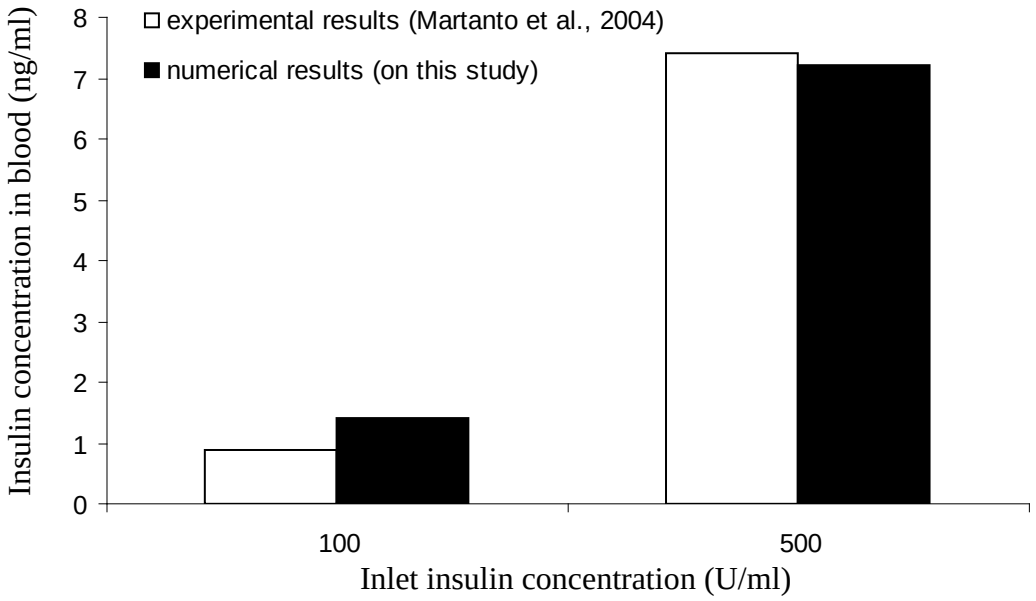

Figure 5.3-Comparison of the simulated blood concentration profile of insulin after applying transdermal delivery by microneedle type F (black column) and the experimental results (blank column) assuming the insertion time of microneedles to be four hours.

5.4.2 Effects of microneedle shapes on insulin distribution in skin

In order to determine the effectiveness of transdermal drug delivery using microneedles, the distribution of blood insulin concentrations for each microneedle model has been obtained. In a previous work involving different needle geometries, Lv et al. (2006) have used a theoretical model to obtain insulin profiles across the skin. They studied both the transient and spatial distribution in the skin tissue as well as in the drug solution of hollow microneedles. However, they have not considered the implications of variations in the microneedle geometry of solid microneedles. In our study, the distribution of insulin concentration across skin for various solid microneedles models has been simulated as shown in Figures 5.4 and 5.5.

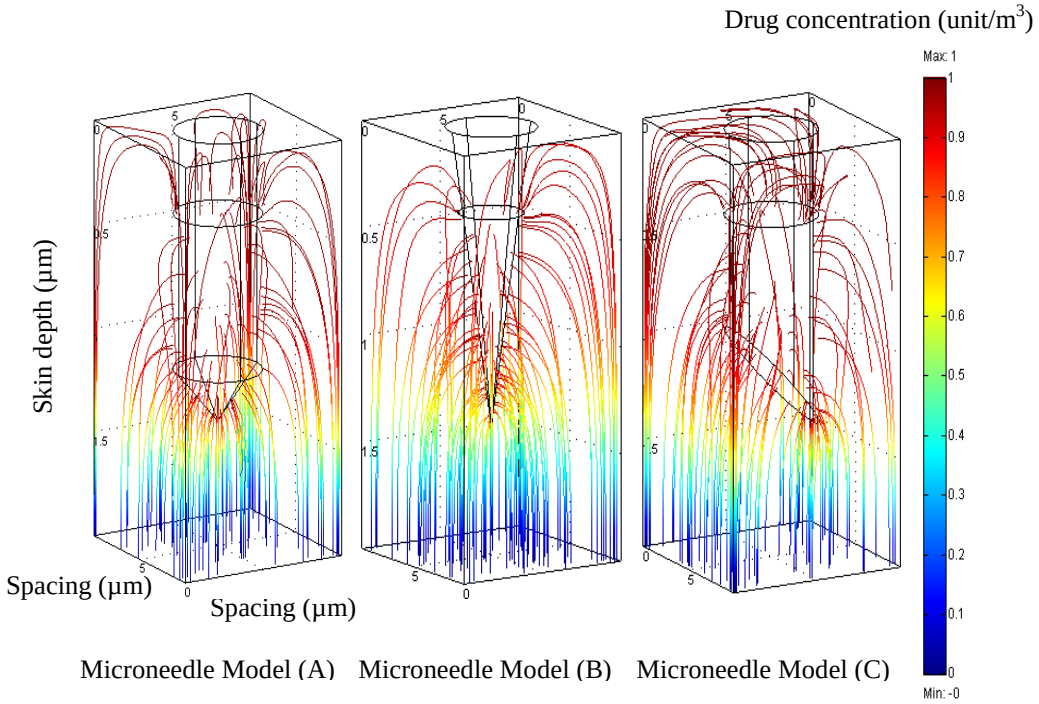

Figure 5.4- Distribution of insulin in skin for microneedle models (A), (B) and (C) (penetration depth is 140 µm and all the remaining dimensions with their design values as mentioned in Table 5.1).

As expected, the insulin concentration decreases gradually towards the blood interface due to sink condition there. It seems the most effective model is microneedle type D as the distribution of insulin concentration (i.e., $0.5 \leq C_{ins} \leq 1$ unit/m^3) covers most of the skin thickness (i.e., 200 µm). On the other hand, microneedle model B results in the least distribution of insulin concentration. The uniform distribution is an important factor that can be observed in microneedle type C and E. In microneedle type C, the drug is distributed mostly on one side. This is due to the cylindrical shape of microneedle with a bevelled tip. However, in microneedle type E, the drug is mainly distributed around the top of the microneedle. This is also due to its arrow-head shape. Back diffusion of insulin has also been observed in all cases. The results show that the distribution of insulin across skin depends on the microneedle geometries.

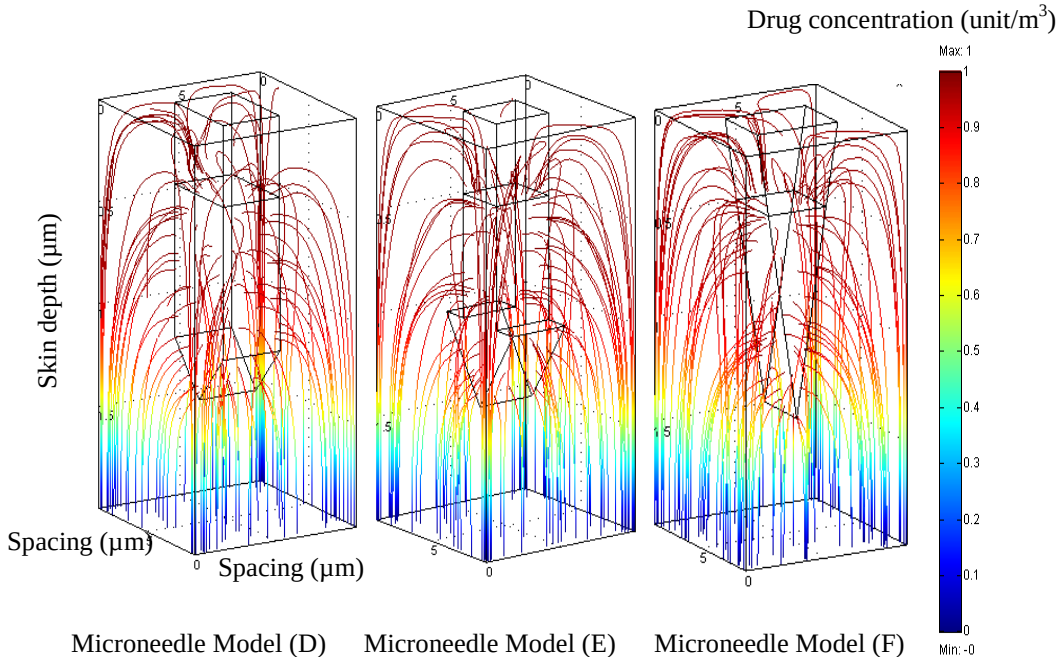

Figure 5.5- Distribution of insulin in skin for microneedle models (D), (E) and (F) (penetration depth is 140 µm and all the remaining dimensions with their design values as mentioned in Table 5.1).

5.4.3 Effects of duration of transdermal drug application and penetration depth

To address the implications of the penetration depth (L) on insulin concentration in the blood, the depth of microneedle penetration for microneedle type D (i.e., rocket needle) has been varied. In addition the penetration depth of the various microneedle model shapes has been varied to examine the influence of L on the steady state insulin concentration in blood ($C_{b,ss}$). The performance of the drug delivery process for microneedle arrays could be improved by relating microneedle geometries to the penetration depth (Teo et al., 2005). The penetration depth of coated microneedles of the same length with various doses was observed (Widera et al., 2006). However, the depth of penetration is increased by increasing the microneedles length while maintaining the same dose (Widera et al., 2006). Cormier et al. (2004) also found a significant reduction in penetration depth for coated microneedles as compared to uncoated microneedles.

Figure 5.6 shows the effects of the duration of application ranging from 4 to 6 hours for various lengths of microneedle and patch surface area of 0.81 cm^2. The steady state insulin concentration in blood ($C_{b,ss}$) does not change that much as there is a constant plateau concentration for each case as shown in Figure 5.6. Penetration depth of microneedles in this model represents the depth to which the microneedle penetrates the skin, and as such, does not directly represent the physical length of the microneedle. However, the time duration within which the drug is active in skin varies depending on the duration of application. As expected, the results indicate that the duration of steady state blood insulin concentration increases, as the duration of application increases.

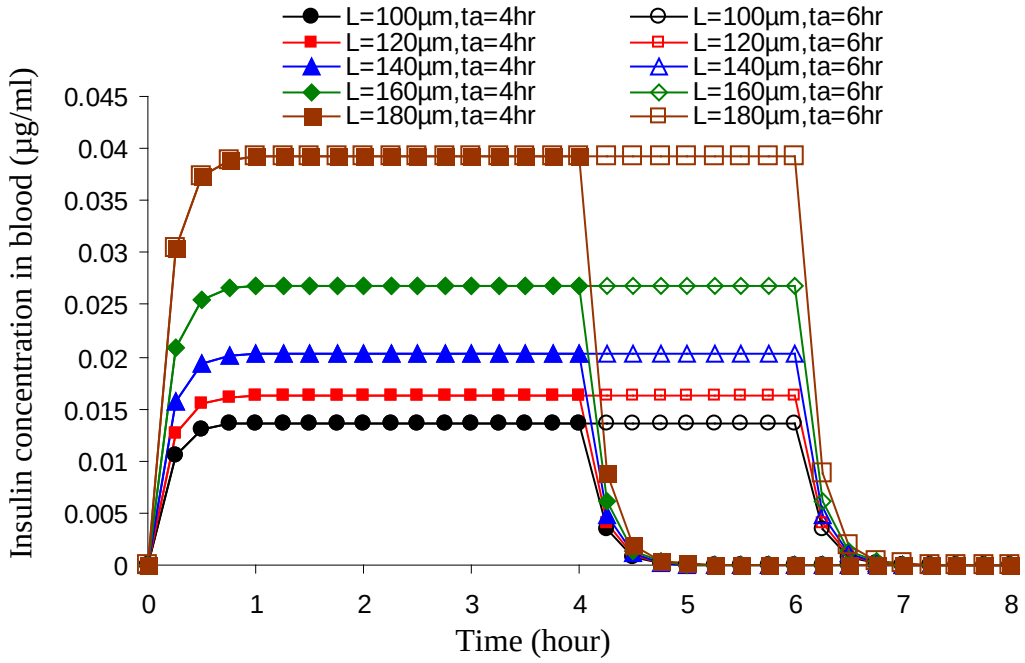

Figure 5.6-Influence of transdermal delivery of insulin for different penetration depth of microneedle and duration of application (t_a) for the input parameters in Table 5.1.

As the effective skin thickness (H_{eff}) decreases with deeper penetration by the microneedles (Davidson et al., 2008), the insulin concentration in blood is increased. This implies that by increasing microneedle penetration depth, the process of transdermal drug delivery using microneedles has been enhanced significantly. In all cases, the steady state blood drug concentration varies between 0.013-0.04 µg/ml depending on values of h/L provided all other parameters remain the same. The result suggests that the implication of changing the

penetration depth of microneedle enhanced the steady state insulin concentration in blood by three fold. Figure 5.7 shows the cumulative amount permeated per unit area of skin for insulin with different penetration depths, which represents equation (5.05). As expected, the cumulative amount of insulin permeated into blood per unit area of skin increases as the penetration depth and the duration of application increase. Altogether, the results indicate that the diffusion of drugs across human skin through the use of microneedles depends on the penetration depth of microneedle. Therefore, the penetration depth of microneedle must be considered in designing, and hence, optimizing any microneedle arrays.

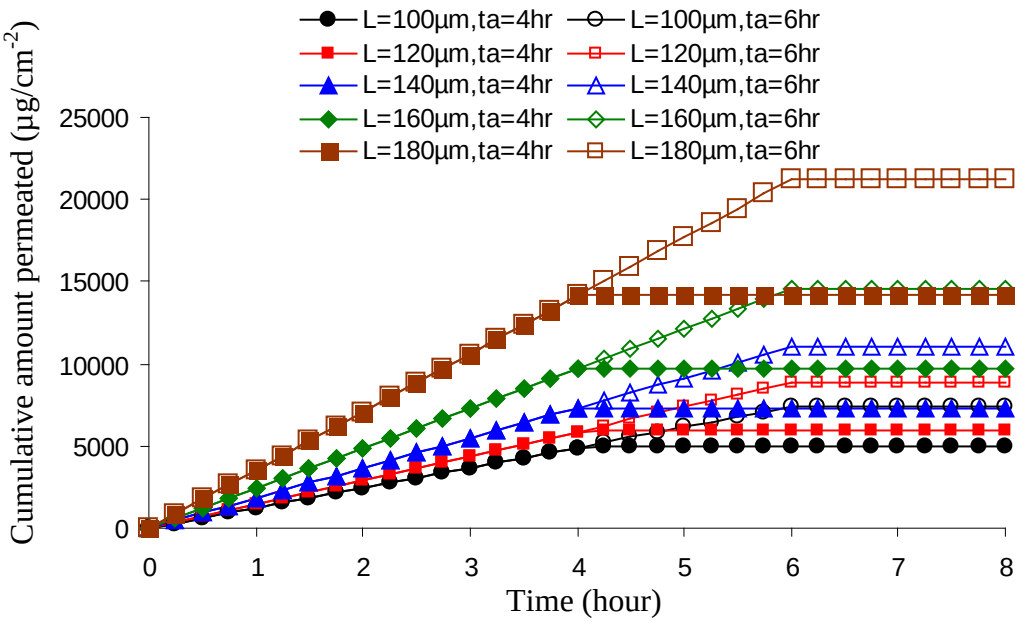

Figure 5.7-Cumulative amount of insulin permeated into blood per unit area of skin with various penetration depths of microneedles for the input parameters in Table 5.1.

The general functional dependency of $\frac{h}{L}$ on $\frac{C_{b,ss}}{C_s}$ is shown in Figure 5.8 (named first curve) and is given by the following relationship:

$$\frac{C_{b,ss}}{C_s} = 1\times10^{-5}\left(\frac{h}{L}\right)^2 - 4\times10^{-5}\left(\frac{h}{L}\right) + 4\times10^{-5};\ 1.11 < \frac{h}{L} < 2;\qquad h=0.02\text{ cm} \qquad (5.06)$$

From Figure 5.8, it appears that a 2nd order polynomial relationship exists between the dimensionless steady state insulin concentration in blood and the dimensionless group (h/L).

When each series of data is fitted to a polynomial trend line, the R^2 value is greater than 0.99, indicating a strong agreement.

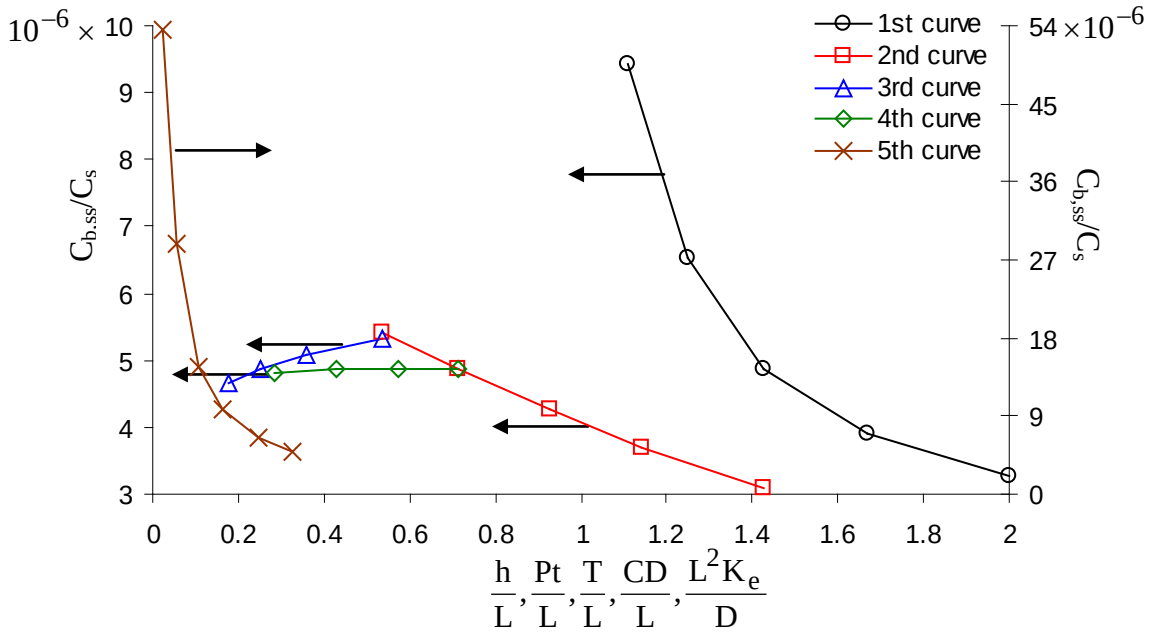

Figure 5.8-Scaling relationship of different dimensionless groups.

To further study the effect of penetration depth, the penetration depth (L) of various microneedles models has been changed to observe the effect on the steady state insulin concentration in blood as shown in Figure 5.9. Microneedle type C has not been included due to the similarity in the geometry of this model, and hence the obtained results, with microneedle model A. Microneedle type D is the best model as it has the highest steady state insulin concentration in blood ($C_{b,ss}$) with a value of 0.039 µg/ml corresponding to a penetration depth of 180 µm. On the other hand, microneedle type B has the lowest steady state insulin concentration in blood ($C_{b,ss}$) with a value of 0.012 µg/ml corresponding to a penetration depth of 100 µm. Over the range of penetration depth tested, the steady state insulin concentration in blood changed by more than 60%, indicating the steady state insulin concentration in blood is a relatively strong function of the penetration depth of microneedle. The results show that there is a proportional relationship between the penetration depth (L)

and steady state insulin concentration in blood. As such the penetration depth is a significant factor in determining the steady state insulin concentration in blood.

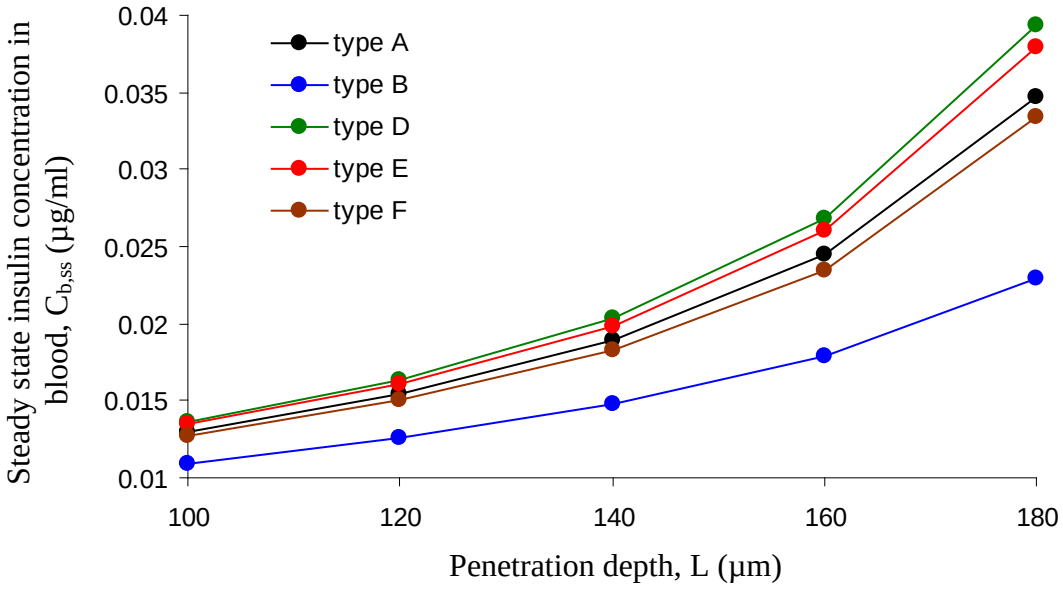

Figure 5.9- Influence of the penetration depth (L) of various microneedles models, coated with insulin, on the steady state insulin concentration in blood ($C_{b,ss}$), assuming that the insertion time of microneedles is four hours (the results of microneedle type C are not included in the figure as they are very similar to the results of microneedle type A).

5.4.4 Effects of centre-to-centre spacing of adjacent microneedles (P_t)

In this section, the centre-to-centre spacing (Pt) of microneedle model has been varied between 75-200 µm to analyze the influence of this parameter on insulin concentration in blood. Microneedle spacing (pitch) is an important parameter and hence appropriate microneedle spacing should be determined (Choi et al., 2006). So far the implications of centre-to-centre spacing have been evaluated in different contexts and rarely on drug concentration in blood. For example, the shear stress acting on microneedle tip with microneedle spacing (i.e., varying from 150 µm to 600 µm) has been examined by Choi et al (2006). These authors have shown that the optimum microneedle spacing is 450 µm as it corresponded to the lowest stress of approximately 34.5 MPa. Closely spaced microneedles are associated with difficulty in insertion due to skin elasticity as reported in a previous study (Davis et al., 2004).

From Figure 5.10, the steady state insulin concentration in blood of insulin varies between 0.019-0.022 µg/ml. Apart from the centre-to-centre spacing, the other dimensions have been kept constant as shown in Table 5.1.

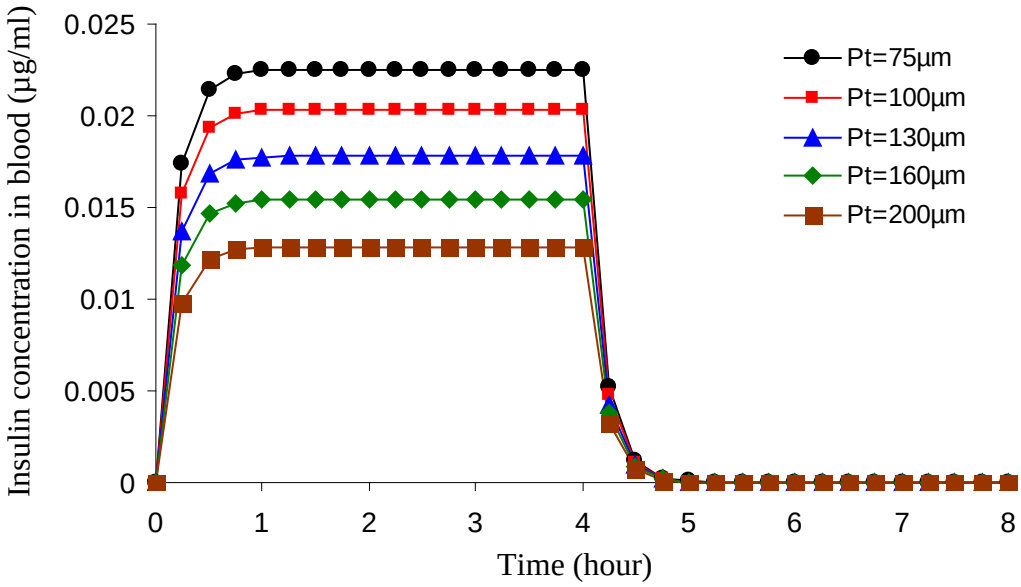

Figure 5.10-Influence of transdermal delivery of insulin for different centre-to-centre spacing for the input parameters in Table 5.1.

As mentioned in the previous results, longer centre-to-centre spacing of microneedles results in higher values of h_e (Davidson et al., 2008). The higher effective skin thickness is offset by the increase in the surface area of the blood circulation interface for a given number of microneedles, which tends to increase the flux of drug molecules into the blood stream. Despite this, increasing microneedle spacing results in generally lower ranges of insulin concentrations. This means that there is an inverse relationship between the microneedle spacing and the insulin concentration in blood. Figure 5.11 shows the cumulative amount permeated per unit area of skin for insulin with different centre-to-centre spacing. As expected, the cumulative amount of insulin permeated into blood per unit area of skin decreases as the microneedle spacing increases. To sum up, the influence of the microneedle spacing on the insulin concentration in blood is less as compared to the previous case (i.e., penetration depth of microneedle). The functional dependency of Pt/L on $C_{b,ss}/C_s$ is shown in

Figure 5.8 (named second curve) and given by the following relation, provided all other parameters remain the same:

$$\frac{C_{b,ss}}{C_s} = 8\times10^{-6} e^{-0.63\left(\frac{Pt}{L}\right)} \quad ; \qquad 0.53 < \frac{Pt}{L} < 1.4 \qquad (5.07)$$

This equation is valid for a given penetration depth (L), in this case L=0.014 cm.

As illustrated in Figure 5.8, the relation between the dimensionless steady state insulin concentration and the dimensionless group (Pt/L) decays exponentially and the R^2 value is greater than 0.99.

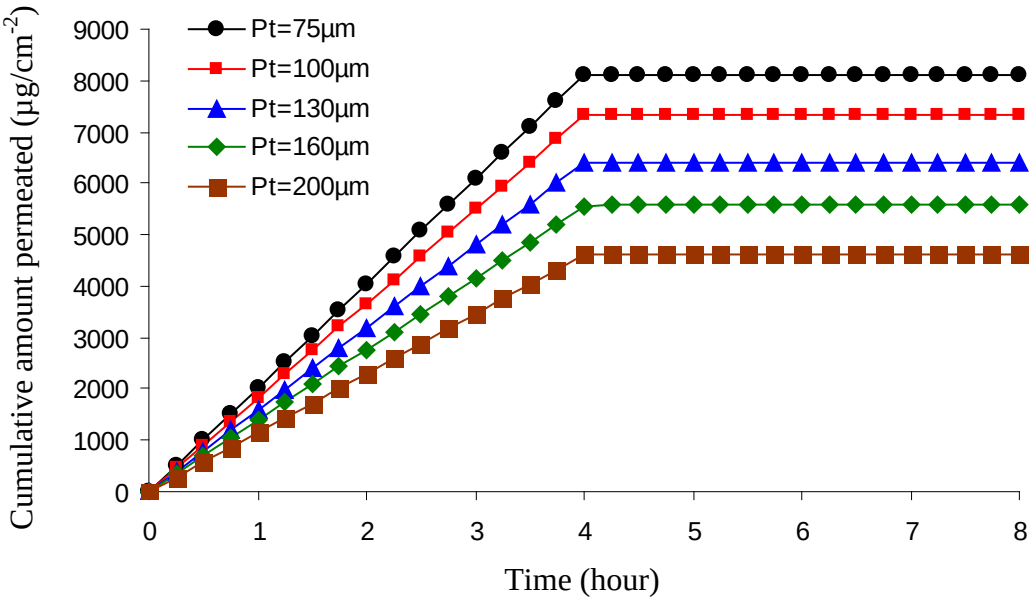

Figure 5.11-Cumulative amount of insulin permeated into blood per unit area of skin with various centre-to-centre spacing of microneedles for the input parameters in Table 5.1.

The centre-to-centre spacing (Pt) of the microneedle models was varied to study the influence on blood insulin concentrations, as shown in Figure 5.12. As mentioned previously, microneedle type A and microneedle type C have been found to be indistinguishable so microneedle type C has not been plotted. Microneedle type D is the best type as it has the highest steady state insulin concentration in blood ($C_{b,ss}$) with a value of 0.023 µg/ml for a spacing of 75 µm. On the other hand, microneedle type B has the lowest steady state insulin

concentration in blood with a value of 0.008 µg/ml for a spacing of 200 µm. For the range of centre-to-centre spacing studied, the steady state insulin concentration in blood changed by more than 42%. However, the range of steady state insulin concentration in blood is smaller than the range that was obtained by varying the penetration depth of microneedles (>60%). The results indicate there is an inverse relationship between the centre-to-centre spacing (Pt) and the steady state insulin concentration in blood. Altogether, the results indicate that the steady state insulin concentration in blood is not a weak function of microneedle spacing.

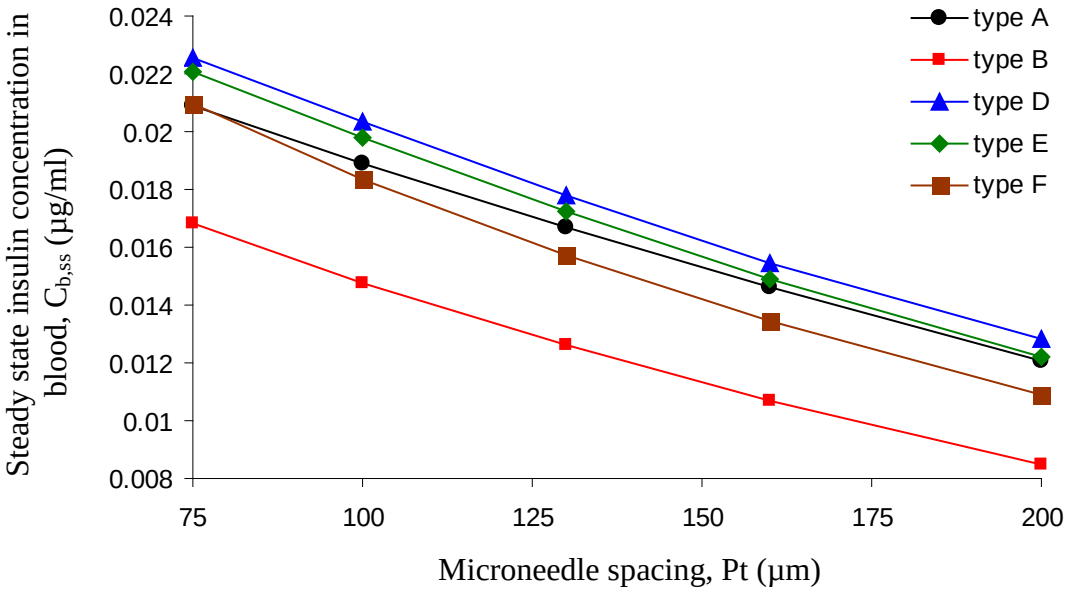

Figure 5.12- Influence of the centre-to-centre spacing (Pt) of various microneedles types, coated with insulin, on the steady state insulin concentration in blood ($C_{b,ss}$), assuming that the insertion time of microneedles is four hours (the results of microneedle type C are not included in the figure as they are very similar to the results of microneedle type A).

5.4.5 Effects of microneedle thickness (T)

The thickness (T) of microneedle type was varied between 25 to 75 µm to examine the influence of the microneedle thickness on the steady state insulin concentration in blood ($C_{b,ss}$). Microneedle thickness has been considered a key factor due to its influence on the force required to fracture the microneedle (Davis et al., 2004). In one study, it was observed that with large microneedle thickness, the margin of safety (i.e. ratio between microneedle fracture and skin insertion force) reached its highest value. Rajaraman and Henderson (2005)

have considered the thickness as an important dimension since it determines the aspect ratio of their fabrication process.

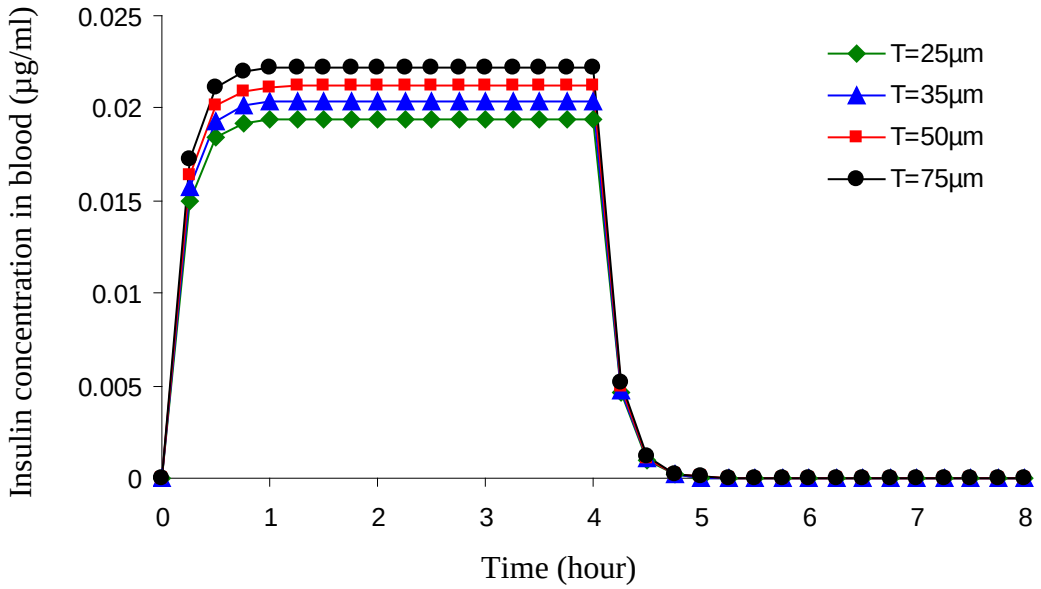

Figure 5.13-Influence of transdermal delivery of insulin for different microneedle thickness for the input parameters in Table 5.1.

The results shown in Figure 5.13 indicate that by increasing the thickness of the microneedles, the steady state insulin concentration in blood ($C_{b,ss}$) can be increased. However, over the range of thicknesses used, the range of $C_{b,ss}$ is generally smaller when compared to the range that has been obtained by varying both penetration depth of microneedle and centre-to-centre spacing of microneedles. This is because increasing microneedle thickness results in less significant increases in P_{eff}, as shown previously (Davidson et al., 2008). All other dimensions have been kept the same as shown in Table 3.1. Overall, the insulin concentration in blood is found to be relatively independent of microneedle thickness in the range studied. Figure 5.14 shows the cumulative amount permeated per unit area of skin for insulin with different microneedle thickness. The cumulative amount of insulin permeated into blood per unit area of skin increases as the microneedle thickness increases. The functional dependency of T/L on $C_{b,ss}/C_s$ is shown in Figure 5.8 (named third curve) and given by the following relation, provided all other parameters remain the same:

$$\frac{C_{b,ss}}{C_s} = 6\times10^{-6}\left(\frac{T}{L}\right)^{0.12} \quad ; \quad 0.17 < \frac{T}{L} < 0.53 \qquad (5.08)$$

This equation is valid for a given penetration depth (L), in this case L=0.014 cm.

From Figure 5.8, it seems that a power relationship exists between the dimensionless steady state insulin concentration in blood and the dimensionless group (T/L). When each series of data is fitted to a power trend line, the R^2 is greater than 0.99, implying a strong agreement.

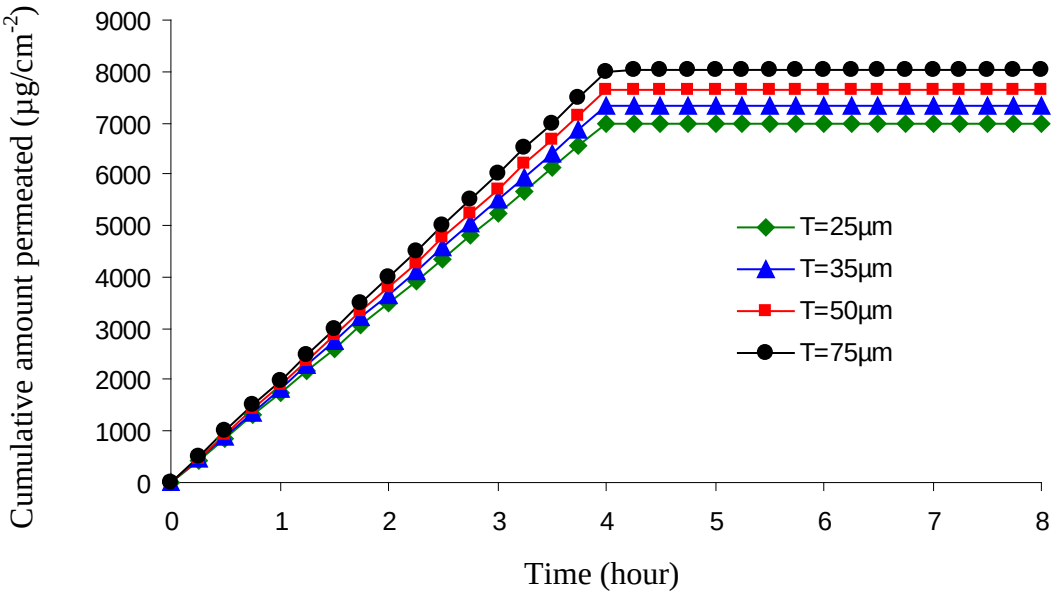

Figure 5.14-Cumulative amount of insulin permeated into blood per unit area of skin with various microneedle thicknesses.

The microneedle thickness (T) of microneedles types D-F was varied to determine the influence on the blood insulin concentration as shown in Figure 5.15. It must be noted that the microneedle thickness is only important for in-plane manufactured microneedles (i.e., microneedles types D-F). Microneedle type D results in the highest steady state insulin concentration in blood ($C_{b,ss}$) with a value of 0.022 µg/ml corresponding to a thickness of 75 µm. On the other hand, microneedle type F has the lowest steady state insulin concentration in blood with a value of 0.017 µg/ml corresponding to a thickness of 25 µm. Over the range of microneedles thicknesses chosen, the steady state insulin concentration was only slightly changed, indicating that it is a relatively weak function of the microneedle thickness. The

results indicate a proportional relationship between microneedle thickness (T) and the steady state insulin concentration in blood. The implication of changing the microneedle thickness has a lower influence on both the insulin concentration in blood and the cumulative amount of insulin permeated into blood per unit area of skin as compared to influences that were obtained by changing both the penetration depth and microneedle spacing.

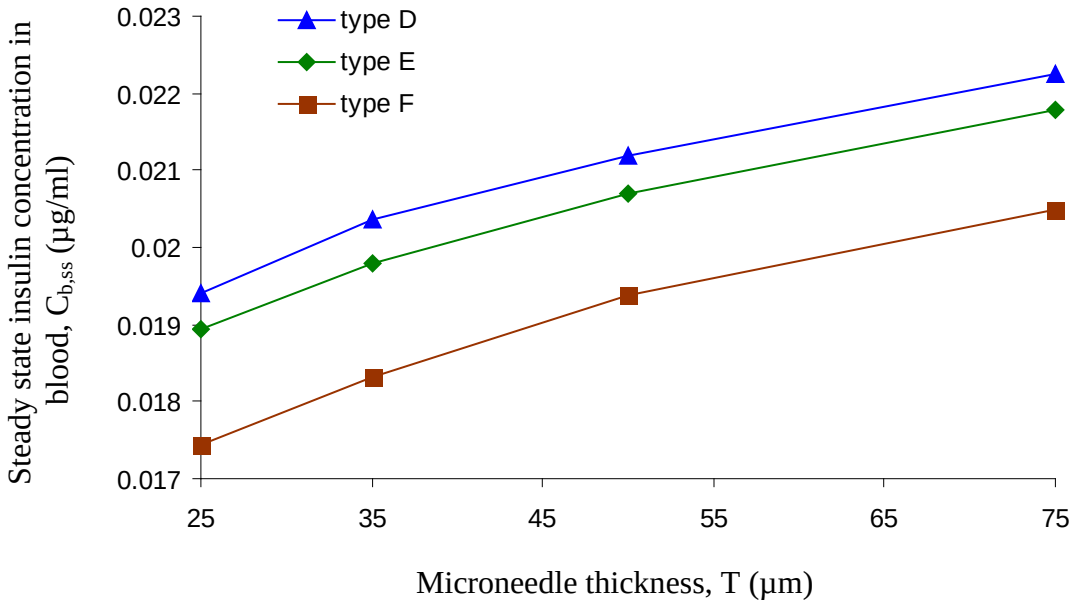

Figure 5.15- Influence of the microneedle thickness (T) of various microneedles types, coated with insulin, on the steady state insulin concentration in blood ($C_{b,ss}$), assuming that the insertion time of microneedles is four hours (the dimensions of these microneedle types are as illustrated in Table 5.1).

5.4.6 Effects of microneedle insulin coating depth (CD)

The effect of the depth of insulin coating (CD) on the insulin concentration in the blood requires further study that is beyond the scope of this research. However, if we assume that CD remains constant during the time that the microneedles are inserted in skin (4 hours in our case), we can perhaps gain an insight on how this affects the blood insulin concentration. Using the above assumption, the depth of insulin coating (CD) on microneedle model was varied between 40 to 100 µm to investigate the influence of this parameter on insulin concentration in the blood. In previous work the drug coating depth (generally 25%-100% of

microneedle length coverage) was examined to study whether uniform drug coating could be achieved (Gill and Prausnitz, 2007). The dose of coated ovalbumin was found to significantly influence the degree of immune response, indicating that the size of dose is a significant factor in transdermal drug delivery through microneedle arrays (Widera et al., 2006). An earlier study presented by Cormier et al. (2004) found that drug delivery efficiency increased with decreasing coating dose of desmopressin as a model drug. In another study, the amount of ovalbumin coated on microneedles was increased by increasing the coating concentration of ovalbumin which in turn also increased the amount of ovalbumin delivered by the microneedles (Matriano et al., 2002).

Similar to what has been obtained for increasing microneedle diameter, increasing the coating depth of insulin on the microneedle does not have a very significant effect on the permeability ratio P_{eff} (Davidson et al., 2008). As a result, the steady state insulin concentration in blood ($C_{b,ss}$) for the range of microneedle diameters being evaluated is almost constant with a value of approximately 0.02 μg/ml. The results for the effect of microneedle coating depth on the steady state insulin concentration in blood are shown in Figure 5.16. All other dimensions have been kept constant as shown in Table 5.1. As a consequence, no differences have been observed for the cumulative amount permeated per unit area of skin for insulin with different microneedle coating depth (data not shown). This means that the insulin concentration in blood is a very weak function of coating depth. The functional dependency of CD/L on $C_{b,ss}/C_s$ is shown in Figure 5.8 (named fourth curve) and given by the following relation, provided all other parameters remain the same:

$$\frac{C_{b,ss}}{C_s} = 3\times10^{-6}\left(\frac{CD}{L}\right)^3 - 5\times10^{-6}\left(\frac{CD}{L}\right)^2 + 3\times10^{-6}\left(\frac{CD}{L}\right) + 4\times10^{-6}$$

$$; 0.28 < \frac{CD}{L} < 0.71 \qquad (5.09)$$

This equation is valid for a given penetration depth (L), in this case L=0.014 cm.

As shown in Figure 5.8, the relation between the dimensionless steady state insulin concentration and the dimensionless group (CD/L) is a 3rd order polynomial increasing and the R^2 value is greater than 0.99.

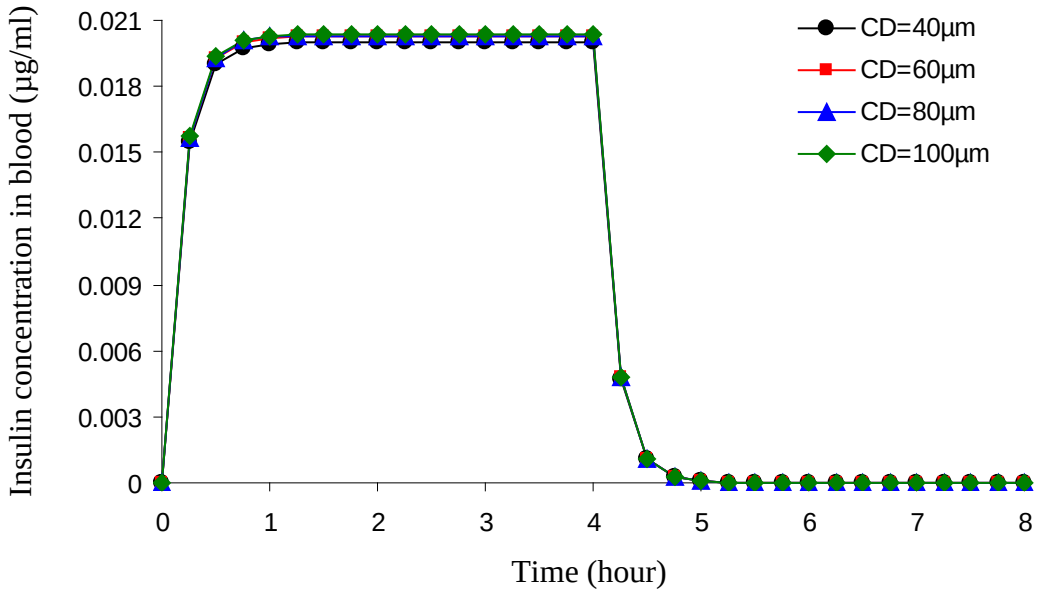

Figure 5.16-Influence of transdermal delivery of insulin for different coating depth for the input parameters in Table 5.1.

The coating depth (CD) was varied on all microneedles models to determine the effect on the insulin concentration in the blood as shown in Figure 5.17. Again, the results from microneedle types A and C are indistinguishable and hence microneedle type C has been omitted from the results. Microneedle type D resulted in the highest steady state insulin concentration in blood $C_{b,ss}$ with a value of 0.02 µg/ml corresponding to a coating depth of 100 µm. In all cases, except microneedle type B, the range of steady state insulin concentration in blood did not change significantly (<5%). This indicates that the steady state blood insulin concentration does not depend significantly on the coating depth. To this end, the variation of coating depth has the lowest influence on both the insulin concentration in blood and the cumulative amount of insulin permeated into blood per unit area of skin as compared to all previous cases.

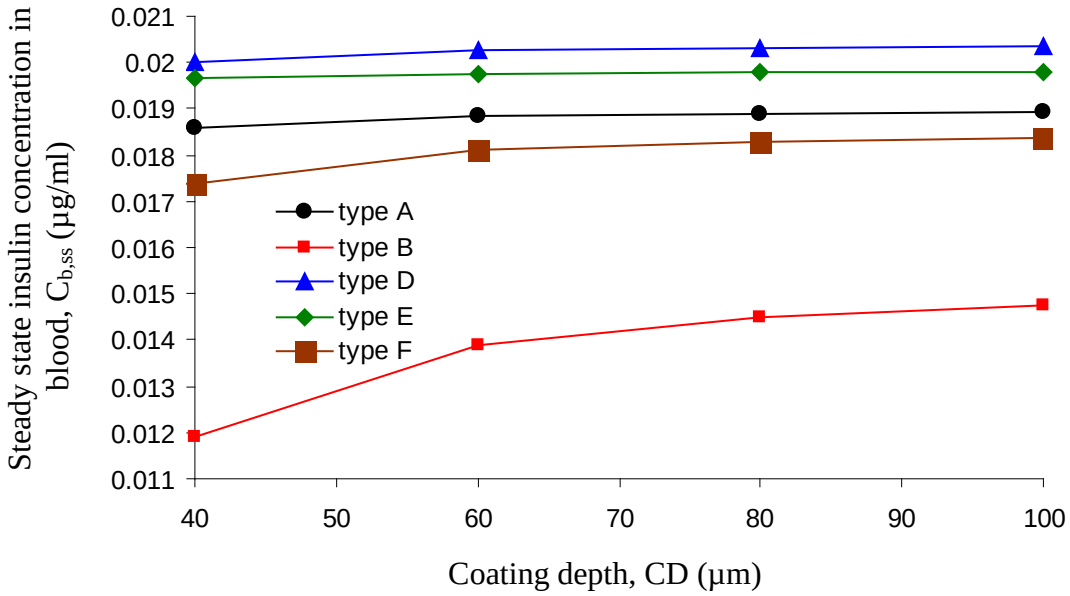

Figure 5.17- Influence of the coating depth (CD) of various microneedle types, coated with insulin, on the steady state insulin concentration in blood ($C_{b,ss}$), assuming that the insertion time of microneedles is four hours (the results of microneedle type C are not included in the figure as they are very similar to the results of microneedle type A).

5.4.7 Effects of pharmacokinetics variables

It has been shown that the drug concentration in blood is mainly controlled by the pharmacokinetics variables if the drug has a long half-life (Shah et al., 1992c). There was a wide variation in the pharmacokinetics variables of many drugs such as fentanyl (Gupta et al. 1992), verapamil (Shah et al 1992c), etc. To evaluate the effects of both the elimination rate constant (K_e) and the volume of distribution (V_b) on the blood drug concentration, different values were chosen as shown in Table 5.1. These reflect the influences of different pharmacokinetic of K_e and V_b variables on blood insulin concentration after applying microneedle arrays as shown in Figure 5.18 and Figure 5.19, respectively. As expected, the insulin concentration in blood varies for different cases depending on the given input parameters. Figure 5.18 reveals how the elimination rate constant influences the insulin concentration in blood. The result indicates that by changing the elimination rate constant, the insulin concentration in blood is increased by 10 times.

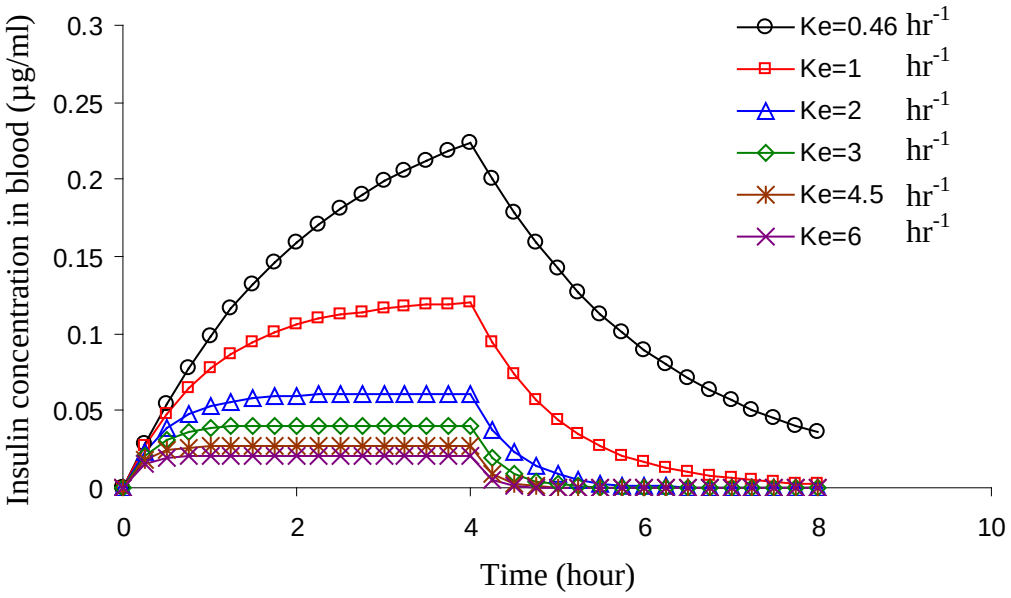

Figure 5.18-Influence of transdermal delivery of insulin for different elimination rate constant for the input parameters in Table 5.1.

For example, by decreasing the elimination rate constant from 6 $hr^{-1}$to 0.46 hr^{-1}, the insulin concentration in blood is increased to 0.24 µg/ml which enhances the insulin delivery. This means that the insulin concentration in blood depends on elimination rate constant.

For given parameters, the functional dependency for elimination rate constant (K_e), as shown in Figure 5.8 (fifth curve), is governed by the following scaling relationship;

$$\frac{C_{b,ss}}{C_s} = 2\times10^{-6}\left(\frac{L^2K_e}{D}\right)^{-0.94} \quad ; \quad 0.02 < \frac{L^2K_e}{D} < 0.32 \qquad (5.10)$$

This scaling equation is valid for a given penetration depth, in this case L=0.014 cm.

From Figure 5.8, it suggests that a power relationship exists between the dimensionless steady state insulin concentration in blood and the dimensionless group (L^2K_e/D). When each series of data is fitted to a power trend line, the R^2 is greater than 0.99, implying a strong agreement.

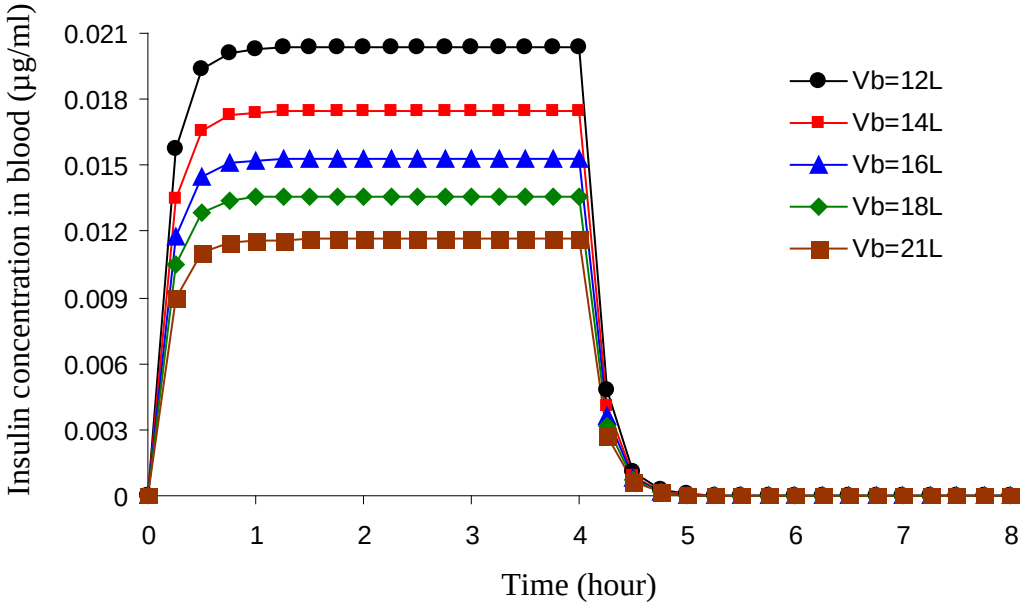

Figure 5.19-Influence of transdermal delivery of insulin for different volume of distribution for the input parameters in Table 5.1.

Figure 5.19 depicts the influence of varying the volume of distribution on insulin concentration in blood. The figure shows clearly that by changing the volume of distribution, the insulin concentration in blood is increased by about two folds. For example, the steady state insulin concentration in blood increases to 0.02 µg/ml when reducing the volume of distribution from 21 L to 12 L. This shows that the insulin concentration in blood also depends on the volume of distribution.

Although these profiles have different distributions, they show that pharmacokinetic variables (i.e., elimination rate constant) have significant effects on insulin delivery using microneedles. This simulation is useful to predict the quantitative influence of pharmacokinetic variables on blood drug concentration. The cumulative amount permeated per unit area of skin for various pharmacokinetics parameters are all the same. This is because the cumulative amount permeated per unit area of skin is not a function of both elimination rate constant and volume of distribution as shown in Equation (5.05). Therefore, the results of this implication have not been included.

The functional dependency of volume of distribution (V_b) for microneedle injection of insulin is shown in Figure 5.20 which follows the scaling relation as below;

$$\frac{C_{b,ss}}{C_s} = 38083\left(\frac{V_b}{L^3}\right)^{-1} \quad ; \quad 4.4\times10^9 < \frac{V_b}{L^3} < 7.6\times10^9 \qquad (5.11)$$

This scaling equation is also valid for a given microneedle length, in this case L=0.014 cm. The other parameters D, h and C_s are assumed constant for both cases as shown in Table 5.1. As shown in Figure 5.20, the relation between the dimensionless steady state insulin concentration and the dimensionless group (V_b/L^3) is exponentially decreasing and the R^2 value is greater than 0.99.

These relationships can be effective in terms of simulation time to determine the effects of both elimination rate constant and volume of distribution on blood drug concentration for real life problems. The more detailed evaluations should be performed with simultaneous consideration for the differences in skin structures and pharmacokinetic variables. Altogether, the diffusion of drugs across skin through the use of microneedles is related to the pharmacokinetics variables.

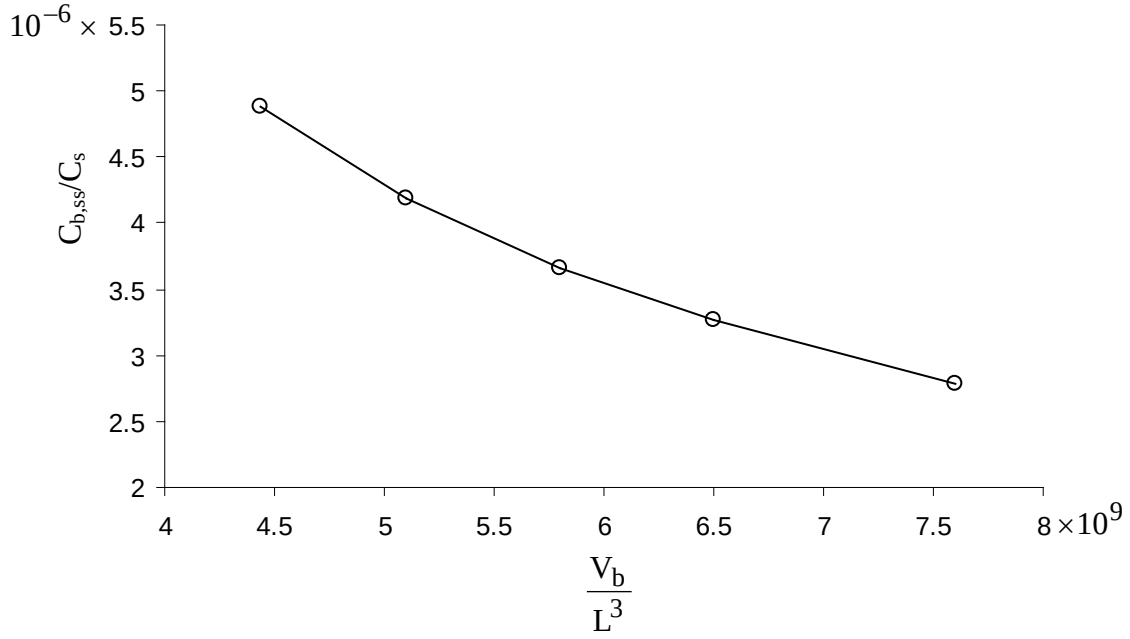

Figure 5.20-Scaling relationship of the dimensionless group $\frac{V_b}{L^3}$.

5.4.8 Effects of patch surface area of microneedle

Since the first fabrication of the microneedles for drug delivery, there have been many different sizes of the microneedles surface areas. Some of them are relatively small with a surface area of 0.04 cm^2 (Teo et al., 2005) while others have larger area up to of 0.81 cm^2 (Park et al., 2005). In this work, we have carried out simulations to synthesise the effects of the size of the patch on drug delivery, as shown in Figure 5.21. The surface area represents the perpendicular area of the direction of the drug diffusion for a patch with a uniform area. Therefore, $\left(\frac{dQ}{dt}\right)S_a$ in equation (3.08) represents the drug penetration rate into blood that passes an area inclined perpendicularly to the direction of diffusion per unit time.

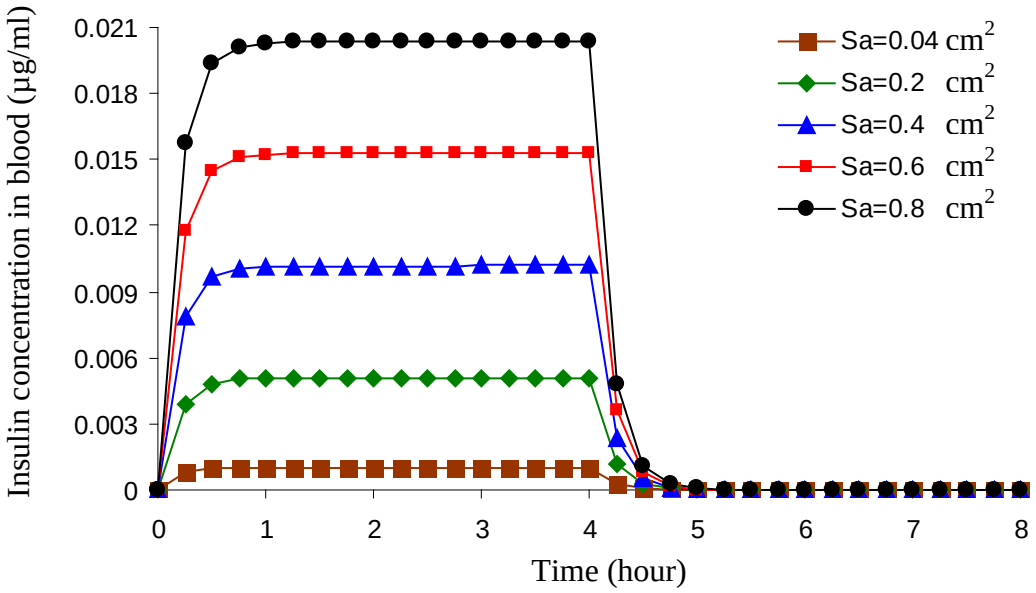

Figure 5.21-Influence of transdermal delivery of insulin for various sizes of patch for the input parameters in Table 5.1.

In Figure 5.21, the duration of application is 4 hours while the size of the patch varies from 0.04 cm^2 to 0.81 cm^2. We can see that the steady state blood insulin concentration ($C_{b,ss}$) varies between 0.001 and 0.02 µg/ml and there is a steady-state concentration (the plateau) after certain duration of application. This implies that there is a proportional relationship between the size of the array (S_a) and the blood insulin concentration. This relationship must

be taken into consideration while designing microneedle array systems in practice. However, no differences have been observed for the cumulative amount permeated per unit area of skin for insulin with different patch size (data not shown). Overall, the insulin concentration in blood is a strong function of patch size. This is because the variation of patch size has a significant influence (>90%) on the insulin delivery using microneedles as discussed previously.

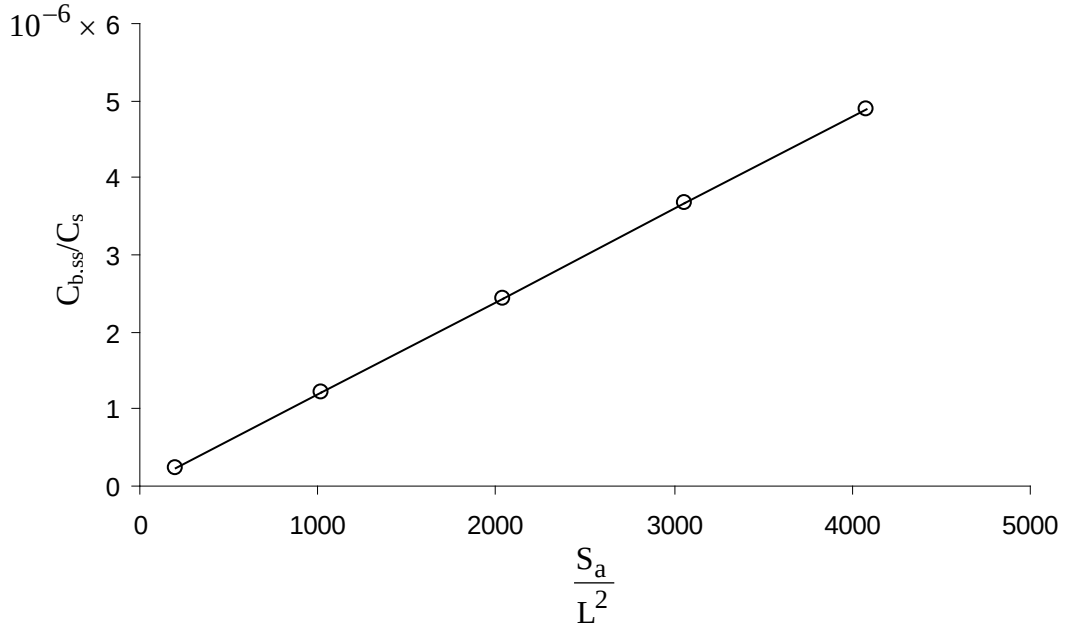

Figure 5.22-Scaling relationship of the dimensionless group $\frac{S_a}{L^2}$.

The functional dependency of $\frac{S_a}{L^2}$ on $\frac{C_{b,ss}}{C_s}$ is as shown in Figure 5.22 and given by the following relation provided all other parameters remain the same:

$$\frac{C_{b,ss}}{C_s} = 0.0012\left(\frac{S_a}{L^2}\right) + 0.0003 \quad ; \quad 204 < \frac{S_a}{L^2} < 4081 \qquad (5.12)$$

This equation is valid for a given microneedle length (L), in this case L=0.014 cm.

From Figure 5.22, it suggests that a linear relationship exists between the dimensionless steady state insulin concentration in blood and the dimensionless group (S_a/L^2).

5.4.9 Effects of skin thickness

The distance from the skin surface to dermal circulation represents the skin thickness. This can be a function of age, anatomical region, race and sex (Lee and Hwang, 2002). If we change the skin thickness while maintaining the same length of the microneedles, then there will be a change in effective diffusion length and hence, insulin concentration in blood. The implications of changing skin thickness while keeping a constant length of the microneedle are shown in Figure 5.23. By reducing the skin thickness, the effective skin thickness is also reduced which enhances the insulin concentration in blood by 3 times. For example, by reducing the skin thickness from 240 µm to 160 µm, the steady state insulin concentration in blood is significantly increased to 0.04 µg/ml.

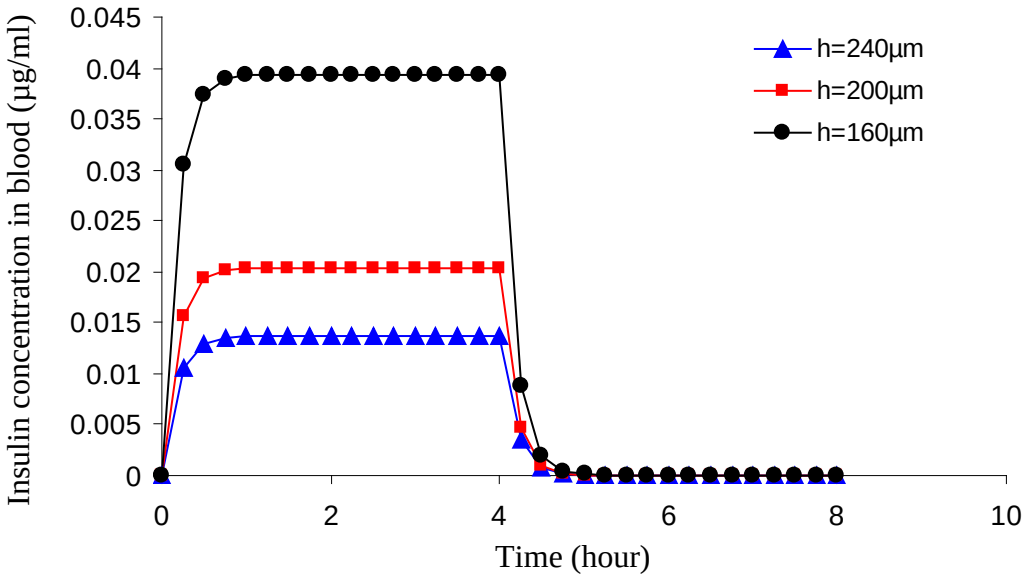

Figure 5.23-Influence of transdermal delivery of insulin for various skin thicknesses for the input parameters in Table 5.1.

Furthermore, Figure 5.24 shows the cumulative amount permeated per unit area of skin for insulin with different skin thicknesses. Changing the skin thickness has a significant influence on the cumulative amount permeated per unit area of skin. As expected, cumulative amount of insulin permeated into blood per unit area of skin increases as the skin thickness decreases.

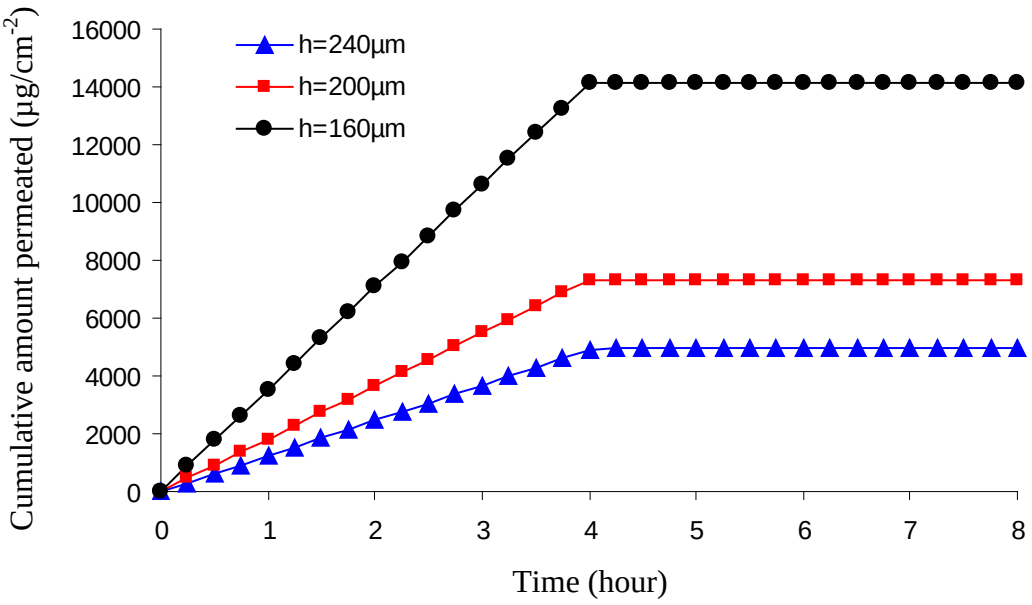

Figure 5.24-Cumulative amount of insulin permeated into blood per unit area of skin with various skin thicknesses.

As mentioned previously, the steady state insulin concentration in blood is a function of number of variables for a given skin thickness. Such a dependency is given by the following scaling relationship for cases where 0.016 cm < h < 0.024 cm:

$$\frac{C_{b,ss}}{C_s} = -1\times10^{18}\left(\frac{S_a\times L^3\times K_e\times T\times Pt}{V_b\times h\times D\times CD}\right)^3 + 2\times10^{11}\left(\frac{S_a\times L^3\times K_e\times T\times Pt}{V_b\times h\times D\times CD}\right)^2$$
$$-11904\left(\frac{S_a\times L^3\times K_e\times T\times Pt}{V_b\times h\times D\times CD}\right) + 0.0002$$

$$; \ 4.43\times10^{-8} < \frac{S_a\times L^3\times K_e\times T\times Pt}{V_b\times h\times D\times CD} < \ 6.64\times10^{-8} \qquad (5.13)$$

From Figure 5.25, it suggests that a 3rd order polynomial relationship exists between the dimensionless steady state insulin concentration in blood and the dimensionless group $\left(\frac{S_a\times L^3\times K_e\times T\times Pt}{V_b\times h\times D\times CD}\right)$.

Such scaling relationship is useful to determine the steady state drug concentration in blood where there are no modelling or experimental results, as shown in Figure 5.25 for different values of skin thickness (h). It must be pointed out that the skin thickness has been varied

while maintaining the rest of variables constant. The figure shows that the thickness of skin is an important parameter for the process of drug delivery by using microneedles array.

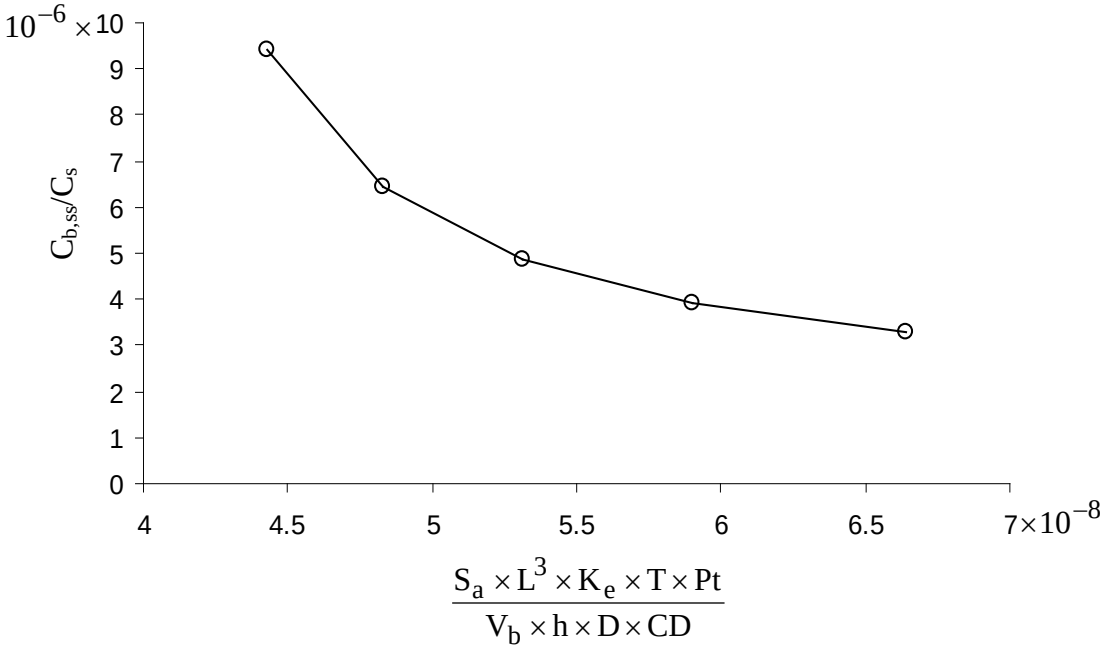

Figure 5.25-Scaling relationship of the dimensionless group $\frac{S_a \times L^3 \times K_e \times T \times Pt}{V_b \times h \times D \times CD}$.

5.4.10 Effects of microneedle diameter (d)

To assess how the microneedle diameter (d) affects the blood insulin concentration, the diameter of microneedle type C (i.e., bevelled needle at a constant tip angle of 45º) has been varied. In addition, the diameter of each microneedle model was varied to evaluate the influence on the steady state insulin concentration in blood ($C_{b,ss}$). Khumpuang et al. (2005) have claimed that the microneedle diameter should have a diameter greater than the diameter of white blood cell (≈ 20 μm) in order to avoid any problem that may arise from blood clogging. In general, larger diameters are advantageous in allowing greater mechanical stability (Ovsianikov and Chichkov, 2007) as the force required to buckle the microneedle during insertion to the skin increases (Park et al., 2007). Teo et al. (2005) have shown that microneedle-mediated drug delivery could be enhanced by increasing microneedle diameters. These results agreed well with the simulations presented by Haider et al. (2001). In another

study, it has been shown that microneedle diameter is related to microneedle density, i.e., the number of microneedle per unit area (Stoeber and Liepmann, 2005).

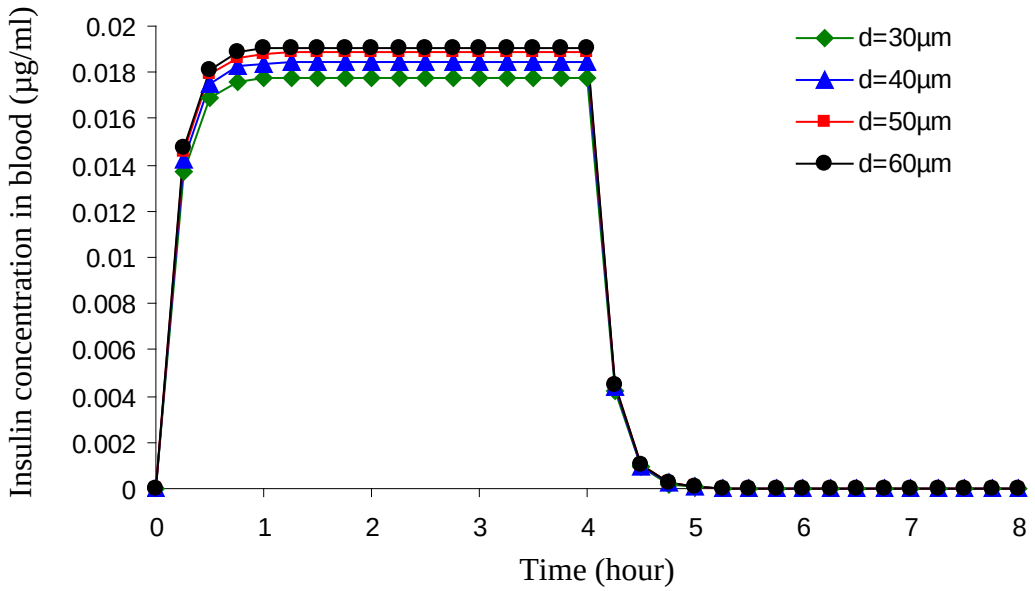

Figure 5.26-Influence of transdermal delivery of insulin for various diameter of microneedle type C for the input parameters in Table 5.1.

In previous results presented by Davidson et al. (2008) it has been shown that varying microneedle diameter does not have a significant influence on the effective permeability across skin (P_{eff}). This agrees well with our results as the steady state insulin concentration in blood ($C_{b,ss}$) for various diameters did not change significantly (<10%) and there is a plateau in insulin concentration of approximately 0.019 µg/ml, as shown in Figure 5.26. This indicates that by increasing microneedle diameter, the process of transdermal drug delivery using microneedles has not been enhanced significantly. As a result, the insulin concentration in blood is a weak function of microneedle diameter. Other model dimensions have been kept constant as shown in Table 5.1.

The microneedle diameter (d) of both microneedles types A and C was varied to observe the influence on steady state insulin concentration as shown in Figure 5.27. Microneedle type A is

the resulted in the highest steady state insulin concentration in blood ($C_{b,ss}$) with a value of 0.0192 µg/ml corresponding to a diameter of 60 µm. However, the steady state insulin concentrations in blood of both microneedles models were not significantly different (<10%), indicating that the steady state insulin concentration in the blood does not strongly depend on the microneedle diameter. Our results suggest that there has been a proportional relationship between microneedle diameter (d) and steady state insulin concentration in blood. To sum up, the range of steady state insulin concentration is quite small for each microneedle when compared to the range that was obtained by varying other parameters (e.g., penetration depth, centre-to-centre spacing).

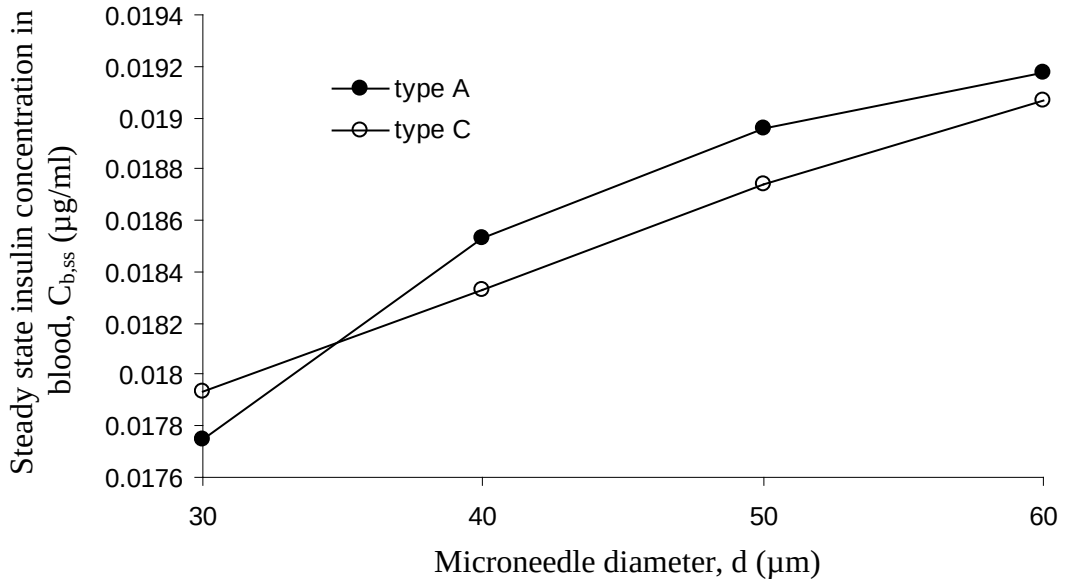

Figure 5.27- Influence of the diameter (d) of various microneedles models, coated with insulin, on the maximum insulin concentration in blood ($C_{b,max}$), assuming that the insertion time of microneedles is four hours.

5.5 Summary

A parametric analysis for transdermal delivery of high molecular weight drug (i.e., insulin) from microneedles has been presented. The simulations have allowed us to identify the significance of various factors that influence the drug delivery while designing microneedle arrays. In addition, the steady state insulin concentration in blood of various microneedle

types has been examined. It has been found that both the elimination rate constant and the surface area of the patch are the most significant factors in determining the steady state insulin concentration in blood ($C_{b,ss}$), followed by the skin thickness, penetration depth, volume of distribution and centre-to-centre spacing, respectively. Other parameters such as microneedle thickness, microneedle diameter and coating depth had a less significant effect on the steady state insulin concentration in blood, respectively. Microneedle type D (rocket needle) was the best type in terms of penetration depth, microneedle thickness, coating depth and centre-to-centre spacing while, microneedle type A (cylindrical needle) was the best type in terms of microneedle diameter. In addition, a scaling analysis has also been done which shows the functional dependence of insulin concentration in blood on other variables of skin and microneedle arrays.

CHAPTER 6

Optimization of Microneedles Arrangements

6.1 Introduction

Although there has been an increase of up to three orders of magnitude in drug permeability in skin by using microneedles of various types and geometries (Park et al., 2005), generally drug permeability across skin has not been considered as a critical parameter in designing microneedles in most previous studies. One of main focuses in transdermal drug delivery research is to increase the permeability of the drug penetrating the skin. The drug permeability across skin has been reported as a key factor that determines the efficiency of transdermal drug delivery process (Wilke et al., 2006). To deliver drugs across human skin for any medical reasons, the transport of drugs needs to be enhanced. It seems one way to achieve this is by increasing the permeability across skin by artificial means which reduces the resistance of skin barrier to enhance the delivery of drugs. As expected, this necessitates knowing various factors that affect permeability across skin when using microneedle arrays. In principle, permeability across skin can be increased as a result of optimum microneedle dimensions. However, it is difficult to reach an optimum design without understanding the transport properties of skin, e.g., permeability across skin (Al-Qallaf et al., 2007; Zahn et al., 2005). Permeability across skin represents the path length of a molecule across a given skin thickness over unit time (Al-Qallaf and Das 2008; Environmental Protection Agency, 1992). Teo et al. (2006) reviewed different microneedle designs that are currently being used for transdermal drug delivery. So far, microneedle systems with various dimensions have been fabricated with limited consideration of how to increase permeability across skin (Al-Qallaf and Das 2009a,b; Al-Qallaf and Das, 2008).

Al-Qallaf and Das (2008) present a framework developed specifically to design optimum microneedle arrays (e.g., number of microneedles, microneedle radius, etc) for transdermal

drug delivery with a view to increase drug permeability in skin, called permeability across skin hereafter. The framework includes the centre-to-centre spacing (pitch) of the microneedles to avoid any overlapping of the microneedle upon insertion into skin. The developed framework considers both solid and hollow microneedles which expand the scope of the current literature on microneedles for transdermal drug delivery. To provide quantitative analysis of in vitro skin permeation of drug from microneedles, Al-Qallaf and Das (2008) have theoretically studied the influence of microneedle geometry on permeability across skin. This is done by using an in-house optimization model based on a Java program. The developed model also correlated the variation of skin thickness to permeability across skin. This is expected to lead to optimum microneedle design for each case study. The process of transdermal drug delivery has been improved by reaching the highest value of permeability across skin. This is confirmed by comparing the optimized design with an existing design (McAllister et al., 2003). In another work, Al-Qallaf and Das (2009a) have expanded the range of geometrical parameters such as microneedle radius, surface area of microneedles etc, from what are available in the current literature with the main aim to optimise these parameters. Permeability across skin has been correlated to the variation of skin thickness depending on anatomical region and sex (Al-Qallaf and Das, 2009a) or on age and race (Al-Qallaf and Das, 2008). It is shown that correlation for predicting permeability of viable epidermis for high molecular weight can be developed which are envisaged to help design of the drug delivery devices. A relationship is presented between permeability across skin and diffusion coefficient for the optimum of both the solid and hollow microneedles for various drugs (Al-Qallaf and Das, 2008). Previously obtained results (Al-Qallaf et al., 2007) of the maximum blood concentration are combined with the current results to demonstrate the optimum microneedle design.

In those previous studies, we have initiated investigations on optimizing the square patch of microneedle arrays (Al-Qallaf and Das, 2009a; Al-Qallaf and Das, 2008). However, it has been realized that since the first fabrication of microneedles a large variety of microneedle distribution have been proposed such as square (Kim and Lee, 2007; Ji et al., 2006), hexagonal (Widera et al., 2006; Matriano et al., 2002), triangular (Perennes et al., 2006) and rectangular (Park et al., 2005). Aggarwal and Johnston (2004) investigated the influence of various patterns (e.g., square, rectangular, etc) on buckling force, bending force and bending stress. Our previous work (Al-Qallaf and Das, 2009a; Al-Qallaf and Das, 2008) have attempted to study and hence optimize the square patch with a square microneedle distribution to maximize the permeability across skin. While the developed framework (Al-Qallaf and Das, 2009a; Al-Qallaf and Das, 2008) is useful, it seems it is also necessary to develop the wider applications of the framework to non-square distributions of the patterns so as to optimize them for transdermal drug delivery (Al-Qallaf and Das, 2009b). To address this issue, we have extended our previous work (Al-Qallaf and Das, 2009a; Al-Qallaf and Das, 2008) to consider non-square patterns (i.e., rectangular) as well as the distribution of microneedles such as triangular and diamond (Al-Qallaf and Das, 2009b). Therefore, we have optimized and compared the microneedle arrays of both square and rectangular patch to maximize permeability across skin of both solid and hollow microneedles. The optimization framework of considering both the microneedle pattern as well as the distributions allows us to identify the optimum pattern and distribution to enhance the performance of microneedles array. It must be pointed out that in the present context ‘pattern’ means the shape of the microneedles array (i.e., square or rectangular) and ‘distribution’ means the arrangement of the microneedles inside an array (i.e., triangular or diamond). In the present context, the most important issue is to be able to fabricate the most accurate microneedles. Hence, overdesigning them was not considered to be a very important issue in this work. Contrary to many engineering systems (e.g., road bridge), overdesigning the microneedles may have an

adverse effect on the drug delivery behaviour (e.g., substantial increase of drug concentration above the safe limit). As stated previously, the main aim of microneedles is to create preferential pathways to deliver drug. In fact, the development of these systems aims for transdermal drug delivery with patients' safety, comfort, etc. (Prausnitz et al., 2004) which may not be possible if they are overdesigned.

6.2 Modelling strategy

6.2.1 Governing equations for permeability across skin

To develop the current framework, a simple theoretical in vitro model has been adopted to calculate the permeability across skin (K) using the following equation (McAllister et al., 2003):

$$K = f\frac{D}{L_h} \tag{6.01}$$

f represents the fractional skin area after insertion by microneedles, D is the diffusivity of the skin to the drug molecule and L_h is the length of a hole in skin. The theoretical model represents both the solid and hollow microneedles as shown in Figure 6.1. It must be pointed out that the hole length (L_h) represents the skin thickness (h) in case of solid microneedles, while this represents the microneedle length (L_m) in case of hollow microneedles. This is because the drug molecules do not move through the microneedle itself in case of solid microneedle but traverse through various disruptions in the skin from the donor compartment (i.e, microneedle arrays) to the receiver compartment (e.g., blood flow). On the other hand, when the molecules move through their bores in case of hollow microneedle, the path length represents the microneedle length as shown in Figure 6.1(a). When the microneedles are inserted, a circular shaped domain (hole) is obtained with a radius corresponding to the radius of the microneedle and an annular gap width (W) as shown in Figure 6.1(b).

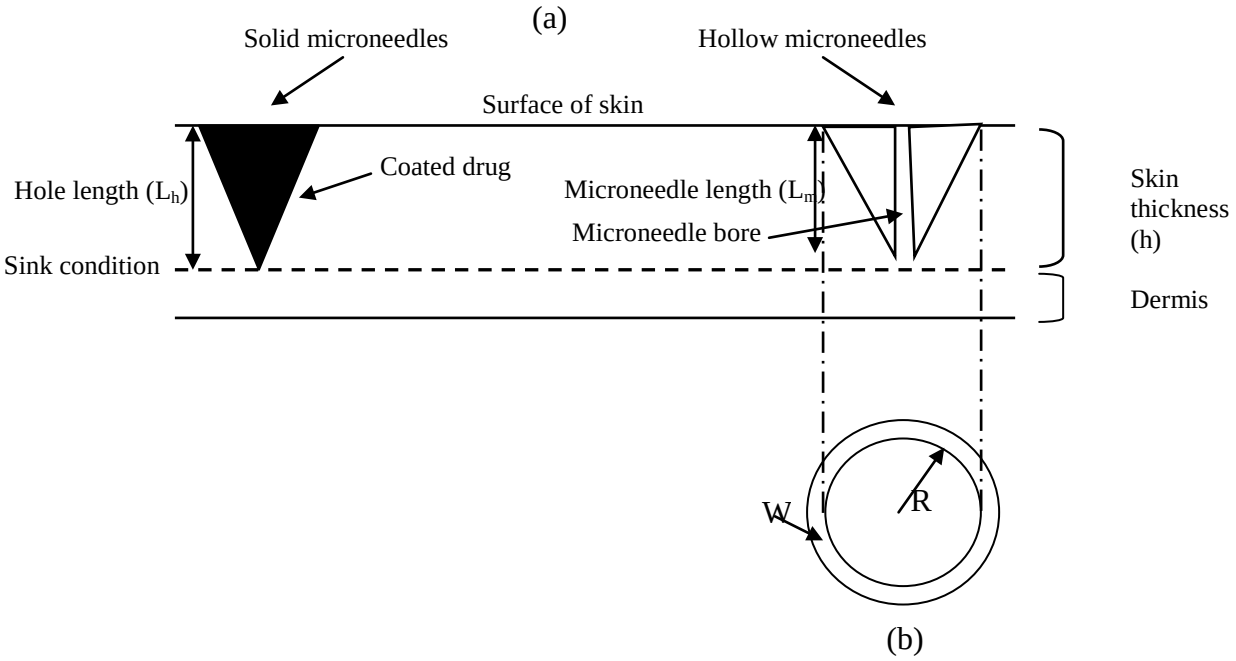

Figure 6.1- The Schematic diagram of solid and hollow microneedles (a) side view, (b) top view (W is the annular gap width, R is microneedle radius).

The fractional area with the insertion of the microneedles can be calculated based on the following equations:

$$f = N\pi\frac{(R+W)^2 - R^2}{A} \qquad (6.02)$$

N is the total number of microneedles for a given patch, R is the radius of the microneedle, W is the annular gap width and A is the area of a given microneedle arrays. These equations are for calculating permeability. As equations (6.01) & (6.02) show, there are different variables that should be considered in designing microneedles arrays which include the radius of microneedles (R), surface area of microneedle arrays (A) and the total number of the microneedles (N). There is a fourth parameter, skin thickness, which is assumed to be constant. But in our case, it is a very important factor, e.g., how skin thickness varies in terms of different classifications (Lee and Hwang, 2002).

The main purpose of this study is to maximize permeability across skin (K) in equation (6.01) for the case where the microneedles are inserted by adopting equation (6.02) and assuming

that it is a square patch so that the total numbers of microneedles (N) is n^2 where n is the number of microneedles per row. Assuming that the diffusion coefficient (D) and skin thickness (L) are constants and the annular gap width (W) is a function of microneedle radius (R) as:

$$W = \varepsilon R \tag{6.03}$$

Where ε is the ratio of annular gap width to the radius of microneedle, we have the following constraint equations;

$$n_{min} \le n \le n_{max} \tag{6.04}$$

$$R_{min} \le R \le R_{max} \tag{6.05}$$

$$A_{min} \le A \le A_{max} \tag{6.06}$$

Combining equations (6.02) and (6.03):

$$f = \pi \frac{NR^2}{A} \varepsilon(\varepsilon + 2) \tag{6.07}$$

Here $\varepsilon = \frac{W}{R}$ (6.08)

Combining equations (6.01) and (6.07), permeability across skin for cases when microneedles are inserted is:

$$K = c\pi \frac{NR^2}{A} \frac{D}{L_h} \tag{6.09}$$

Where $c = \varepsilon(\varepsilon + 2)$ (6.10)

In equation (6.09), c is dimensionless constant.

6.2.2 Model assumptions

To develop the theoretical model, the following assumptions have been made:

(a) Viable epidermis is a homogenous medium (Gui and Liu, 2005).

(b) The drug injected by either solid or hollow microneedles is delivered into two parts. The first part is the epidermis and the second part is the dermis where the drug is absorbed into blood vessel. The sink condition (100% absorption) occurs at the interface between the epidermis and dermis.

6.2.3 Formation of optimization problem for square microneedle arrays

Since L_h, D, c and π are constants, the problem statement can be reformulated as follows:

$$g = \frac{n^2 R^2}{A} \tag{6.11}$$

Where g is the optimization function which is derived from equation (6.02) (i.e., π is constant) and N equals n^2, where n is the number of microneedles per row, assuming that the microneedles array is a square patch. Therefore, the permeability across skin when microneedles are inserted can be introduced as:

$$K = c\pi g \frac{D}{L_h} \tag{6.12}$$

From the investigation of the function in equation (6.11), it is obvious that g has its maximum value at maximum n and R and minimum A. Further, the permeability across skin (K) is maximum when the value of g is maximum. Therefore, the desired solution for g would simply be:

$$(n^2, R, A) \rightarrow (n_{max}, R_{max}, A_{min})$$

However, careful study of the microneedles patch geometry as shown in Figure 6.2 reveals that there is another physical and manufacturing constraint which is the pitch (Pt), the centre-to-centre distance between two adjacent microneedles. This new constraint is given as follows:

$$P_t \geq \alpha R \tag{6.13}$$

Where $\alpha > 2.0$

Here α is the aspect ratio of the pitch over radius of microneedle. Noting that, in order to determine the pitch we have assumed that in a given row of an array, the total distance for this row (X) is given by the following equation:

$$X = nP_t \tag{6.14}$$

Therefore, the area of a square array is:

$$A = n^2 P_t^2$$

$$\text{or, } P_t = \frac{\sqrt{A}}{n} \tag{6.15}$$

The constraint equations (6.04-6.06) are reformulated to include the new following constraint:

$$\frac{\sqrt{A}}{n} \geq \alpha R \tag{6.16}$$

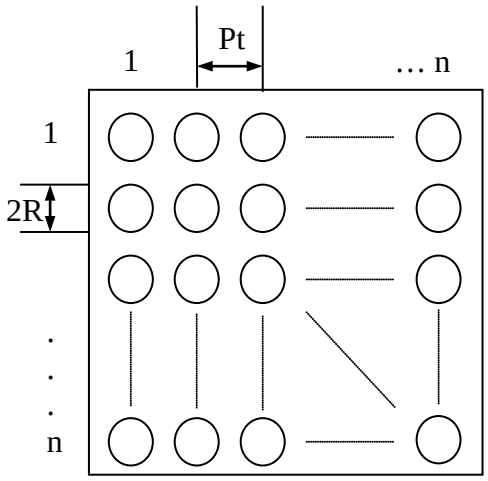

Figure 6.2- The Schematic diagram of a square patch. The aspect ratio (α) is the ratio of the pitch (P_t) over microneedle radius R.

6.2.4 Formation of optimization problem for non-square microneedle arrays

To further study the case of square patch, we have investigated the influence of changing the pattern by introducing the diamond and triangular patterns as shown in Figure 6.3. The idea of the microneedles distribution is analogous to the packing of tubes in heat exchangers, where the tubes in the heat exchangers represent the microneedles (Hewitt, 1990; Perry et al., 1984).

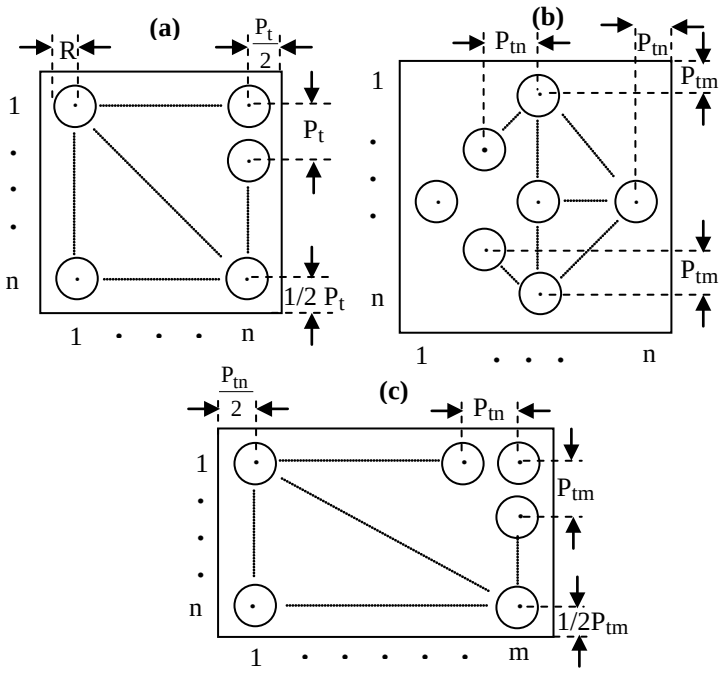

Figure 6.3- The schematic diagrams (top view) of: (a) square pattern with a square patch microneedle array, (b) diamond/triangular pattern with a square patch microneedle array and (c) rectangular pattern with a rectangular patch microneedle array. Here R is the radius of microneedles, P_t is the pitch in x or y direction of square pattern, P_{tn} and P_{tm} are the pitch in x and y direction of diamond, triangular and rectangular pattern, respectively.

The pitch of the diamond pattern per row (P_{tn}) or per column (P_{tm}) is given as follows:

$$P_{tn} = P_{tm} = 0.707 \times P_t \tag{6.17}$$

Therefore, the area of a square array for the diamond pattern is:

$$A = 2n \times P_{tn} \times 2m \times P_{tm} \tag{6.18}$$

Here, m is the total number of microneedles per column and assuming n equals m since the patch has a square shape. By combining equations (6.13), (6.17) and (6.18), the new constraint of the diamond pattern is:

$$\frac{\sqrt{A}}{1.414 \times \sqrt{n \times m}} \geq \alpha R \tag{6.19}$$

Although n equals m and P_{tn} equals P_{tm}, the ranges of both P_{tn} and P_{tm} are different according to the reported values in the literature. Therefore, we define the total number of microneedles and pitch per either row or column as n and m so that the optimisation program can iterate the

input parameters depending on the selected range for n and m. The values of microneedle pitch (P_{tn}) and (P_{tm}) for all patterns are explained in Table 6.1.

Table 6.1. The values of microneedle pitch for various patterns and types. Here, 'pattern' means the distribution of the microneedles inside an array and 'type' means the shape of the pattern.

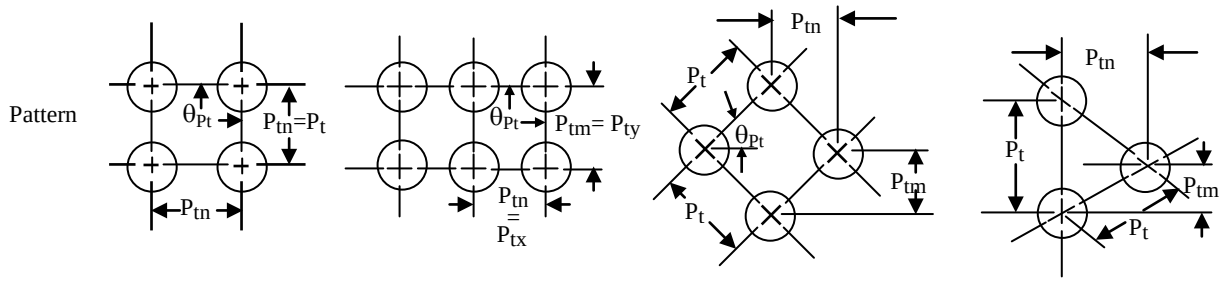

Type	Square	Rectangular	Diamond	Triangular
θ_{Pt}	90^o	90^o	45^o	30^o
P_{tn}	P_t	P_{tx}	$0.707P_t$	$0.866P_t$
P_{tm}	P_t	P_{ty}	$0.707P_t$	$0.5P_{tn}$

In case of the triangular pattern, the pitch for each per row (P_{tn}) is given as follows:

$$P_{tn} = 0.866 \times P_t \tag{6.20}$$

On the other hand, the pitch of the triangular pattern for each column (P_{tm}) is given as follows:

$$P_{tm} = 0.5 \times P_t \tag{6.21}$$

By combining equations (6.13), (6.18), (6.20) and (6.21) we find that the area of a square patch for both the triangular and diamond patterns is equal. Therefore, the new constraint of triangular pattern is:

$$\frac{\sqrt{A}}{1.316 \times \sqrt{n \times m}} \geq \alpha R \tag{6.22}$$

The input parameters for solving these equations are as shown in Table 6.2 which are mostly adopted from reported literature.

Table 6.2. The input geometrical parameters used in this work for optimizing solid and hollow microneedle arrays.

	Square/Diamond/Triangular Pattern		**Rectangular Pattern**		
Parameters	Solid	Hollow	Solid	Hollow	Scaling Parameters
N	$10^{D} \le n \le 20^{E}$	$4^{H} \le n \le 20^{A}$	$3^{I} \le n \le 10^{C}$	$4^{M} \le n \le 10^{N}$	1
M	-	-	$4^{I} \le m \le 20^{C}$	$8^{M} \le m \le 20^{N}$	1
R	$0.0025^{B} \le R \le 0.0075^{D}$	$0.004^{A} \le R \le 0.015^{G}$	$0.005^{J} \le R \le 0.01^{K}$	$0.005^{M} \le R \le 0.0125^{N}$	0.0005
A	$0.04^{D} \le A \le 0.81^{C}$	$0.04^{D} \le A \le 0.56^{F}$	$0.03^{K} \le A \le 1.6^{L}$	$0.02^{M} \le A \le 0.64^{N}$	0.01
α	$2.7^{D} \le \alpha \le 12^{C}$	$3.1^{A} \le \alpha \le 25^{F}$	$3.5^{K} \le \alpha \le 40^{J}$	$3.2^{N} \le \alpha \le 16^{N}$	-
P_{tn}	-	-	$0.035^{K} \le P_{tn} \le 0.2^{J}$	$0.03^{M} \le P_{tn} \le 0.04^{N}$	0.001
P_{tm}	-	-	$0.035^{K} \le P_{tm} \le 0.2^{J}$	$0.03^{M} \le P_{tm} \le 0.08^{N}$	0.001

n: number of microneedles per row; m: number of microneedles per column; R: microneedle radius; A: surface area of microneedles array; α: the aspect ratio of pitch over radius; P_{tn}: the pitch in x direction, the distance between two adjacent microneedles per row and P_{tm}: the pitch in y direction, the distance between two adjacent microneedles per column.
[A]Kaushik et al. (2001), [B]Shikida et al. (2006), [C]Park et al. (2005), [D]Teo et al. (2005), [E]Xie et al. (2005), [F]Wu et al. (2007), [G]Khumpuang et al. (2007), [H]Verbaan et al. (2007), [I]Choi et al. (2006), [J]Han et al. (2007), [K]Miyano et al. (2005), [L]Martanto et al. (2004), [M]Khumpuang et al. (2006) and [N]Park et al. (2007).

To expand the scope of this work further, we have included the rectangular patch as shown in Figure 6.3. The optimization function (g) of this patch can be introduced as:

$$g = \frac{(n \times m)R^2}{A} \tag{6.23}$$

Here, n is not necessarily equal to m. The area of a rectangular patch is:

$$A = n \times P_{tn} \times m \times P_{tm} \tag{6.24}$$

Hence, the new constraints for the rectangular patch are given as:

$$\frac{A}{n \times m \times P_{tn}} \ge \alpha R \tag{6.25}$$

$$\frac{A}{n \times m \times P_{tm}} \ge \alpha R \tag{6.26}$$

Therefore, the optimization function (g) in equation (6.23) is maximized by considering the constraint equations (6.04-6.06) along with the following constraint:

$$m_{min} \leq m \leq m_{max} \quad (6.27)$$

$$P_{tn\ min} \leq P_{tn} \leq P_{tn\ max} \quad (6.28)$$

$$P_{tm\ min} \leq P_{tm} \leq P_{tm\ max} \quad (6.29)$$

In some cases, we have expanded the microneedle geometries to cover a broader range of parameters. For example, n_{max} of rectangular patch has been increased to 20 for both solid and hollow microneedles and, also the aspect ratios (α) of square, diamond and triangular patterns of solid microneedles have been extended to 20 as compared to the reported values. On the other hand, the aspect ratios of hollow microneedle for diamond and triangular patterns have been increased to 30 and for square and rectangular patterns to 40.

6.2.5 Method of solution

The optimization equations (6.11) and (6.23) along with their constraint equations were implemented and solved using an optimization model (Figure 6.4). In this study, an in-house algorithm has been developed to search the whole space for (n, R, A) by comparing each value of the g function at every point in the discrete space until it finds the optimum value which then mark corresponding (n, R, A) as the optimum values. These optimum values of n, R, A are obtained for a given set of data by which the value of the optimized function (g) as defined in equations (6.11) and (6.23) reaches its maximum value. The main idea of our algorithm is to iterate through the whole space of (n, R, A) until it finds the optimum of (n, R, A) at which g is maximum provided that the geometrical condition is fulfilled. Moreover, in order to do this iteration, a scale (step size) must be defined by the user for each parameter. For the purpose of our work, a Java swing program, ‘Microneedle System Optimization’ has been constructed to implement the above mentioned procedure which is explained in the flowchart in Figure 6.5.

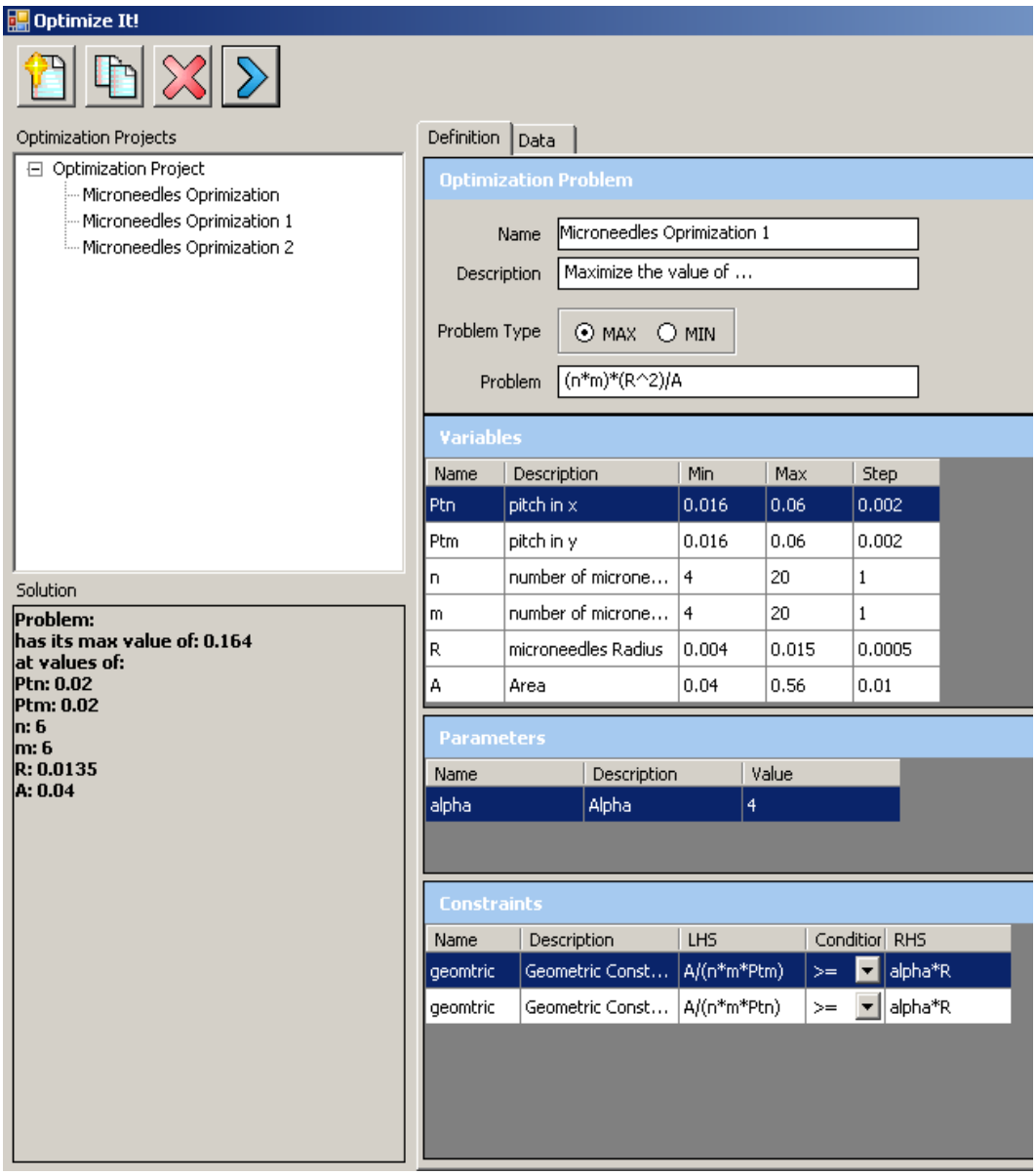

Figure 6.4- Graphical user interface of in-house Java program used for microneedles system optimization.

This optimization algorithm solves a problem that appeared when using other available software. For example, the commercial software Excel solver uses an optimization method called generalized reduced gradient (GRG). The GRG optimization method depends on the calculation of gradient second order partial differentiation. This requires the function under optimization to be continuously differentiable function within the optimization space. Since the problem under study is not continuous, it has an integer variable n, so it is not expected to get feasible results for this problem using Excel solver (Fylstra et al., 1998).

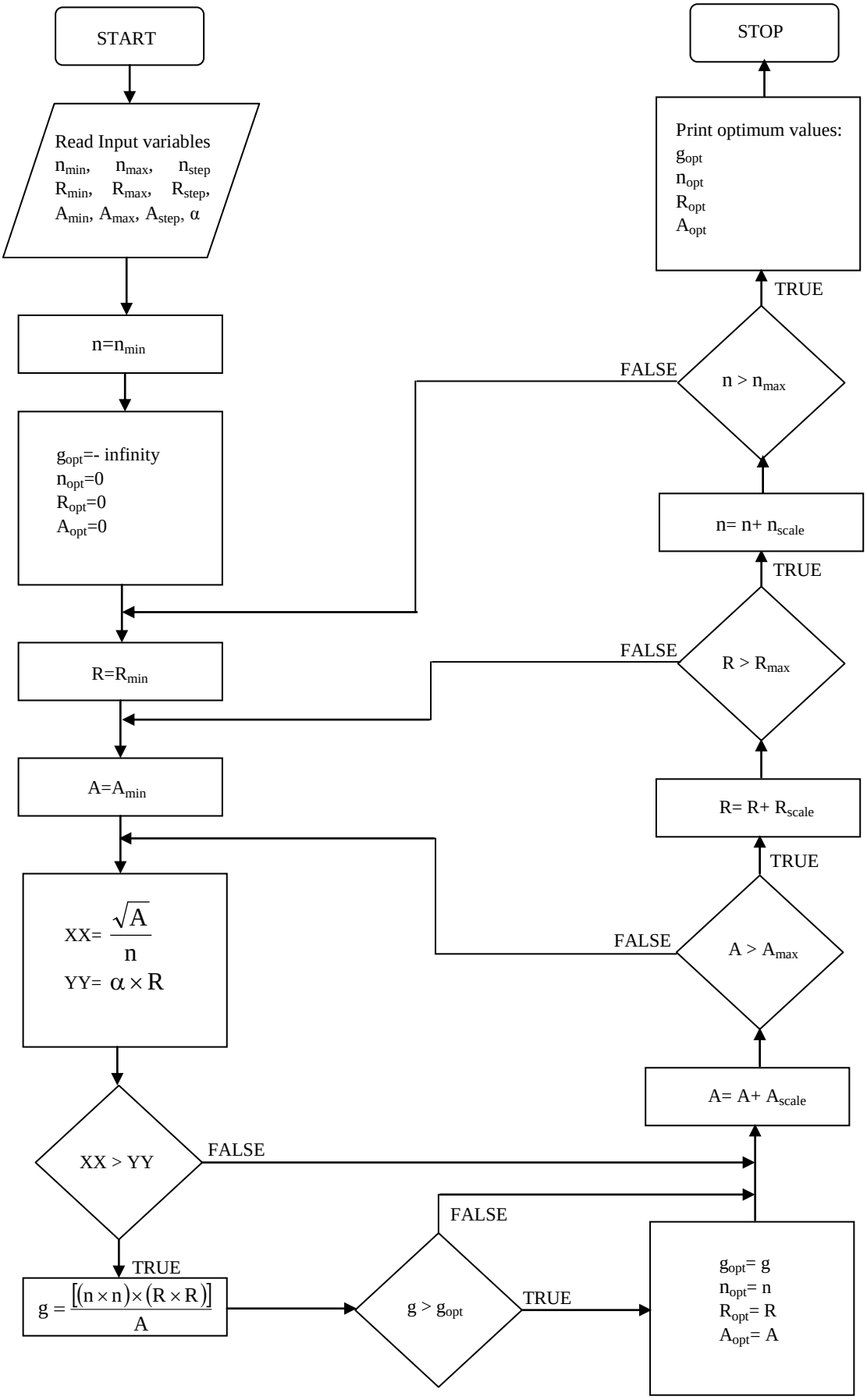

Figure 6.5- Algorithm used in Java program for microneedles system optimization.

The optimization algorithm follows total enumeration approach that search the whole space to find all feasible solutions. This technique can be applied sufficiently for problems with small dimensions (Streichert and Ulmer, 2005). This optimization algorithm ensures locating a global optima solution by performing total enumeration method (Han and Liu, 2008; Kargahi et al., 2006; Subramanian, 1999). In other words, this algorithm has the ability to compare with every possible solution in order to guarantee determining the global optima solution (Han and Liu, 2008). The algorithm involves both step size and input parameters that must be defined by the user.

6.3 Results and discussions

Some typical results of the developed optimization model for the input parameters (Table 6.2) for both solid and hollow microneedles are listed in Table 6.3. As stated before, our approach of optimization involves developing a method to maximize the permeability across skin to obtain optimum microneedle design of various patterns with different geometries for solid and hollow microneedles. Therefore, the purpose of these simulations is to identify both the optimum pattern and distribution of microneedles to enhance the performance of microneedles array. The results presented in Table 6.3 show that in case of solid and hollow microneedles, the maximum values the optimization function (g) are approximately 0.081 and 0.13, respectively.

Table 6.3. The optimum parameters found using the developed framework for both solid and hollow microneedles for various patterns.

	Solid Microneedles				**Hollow Microneedles**			
Pattern	Array	R	A	g	Array	R	A	g
Square	17×17	0.0065	0.15	0.081	15×15	0.0135	0.42	0.098
Diamond	16×16	0.0055	0.19	0.41	11×11	0.011	0.3	0.049
Triangular	12×12	0.006	0.11	0.047	9×9	0.0115	0.19	0.056
Rectangular	20×20	0.01	0.49	0.081	10×15	0.0125	0.18	0.130

As discussed below, various microneedle patterns and their geometries (e.g., number of microneedles per row, microneedle radius, etc) have been optimized and analysed to address

their influences in terms of the optimization function (g), and thereby, the design of microneedle. The outcome of the simulations allowed us to identify the optimum dimensions of microneedles by reaching the highest values of the optimization function (g). These optimum dimensions have been used in equation (6.12) to determine the optimums permeability across skin. This has been done by either varying the classification of skin thickness in case of solid microneedles or microneedle length in case of hollow microneedles. Moreover, the optimum dimensions of both solid and hollow microneedles have been correlated with the diffusion coefficient to derive various correlations for different microneedles shapes and patterns.

6.3.1 Optimization of surface area of patch

The design of microneedle arrays is constrained by a number of parameters including the surface area of microneedle arrays (Gill and Prausnitz, 2007; Al-Qallaf and Das, 2009a,b; Al-Qallaf and Das, 2008, Al-Qallaf et al., 2007). Since the first fabrication of the microneedles for drug delivery, there have been many different sizes of both the solid and hollow microneedles with different patch surface area as shown in Table 6.1. Some researchers relate the surface area to the number of microneedles and call it microneedle density (Cormier et al., 2004). However, the microneedle density may vary for a given surface area of the arrays. As a result, the implications of the surface area and the microneedle density of the drug transport behaviour are not clear. For the purpose of this section, the surface area of microneedle arrays has been studied with a view to optimize this parameter and hence, enhance the drug delivery process. As shown in equations (6.11) and (6.23), there is an inverse relationship between the surface areas of square and rectangular patch and, the optimization function (g). A simulation has been carried out to present the influence of this inverse relationship for different microneedle patterns for both solid and hollow microneedles (Figure 6.6).

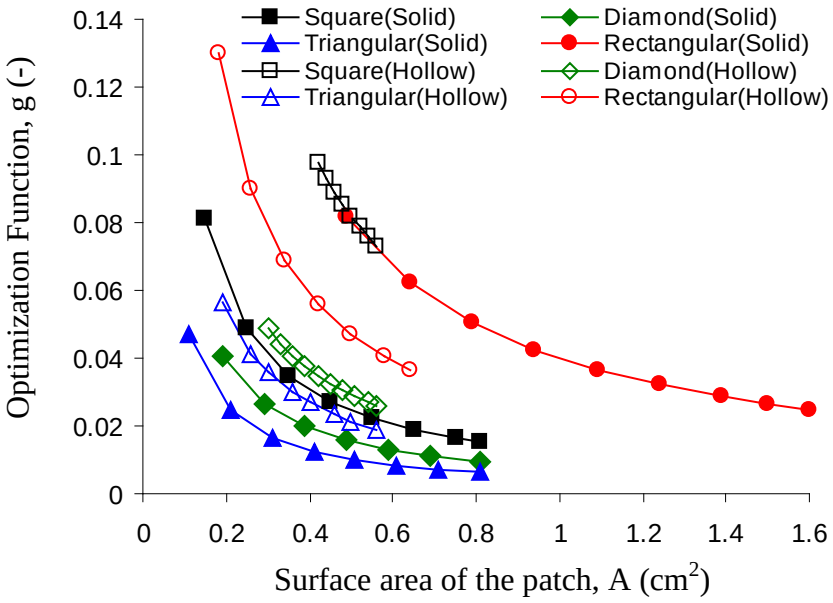

Figure 6.6- The relation between optimization function (g) and the microneedle surface area (A) of solid (dark markers) and hollow (blank markers) microneedles of various patterns with their optimum values in Table 6.3 when aspect ratio (α) of solid and hollow microneedles is 3.5 and 3.2, respectively.

It must be pointed out that the optimum microneedle surface area means the highest value of the optimization function (g). This is because in case of higher values of (g), the transdermal drug transport is enhanced due to increased permeability across skin. Based on the optimum results listed in Table 6.3, the optimization approach suggests that the best microneedle pattern for solid microneedle is either the square or the rectangular patch corresponding to an optimization function (g) of 0.081 and a surface area of 0.15 cm^2 and 0.49 cm^2, respectively. On the other hand, the best microneedle pattern for hollow microneedle is the rectangular pattern corresponding to an optimization function (g) of 0.13 and a surface area of 0.18 cm^2. The simulations show that the rectangular patterns of both solid and hollow microneedles give the highest values of optimization function (g) and hence, higher permeability across skin. As shown in Figure 6.6, the lowest optimum values of the microneedle surface area in case of solid and hollow microneedles are 0.8 cm^2 and 0.58 cm^2 for triangular pattern in both cases. Altogether, by optimizing the microneedle surface area, the process of transdermal delivery using microneedles has been enhanced. The general practical implications of these results,

e.g., the suitable patterns for a given scenario (e.g., skin thickness), are discussed in the following sections.

6.3.2 Optimization of microneedle radius

The radius of microneedles has a significant ability to increase the permeability across the skin. In a previous study, the transdermal drug delivery has been increased by changing the radii of the microneedles (Teo et al., 2005). They used a microneedle array with a radius of 0.005 cm and then increased the radius to 0.015 cm. The result was promising because it enhanced the flux by 10 times (Teo et al., 2005). The implications of studying the influence of the proportional relationship between the optimization function (g) and microneedle radius as shown in equations (6.11) and (6.23) are illustrated in this section. Figure 6.7 shows the dependence of the optimization function (g) on the microneedle radius (R) of both solid and hollow microneedles for the tested patterns with corresponding optimum surface area of microneedle array as listed in Table 6.3.

The optimum value has been defined when the highest value of g function is reached. This is because we are seeking the maximum permeability across skin and hence, the maximum values of g function. Among the microneedle pattern evaluated, the highest and lowest optimum values of the microneedle radius in case of solid microneedles are 0.01 cm and 0.0055 cm for rectangular and diamond patterns, respectively (Figure 6.7). Moreover, the highest and the lowest optimum values of the microneedle radii in case of hollow microneedles are 0.0135 cm and 0.0115 cm for square and triangular patterns, respectively. This figure suggests that reaching the optimum value for a given geometry (i.e., microneedle radius) is not always the best approach to increase permeability across skin. For example, the highest optimum value of the microneedle radius in case of hollow microneedle is 0.0135 cm corresponding to an optimization function (g) of 0.098. However, it is clear that hollow microneedle reaches its maximum optimization function (g) at a value of 0.13 corresponding

to a microneedle radius of 0.0125 cm. It is noticed that the optimization function (g) depends on all the input parameters which are connected to one another. Therefore, in order to reach the highest value of the optimization function (g), the input parameters must be optimized too. As stated previously, the best microneedle pattern for solid microneedle is either the square or the rectangular pattern corresponding to an optimization function (g) of 0.081 and a radius of 0.0065 cm and 0.01 cm, respectively. In contrast, the best microneedle pattern for hollow microneedle is the rectangular pattern corresponding to an optimization function (g) of 0.13 and a radius of 0.0125 cm. The results suggest that optimizing microneedle radius to maximize the optimization function (g) is valuable for enhancing the optimized permeability across skin (K). These results agreed well with a previous experimental result presented by Teo et al. (2005).

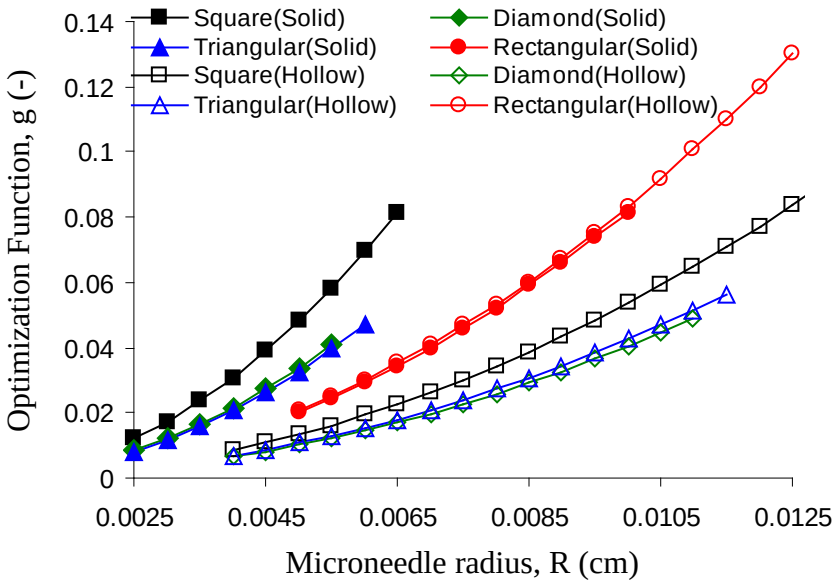

Figure 6.7- The relations between optimization function (g) and the microneedle radius (R) of solid (dark markers) and hollow (blank markers) microneedles of various patterns with their optimum values in Table 6.3 when aspect ratios (α) of solid and hollow microneedles is 3.5 and 3.2, respectively.

6.3.3 Optimization of the number of microneedles per row

A number of different microneedle designs that vary in the total number of microneedles have appeared in the literature for both solid and hollow microneedles as shown in Table 6.4. Park

et al. (2006) found that permeability across skin increases by increasing the number of microneedles. In another study, the total number of microneedles has been changed for two model drugs (i.e., calcein and bovine serum albumin (BSA)). The results show that when the number of microneedles equals 100, permeability across skin increases four fold as compared to another design where the number of microneedles is 20 for the same model drugs (Park et al., 2005). The efficiency of transdermal drug delivery has been improved by increasing the number of microneedles (Stoeber and Liepmann, 2005). In some cases, the number of microneedles is related to the surface area of patch which then defines as microneedle density as explained previously. In general, a high microneedle density is needed in order to increase the penetration efficiency (Shikida et al., 2006). Therefore, the influence of the number of microneedles on the performance of the microneedles array has been addressed previously. Nevertheless, we believe that it is also necessary to consider how to optimize the total number of microneedles (N_t) in a given patch for a given pattern. The implications of changing the optimum number of microneedles of both per row (n) and per column (m) on the optimization function (g) for various microneedle patterns is shown in Figure 6.8.

It must be pointed out that the total number of microneedles in Figure 6.8 are explained in Table 6.4 for clarification. The optimization function for both solid and hollow microneedles varies almost linearly with the total number of microneedles for all cases of microneedle patterns. The results in Figure 6.8 indicate that the highest optimization function in terms of solid microneedles happens for either the square or rectangular patterns, whereas, in terms of hollow microneedles it happens for the rectangular pattern. On the other hand, the lowest optimization functions for both solid and hollow microneedles happen for the diamond pattern. The results illustrate that the optimization function depends on the number of microneedles, surface area of the patch, and microneedle radius which should be optimized to reach the highest value of this optimization function.

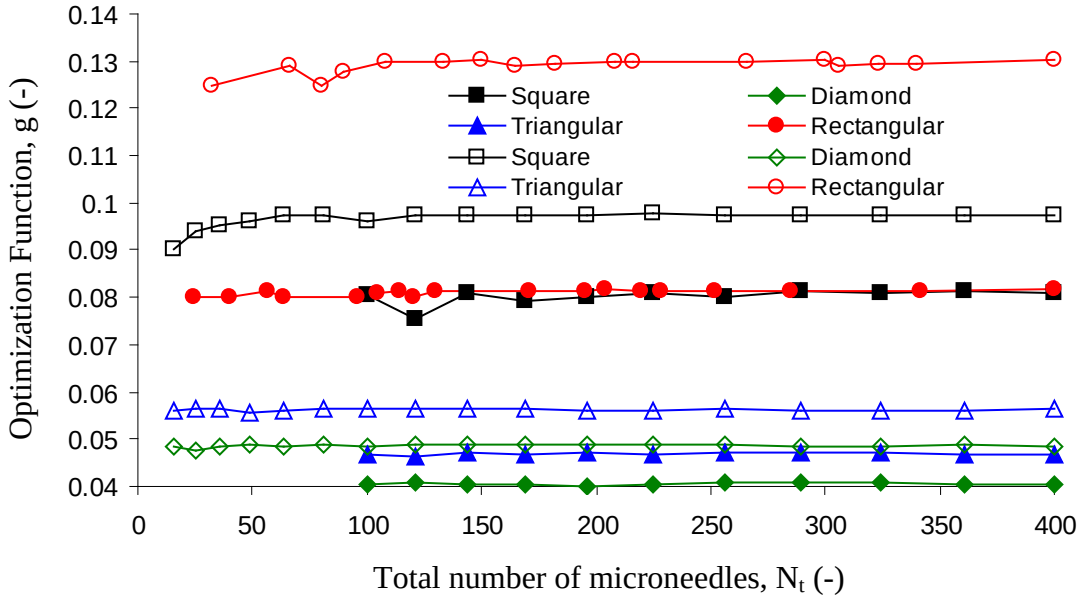

Figure 6.8- The relation between the optimization function (g) and the optimum total number of microneedles (N_t) in Table 6.4 for solid (dark markers) and hollow (blank markers) microneedles of various patterns when aspect ratio (α) of solid and hollow microneedles is 3.5 and 3.2, respectively.

Table 6.4. The total number of microneedles in an array for various optimum microneedle arrays.

Solid Microneedles						Hollow Microneedles					
Square, Diamond and Triangular	Array	N_t	Rectangular	Array	N_t	Square, Diamond and Triangular	Array	N_t	Rectangular	Array	N_t
	10×10	100		3×19	57		4×4	16		4×8	32
	11×11	121		4×6	24		5×5	25		5×18	90
	12×12	144		5×8	40		6×6	36		6×11	66
	13×13	169		6×16	96		7×7	49		7×19	133
	14×14	196		7×15	105		8×8	64		8×10	80
	15×15	225		8×15	120		9×9	81		9×12	108
	16×16	256		9×19	171		10×10	100		10×15	150
	17×17	289		10×13	130		11×11	121		11×15	165
	18×18	324		11×20	220		12×12	144		12×18	216
	19×19	361		12×19	228		13×13	169		13×14	182
	20×20	400		13×5	195		14×14	196		14×19	266
				14×18	252		15×15	225		15×20	300
				15×19	285		16×16	256		16×13	208
				16×4	64		17×17	289		17×20	340
				17×12	204		18×18	324		18×17	306
				18×19	342		19×19	361		19×17	323
				19×6	114		20×20	400		20×20	400
				20×20	400						

The optimum designs may offer variety of benefits for designing microneedle geometries for a given purpose, e.g., reducing the cost of fabrication (fewer microneedles), medical reasons (smaller microneedle radius) since that all designs have almost the same value of optimization

function for a given pattern and type as shown in Figure 6.8. Overall, the finding indicates that the total number of microneedles, surface area of microneedle arrays, and microneedle radius are all connected to each other.

6.3.4 Optimization of the aspect ratio (α)

The aspect ratio of the microneedle geometry has been defined in different ways so far. For example, Huang and Fu (2007) define it as the base over tip diameter. Park et al. (2005) describe it as the ratio of microneedle length to tip diameter. In other case, the aspect ratio refers to the length over width of the microneedles (Davis et al, 2005). The ratio of needle height to base diameter has been called as the aspect ratio too (Wilke et al., 2005). In this work, the aspect ratio (α) is defined as the ratio of the centre-to-centre distance between two microneedles (pitch) to the microneedle radius (R). In general, this parameter should be greater than 2.0 so that an overlapping between any two microneedles does not occur. Further, if the pitch is too small (<2.0), then the needles are placed too close to one another which may prevent them from pain free penetration of the skin due to their mechanical strengths and reaching the targeted depth (Miyano et al., 2005). Figure 6.9 illustrates the optimum pitch (P_t) as a function of aspect ratio (α) for both solid and hollow microneedles of various microneedle patterns. Figure 6.9 depicts that in case of rectangular pattern for both solid and hollow microneedles, the aspect ratio has no obvious influence on the optimum pitch. This means that the optimum pitch occurs at the minimum pitch of either per row (P_{tn}) or per column (P_{tm}). On the other hand, in case of other pattern, the optimum pitch for both solid and hollow microneedles varies nonlinearly with the aspect ratio. Moreover, the triangular and diamond patterns of solid and hollow microneedles, respectively, show partially different behaviour than the other patterns types as the highest optimum pitch does not occur at the highest aspect ratio. This is clear from Figure 6.9 as the highest optimum pitch for the triangular and diamond patterns of solid and hollow microneedles occurs at an aspect value of 12 and 25 instead of 20 and 30, respectively. In all cases, the range of optimum pitch is large

for triangular pattern (66%) when compared to the range that was obtained by varying the aspect ratio for rectangular pattern.

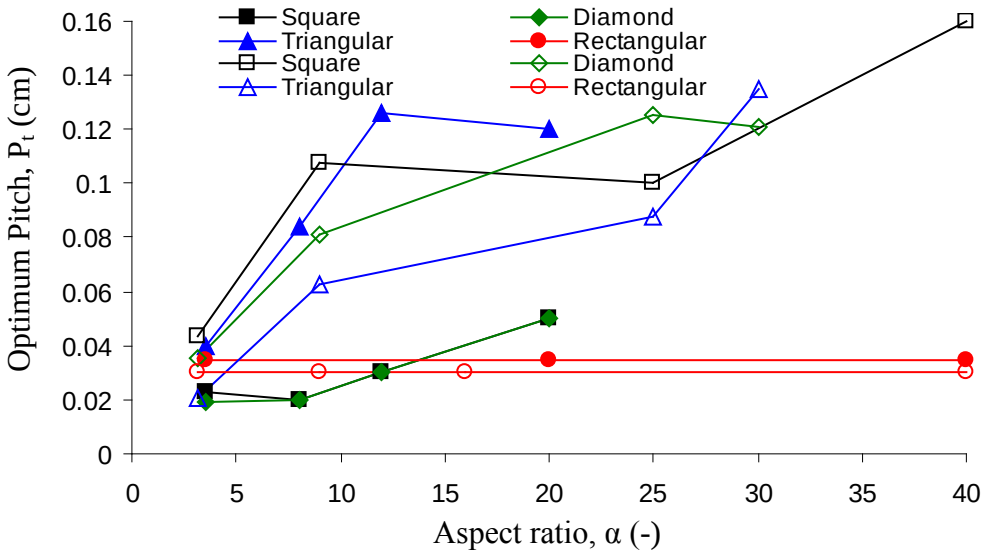

Figure 6.9- Influence of the aspect ratio of pitch over microneedle radius (α) of solid (dark markers) and hollow (blank markers) microneedles on the optimum pitch (P_t) for various patterns.

Figure 6.10 reveals how the aspect ratio of solid and hollow microneedles of various microneedle patterns influences the optimization function. As shown in Figure 6.10, there is an inverse relationship between the optimization function and the aspect ratio for all cases of microneedles patterns for both solid and hollow microneedles except in case of rectangular pattern of solid microneedles. Therefore, for a rectangular pattern, changing the aspect ratio does not affect the optimization function significantly. Moreover, the optimization function reaches its highest values at the minimum aspect ratio for all microneedle patters. The results in Figure 6.10 indicate that the highest optimization function (g) in terms of solid microneedles happens for the square pattern, whereas, in terms of hollow microneedles it happens for the rectangular pattern.

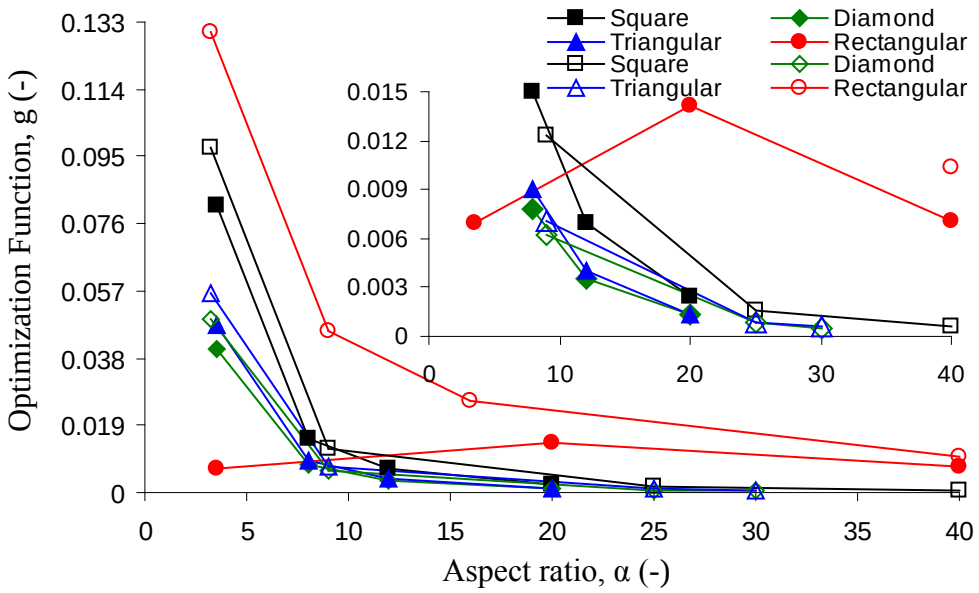

Figure 6.10- Influence of the aspect ratio of pitch over microneedle radius (α) of solid (dark markers) and hollow (blank markers) microneedles on our optimization function (g) for various patterns.

6.3.5 Effect of the skin thickness

As well known, there is strong evidence that the skin thickness can vary according to age, race, anatomical region and sex (Lee and Hwang, 2002; Fenske and Lober, 1986). Skin thickness therefore can play an important role as a barrier against any injected drugs. In a previous work, we have studied the influence of skin thickness of various anatomical regions (Al-Qallaf and Das, 2009a; Al-Qallaf et al., 2007), sex (Al-Qallaf and Das, 2009a), age group and race (Al-Qallaf and Das, 2009b) on permeability across skin for various drugs of the square patch. In this work, we evaluate the effects of skin thickness for all skin thickness classifications on drug permeation in skin of various patterns. As explained previously, the path length of skin disruption made by solid microneedles represents the effective diffusion length (i.e., thickness of the skin) and there is an inverse relationship between the skin thickness (h) and permeability across skin (K) as shown in equation (6.01). The dependency of the thickness of skin (h) for various age groups (Artz et al., 1979) on permeability across skin (K) for insulin as a model drug is shown in Figure 6.11.

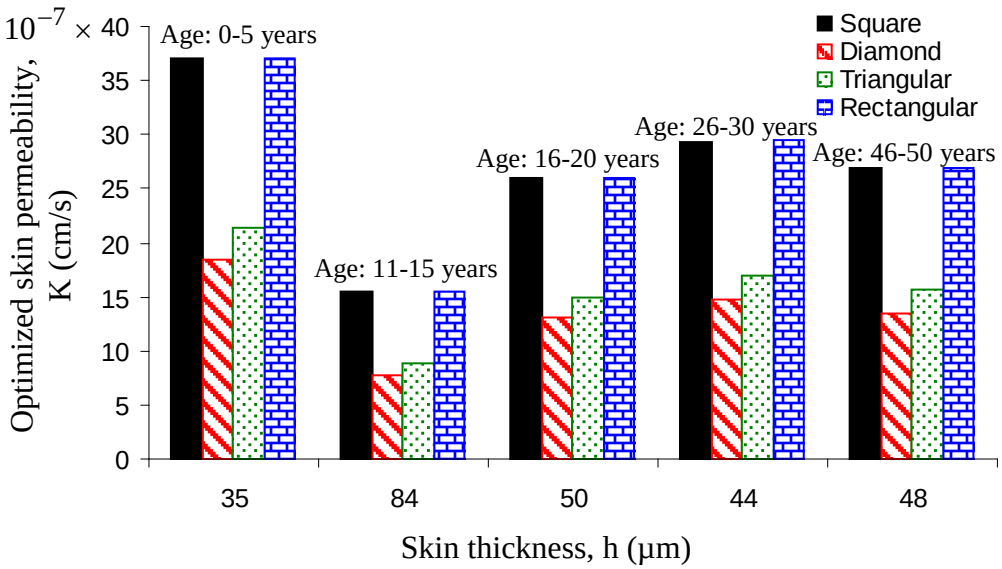

Figure 6.11- Influence of skin thickness (h) of solid microneedles for the optimum microneedles array of various patterns listed in Table 6.3 for various group ages (Artz et al 1979) for a given anatomical region (i.e., medial thigh) on the optimized permeability across skin (K).

For a given skin thickness, the optimized permeability across skin for either square or rectangular patterns is higher as compared to the other microneedle patterns. In addition, the difference in the optimized permeability across skin for a given microneedle pattern between the skin thickness of age group (0-5) and age group (11-15) proves the necessity of considering the skin thickness. For a given microneedle pattern, the optimized permeability across skin is maximum for age group (0-5) and minimum for age group (11-15), whereas, the remaining group ages are between the maximum and minimum values of the optimized permeability across skin. This indicates that skin thickness in terms of age must be considered in designing microneedles more specifically for age group (0-5) and (11-15) as compared to the other group ages.

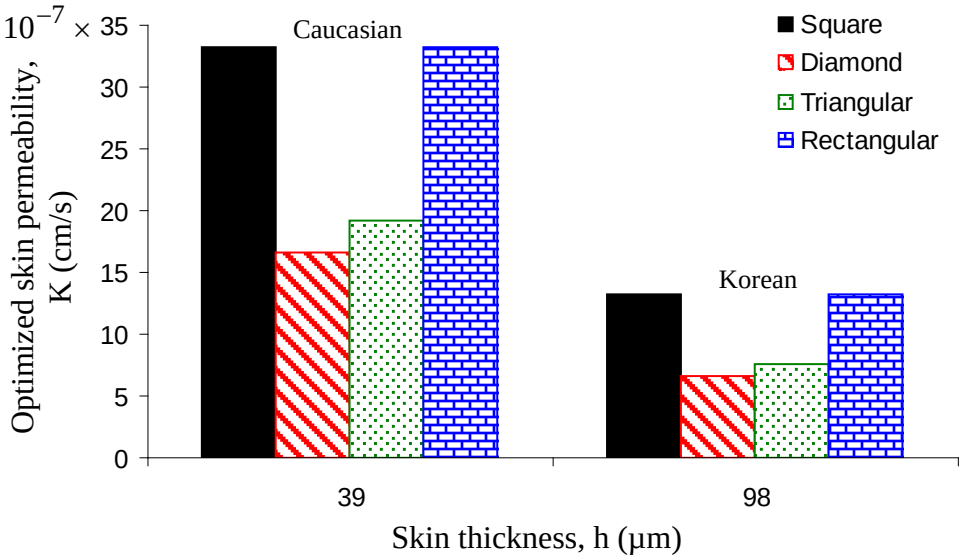

Figure 6.12- Influence of skin thickness (h) of solid microneedles for the optimum microneedles array of various patterns listed in Table 6.3 for different races (Lee and Hwang 2002) for a given anatomical region (i.e., chest) on the optimized permeability across skin (K).

Figure 6.12 shows the effect of the skin thickness of different races (i.e., Korean and Caucasian) on the optimized permeability across skin for various microneedle patterns. The optimized permeability across skin for either square or rectangular pattern is higher when compared with the other microneedle patterns for a given race. In all cases of microneedle patterns, the optimized permeability across skin of Caucasian race increases approximately 3 times more than Korean race. The range of optimized permeability across skin is relatively large for each microneedle pattern (60%) when compared to the range that was obtained by varying skin thickness in terms of age (9-58%). This means that the skin thickness in terms of race is a relatively major factor that must be taken into consideration when designing microneedles.

The evaluations of the optimized permeability across skin as a function of skin thickness with respect to various anatomical regions are shown in Figure 6.13. Also, in these evaluations, the optimized permeability across skin is higher in either square or rectangular pattern than both the diamond and triangular patterns. Further, for a given microneedle pattern the optimized permeability across skin is higher in the abdomen as compared to both the back and back of

the leg. The range of optimized permeability across skin is quite small for each microneedle pattern (9-35%) when compared to the range that was obtained by varying skin thickness in terms of race. However, the difference in optimized permeability across skin shows the necessity of considering the variation of optimized permeability across skin according to anatomical site.

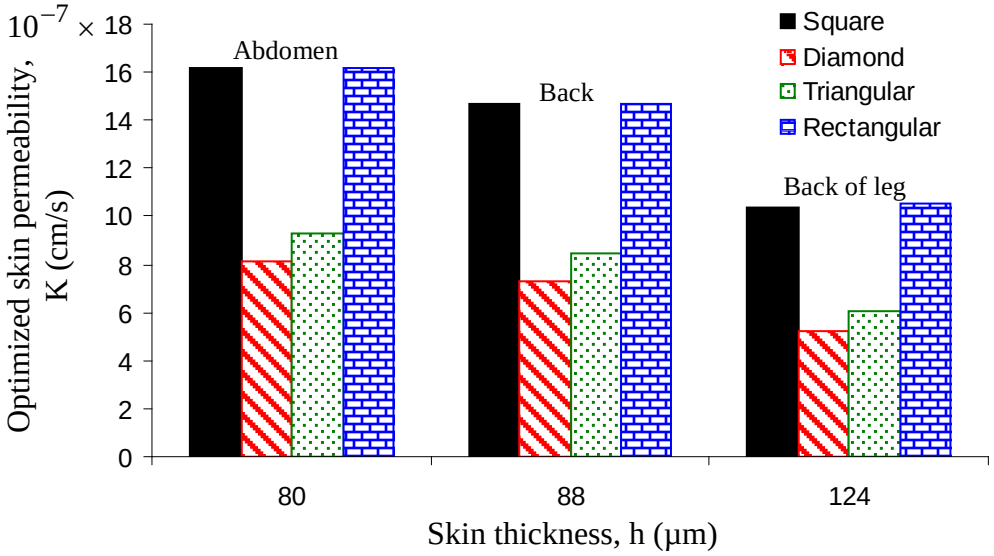

Figure 6.13- Influence of skin thickness (h) of solid microneedles for the optimum microneedles array of various patterns listed in Table 6.3 for different anatomical region (Lee and Hwang 2002) for a given sex (i.e., male) on the optimized permeability across skin (K).

Figure 6.14 presents the implications of changing the skin thickness in terms of sex group for various microneedle patterns. As expected, the optimized permeability across skin reaches its highest value at either the square or rectangular pattern for both sexes (i.e., female and male). Also, for a given microneedle pattern the optimized permeability across skin is higher in female than male. The range of optimized permeability across skin is relatively large for each microneedle pattern (40%) when compared to the range that was obtained by varying skin thickness in terms of anatomical region. These results justified our claim of considering the classification of skin thickness when designing microneedle arrays as well as when fabricating a given microneedle pattern. Altogether, the result implies that the degree of skin thickness effect is race > age > sex > anatomical region.

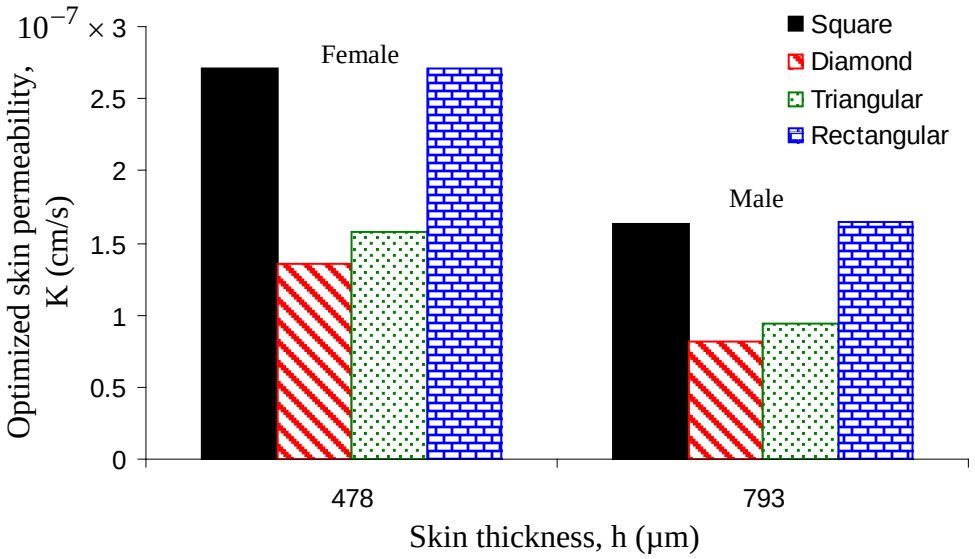

Figure 6.14- Influence of skin thickness (h) of solid microneedles for the optimum microneedles array of various patterns listed in Table 6.3 for different sex (Lee and Hwang 2002) for a given anatomical region (i.e., sole) on the optimized permeability across skin (K).

6.3.6 Effect of the microneedle length

As explained previously, the hole length (L_h) represents the length of microneedle arrays in case of hollow microneedles. Also, the inverse relationship between the microneedle length (L) and permeability across skin as shown in equation (6.01) motivated us to investigate this parameter as discussed below. To address this point, the influence of this parameter has been investigated for various microneedle patterns on the optimized permeability across skin for hollow microneedle arrays. As shown in Figure 6.15 different dimensions of microneedle lengths have been compared. As expected, the lower the microneedle length is, the higher the optimized permeability across skin is. As opposed to the case of solid microneedles, the optimized permeability across skin for a given microneedle length reaches its highest value in the rectangular pattern only. The observations of the simulations carried out indicate that the optimized permeability across skin reaches its lowest value in the diamond pattern for both cases, solid and hollow microneedles. The result indicates that the influence of microneedle length for each microneedle pattern is relatively higher (33-67%) than the influence of skin

thickness on optimized permeability across skin. The result illustrates that the optimized permeability across skin is a function of microneedle length and skin thickness in hollow and solid microneedle arrays, respectively and hence the necessity of considering these parameters for the fabrication of microneedle arrays.

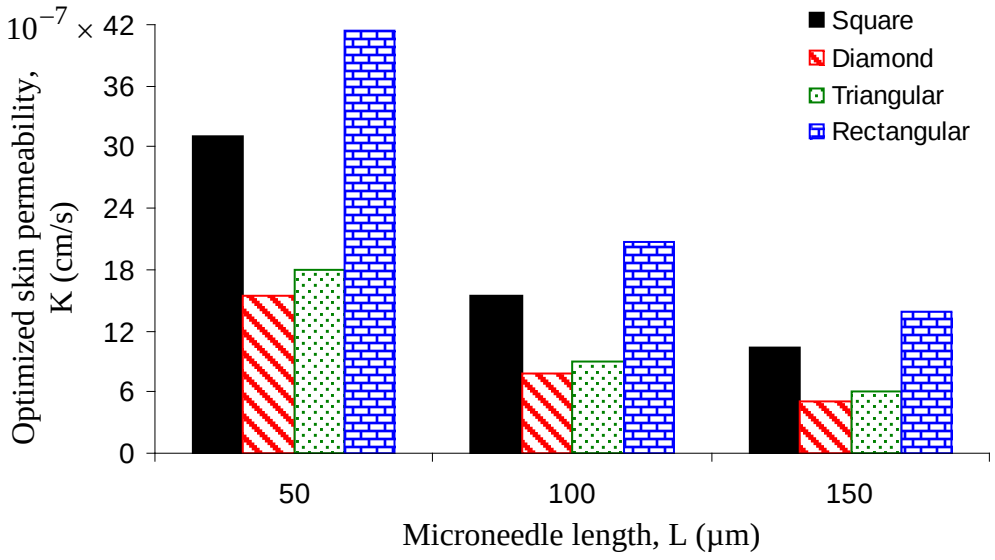

Figure 6.15- Influence of microneedle length (L) of hollow microneedles for the optimum microneedle array of various pattern listed in Table 6.3 on the optimized permeability across skin (K).

6.3.7 Effect of permeability across skin

The optimum microneedles in case of solid microneedles in Table 6.3 were investigated for different model drugs (McAllister et al., 2003). This investigation is particularly useful to compare the optimized permeability across skin of the developed framework presented with respect to various microneedle patterns. Figure 6.16 reflects the influences of four microneedle patterns for various model drugs (i.e., insulin is hexameric insulin, BSA is bovine serum albumin, nano(25) and nano(50) are nanosphere particles with molecular radii of 25 nm and 50 nm, respectively) on the optimized permeability across skin after applying optimised microneedle systems (solid microneedles). As expected, permeability across skin dramatically decreases as the diffusion coefficient of the model drugs decreases. The results also show that permeability across skin reaches its highest value when calcein is delivered.

This is obviously expected because calcein has both the highest diffusion coefficient ($6\times10^{-6}\,cm^2/s$) (McAllister et al., 2003) and the lowest molecular weight (623 Da) (Nishimura and Lemasters, 2001) among the model drugs. In all cases, the optimized permeability across skin is maximum for either the square or rectangular pattern and minimum for the diamond pattern.

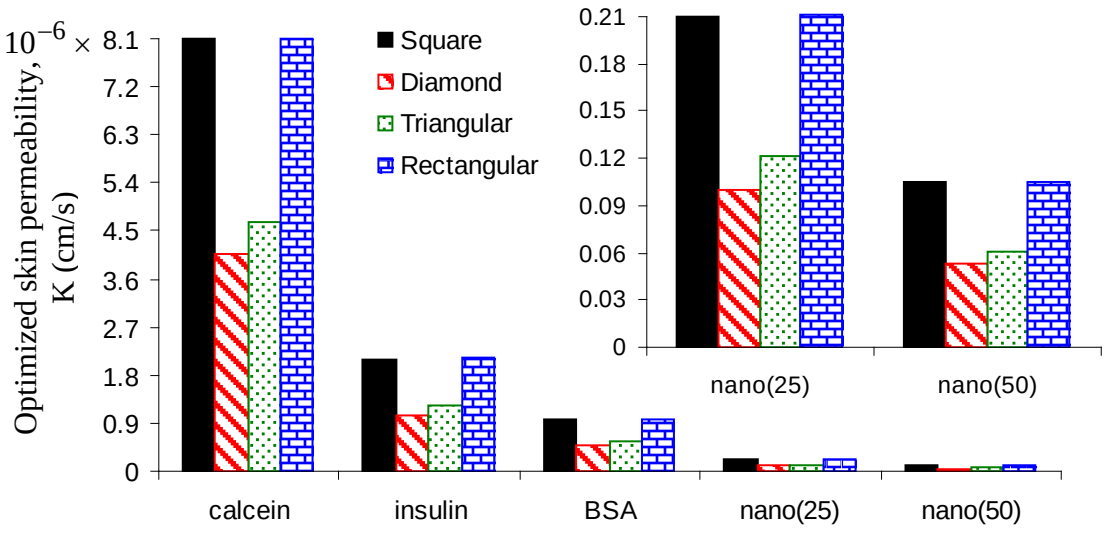

Figure 6.16- Influence of applying our optimization model for solid microneedles of the optimum microneedles listed in Table 6.3 on the optimized permeability across skin (K) for different drugs.

Moreover, the influence of various microneedle patterns for these model drugs on the optimized permeability across skin after applying optimized microneedle system (hollow microneedles) is presented in Figure 6.17. Also, in these measurements, the optimized permeability across skin decreases by decreasing the diffusion coefficient of the model drugs. In all cases, the optimized permeability across skin is maximum for the rectangular pattern and minimum for the diamond pattern. The results in both Figure 6.16 and Figure 6.17 suggest that the microneedle pattern is an important parameter to consider for optimizing and hence, enhancing the transdermal drug delivery using microneedles.

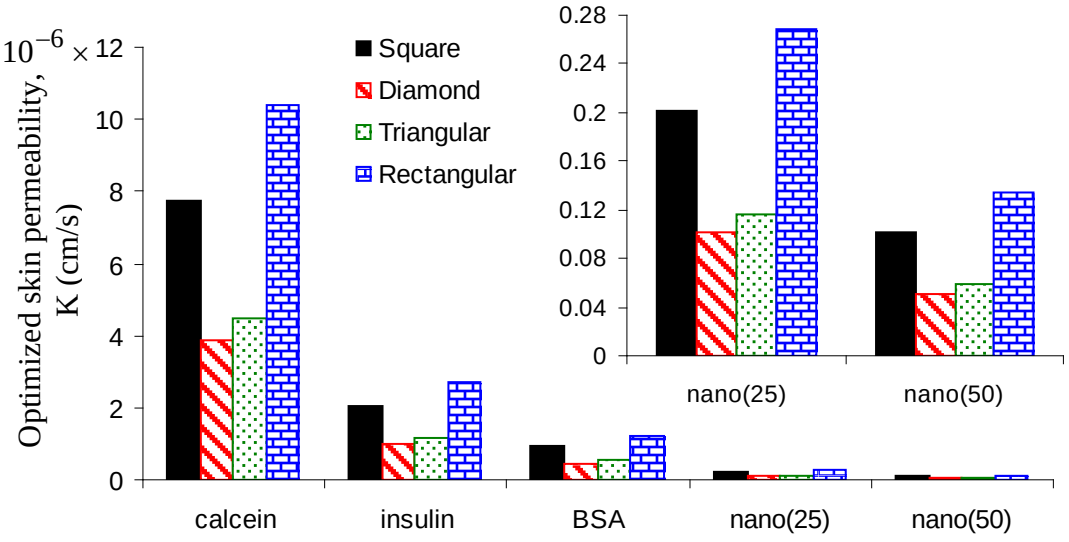

Figure 6.17- Influence of applying our optimization model for hollow microneedles of the optimum microneedles listed in Table 6.3 on the optimized permeability across skin (K) for different drugs.

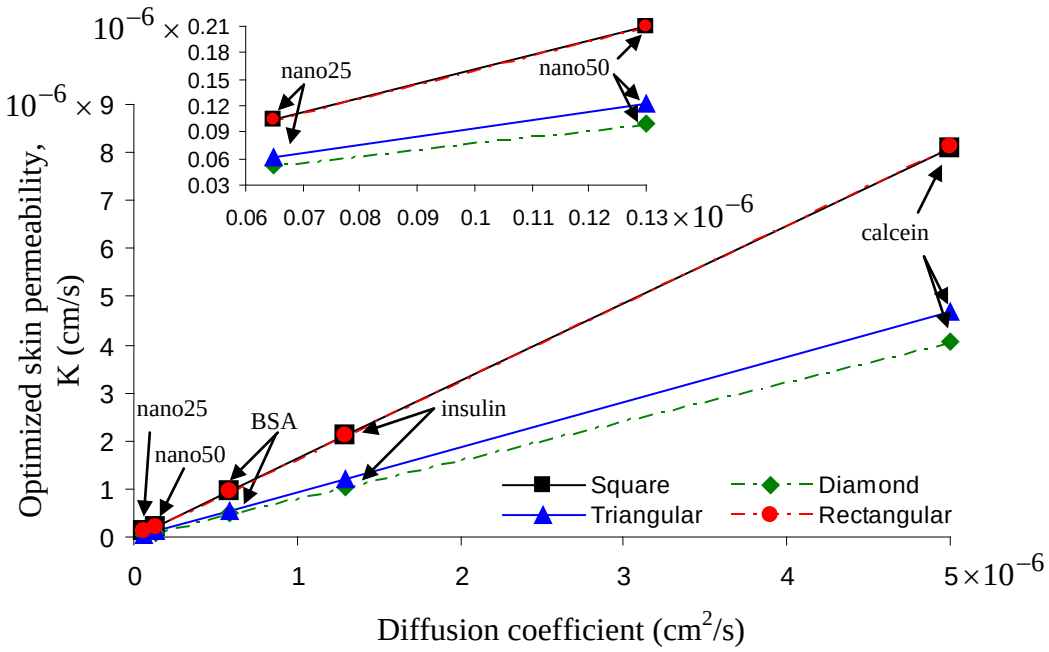

Figure 6.18- Relationship between the optimized permeability across skin (K) and diffusion coefficient (D) of the optimum solid microneedles listed in Table 6.3 for various drugs.

Another aim of this work is to formulate a relationship between the optimized permeability across skin and diffusion coefficient of the proposed model drugs with various microneedle models. This attempt is presented in Figure 6.18 and Figure 6.19 for the case of solid and hollow microneedles, respectively. As shown in both figures, it seems there is a linear relationship in all microneedle patterns. These correlations are listed in Table 6.5 for all

microneedles patterns types corresponding to their optimum geometries in Table 6.3. It must be pointed out that these correlations are valid for a diffusion coefficient ranges as $6.5\times10^{-8} \le D \le 5\times10^{-6}$ cm^2/s. In Figure 6.18, the trend lines of both the square and rectangular patterns in terms of solid microneedle are almost the same. This is expected since the optimization function (g) for both patterns is almost equal as discussed previously. On the other hand, the trend lines of both the square and rectangular patterns for hollow microneedle are apart as shown in Figure 6.19. This is expected since that the optimization functions (g) for both cases are different.

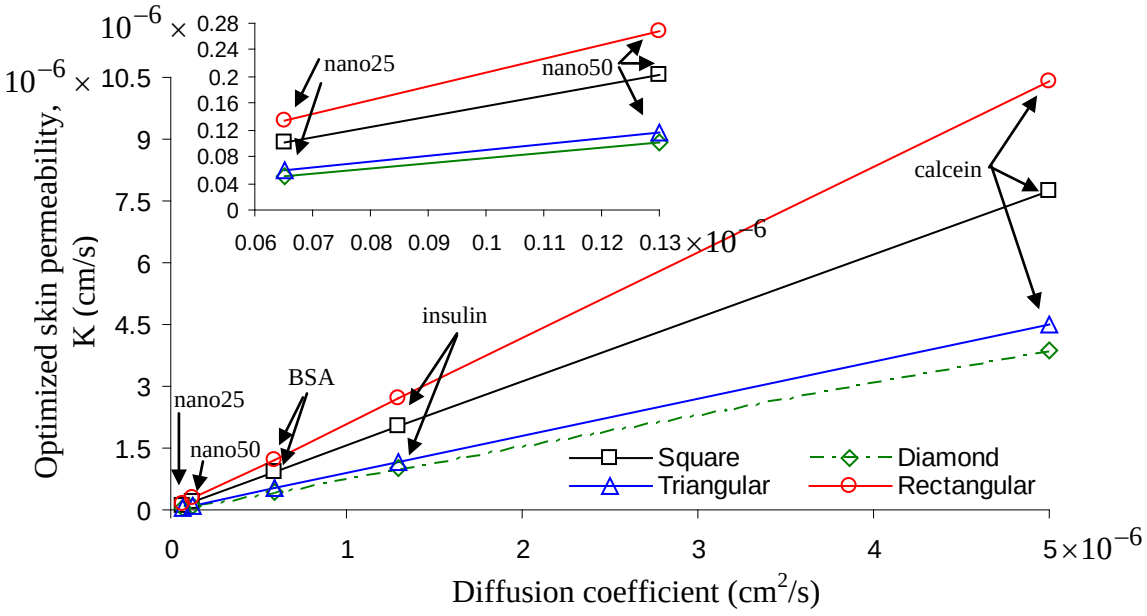

Figure 6.19- Relationship between the optimized permeability across skin (K) and diffusion coefficient (D) of the optimum hollow microneedles listed in Table 6.3 for various drugs.

Table 6.5. The correlations of various microneedles patterns for both solid and hollow microneedles corresponding to their optimum dimensions in Table 6.3.

Microneedle types / **Pattern**	Solid	Hollow
Square	$K = 1.618\times D - 0.0008$	$K = 1.5519\times D + 0.0007$
Diamond	$K = 0.8125\times D - 0.0029$	$K = 0.776\times D + 0.0003$
Triangular	$K = 0.936\times D + 0.0007$	$K = 0.8959\times D + 0.0014$
Rectangular	$K = 1.622\times D + 0.0002$	$K = 2.0806\times D - 0.0054$

Where K is the optimized permeability across skin (cm/s) and D is the diffusion coefficient of various drugs in skin (cm^2/s). It must be pointed out that these correlations are valid for a diffusion coefficient ranges as $6.5\times10^{-8} \le D \le 5\times10^{-6}$ cm^2/s.

In chapter 5, the influence of microneedle dimensions (i.e., surface area of patch) on insulin concentration in blood has been studied. Therefore, in Figure 6.20, the permeability across skin of insulin for various patterns has been plotted with the steady state insulin concentration in blood for the optimum solid microneedle to determine the intercept point. This intercept point shows the optimum surface area of patch of solid microneedles. The result shows that the highest and lowest value of the microneedle surface area are 0.87 cm^2 and 0.33 cm^2 for rectangular and triangular patterns, respectively. In all cases, the best microneedle pattern for solid microneedle is rectangular pattern corresponding to an optimized permeability across skin of 9×10^{-7} cm/s and a steady state insulin concentration in blood of 0.023 µg/ml. In some cases, where the drug concentrations in blood and permeability across skin are both considered in manufacturing microneedles, this graph might be useful.

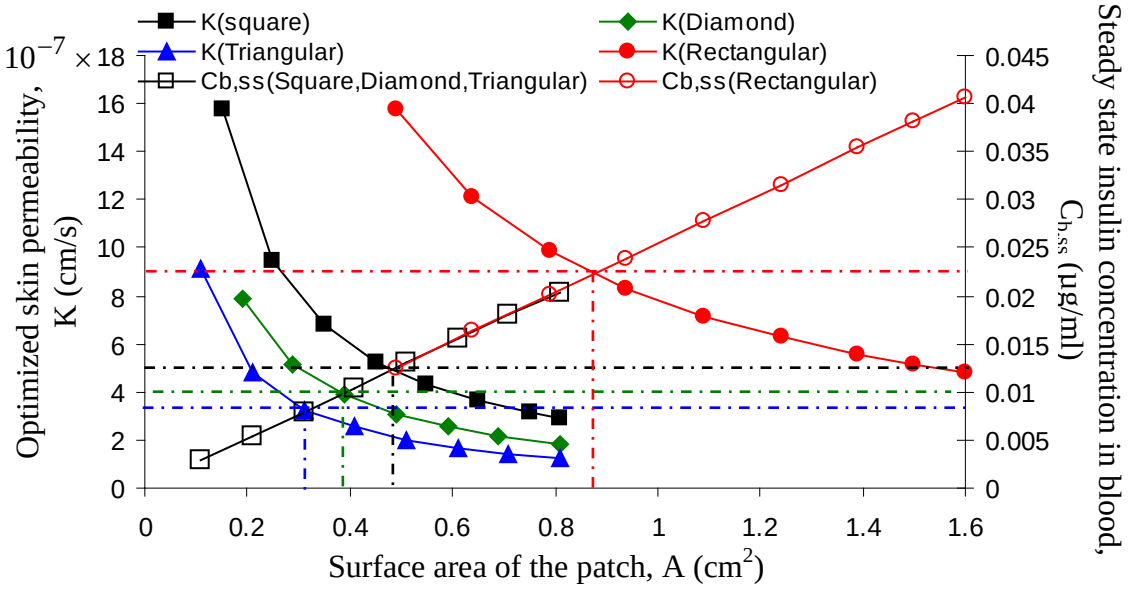

Figure 6.20- The optimum point (intercept) between permeability across skin (K) and steady state insulin concentration in blood ($C_{b,ss}$) of the optimum solid microneedles for different microneedle patterns with various surface area of patch.

To evaluate the usefulness of our optimization model on increasing permeability across skin, the dimensions of our optimized model were compared with a previous model as shown in Table 6.6. The results of permeability across skin for both designs have been given in Figure 6.21. In our work, the microneedle arrays proposed by McAllister et al. (2003) have been

optimized. The result shows an increase of 8 fold for permeability across skin when using our optimized model, which improves the process of transdermal drug delivery. This is due to the effects of increasing microneedle radius and decreasing the surface area of the patch. This has been done with the consideration of keeping the same number of microneedles per row (i.e., n=20) and aspect ratio of pitch over microneedle radius (i.e., α=3.75). Therefore, the permeability across skin can be increased by adjusting the optimum parameters (e.g., number of microneedles, microneedle radius, etc.) of the microneedle.

Table 6.6 Values of parameter for McAllister's (McAllister et al., 2003) and our optimized design.

	Design of McAllister et al. (2003)	Our optimized design
Number of microneedles per row, n (-)	20	20
Microneedle radius, R (cm)	0.001	0.0019
Surface Area of the Patch, A (cm)	0.09	0.04
Pitch, Pt (cm)	0.015	0.01
Aspect ratio, α (-)	3.75	3.75

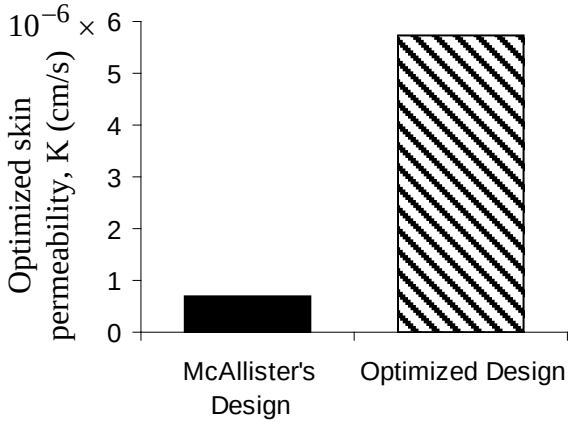

Figure 6.21- Effect of the optimization function (g) on McAllister's design (McAllister et al. 2003) before and after applying it on optimized permeability across skin (K).

6.4 Summary

This study presents an optimization framework for transdermal delivery of both low and high molecular weight drugs from microneedle. The optimization process is based on determining an optimisation function (g) for various microneedle patterns (e.g., square, diamond,

triangular, etc.). We argue that higher the value of g is, the higher the drug permeability in skin is. The outputs of the developed framework have allowed us to identify the optimum design of both solid and hollow microneedles. In particular, the results have been used to predict permeability across skin of both low and high molecular weight drugs using microneedle systems. Also, optimum designs based on different skin thickness (e.g., race, age, etc.) for transdermal delivery of drugs have been suggested.

CHAPTER 7

Effect of Skin Metabolism

7.1 Introduction

A number of mathematical frameworks have been developed for evaluating both the skin permeation and blood concentration of drug delivered using microneedle arrays (Al-Qallaf and Das, 2009a,b; Al-Qallaf and Das, 2008; Davidson et al., 2008; Al-Qallaf et al., 2007; Lv et al., 2006; McAllister et al., 2003). However, in almost all of these cases, the metabolism of the drug has not been considered. Consequently the skin permeation and blood concentration of the drug have been modelled assuming no drug metabolism in the viable skin. For example, we have previously evaluated the effects of volume of distribution (V_b) and elimination rate constant (K_e) on the fentanyl concentration in blood without considering the skin metabolism (Al-Qallaf et al., 2007). Other general mathematical models for molecule transport across skin have been also proposed which have not included the influence of skin metabolism, see e.g., the reviews by Godin and Touitou (2007) and, Yamashita and Hashida (2003). Similarly, Simon et al. (2006) proposed a mathematical model of iontophoretic transdermal drug delivery and assumed no drug metabolism in the viable skin. Although these modelling studies were useful, there are a number of situations where drug metabolism in skin during transdermal delivery in general, and microneedle arrays specifically, might be important. For example, Yamashita and Hashida (2003) argue that the skin metabolism may be an important factor for developing transdermal drug delivery approach. Indeed many studies considered the influence of drug metabolism in skin (e.g., Boderke et al., 2000; Sugibayashi et al., 1999; Bando et al., 1997; Auton, 1993). However, these studies are insufficient in determining the implications of the skin metabolism for transdermal drug delivery using microneedles. This is obvious because the drugs are injected in the viable epidermis in this case instead of the top of the skin, and the influence of the path lengths for drug transport across skin on the kinetics of metabolism may be different. This has been explained in more detail in section 7.2.

The purpose of the study in this chapter is to develop a mathematical framework to examine the importance of considering skin metabolism for drug delivery using microneedle arrays. In particular, we are interested to determine the implications of verapamil delivery using microneedle arrays. Verapamil is used for many medical purposes such as preventing the heart attack (Simonetti et al., 1986), lowering blood pressure (Trewet and Ernst, 2008), and stopping cluster headache attacks (Tobin and Flitman, 2008) and diarrhea due to microscopic colitis (Scheidler and Meiselman, 2001). The administration of verapamil is often done orally. However it has been shown that the bioavailability of verapamil may be reduced by 80-90% if the oral route is chosen (Choi et al., 2008; Michel, 2006). On the other hand, others argue that it can be delivered by transdermal route which seems to improve the bioavailability of verapamil (Shah et al., 1992a). Shah et al. (1992b) concluded that not all the amount of delivered verapamil reached the blood circulation. One of the possible reasons to explain this effect was that the verapamil could be metabolized in the skin (Shah et al., 1992b).

Assuming that one wishes to adopt transdermal routes for delivery of verapamil, it is not certain what role the microneedle arrays could play for its delivery. To this end, one needs to determine the advantage of microneedles over a normal patch for verapamil delivery and determine the implications of verapamil metabolism in skin. To address these issues, we have carried out simulations for both transdermal patch (without microneedles) and microneedle arrays in this chapter.

As mentioned previously, many theoretical models of transdermal drug delivery have been proposed to study the influence of skin metabolism. However, most of these models have studied the influence of skin metabolism for the full skin thickness (i.e., the stratum corneum and viable skin together). In fact, skin metabolism occurs primarily in the viable epidermis

(Amsden and Goosen, 1995). In order to validate this fact we have carried simulations of the transdermal patch with two hypothetical cases. To make a logical comparison, the simulations of these two hypothetical cases have been carried out for the same transdermal drug delivery system (i.e., patch) with the same input parameters. The first case represents the transdermal patch on the top of the stratum corneum. The second case represents a hypothetical case where the patch is on top of the viable epidermis. A comparison for these two hypothetical cases has been presented to show the influence of skin metabolism. Based on the result of this comparison, we have carried out another simulation for the microneedle arrays. The simulations of microneedles have been carried out by adopting a previous microneedle model (Davidson et al., 2008).

In this work, a study of both skin permeation and verapamil concentration in blood have been carried out based on a diffusion model including a metabolic process. Improving upon our previous work (Davidson et al., 2008; Al-Qallaf et al., 2007), we have introduced mono and bi-layer diffusion models with two compartment model to estimate verapamil concentration in blood when either applied as a patch or injected using microneedle. In all cases, the cumulative amounts of verapamil permeated per unit area of skin with and without skin metabolism have been numerically determined. Moreover, the distribution of verapamil across skin for the transdermal delivery using microneedles has been obtained. Therefore, the analysis of both verapamil permeation and the verapamil concentration in blood are thought to be useful. In particular, this is important to identify the impact of skin metabolism when applying the transdermal delivery of verapamil using microneedles. In fact, this helps to clarify the argument about the assumption of neglecting skin metabolism in viable skin as discussed previously.

7.2 Modelling strategy

A schematic diagram of the developed mathematical framework of transdermal delivery of verapamil for both the patch and microneedle arrays is illustrated in Figure 7.1.

Figure 7.1- Schematic diagram of transdermal drug delivery for both patch and microneedle arrays, adopted from (Al-Qallaf et al., 2007) (i.e., the volume of distribution in tissue V_t is defined in section 7.2.3).

There are two main transdermal drug delivery systems in the figure: a transdermal patch containing verapamil at a homogeneous concentration (Shah et al., 1992c) and a microneedle array coated with verapamil solution (Davidson et al., 2008). Application of the transdermal patch is divided into two hypothetical cases that represent application on the top of either the stratum corneum or viable epidermis. In the first case, verapamil penetrates the stratum corneum, partitions towards and penetrates the viable epidermis and then enters the blood circulation (Tojo, 1987). In the second case, verapamil diffuses across the viable epidermis and then is absorbed by the blood circulation. Although this is a hypothetical case designed purely for the purpose of this chapter, the result obtained for this case is expected to be useful since it has been shown that drug may be metabolized in the viable epidermis (Amsden and Goosen, 1995). In the figure, S_a is the surface area of both the transdermal patch and

microneedle arrays, L is the penetration depth of microneedles, H_{eff} is the effective skin thickness (i.e., effective path length of molecules in tissue) that verapamil molecules can pass in the tissue from microneedle which depends on the needle geometry (Davidson et al., 2008). Verapamil is defined to get absorbed into two compartments (i.e., blood compartment and tissue compartment) with first order elimination kinetics (Tojo, 1987).

7.2.1 Model assumptions

The mathematical framework in this work is based on the following assumptions:

(1) The skin metabolism is defined to follow first order kinetics (Lee et al., 1996; Sato and Mine, 1996; Tojo et al., 1985; Hadgraft, 1980; Yu et al., 1979). This assumption has been chosen since most of the mathematical models that have been presented to describe the metabolic kinetics of drug during its diffusion through skin follow the first order kinetics as compared to Michaelis-Menten kinetics (Sugibayashi et al. 1999; Sugibayashi et al., 1996; Higuchi et al., 1983). Furthermore, Lipscomb and Poet (2008) concluded that in vivo drug concentration is usually below the Michaelis-Menten constant (Km) which leads to essentially consider the first order kinetics. In particular, the transdermal drug delivery has been reported to follow first order kinetics (Papa et al., 2009; Prodduturi et al., 2009; Shakeel et al., 2008).

(2) The distribution of the enzyme in the viable skin is assumed to be uniform (Boderke et al., 2000). Liu et al. (1990) proposed a theoretical diffusion model to examine the enzyme distribution. This model was based on the assumption of uniform enzyme distribution. The outcome of this study supports this assumption since the theoretical results agreed well with their experimental data. In another study, a mathematical absorption model with skin enzyme distribution has been developed (Hikima et al., 2006). The investigation shows a uniform enzyme distribution across skin. No significant differences have been observed between the uniform enzyme distribution model and non-uniform enzyme distribution model (Sugibayashi

et al., 1999; Tojo et al., 1994). Therefore, this assumption is easily applicable to represent the drug diffusion profile across skin (Bando et al., 1996) which leads to a simplified theoretical model (Yamaguchi et al., 2006; Boderke et al., 2000).

(3) For the simulations carried out using SKIN-CAD® (Biocom Systems, 2006), the transport of verapamil across skin is described by one-dimensional diffusion model (Lv et al., 2006; Boderke et al., 2000). For the sake of simplicity, the one-dimensional diffusion has been assumed as this allows one to consider the effects of drug metabolism alone and not any other effects (e.g., dimensionality). Such assumption has been used in many mathematical models to describe the transdermal drug delivery using microneedles (Lv et al., 2006; McAllister et al., 2003). In particular, several studies have been obtained by carrying out simulations using SKIN-CAD® which assume one-dimensional method (Kimura and Tojo, 2007; Tojo and Hikima, 2007; Mori et al., 2003). The numerical results agreed well with the experimental data.

(4) The diffusion coefficients are assumed to be constant in each layer (Boderke et al., 2000) although they may be different. The Diffusion coefficient of verapamil has been shown to be three orders of magnitude less in the stratum corneum as compared to viable skin (Shah et al., 1992a). It has been defined that the diffusion coefficient in the viable epidermis and dermis are of the same magnitude (Yamaguchi et al., 2008; Tojo, 2005). Therefore, it is acceptable to assume a constant value of the diffusion coefficient across the viable skin.

(5) All the verapamil molecules are assumed to be taken up by the blood circulation (Al-Qallaf et al., 2007). This assumption has been previously explained in detail in section 5.3.1.

(6) The body pharmacokinetics is defined to follow two-compartment model (Shah et al., 1992c; Anderson et al., 1982). The two-compartment model for verapamil has been chosen in

consistency with previous studies which indicate this to be a better model as compared to the one-compartment model (Bertera et al., 2008; Syvanen et al., 2008). Ahmed et al. (1992) investigated the pharmacokinetic behaviour of verapamil for a range of models. Their results showed that the two-compartment model was the most appropriate model as compared to one-compartment and three-compartment models.

(7) At x=h (Fig.7.1), the concentration of verapamil is defined to be zero (sink condition) (Al-Qallaf et al., 2007; Mori et al., 2003; Tojo et al., 1989). This assumption has been previously explained in detail in section 3.3.

(8) The back diffusion of verapamil in skin is ignored (Al-Qallaf et al., 2007; Tojo, 2005; Shah et al., 1992c). This has been done since the diffusion coefficient of verapamil is small in the stratum corneum (Shah et al., 1992c). Therefore, it seems to be acceptable to ignore the back diffusion (Tojo, 2005).

7.2.2 Governing equations characterizing the skin concentration

The skin is represented by a bi-layer model which has two layers, stratum corneum and viable skin. In the case of neglecting the skin metabolism, the movement of verapamil across skin (Figure 7.1) is based on Fick's second law as:

Across the stratum corneum

$$\frac{\partial C_{sc}}{\partial t} = D_{sc}\frac{\partial^2 C_{sc}}{\partial x^2}; \qquad 0 < x < h_{sc} \tag{7.01}$$

Across the viable skin

$$\frac{\partial C_{vs}}{\partial t} = D_{vs}\frac{\partial^2 C_{vs}}{\partial x^2}; \qquad h_{sc} < x < h \tag{7.02}$$

The initial verapamil concentration in skin is assumed to be zero. The boundary conditions used in this work for solving all the governing equations are:

At the surface of the skin, the verapamil concentration is:

$C = C_s$ at $x = 0$ $(0 < t \leq t_a)$ (7.03)

Verapamil is assumed to be delivered at a constant rate, i.e., a constant skin surface concentration is maintained (Shah et al., 1992c).

At the interface between stratum corneum and viable skin, the verapamil concentration is:

$C_{sc} = K_{sc/vs} C_{vs}$ at $x = h_{sc}$ $(0 < t)$ (7.04)

At the bottom of the skin epidermis, the concentration of verapamil is:

$C = 0$ at $x = h$ $(0 < t)$ (7.05)

where C is the verapamil concentration, D is the diffusion coefficient and the subscripts s, sc and vs represent the skin surface, the stratum corneum and the viable skin, respectively, t is time, x is the distance in a given skin layer, $K_{sc/vs}$ is the partition coefficient between the stratum corneum and the viable skin, t_a is the duration of application of the drug delivery system, h_{sc} is the stratum corneum thickness and h is the skin thickness (i.e., distance to blood vessel).

As is well known, the metabolic reaction occurs in the viable skin and not in the stratum corneum (Tojo, 2005; Schaefer et al., 1982). Therefore, in the case of considering the metabolism the following equation is used instead of equation (7.02):

$$\frac{\partial C_{vs}}{\partial t} = D_{vs} \frac{\partial^2 C_{vs}}{\partial x^2} - K_m C_{vs} \quad (7.06)$$

where K_m is the first order metabolic reaction rate constant.

As shown in Figure 7.1, solid microneedles pierce the stratum corneum allowing verapamil to effectively bypass this barrier to diffusion. Therefore, the skin is represented by a mono-layer diffusion model in this work. The injected verapamil by microneedles diffuses across viable

skin obeying Fick's second law until it reaches blood vessels (Al-Qallaf et al., 2007; Tojo, 2005; Boderke et al., 2000).

7.2.3 Governing equations characterizing the blood concentration

The verapamil concentration in blood after imposing the transdermal drug delivery is given by the following two-compartmental pharmacokinetic model (Tojo, 2005):

$$V_b \frac{dC_b}{dt} = \left(\frac{dQ}{dt}\right) S_a - (K_e + K_{12}) C_b V_b + K_{21} C_t V_t \qquad (7.07)$$

$$V_t \frac{dC_t}{dt} = K_{12} C_b V_b - K_{21} C_t V_t \qquad (7.08)$$

where K_e is the elimination rate constant from the blood compartment, K_{12} and K_{21} are the transfer rate constants between compartments, dQ/dt is the penetration rate of verapamil through the skin, S_a is the surface area of the delivery system, V_b and V_t are the volumes of distribution in the blood and the tissue compartments, respectively, C_b and C_t are verapamil concentrations in the blood and the tissue compartments, respectively. The tissue compartment refers to the poorly perfuse non-fatty tissues such as muscle.

The governing equations with the initial and boundary conditions (7.01) – (7.08) have been implemented and solved using the software, SKIN-CAD® (Biocom Systems, 2006). In this work, we have predicted verapamil concentration in blood for the transdermal drug delivery with and without skin metabolism by using mono-layer and bi-layer diffusion models in case of applying the microneedle arrays and the patch, respectively.

The diffusion of coated verapamil has been modelled in 3D using the software, FEMLAB® (Comsol, 2005). The steady state diffusive flux of verapamil through the blood interface has been calculated by assuming that the concentration of verapamil on the needle surface is constant (Davidson et al., 2008). This allows us to obtain the effective skin thickness by

determining the flux from the simulations. As mentioned previously, the effective skin thickness (H_{eff}) in case of applying solid microneedles is calculated as (Davidson et al., 2008):

$$H_{eff} = D_{vs} \frac{C_a}{J_{ss}} \quad (7.09)$$

where C_a is verapamil concentration at the coated surface area of microneedles and J_{ss} is the average steady-state flux through the blood interface. This is then used as an input parameter for SKIN-CAD®. This approach has been adopted following the work by Davidson et al. (2008), which have previously shown that the effective skin thickness is influenced by the microneedle geometry. Equation (7.09) determines the effective path length of drug molecules once released from the microneedles.

7.3 Results and discussions

The impacts of the pharmacokinetic variables with skin metabolism have been studied by Shah et al. (1992c). However, this study was based on transdermal drug delivery by transdermal patch on the top of stratum corneum. According to Shah et al. (1992c) there is a large difference in the pharmacokinetics variables of verapamil. Following this study we have evaluated the influence of pharmacokinetic variables on verapamil with the consideration of skin metabolism for both transdermal patch and microneedle arrays. The values of the pharmacokinetics variables, which were used in our simulations, are shown in Table 7.1.

Table 7.1. Pharmacokinetics variables of verapamil obtained from the references.

Parameters / References	$V_b \times 10^4$ (ml)	$V_t \times 10^4$ (ml)	$K_e \times 10^{-4}$ (s^{-1})	$K_{12} \times 10^{-4}$ (s^{-1})	$K_{21} \times 10^{-4}$ (s^{-1})
Koike et al. (1979)	6.47	8.34	1.50	6.22	3.94
Eichelbaum et al. (1981)	27.39	13.14	0.79	2.12	2.78
Anderson et al. (1982)	2.63	5.18	1.58	2.19	1.11

V_b and V_t are the volumes of distribution in the blood and the tissue compartments, respectively, K_{12} and K_{21} are the transfer rate constants between compartments and K_e is the elimination rate constant from the blood compartment.

To further quantify the influence of skin metabolism, we have hypothetically considered the patch at the top of viable epidermis with and without skin metabolism. We hypothesized this case since the metabolic process occurs in the viable epidermis as mentioned previously.

Table 7.2. Model parameters used in this work for analyzing the blood concentration of verapamil penetrated through the skin with and without skin metabolism for both patch and microneedle arrays (Tojo, 1987; Shah et al., 1992c; Al-Qallaf et al., 2007).

Parameters	Patch		Microneedles	
	case one[a]	case two[b]	case one[c]	case two[d]
Duration for medication (calculation): t_m (hour)	48		8	
Duration of application: t_d (hour)	24		4	
Surface area of microneedle arrays/patch: S_a (cm^2)	80		2	
Thickness of stratum corneum: h_{sc} (cm)	0.002	-	-	
Distance to blood vessel: h (cm)	0.02	0.018	0.02	
Effective skin thickness: H_{eff} (cm)	-	-	0.00819	0.00827
Diffusion coefficient in stratum corneum: D_{sc} (cm^2/s)	7×10^{-11}	-	-	
Diffusion coefficient in viable skin: D_{vs} (cm^2/s)	7×10^{-8}			
Stratum corneum/viable skin partition coefficient: $K_{sc/vs}$ (-)	8	-	-	
Volume of distribution: V_b(ml)	variable			
Volume of distribution: V_t(ml)	variable			
Elimination rate constant: K_e (s^{-1})	variable			
Transfer rate constant: K_{12} (s^{-1})	variable			
Transfer rate constant: K_{21} (s^{-1})	variable			
Skin surface concentration: C_s (mg/ml)	344	43	43	
First order reaction metabolic rate constant: K_m (s^{-1})	5.61×10^{-4}		-	5.61×10^{-4}

[a]On the top of the stratum corneum, [b]on the top of the viable epidermis (i.e., with and without metabolism for both "a" and "b"), [c]without metabolism and [d]with metabolism.

The philosophy of this modelling strategy relies on comparing two hypothetical cases of transdermal delivery of verapamil using patch. This comparison is useful to evaluate the influence of skin metabolism and hence whether to consider the metabolic process in case of coated microneedles with verapamil. To achieve a logical result, those two cases have been simulated with a transdermal patch with the same input parameters. Based on this result, we

have carried out simulations of transdermal delivery of verapamil using microneedles. The input parameters of those simulations are shown in Table 7.2.

7.3.1 Effect of skin metabolism in case of patch

To examine the implications of skin metabolism in transdermal drug delivery of patch, we have simulated cumulative amount permeated across the skin and blood concentration of verapamil with and without skin metabolism using model parameters as shown in both Table 7.1 and Table 7.2. As previously explained, this has been done by comparing one case where the transdermal patch is applied on the top of the stratum corneum (i.e., case one) with a hypothetical case where it is applied on the top of the viable epidermis without the stratum corneum (i.e., case two).

Figure 7.2- The effect of skin metabolism on the cumulative amount of verapamil permeated into blood per unit area of skin following transdermal delivery using patch (i.e., on the top of the stratum corneum) for the input parameter adopted from (Anderson, 1982).

Figure 7.2 shows the cumulative amount of verapamil permeated per unit area of skin with and without metabolism when using the patch for case one. The cumulative amounts of verapamil permeated per unit area of skin with and without metabolism reached approximately 360 $\mu g/cm^2$ and 830 $\mu g/cm^2$, respectively, in 24 hours during the patch

application. The calculated permeation flux without skin metabolism is approximately 2.3 times higher than that with skin metabolism during the patch application. The results seem to suggest that skin metabolism is an important factor for the transdermal delivery of verapamil. The effects of skin metabolism on the blood verapamil concentration using patch for case one are shown in Figure 7.3. These simulations have been done using various literature values for pharmacokinetic parameters as shown in Table 7.1. The maximum verapamil concentration in blood ($C_{b,max}$) is different between the two cases (i.e., with and without metabolism). In case of considering skin metabolism, the maximum verapamil concentration in blood ($C_{b,max}$) for the pharmacokinetics parameters given by Anderson et al. (1982), Koike et al. (1979) and Eichelbaum et al. (1981) reached 0.09, 0.04 and 0.02 µg/ml, respectively. On the other hand, it reached 0.21, 0.09 and 0.04 µg/ml in case when skin metabolism is not considered. As expected, the results indicate that skin metabolism has a noticeable influence for the transdermal delivery of patch on the top of the stratum corneum.

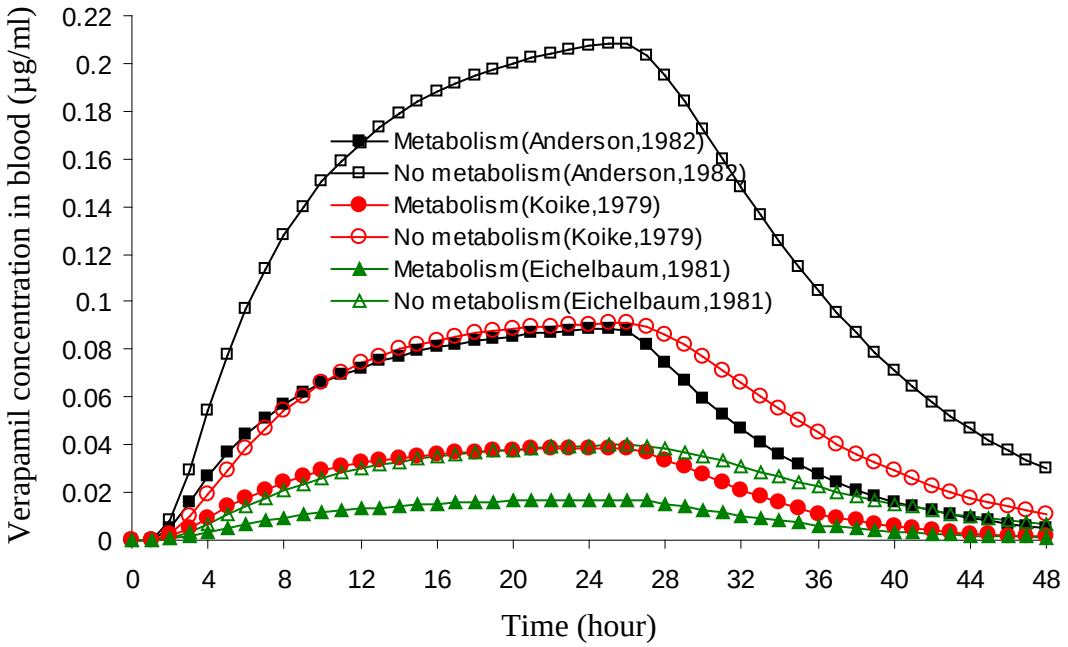

Figure 7.3- The effects of various pharmacokinetic parameters with and without skin metabolism on the blood verapamil concentration following transdermal delivery using patch (i.e., on the top of the stratum corneum).

This result agrees well with the results presented by Shah et al. (1992c) qualitatively. Overall, the obtained results show that the skin metabolism is a relatively important factor for the process of transdermal delivery of verapamil if a patch is used (case one) since the difference in both the maximum blood concentration and cumulative amount of verapamil permeated into blood per unit area of skin are more than double as compared between both cases (i.e., with and without skin metabolism).

Figure 7.4- The effect of skin metabolism on the cumulative amount of verapamil permeated into blood per unit area of skin following transdermal delivery using patch (i.e., on the top of the viable epidermis) for the input parameter adopted from (Anderson, 1982).

In contrast, Figure 7.4 represents the cumulative amount of verapamil permeated per unit area of skin with and without skin metabolism for transdermal delivery by applying the patch on the top of the viable epidermis (case two). As explained previously, this case has been proposed to identify the importance of whether to consider the metabolic process in viable epidermis by comparing this case (i.e., case two) with the previous case (i.e., case one). The cumulative amounts of verapamil permeated per unit area of skin with and without metabolism reached approximately 9700 $\mu g/cm^2$ and 14000 $\mu g/cm^2$, respectively, in 24 hours.

A less remarkable difference has been observed by comparing the simulated data with and without skin metabolism.

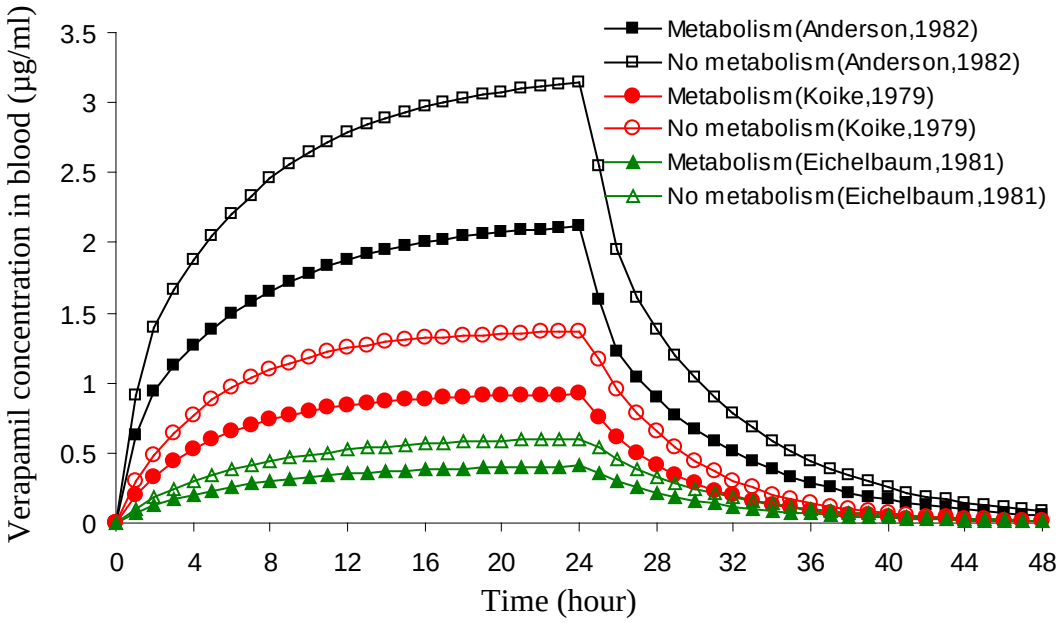

Figure 7.5- The effects of various pharmacokinetic parameters with and without skin metabolism on the blood verapamil concentration following transdermal delivery using patch (i.e., on the top of the viable epidermis).

The simulated blood concentrations in case two are shown in Fig. 7.5. Less observable differences have been shown for this case as compared with the previous case. This is because the differences in the maximum blood concentration between both cases (i.e., with and without skin metabolism) are less (<30%) than the previous case (>50%) for all the pharmacokinetic parameters presented. For example, in case of considering skin metabolism, the maximum verapamil concentration in blood ($C_{b,max}$) for the pharmacokinetics parameters given by Anderson et al. (1982) reached 2.2 µg/ml, whereas, it reached 3.2 µg/ml in case when skin metabolism is not considered. Therefore, these simulations show that the skin metabolism has a lower influence which could be neglected as compared with the case of transdermal delivery of verapamil by applying the patch on the top of stratum corneum (case

one). The result of this case motivated us to further study the influence of skin metabolism during the injection of microneedles as discussed below.

7.3.2 Effect of skin metabolism in case of microneedle systems

Motivated with the previous results and to further study the skin metabolism effect, we have carried out simulations of transdermal delivery of verapamil using microneedle arrays with and without considering skin metabolism in the microneedle model as shown in Figure 7.6.

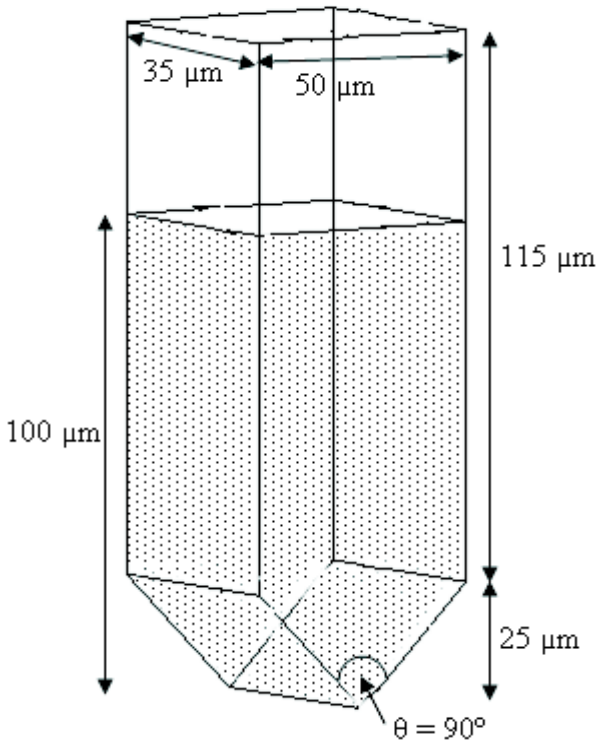

Figure 7.6- Schematic diagram of a microneedle model used in this work (i.e., the dotted area represents the surface area coated with verapamil).

In case of not considering the skin metabolism effects, equation (7.02) has been used to describe verapamil transport across skin. On the other hand, in case of considering the skin metabolism effects, equation (7.06) has been used. Then the average flux of both cases has been determined by using FEMLAB® as discussed previously in section 7.2. The effective skin thickness (H_{eff}) of transdermal delivery of verapamil using microneedles with and without skin metabolism has been calculated according to equation (7.09) for the parameters

shown in Table 7.2. The utility of using the effective skin thickness has been previously explained in section 7.2. This has been used as an input parameter to calculate the verapamil concentration in blood by using SKIN-CAD®. No significant difference has been observed in the effective skin thickness (<1%) for both cases (i.e., with and without skin metabolism). This similarity appears because the effective skin thickness mainly depends on the flux at the blood interface which was almost the same for both cases since that microneedle reach much nearer to the blood interface where the drugs have only minimal contact with the dermal enzyme (Steinstrasser and Merkle, 1995; Martin et al., 1987).

Figure 7.7- The effect of skin metabolism on the cumulative amount of verapamil permeated into blood per unit area of skin following transdermal delivery using microneedle arrays for the input parameter adopted from (Anderson, 1982).

Figure 7.7 shows the cumulative amount permeated per unit area of skin for verapamil with and without metabolism. The cumulative amounts of verapamil permeated per unit area of skin with and without metabolism reached approximately 4900 μg/cm^2 and 5400 μg/cm^2, respectively. These figures also show that the differences between both cases (i.e., with and without skin metabolism) are lower as compared with the previous cases (i.e. case one and two). This result is consistent with our claim to not consider skin metabolism when designing

microneedle arrays. The verapamil concentration in blood starts to reduce after four hours as the duration of application is 4 hours as shown in Figure 7.8. In all cases, insignificant differences have been observed between both cases (i.e., with and without skin metabolism) (6-9%) when compared to case one (>50%). This is because the maximum verapamil concentration in blood ($C_{b,max}$) in both cases (i.e., with and without skin metabolism) for the pharmacokinetic parameters given by Anderson et al. (1982), Koike et al. (1979) and Eichelbaum et al. (1981) reached approximately 0.1 µg/ml, 0.04 µg/ml and 0.01 µg/ml, respectively. Altogether, the obtained results show that the skin metabolism is a relatively weak function of the process of transdermal delivery of verapamil if microneedle is used since the difference in both the maximum blood concentration and cumulative amount of verapamil permeated into blood per unit area of skin are almost the same as compared between both cases (i.e., with and without skin metabolism).

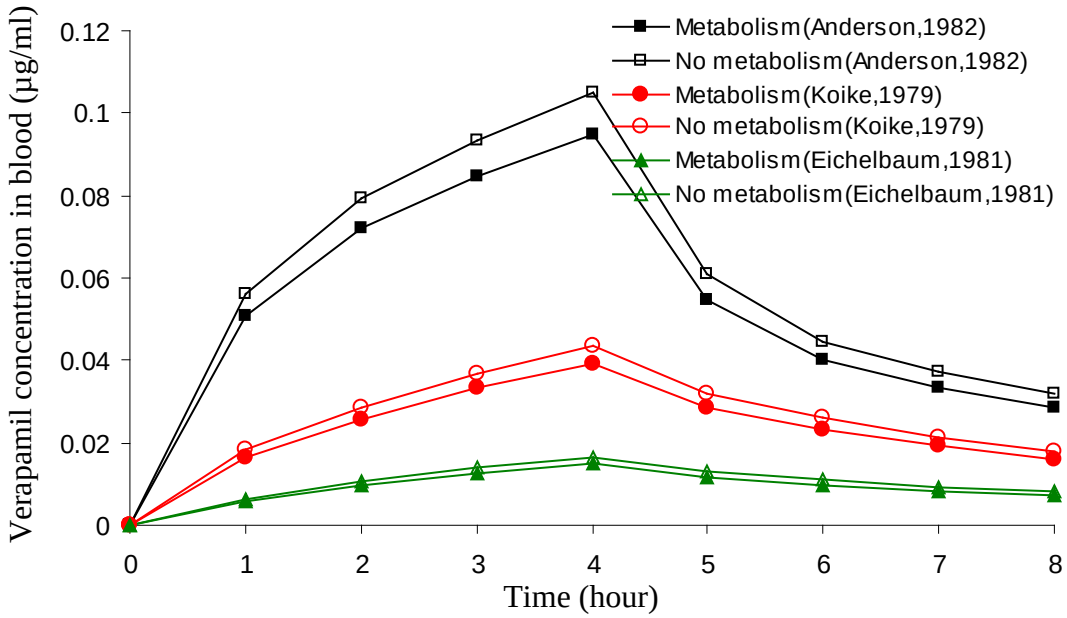

Figure 7.8- The effect of various pharmacokinetics parameters with and without skin metabolism on the blood verapamil concentration following transdermal delivery using microneedle arrays.

To further achieve a better knowledge of the transdermal delivery of verapamil using microneedles, the distribution of verapamil across skin in 3D has been obtained as shown in

Figure 7.9. This figure shows the distribution of verapamil concentration across skin without metabolism. This simulation has been utilized to determine the effective skin thickness (H_{eff}) in order to use this value as an input parameter for the previous simulations which mimic the transdermal delivery of verapamil using microneedles. However, the distribution of verapamil concentration across skin with metabolism has not been presented since the concentration profile of both cases (i.e., with and without metabolism) are almost the same as shown previously in Figure 7.8.

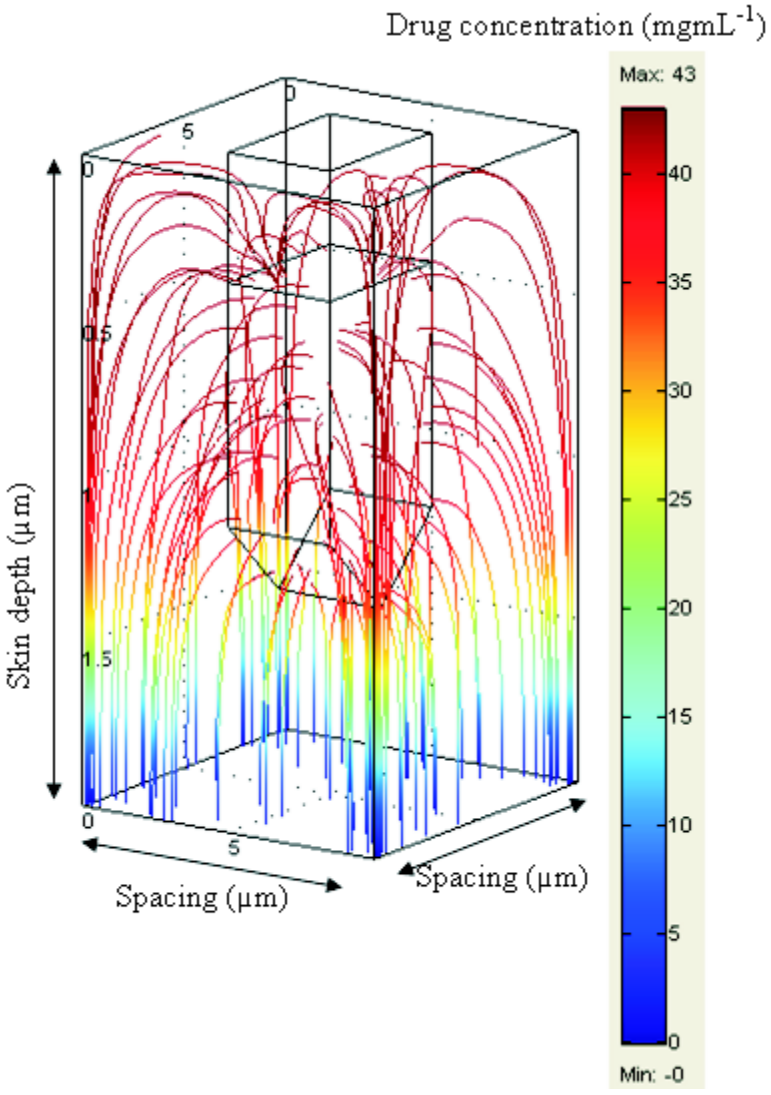

Figure 7.9- Distribution of verapamil across skin without metabolism in 3D of the microneedle model.

All together, our result implies that the degree of skin metabolism effect is transdermal patch (case one) > transdermal patch (case two) > microneedles. This result indicates that skin metabolism will greatly influence the transdermal delivery of verapamil in the skin including the diffusion barrier (i.e., stratum corneum) and will not influence so much when the diffusion barrier is bypassed and the diffusion path length of the viable epidermis decreases. This conclusion accords well with the results conducted by Boderke et al. (2000). To sum up, the findings indicate that not only the transdermal delivery of verapamil using microneedles has been improved but also the influence of skin metabolism has been reduced as compared with the transdermal delivery using patch.

7.4 Summary

Various theoretical studies have been proposed to predict the drug transport behaviour after drug injection using microneedles. However, it is important to examine considering the effects of biological factors such as skin metabolism. A mathematical model for microneedle systems is introduced and applied to simulate the verapamil transport with metabolism in the skin. A comparative analysis for a transdermal delivery of verapamil from microneedle is presented in this chapter. The results indicate that the skin metabolism does not affect markedly the skin permeation after verapamil injection using microneedles.

CHAPTER 8

Conclusions and Future Work

8.1 Conclusions

- The utility of microneedle system for transdermal drug delivery has been demonstrated in this DPhil thesis. The simulations show that the microneedle array enhances the transdermal delivery of drugs (e.g., fentanyl) as compared to the transdermal patch (without microneedles) (section: 3.6).

- It has been found that both the elimination rate constant and the surface area of the patch were the most significant factors in determining the steady state drug concentration in blood ($C_{b,ss}$), followed by the skin thickness, penetration depth, volume of distribution and centre-to-centre spacing, respectively. Other parameters such as microneedle thickness, microneedle diameter and coating depth had a less significant effect on the steady state drug concentration in blood, respectively (section: 5.5).

- By decreasing the pharmacokinetic variables (i.e., elimination rate constant and volume of distribution) and skin thickness, the steady state drug concentration in blood increases (sections: 5.4.7, 5.4.9).

- By increasing the penetration depth, diameter, thickness and coating depth of microneedle, both the steady state drug concentration in blood and the effective permeability across skin increase and the effective skin thickness decreases. On the other hand, by increasing the microneedle spacing, both the steady state drug concentration in blood and the effective permeability across skin decrease and the

effective skin thickness increases (sections: 4.5.3, 4.5.4, 4.5.5, 4.5.6, 4.5.7, 5.4.3, 5.4.4, 5.4.5, 5.4.6, 5.4.10).

- Microneedle type D (rocket needle) was the best type in terms of penetration depth, microneedle thickness, coating depth and centre-to-centre spacing while, microneedle type A (cylindrical needle) was the best type in terms of microneedle diameter (section: 5.5).

- The dimensional analysis carried out in this work shows various relations (e.g., polynomial, power, etc.) between the dimensionless steady state insulin concentration in blood and different dimensionless groups. The developed relationships make the problem under consideration simpler to analyse and allow us to correlate multi-scale behaviour of drug delivery using microneedles (section: 5.5).

- The results of this study indicate that the duration of steady state drug concentration increases as the duration of application increases (section: 5.4.3).

- It has been found that the depth of penetration from the microneedle array was the most important factor in determining both the effective skin thickness and permeability across skin, followed by the centre-to-centre spacing. Other microneedle dimensions such as the diameter in cylindrical needles, the thickness in flat needles, and the coating depths were less significant (section: 4.6).

- For a given centre-to-centre spacing, the effective skin thickness is only slighter higher in the hexagonal pattern than the square pattern (section: 4.5.8).

- The differences in optimized permeability across skin show the necessity of considering the variation of skin thickness when applying microneedle arrays into human skin. The results show that the degree of skin thickness effect is race > age > sex > anatomical region (section: 6.3.5).

- Our optimization technique showed that the optimized permeability across skin was increased by eightfold compared with some previous design (McAllister et al., 2003) (section: 6.3.7).

- The steady state insulin concentration in blood of the optimum solid microneedle was determined, and plotted against optimized permeability across skin for various patterns. The data show that the best microneedle pattern for solid microneedle was the rectangular pattern (section: 6.3.7).

- The simulations carried out indicate that the optimized permeability across skin reaches its highest value by adopting the rectangular pattern for both solid and hollow microneedles (section: 6.3.1).

- The results presented in this thesis suggest that by reducing the aspect ratio, the optimized permeability across skin of drugs can be increased. This implies that the aspect ratio is a key parameter while adjusting the dimensions of microneedles (section: 6.3.4).

- An attempt has been done in this thesis to formulate a relationship between the diffusion coefficient and the optimized permeability across skin for various

microneedle patterns of both solid and hollow microneedles. The result shows that there is a linear relationship in all microneedle patterns (section: 6.3.7).

- The result illustrate that the optimization function (g) depends on the number of microneedles, surface area of the patch, and microneedle radius which should be optimized to reach the highest value of this optimization function (section: 6.3.3).

- A study of both skin permeation and drug concentration in blood has been carried out based on a diffusion model including a metabolic process. The result indicates that the degree of skin metabolism effect is transdermal patch (case one) > transdermal patch (case two) > microneedles (section: 7.3.2).

8.2 Future work

This study presented theoretical results of using microneedles to deliver drugs across skin. While building on these results, further examinations are recommended to improve this novel study. Thus, future studies are needed to understand the skin deformation and its influence on the penetration depth during injection. Experimental work which involves real-time imaging once the microneedle has been injected would provide an accurate estimation of the effective skin thickness. This will improve the results carried out by the numerical simulations and hence to obtain a relationship between the penetration depth of microneedle and the skin deformation.

The transdermal drug delivery using microneedle has been shown to be strongly dependent on the classification of skin thickness (i.e., sex, age, etc). Therefore, combining the optimization dimensions presented in this thesis with the variation of skin thicknesses should be carried out. Experimental studies of the influence of skin thickness on permeability across skin will

serve a good guidance for any numerical study in the future. In addition, the outcome of these experiments will expand the fabrication of microneedle based on a certain classification of skin thickness to achieve optimal microneedle design and thereby reduce the resistance offered by skin tissue.

Future work should focus on determining the implications of any dissolution phenomena around the coated microneedles. The mathematical model presented in this thesis was based on the assumption of constant concentration around the coated area of the solid microneedle. This has been done due to the lack information of the drug dissolution using microneedle in the literature. Therefore, experimental studies could be carried out to show the dissolution rate constant to use it as an input parameter for any numerical study in the future.

In the past decade, many theoretical models have been proposed to correlate the diffusion coefficient in the stratum corneum. This is because the stratum corneum has been considered as the main barrier of the transdermal drug delivery. However, with the new invention of the microneedle array, one should pay attention to the mass transfer of both low and high molecular weight drugs. Therefore, more experimental study is required to develop a mathematical framework of the diffusion coefficient across the viable skin. To date, all the values of diffusion coefficients in the viable skin have been determined either by adopting an equation such as Stokes-Einstein equation, an empirical correlation, etc., or an estimation based on the diffusion coefficient across the stratum corneum.

Our findings show that the pharmacokinetic parameters are important on defining the drug concentration in blood. However, based on the literature there are a large variation of these values. Therefore, experimental studies should be presented to explain this variation and

hence to recommend the best values to be taken for transdermal drug delivery using microneedles.

The partition coefficient mainly occurs between the stratum corneum and the viable epidermis. One way to enhance the efficiency of the numerical study presented in this thesis is to consider the partitioning of the drug during the injection. This could be done by presenting an experimental study to examine whether this could influence the mass transfer of drug across skin tissue.

In this work, we have studied six solid microneedle models by using insulin as a model drug. However, this study could be improved by expanding more models since different shapes of microneedle could be fabricated in the future. This would provide a better result by comparing our findings with these new models which provide a wider view for the users to obtain the optimum model.

The optimized designs should be fabricated and run an experimental study. Once these microneedles have been fabricated then they should be tested clinically. In addition, the fabrication process of these optimized designs could be linked with different issues such as comparing the material strength of these optimized designs for different materials (e.g., metal, polymers, silicon, etc.).

REFERENCES

Abrams, S.A., O'Brien, K.O., Liang, L.K., Stuff, J.E. (1995) Differences in calcium absorption and kinetics between black and white girls aged 5-16. J. Bone Miner. Res., 10, 829-833.

Ahmed, J.H., Elliott, H.L., Meredith, P.A., Reid, J.L. (1992) Low-dose verapamil in middle-aged and elderly patients with angina pectoris: No evidence of increased susceptibility to the cardiac effects. Cardiovascular Drugs and Therapy, 6, 153-158.

Aggarwal, P., Johnston, C.R. (2004) Geometrical effects in mechanical characterizing of microneedle for biomedical applications. Sensors and Actuators B, 102, 226-234.

Alarcon, J.B., Hartley, A.W., Harvey, N.G., Mikszta, J.A. (2007) Preclinical evaluation of microneedle technology for intradermal delivery of influenza vaccines. Clin. Vaccine Immunol., 14(4), 375–381.

Al-Qallaf, B., Das, D.B., Mori, D., Cui, Z.F. (2007) Modelling transdermal delivery of high molecular weight drugs from microneedle systems. Philos. T. Roy. Soc. A., 365, 2951-2967.

Al-Qallaf, B., Das, D.B. (2008) Optimization of square microneedle arrays for increasing drug permeability in skin. Chemical Engineering Science, 63, 2523-2535.

Al-Qallaf, B., Das, D.B. (2009a) Optimizing microneedle arrays to increase skin permeability for transdermal drug delivery. Annals of the New York Academy of Sciences, 1161, 83-94.

Al-Qallaf, B., Das, D.B. (2009b) Optimizing microneedle arrays for transdermal drug delivery: Extension to non-square distribution of microneedles. Journal of Drug Targeting, 17(2), 108-122.

Ambrose, C.G., Clanto, T.O. (2004) Bioabsorbable implants: review of clinical experience in orthopedic surgery. Ann. Biomed.Eng., 32(1), 171–177.

Amsden, B.G., Goosen M.F.A. (1995) Transdermal delivery of peptide and protein drugs: an overview. AIChE, 41(8), 1972-1997.

Anderson, P., Bonderson, U., Sylvcn, C. (1982) Clinical pharmacokinetics of verapamil in patients with a trial fibrillation. European Journal of Clinical Pharmacology, 23(1), 49-57.

Arora, A., Prausnitz, M.R., Mitragotri, S. (2008) Micro-scale devices for transdermal drug delivery. International Journal of Pharmaceutics, 364, 227-236.

Artz, C.P., Moncrief, J.A., Pruitt, B.A. (1979) Burns: a team approach. Saunders, Philadelphia, 22-24.

Auton, T.R. (1993) Concentration-flux relations for a multicellular biological membrane with metabolism. Mathematical Biosciences, 115(1), 103-117.

Aziz, N.A, Majlis, B.Y. (2006) Fabrication study of solid microneedles array using HNA. Proceeding of IEEE International Conference on Semiconductor Electronics, ICSE2006, December 6-8, Kuala Lumpur, Malaysia.

Bal, S.M., Caussin, J., Pavel, S., Bouwstra, J.A. (2008) In vivo assessment of safety of microneedle arrays in human skin. European Journal of Pharmaceutical Sciences, 35(3), 193-202.

Baksu, B., Baksu, A., Göker, N., Citak, S. (2009) Do different delivery systems of hormone therapy have different effects on psychological symptoms in surgically menopausal women? A randomized controlled trial. Maturitas, 62, 140–145.

Bando, H., Sahashi, M., Takagi, T., Yamashita, F., Takakura, Y., Hashida, M. (1996) Analysis of in vitro skin penetration of acyclovir prodrugs based on a diffusion model with a metabolic process. International Journal of Pharmaceutics, 135, 91-102.

Bando H., Sahashi M., Yamashita F., Takakura Y., Hashida M. (1997) In vivo evaluation of acyclovir prodrug penetration and metabolism through rat skin using a diffusion/ bioconversion Model. Pharmaceutical Research, 14, 1, 56–62.

Banks, S.L., Pinninti, R.R., Gill, H.S., Crooks, P.A., Prausnitz, M.R., Stinchcomb, A.L. (2008) Flux across microneedle-treated skin is increased by increasing charge of naltrexone and naltrexol in vitro. Pharmaceutical Research, 25(7), 1677-1685.

Barbero, A.M., Frasch, H.F. (2005) Modeling of diffusion with partitioning in stratum corneum using a finite element model. Ann. Biomed. Eng., 33(9), 1281–1292.

Barbero, A.M., Frasch, H.F. (2005) Modeling of diffusion with partitioning in stratum corneum using a finite element model. Ann. Biomed. Eng., 33(9), 1281–1292.

Barker, D.E. (1951) Skin thickness in the human. Plast. Reconstr. Surg., 7, 115-116.

Barry, B.W. (2001) Novel mechanisms and devices to enable successful transdermal drug delivery. Eur. J. Pharm. Sci., 14, 101-114.

Becker, S.M., Kuznetsov, A.V. (2008) Thermal in vivo skin electroporation pore development and charged macromolecule transdermal delivery: A numerical study of the influence of chemically enhanced lower lipid phase transition temperatures. International Journal of Heat and Mass Transfer, 51, 2060–2074.

Bertera, F.M., Mayer, M.A., Opezzo, J.A.W., Taira, C.A., Hocht, C. (2008) Comparison of different pharmacodynamic models for PK-PD modeling of verapamil in renovascular hypertension. Journal of Pharmacological and Toxicological Methods, 57, 212-219.

Blank, I.H. (1964) Penetration of low-molecular-weight alcohols into skin. I. Effect of concentration of alcohol and type of vehicle. J. Invest. Dermatol., 43, 415-420.

Blank, I.H., Scheuplein, R.J. (1969) Transport into and within skin. Br. J. Derm., 81 (supplement 4), 4-10.

Bloom, W., Fawcett, D.W. (1975) A textbook of histology, 10th edn. Lippincott, Philadelphia, 563-594.

Biocom system, Inc. (2006) SKIN-CAD®. Simulator for skin pharmacokinetics. Biocom system, Inc., Fukuoka, Japan.

Boderke P., Schittkowski K., Wolf M., Merkle H. P. (2000) Modeling of diffusion and concurrent metabolism in cutaneous tissue. Journal of Theoretical Biology, 204, 393-407.

Bommannan, D., Potts, R.O., Guy, R.H. (1990) Examination of the stratum corneum barrier functions in vivo by infrared spectroscopy. J. Invest. Dermatol., 95, 403-408.

Bosman, I. J. (1996) Transdermal delivery of anticholinergic bronchodilators: methodological and clinical aspects. Dissertation, University of Groningen, Netherlands.

Braybrook, J.H. (1997) Biocompatibility: Assessment of Medical Devices and Materials, Wiley, New York.

Buckingham, E. (1914) On physically similar systems: illustrations of the use of dimensional equations. Phys. Rev., 4, 345-376.

Capes, S.E., Hunt, D., Malmberg, K., Pathak, P., Gerstein, H.C. Stress hyperglycemia and prognosis of stroke in nondiabetic and diabetic patients. Stroke, 32, 2426-2432.

Chabri, F., Bouris, K., Jones, T., Barrow, D., Hann, A., Allender, C., Brain, K., Birchall, J. Microfabricated silicon microneedles for nonviral cutaneous gene delivery. Br. J. Dermatol., 150(5), 869–877.

Chakraborty, S., Tsuchiya, K. (2008) Development and fluidic simulation of microneedles for painless pathological interfacing with living systems. Journal of Applied Physics, 103, 114701-1–114701-9.

Chen, B., Wei, J., Tay, F.E.H., Wong, Y.T., Iliescu, C. (2008) Silicon microneedle array with biodegradable tips for transdermal drug delivery. Microsystem Technologies, 14(7), 1015-1019.

Choi, J.W., Park, I.B., Ha, Y.M., Jung, M.G., Lee, S.W. and Lee, S.H. (2006) Insertion force estimation of various microneedle array-type structures fabricated by a Microstereolithography Apparatus, In: Proceedings of International Joint Conference, October 18-21, Bexco, Pusan, Korea.

Choi, D.H., Shin, W.G., Choi, J.S. (2008) Drug interaction between oral atorvastatin and verapamil in healthy subjects: effects of atorvastatin on the pharmacokinetics of verapamil and norverapamil. European Journal of Clinical Pharmacology, 64(5), 445-449.

Comsol, A.B. (2005) FEMLAB® 3 multiphysics modelling, Documentation, Comsol AB., Stockholm, Sweden.

Cormier, M., Johnson, B., Ameri, M., Nyam, K., Libiran, L., Zhang, D.D., Daddona, P. (2004) Transdermal delivery of desmopressin using a coated microneedle array patch system. Journal of Controlled Release, 97, 503-511.

Coulman, S.A., Anstey, A., Gateley, C., Morrissey, A., McLoughlin, P., Allender, C., Birchall, J.C. (2009) Microneedle mediated delivery of nanoparticles into human skin. International Journal of Pharmaceutics, 366, 190–200.

Crank, J. (1979) The mathematical of diffusion. 2nd edition, Oxford University Press, Oxford.

Cross, S.E., Roberts, M.S. (1993) Subcutaneous absorption kinetics of interferon and other solutes. J. Pharm. Pharmacol., 45, 606-609.

Cross, S.E., Roberts, M.S. (2004) Physical enhancement of transdermal drug application: Is delivery technology keeping up with pharmaceutical development?. Current Drug Delivery, 1, 81-91.

Davidson, A., Al-Qallaf, B., Das, D.B. (2008). Transdermal drug delivery by coated microneedles: geometry effects on effective skin thickness and drug permeability. Chemical Engineering Research and Design, 86, 1196-1206.

Davis, S.P. (2003) Hollow microneedles for molecular transport across skin. Ph.D. thesis, Georgia Institute of Technology, USA.

Davis, S.P., Landis, B.J., Adams, Z.H., Allen, M.G., Prausnitz, M.R. (2004) Insertion of microneedles into skin: measurement and prediction of insertion force and needle fracture force. Journal of Biomechanics, 37, 1155-1163.

Davis, S.P., Martanto, W., Allen, M.G., Prausnitz, M.R. (2005) Hollow metal microneedles for insulin delivery to diabetic rats. IEEE T. Bio-med Eng., 52, 909-915.

Dean, C.H., Alarcon, J.B., Waterston, A.M., Draper, K., Early, R., Guirakhoo, F., Monath, T.P., Mikszta, J.A. (2005) Cutaneous delivery of a live, attenuated chimeric flavivirus vaccine against Japanese encephalitis (ChimeriVax)-JE) in non-human primates, Hum. Vaccin., 1(3), 106–111.

De Rigal, J., Escoffier, C., Querleux, B., Faivre, B., Agache, P., Leveque, J.L. (1989) Assessment of aging of the human skin by in vivo ultrasonic imaging. J. Invest. Dermatol., 93, 621-625.

Diehl, K.H., Hull, R., Morton, D., Pfister, R., Rabemampianina, Y., Smith, D., Vidal, J.M., Vorstenbosch, C. (2001) A good practice guide to the administration of a substances and removal of blood, including routes and volumes. Journal of Applied Toxicology, 21, 15-23.

Diridollou, S., Vabre, V., Berson, M., Viallant, L., Black, D., Lagarde, J.M., Gregoire, J.M., Gall, Y., Patat, F. (2001) Skin ageing: changes of physical properties of human skin in vivo. Int. J. Cosmet. Sci., 23, 353-362.

Donnelly, R.F., Morrow, D.I.J., McCarron, P.A., Woolfson, A.D., Morrissey, A., Juzenas, P., Juzeniene, A., Lani, V., McCarthy, H.O., Moan, J. (2009) Microneedle arrays permit enhanced intradermal delivery of a preformed photosensitizer. Photochemistry and Photobiology, 85, 195-204.

Eichelbaum, M., Somogyi, A., Unruh, G.E.V., Dengler, H.J. (1981) Simultaneous determination of the intravenous and oral pharmacokinetic parameters of D,L-verapamil using stable isotope-labelled verapamil. European Journal of Clinical Pharmacology, 19(2), 133-137.

Environmental Protection Agency. (1992) Risk assessment forum. Guidelines for exposure assessment (FRL-41295-5).Washington, DC. http://www.epa.gov/NCEA/raf/PDFs/exposure.pdf.

Escoffier, C., De Rigal, J., Rochefort, A.,Vasselet, R., Leveque, J.L., Agache, P.G. (1980) Age-related mechanical properties of human skin: an in vivo study. J. Invest. Dermatol., 93, 353-357.

Farahmand, S., Maibach, H.I. (2009) Transdermal drug pharmacokinetics in man: Interindividual variability and partial prediction. International Journal of Pharmaceutics, 367, 1–15.

Feldmann, R.J., Maibach, H.I. (1967) Regional variation in percutaneous penetration of ^{14}C Cortisol in man. J. Invest. Dermatol., 48(2), 181-183.

Fenske, N.A., Lober, C.W. (1986) Structural and functional changes of normal aging skin. J. Am. Acad. Dermatol., 48, 571-585.

Fernandez, L.J., Altuna, A., Tijero, M., Gabriel, G., Villa, R., Rodriguez, M.J., Batlle, M., Vilares, R., Berganzo, J., Blanco, F.J. (2009) Study of functional viability of SU-8-based microneedles for neural applications. J. Micromech. Microeng., 19, doi:10.1088/0960-1317/19/2/025007.

Foreman, M.I., Kelly, I. (1976) The diffusion of nandrolone through hydrated human cadaver skin. Br. J. Dermatol., 95, 265–270.

Fylstra, D., Lasdon, L., Watson, J. (1998) Design and use of the microsoft excel solver. Interfaces, 28(5), 29-55.

Ghanem, A.H., Mahmoud, H., Higuchi, W.I. (1992) The effects of ethanol on the transport lipophilic and polar permeants across hairless mouse skin. Methods/validation of a novel approach. Int. J. Pharm., 78, 137-156.

Gardeniers, H.J.G.E, Luttge, R., Berenschot, E.J.W., de Boer, M.J., Yeshurun, S.Y., Hefetz, M., van't Oever, R., van den Berg, A. (2003) Silicon micromachined hollow microneedles for transdermal liquid transport. J. MEMS, 12, 855-862.

Gass, M.L.S., Bassuk, S.S., Manson, J.A.E. (2009) Reassessing benefits and risks of hormone therapy. American Journal of Lifestyle Medicine, 3, 29-43.

George, K., Kubota, K., Twizell, E.H. (2004) A two-dimensional mathematical model of percutaneous drug absorption. Biomed. Eng. Online, 3, 18.

Gill, H.S., Prausnitz, M.R. (2007) Coated microneedles for transdermal delivery. Journal of Controlled Release, 117, 227-237.

Gniadecka, M., Jemec, G.B.E. (1998) Quantitative evaluation of chronological ageing and photoageing in vivo: studies on skin echogenicity and thickness. Br. J. Dermatol., 139, 815-821.

Gniadecka, M., Gniadecki, R., Serup, J. Sondergaard, J. (1994) Ultrasound structure and digital image analysis of the subepidermal low echogenic band in aged human skin: diurnal changes and interindividual variability. J. Invest. Dermatol., 102, 362-365.

Gniadecka, M., Jemec, G.B.E. (1998) Quantitative evaluation of chronological ageing and photoageing in vivo: studies on skin echogenicity and thickness. Br. J. Dermatol., 139, 815-821.

Godin, B.S., Touitou, E. (2007) Transdermal skin delivery: Predictions for humans from in vivo, ex vivo and animal models. Advanced Drug Delivery Reviews, 59(11), 1152-1161.

Golla, S., Neely, B.J., Whitebay, E., Madihally, S.V., Robinson, R.L.JR., Gasem, K.A. (2009) Virtual design of chemical penetration enhancers for transdermal drug delivery. Journal of Pharmaceutical Sciences, doi:10.1002/jps.21681.

Goyal, A., Mandapurama, S., Michniak, B., Simona, L. (2007) Application of orthogonal collocation and regression techniques for recovering parameters of a two-pathway transdermal drug-delivery model. Computers and Chemical Engineering, 31, 107-120.

Griss, P., Stemme, G. (2003) Side-opened out-of-plane microneedles for microfluidic transdermal liquid transfer. Journal of Microelectromechanical Systems, 12(3), 296–301.

Gui, L., Liu, J. (2005) Study on the heat and fluid transport inside the biological tissues subject to boiling saline-based tumor hyperthermic injection. Heat Transfer Engineering, 26, 73-84.

Gupta, S.K., Southam, M., Gale, R., Huang, S.S. (1992) System functionality and physicochemical model of Fentanyl transdermal system. J. Pain symptom Manage., 7, S17-S26.

Guy, R., Hadgraft, J., Maibach, H. (1982) A pharmacokinetic model for percutaneous absorption. Int. J. Pharm., 11, 119–129.

Hadgraft, J. (1980) Theoretical aspects of metabolism in the epidermis. International Journal of Pharmaceutics, 4, 229-239.

Hallow, D.M., Seeger, R.A., Kamaev, P.P., Prado, G.R., LaPlaca, M.C., Prausnitz, M.R. (2008) Shear-induced intracellular loading of cells with molecules by controlled microfluidics. Biotechnology and Bioengineering, 99(4), 846-854.

Haider, I., Pettis, R.J., Davison, N., Clarke, R., Zahn, J.D. (2001) Biomedical and fluid flow characterization of microneedle-based drug delivery devices. In Proceedings of the 25th Annual Meeting of the American Society of Biomechanics, August, San Diego, California, USA (Abstract).

Han, Z., Liu, K.J.R. (2008) Resource allocation for wireless networks; Basics, technique, and applications. Cambridge university press, UK.

Han, M., Hyun, D.H., Park, H.H., Lee, S.S.L., Kim, C.H., Kim, C.G. (2007) A novel fabrication process for out-of-plane microneedle sheets of biocompatible polymer. J. Micromech. Microeng., 17, 1184-1191.

Hansen, R.N. (2004) Glucose Homeostasis. A Biosimulation Approach, Technical University of Denmark, Copenhagen.

Haq, M.I., Smith, E., John, D.N., Kalavala, M., Edwards, C., Anstey, A., Morrissey, A., Birchall, J.C. (2009) Clinical administration of microneedles: skin puncture, pain and sensation. Biomed Microdevices, 11, 35–47.

Hashida, M., Okamoto, H., Sezaki, H. (1988) Analysis of drug penetration through skin considering donor concentration decrease. Journal of Pharmacobio-Dynamics, 11(9), 636–644.

Hashmi, S., Ling, P., Hashmi, G., Reed, M., Gaugler, R., Trimmer, W. (1995) Genetic transformation of nematodes using arrays of micromechanical piercing structures, Bio. Techniques, 19, 766-770.

He, N., Warner, K.S., Higuchi, W.I., Li, S.K. (2005) Model analysis of flux enhancement across hairless mouse skin induced by chemical permeation enhancers. International Journal of Pharmaceutics, 297, 9-21.

Henry, S., McAllister, D.V., Allen, M.G., Prausnitz, M. R. (1998) Microfabrication microneedles: A novel approach to transdermal drug delivery. J. Pharm. Sci., 87(8), 922-925.

Hewitt, G.F. (1990) Hemisphere handbook of hear exchanger design. Hemisphere, New York.

Higuchi, W.I., Gordon, N.A., Fox, J.L., Ho, N.F.H. (1983) Transdermal delivery of prodrugs. Drug Development and Industrial Pharmacy, 9(4), 691-706.

Hikima, T., Maibach, H.I., Tojo, K. (2006) Skin enzymes distribution in transdermal drug delivery. The Annual AIChE Meeting, San Francisco, USA.

Hoffmann, K., Dirschka, T.P., Stucker, M., el-Gammal, S., Altmeyer, P. (1994) Assessment of actinic skin damage by 20 MHz sonography. Photodermatol. Photoimmunol. Photomed., 10, 97-101.

Holbrook, K.A. (1994) Ultrastructure of the Epidermis: Chapter 1 of the Keratinocyte Handbook, edited by Leigh, I.M. and Lane, E.B., Watt, F.M., Cambridge, Great Britain, Cambridge University Press, 3–39.

Howard, A., Mercer, P., Nataraj, H.C., Kang, B.C. (1997) Bevel-down superior to bevel-up in intradermal skin testing. Ann. Allergy Asthma Immunol., 78, 594–596.

Hsu, C.C., Chen, Y.T., Tsai, C.H., Kang, S.W. (2007) Fabrication of microneedles, In: Proceedings of the 2nd IEEE International Conference on Nano/Micro Engineered and Molecular Systems, January 16-19, Bangkok, Thailand.

Huang, H., Fu, C. (2007) Different fabrication methods of out-of-plane polymer hollow needle arrays and their variations. J. Micromech. Microeng., 17, 393-402.

http://www.pharmpress.com/shop/samples/T&T-ch1.pdf.

Isowaki, A., Ohtori, A., Matsuo, Y., Tojo, K. (2003) Drug delivery to the eye with a transdermal therapeutic system. Biol. Pharm. Bull., 26(1), 69-72.

Ito, Y., Hagiwara, E., Saeki, A., Sugioka, N. and Takada, K. (2006) Feasibility of microneedles for percutaneous absorption of insulin. European Journal of Pharmaceutical Science, 29, 82-88.

Izumi, H., Aoyagi, S. (2007) Novel fabrication method for long silicon microneedles with three-dimensional sharp tips and complicated shank shapes by isotropic dry etching. Transactions on Electrical and Electronic Engineering IEEJ Trans, 2, 328-334.

Ji, J., Tay, F.E.H., Miao, J. (2006) Microfabricated silicon microneedle array for transdermal drug delivery. Journal of Physics, Conference Series, 34, 1127–1131.

Jiang, J. (2006). Ocular drug delivery using microneedles. Ph.D. thesis. Georgia Institute of Technology, USA.

Jiang, J., Gill, H.S., Ghate, D., McCarey, B.E., Patel, S.R., Edelhauser, H.F., Prausnitz, M.R. (2007) Coated Microneedles for Drug Delivery to the Eye. Investigative Ophthalmology & Visual Science, 48(9), 4038-4043.

Jiang, J., Moore, J.S., Edelhauser, H.F., Prausnitz, M.R. (2009) Intrascleral drug delivery to the eye using hollow microneedles. Pharmaceutical Research, 26(2), 395-403.

Johnson, J.A. (1997) Influence of race or ethnicity on pharmacokinetics of drug. J. Pharm. Sci., 86(12), 1328-1333.

Joshi, A., Raje, J. (2002) Sonicated transdermal drug transport. Journal of Controlled Release, 83, 13–22.

Kalia, Y.N., Guy, R.H. (2001) Modeling transdermal drug release. Ad. Drug Del. Rev., 48, 159-172.

Kalia, N.Y., Naik, A., Garrison, J., Guy, R.H. (2004) Iontophoretic drug delivery. Adv. Drug Deliv. Rev., 56, 619-658.

Kargahi, M., Anderson, J.C., Dessouky, M.M. (2006) Structural weight optimization of frames using tabu search I: Optimization procedure. Journal of Structural Engineering, 132(12), 1858-1868.

Kaushik, S., Hord, A.H., Denson, D.D., McAllister, D.V., Smitra, S., Allen, M.G., Prausnitz, M.R. (2001) Lack of pain associated with microfabricated microneedles. Anesthesia and Analgesia, 92, 502–504.

Khumpuang, S., Horade, M., Fujioka K., Sugiyama, S. (2005) Through-hole microneedle fabricated by alignment x-ray lithography. Memoirs of the SR Center Ritsumeikan University, No. 7, April, pp.25-30, Japan.

Khumpuang, S., Horade, M., Fujioka K., Sugiyama, S. (2006) Microneedle fabrication using the plane pattern to cross-section transfer method. Smart Mater. Struct., 15, 600-606.

Khumpuang, S., Horade, M., Fujioka K., Kazuya, F., Sugiyama, S. (2007) Geometrical strengthening and tip-sharpening of a microneedle array fabricated by X-ray lithography. Microsyst. Technol., 13, 209-214.

Kielhorn, J., Kollmuß, S.M., Mangelsdorf, I. (2005) International programme on chemical safety environmental health criteria: Dermal absorption. United nations environment programme, International labour organization, World health organization.

Kim, Y.H., Ghanem, A.H., Higuchi, W.I. (1992) Model studies of epidermal permeability. Seminars in Dermatology, 11(2), 145-156.

Kim, K., Lee, J.B. (2007) High aspect ratio tapered hollow metallic microneedle arrays with microfluidic interconnector. Microsystem Technologies, 13, 231-235.

Kimura, C., Tojo, K. (2007) Development of a stick-type transdermal eyelid delivery system of ketotifen fumarate for ophthalmic diseases. Chem. Pharm. Bull., 55(7), 1002-1005.

Kiptoo, P. K., Hamad, M.O., Crooks, P. A., Stinchcomb, A.L. (2006) Enhancement of transdermal delivery of 6-β-naltrexol via a codrug linked to hydroxybupropion. Journal of controlled release, 113:137-145.

Koike, Y., Shimamura, K., Shudo, I., Saito, H. (1979) Pharmacokinetics of verapamil in man. Research Communications in Chemical Pathology and Pharmacology, 24(1), 37-47.

Kolli, C.S., Banga, A.K. (2008) Characterization of solid maltose microneedles and their use for transdermal delivery. Pharmaceutical Research, 25(1), 104-113.

Korinth, G., Schaller, K.H., Drexler, H. (2005) Is the permeability coefficient K_p a reliable tool in Percutaneous absorption studies?. Arch. Tixicol., 79, 155-159.

Koutsonanos, D.G., del Pilar Martin, M., Zarnitsyn, V.G., Sullivan, S.P., Compans, R.W., Prausnitz, M.R., Skountzou, I. (2009) Transdermal influenza immunization with vaccine-coated microneedle arrays. PLoS ONE, 4(3), e4773, doi:10.1371/journal.pone.0004773.

Kraegen, E., Chisholm, D. (1984) Insulin responses to varying profiles of subcutaneous insulin infusion: kinetic modelling studies. Diabetologia, 26(3), 208–213.

Kubota, K., Dey, F., Matar, S., Twizell, E. (2002) A repeated-dose model of percutaneous drug absorption. Appl. Math. Model., 26, 529–544.

Lad, J. (2007). Clinical evaluation of a novel microneedle patch. M.Sc. thesis. Cranfield University, UK.

Lambert, P.H., Laurent, P.E. (2008) Intradermal vaccine delivery: Will new delivery systems transform vaccine administration?. Vaccine, 26, 3197–3208.

Lanke, S.S.S., Kolli, C.S., Strom, J.G., Banga, A.K. (2009) Enhanced transdermal delivery of low molecular weight heparin by barrier perturbation. International Journal of Pharmaceutics, 365, 26–33.

Lee, V.H.L. (1988) Peptide and protein drug delivery systems. Biopharm. Manuf., 1, 24-31.

Lee, A.J., King, J.R., Rogers, T.G. (1996) A multiple-pathway model for the diffusion of drugs in skin. IMA Journal of Mathematics Applied in Medicine & Biology, 13(2), 127-150.

Lee, Y., Hwang, K. (2002) Skin thickness of Korean adults. Surg. Radiol. Anat., 24, 183-189.

Lee, J.W., Park, J.H., Prausnitz, M.R. (2008). Dissolving microneedles for transdermal drug delivery. Biomaterials, 29(13), 2113-2124.

Li, G., Badkar, A., Nema, S., Kolli, C.S., Banga, A.K. (2009) In vitro transdermal delivery of therapeutic antibodies using maltose microneedles. International Journal of Pharmaceutics, 368(1-2), 109-115.

Lipscomb, J., Poet, T.S. (2008) In vitro measurements of metabolism for application in pharmacokinetic modeling. Pharmacology & Therapeutics, 118, 82-103.

Liu, P., Higuchi, W.I., Ghanem, A.H., Bergstrom, T.K., Good, W.R. (1990) Quantitation of simultaneous diffusion and metabolism of β-estradiol in hairless mouse skin: Enzyme distribution and intrinsic diffusion/metabolism parameters. International journal of Pharmaceutics, 64, 7-25.

Lundh, T., Boman, A., Akesson, B. (1997) Skin absorption of the industrial catalyst dimethylethylamine in vitro in guinea pig and human skin and of gaseous dimethylethylamine in human volunteers. Int. Arch. Occup. Environ. Health., 70, 309-313.

Lv, Y.G., Lie, J., Xu, B. (2006) Modeling of transdermal drug delivery with a microneedle array. J. Micromech. Microeng., 16, 2492-2501.

Martanto, W., Davis, S.P., Holiday, N.R., Wang, J., Gill, H.S., Prausnitz, M.R. (2004) Transdermal delivery of insulin using microneedles in vivo. Pharmaceutical Research, 21, 947-952.

Martanto, W., Moore, J.S., Couse, T., Prausnitz, M.R. (2006) Mechanism of fluid infusion during microneedle insertion and retraction. Journal of Controlled Release, 112, 357-361.

Martin, R.J., Denyer, S.P., Hadgraft, J. (1987) Skin metabolism of topically applied compounds. Int. J. Pharm., 39, 23-32.

Matriano, J.A., Cormier, M., Johnson, J., Young, W.A., Buttery, M., Nyam, K., Daddona, P.E. (2002) Macroflux microprojection array patch technology: a new and efficient approach for intracutaneous immunization. Pharm. Res., 19, 63-70.

Matteucci, M., Fanetti, M., Casella, M., Gramatica, F., Gavioli, L., Tormen, M., Grenci, G., De Angelis, F., Di Fabrizio, E. (2009) Poly vinyl alcohol re-usable masters for microneedle replication. Microelectronic Engineering, doi:10.1016/j.mee.2009.01.068.

McAllister, D.V., Allen, M.G., Prausnitz, M.R. (2000) Microfabricated microneedles for gene and drug delivery. Annu. Rev. Biomed. Eng., 2, 289 –313.

McAllister, D.V., Wang, P.M., Davis, S.P., Park J.H., Canatella, P.J., Allen, M.G., Prausnitz, M.R. (2003) Microfabricated needles for transdermal delivery of macromolecules and nanoparticles: fabrication methods and transport studies. PNAS, 100, 13755–13760.

McCarley, K.D., Bunge, A.L. (2001) Pharmacokinetics models of dermal absorption. J. Pharm. Sci., 90(11), 1699-1719.

Meidan, V.M., Michniak, B.B. (2004) Emerging technologies in transdermal therapeutics. Am. J. Ther., 11, 312-316.

Membrino, M.A., (2002). Transdermal delivery of therapeutic compounds by inotophoresis. Ph.D. thesis. University of Florida, USA.

Michaels, A.S., Chandrasekaran, S.K., Shaw, J.E. (1975) Drug permeation through human skin: theory and in vitro experimental measurement. AIChE J., 21, 985-996.

Michel, T., Brunton, L.L., Lazo, J.S., Pharker, K.C. Eds. (2006) Treatment of myocardial ischemia, The pharmacological basics of therapeutics, Goodman & Gilmans, McGraw-Hill, New York, 11th ed.

Mikszta, J.A., Alarcon, J.B., Brittingham, J.M., Sutter, D.E., Pettis, R.J., Harvey, N.G. (2002) Improved genetic immunization via micromechanical disruption of skin-barrier function and targeted epidermal delivery. Nat. Med., 8, 415-419.

Mikszta, A., Sullivan, V.J., Dean, C., Waterston, A.M., Alarcon, J.B., Dekker, J.P. 3rd, Brittingham, J.M., Huang, J., Hwang, C.R., Ferriter, M., Jiang, G., Mar, K., Saikh, K.U., Stiles, B.G., Roy, C.J., Ulrich, R.G., Harvey, N.G. (2005) Protective immunization against inhalational anthrax: a comparison of minimally invasive delivery platforms. J. Infect. Dis., 191(2), 278–288.

Mitragotri, S., Coleman, M., Kost, J. Langer, R. (2000) Transdermal extraction of analytes using low-frequency ultrasound. Pharm. Res., 17, 466-470.

Miyano, T., Tobinaga, Y., Kanno, T., Matsuzaki, Y., Takeda, H., Wakui, M., Hanada, K. (2005) Sugar micro needles as transdermic drug delivery systems. Biomed. Microdevices, 7, 185-188.

Moon, S.J., Lee, S.S. (2003) Fabrication of microneedle array using inclined LIGA process. In Proceedings of the 12th International Conference on Solid-State Sensors, Actuators and Microsystems, Boston, USA, June 8-12, pp. 1546-1549.

Mori, D., Kawamata, H., Tojo, K. (2003) Drug concentration-time profile in the plasma following the dissolution-type transdermal delivery. J. Chem. Eng. Japan, 36(1), 45-48.

Morrissey, A., Wilke, N., Coulman, S.A., Pearton, M., Anstey, A., Gateley, C., Allender, C., Brain, K., Birchall, J.C. (2005) Determination of mechanical properties of silicon and polymer microneedles. In Proceedings the 3rd European Medical and Biological Engineering Conference (EMBEC 05), November 20-25, Prague, Czech Republic.

Mukerjee, E.V., Collins, S.D., Issroff, R.R., Smith, R.L. (2004) Microneedle array for transdermal biological fluid extraction and in situ analysis. Sensors and Actuators A: Physical, 114(2-3), 267-275.

Naegel, A., Hansen, S., Neumann, D., Lehr, C.M., Schaefer, U.F., Wittum, G., Heisig, M. (2008) In-silico model of skin penetration based on experimentally determined input parameters. Part II: Mathematical modelling of in-vitro diffusion experiments. Identification of critical input parameters. European Journal of Pharmaceutics and Biopharmaceutics, 68, 368–379.

Naik, A., Kalia, Y.N., Guy, R.H. (2000) Transdermal drug delivery: overcoming the skin's barrier function. Pharm. Sci. Technol. Today, 3, 318-326.

Nair, A., Reddy, C., Jacob, S. (2009) Delivery of a classical antihypertensive agent through the skin by chemical enhancers and iontophoresis. Skin Research and Technology, doi:10.1111/j.1600-0846.2009.00350.x.

Nicholson, B. (2009) Benefits of extended-release opioid analgesic formulations in the treatment of chronic pain. Pain Practice, 9(1), 71–81.

Nishimura, Y., Lemasters, J.J. (2001) Glycine blocks opening of a death channel in cultured hepatic sinusoidal endothelial cells during chemical hypoxia. Cell Death & Differentiation, 8, 850-858.

Nomeir, A.A., Morrison, R., Prelusky, D., Korfmacher, W., Broske, L., Hesk, D., Mcnamara, P., Mei, H. (2009) Estimation of the extent of oral absorption in animals from oral and intravenous pharmacokinetic data in drug discovery. Journal of Pharmaceutical Sciences, doi:10.1002/jps.21705.

Nordquist, L., Roxhed, N., Griss, P., Stemme, G. (2007) Novel microneedle patches for active insulin delivery are efficient in maintaining clycaemic control: An initial comparison with subcutaneous administration. Pharmaceutical Research, 2007, 24(7), 1381-1388.

Oh, J.H., Park, H.H., Do, K.Y., Han, M., Hyun, D.H., Kim, C.G., Kim, C.H., Lee, S.S., Hwang, S.J., Shin, S.C., Cho, C.W. (2008) Influence of the delivery systems using a

microneedle array on the permeation of a hydrophilic molecule, calcein. European Journal of Pharmaceutics and Biopharmaceutics, 69(3), 1040-1045.

Okamoto, H., Hashida, M., Sezaki, H. (1988) Structure–activity relationship of 1-alkyl or 1-alkenylazacycloalkanone derivatives as percutaneous penetration enhancers. Journal of Pharmaceutical Sciences, 77(5), 418–424.

Okamoto, H., Yamashita, F., Saito, K., Hashida, M. (1989) Analysis of drug penetration through the skin by the two-layer skin model. Pharmaceutical Research, 6(11), 931–937.

O'Riordan, E., Shishkin, G.I. (2008) Parameter uniform numerical methods for singularly perturbed elliptic problems with parabolic boundary layers. Applied Numerical Mathematics, 58, 1761-1772.

Ovsianikov, A., Chichkov, B. (2007) Two photon polymerization of polymer–ceramic hybrid materials for transdermal drug delivery. International Journal of Applied Ceramic Technology, 4(1), 22-29.

Paik, S.J., Byun, S., Lim, J.M., Park, Y., Lee, A., Chung, S., Chang, J., Chun, K., Cho, D. (2004) In-plane single-crystal-silicon microneedles for minimally invasive microfluid systems. Sensors and Actuators A: Physical, 114(2-3), 276-284.

Panchagnula, R. (1997) Transdermal delivery of drugs. Indian Journal of Pharmacology, 29(3), 140–156.

Papa, J., Marton, S., Suvegh, K., Zelko, R. (2009) The influence of metolose structure on the free volume and the consequent metoprolol tartrate release of patches. International Journal of Biological Macromolecules, 44, 6-8.

Park, J.H. (2004) Polymeric microneedles for transdermal drug delivery. Ph.D. thesis, Georgia Institute of Technology, USA.

Park, J.H., Yoon, Y.K., Prausnitz, M.R., Allen, M.G. (2004) High-aspect-ratio tapered structures using an integrated lens technique. In Proceedings of the 17th IEEE International Conference on Micro Electro Mechanical Systems, Maastricht, Netherlands, 383-386.

Park, J.H., Allen, M.G., Prausnitz, M.R. (2005) Biodegradable polymer microneedles: fabrication, mechanics and transdermal drug delivery. Journal of Controlled Release, 104, 51-66.

Park, J.H., Allen, M.G., Prausnitz, M.R. (2006) Polymer microneedles for controlled-release drug delivery. Pharm. Res., 23, 1008-1019.

Park, J.H., Yoon, Y.K., Choi, S.O., Prausnitz, M.R., Allen, M.G. (2007) Tapered conical polymer microneedles fabricated using an integrated lens technique for transdermal drug delivery. IEEE Transactions on Biomedical Engineering, 54(5), 903-913.

Park, J.H., Lee, J.W., Kim, Y.C., Prausnitz, M.R. (2008) The effect of heat on skin permeability. International Journal of Pharmaceutics, 359, 94-103.

Parker, E.R., Rao, M.P., Turner K.L., Meinhart, C.D., MacDonald, N.C. (2007) Bulk micromachined titanium microneedles. Journal of Microelectromechanical System, 16(2), 289-295.

Pavšelj, N., Miklavčič, D. Numerical modeling in electroporation-based biomedical applications. Radiology and Oncology, 42(3), 159-168.

Pearton, M., Allender, C., Brain, K., Anstey, A., Gateley, C., Wilke, N., Morrissey, A., Birchall, J., (2007). Gene delivery to the epidermal cells of human skin explants using microfabricated microneedles and hydrogel formulations. Pharmaceutical Research, 25(2), 407-416.

Perennes, F., Marmiroli, B., Matteucci, M., Tormen, M., Vaccari, L., Fabrizio, E.D. (2006) Sharp beveled tip hollow microneedle arrays fabricated by LIGA and 3D soft lithography with polyvinyl alcohol. J. Micromech. Microeng., 16, 473-479.

Perry, R.H., Green, D.W., Maloney, J.O. (1984) Perry's chemical engineers' handbook. 6th Edition, McGraw-Hill, New York.

Poet, T.S., McDougal, J.N. (2002) Skin absorption and human risk assessment. Chem. Biol. Interact., 140, 19-34.

Potts, R.O., McNeill, S.C., Desbonnet, C.R., Wakshull, E. (1989) Transdermal drug transport and metabolism.II. The role of competing kinetic events. Pharmaceutical Research, 6(2), 119-124.

Power, I., McCormack, J.G. (2008) Advances in patient-controlled analgesia: the role of fentanyl ITS. Medical Devices: Evidence and Research, 1, 49–57.

Prausnitz, M.R. (2004) Microneedles for transdermal drug delivery. Adv. Drug Deliver. Rev., 56, 581-587.

Prausnitz, M.R., Mitragotri, S., Langer, R. (2004) Current status and future potential of transdermal drug delivery. Nature Reviews, 3, 115-124.

Prodduturi, S., Smith, G.J., Wokovich, A.M., Doub, W.H., Westenberger, B.J., Buhse, L. (2009) Reservoir based fentanyl transdermal drug delivery systems: Effect of patch age on drug release and skin permeation. Pharmaceutical Research, 26(6), 1344-1352.

Rajaraman, S., Henderson, H.T. (2005) A unique fabrication approach for microneedles using coherent porous silicon technology. Sensors and Actuators B, 105, 443-448.

Ranade, V.V. (1991) Drug delivery systems.6. Transdermal drug delivery. J. Clin. Pharmacol., 31, 401-418.

Ratner, B.D., Hoffman, A.S., Schoen, F.J., Lemons, J.E. (1996) Biomaterials Science: An Introduction to Materials in Medicine, Academic Press, New York.

Rawlings, A.V. (2006) Ethnic skin types: Are there differences in skin structure and function?. Int. J. Cosmet. Sci., 28, 79-93.

Reddy, M.B., McCarley, K.D., Bunge, A.L. (1998) Physiologically relevant one-compartment pharmacokinetic models for skin. 2. Comparison of models when combined with a systemic pharmacokinetic model. J. Pharm. Sci., 87(4), 482–490.

Reed, M.L., Lye, W.K. (2004) Microsystems for drug and gene delivery. Proceedings of the IEEE, 92(1), 56-75.

Rein H. (1924) Experimental electroendosmotic studies on living human skin. Z. Biol., 81,124.

Richard, S., De Rigal, J., Lacharriere, O., Berardesca, E., Leveque, J.L. (1994) Noninvasive measurement of the effect of lifetime exposure to the sun on the aged skin. Photodermatol. Photoimmunol. Photomed., 10, 164-169.

Ritschel, W.A., Hussain, A.S. (1988) The principles of percutaneous absorption of substances across the skin. Meth. And Find Exptl. Clin. Pharmacol., 10(1), 39-56.

Roberts, M.S., Lai, P.M., Cross, S.E., Yoshida, N.H. (1997) In: Mechanisms of transdermal drug delivery. Marcel Dekker, New York, 291-349.

Rodriguez, A., Molinero, D., Valera, E., Trifonov, T., Marsal, L.F., Pallares, J., Alcubilla, R. (2005) Fabrication of silicon oxide microneedles from macroporous silicon. Sensors and Actuators B, 109, 135-140.

Rougier, A., Lotte, C., Maibach, H.I. (1987) In vivo percutaneous penetration of some organic compound related to anatomical site in humans: predictive assessment by the stripping method. J. Pharm. Sci., 76(6), 451-454.

Roxhed, N. (2007). A fully intergrated microneedle-based transdermal drug delivery system. Ph.D. thesis. Royal Institute of Technology, Stockholm, Sweden.

Roxhed, N., Gasser, T.C., Griss, P. (2007) Penetration-enhanced ultrasharp microneedles and prediction on skin interaction for efficient transdermal drug delivery. Journal of Microelectromechanical Systems, 16(6), 1429-1440.

Roxhed, N., Griss, P., Stemme, G. (2008) Membrane-sealed hollow microneedles and related administration schemes for transdermal drug delivery. Biomed. Microdevices, 10, 271–279.

Rudman, D., Feller, A.G., Nagraj, H.S., Gergans, G.A., Lalitha, P.Y., Goldberg, A.F., Schlenker, R.A., Cohn, L., Rudman, I.W., Mattson, D.E. (1990) Effects of human growth hormone in men over 60 years old. The New England Journal of Medicine, 323, 1-6.

Rudolph, R., Fisher, J.C., Ninnemann, J.L. (1980) Skin grafting. Little Brown, Boston.

Runyan, W.R., Bean, K.E. (1990) Semiconductor integrated circuit processing technology, Addison-Wesley, New York.

Rushmer, R.F., Buettner, K.J.K., Short, J.M., Odland, G.F. (1966) The Skin. Science., 154, 343-348.

Sadrzadeh, N., Glembourtt, M.J., Stevenson, C.L. (2007) Peptide drug delivery strategies for the treatment of diabetes. Journal of Pharmaceutical Sciences, 96(8), 1925-1954.

Sammoura, F., Kang, J.J., Heo, Y.M., Jung, T.S., Lin, L. (2007) Polymeric microneedle fabrication using a microinjection molding technique. Microsystem Technologies, 13, 517-522.

Santini, J.T., Richards, A.C., Scheidt, R.A., Cima, M.J., Langer, R.S. (2000) Microchip technology in drug delivery. Annals of Medicine, 32(6), 377–379.

Sartorelli, P., Aprea, C., Cenni, A., Novelli, M.T., Orsi, D., Palmi, S., Matteucci, G. (1998). Prediction of percutaneous absorption from physiochemical data: A model based on data of in virto experiments. Ann. Occup. Hyg., 42(4), 267-276.

Sartorelli, P., Anderson, H.R., Angerer, J., Corish, J., Drexler, H., Goen, T., Griffin, P., Hotchkiss, S.A.M., Larese, F., Montomoli, L., Perkins, J., Schmelz, M., van de Sandt, J., Williams, F. (2000) Percutaneous penetration studies for risk assessment. Environmental Toxicology Pharmacology, 8, 133–152.

Sato, K., Mine, T. (1996) Analysis of in vitro rat skin permeation and metabolism of SM-10902, prodrug of synthetic prostacyclin analogue. International Journal of Pharmaceutics, 135(1-2), 127-136.

Schaefer, H., Zesch, A., Stuttgen, G. (1982) Skin Permeability, Chapter 3, Springer-Verlag, New York.

Schaefer, H., Redelmeier, T.E. (1996) Skin barrier: Principles of percutaneous absorption, New York, Karger.

Scheidler, M.D., Meiselman, M. (2001) Use of verapamil for the symptomatic treatment of microscopic colitis. J. Clin. Gastroenterol., 32(4), 351–352.

Scheuplein, R.J. (1965) Mechanism of percutaneous adsorption I. Routes of penetration and the influence of solubility. J. Invest. Dermatol., 45, 334-345.

Scheuplein, R.J. (1967) Mechanism of percutaneous absorption II. Transient diffusion and the relative importance of various routes of skin penetration. J. Invest. Dermatol., 48, 79-88.

Scheuplein, R.J., Blank, I.H. (1971) Permeability of the skin. Physiol. Rev., 51, 702-747.

Scheuplein, R.J. (1978) Permeability of the skin: A review of major concepts. Curr. Probl. Dermatol., 7, 172-186.

Seidenari, S., Pagnoni, A., DiNardo, A., Giannetti, A. (1994) Echographic evaluation with image analysis of normal skin: Variations according to age and sex. Skin Pharmacol., 7, 201-209.

Seidenari, S., Giusti, G., Bertoni, L., Magnoni, C., Pellacani, G. (2000) Thickness and echogenicity of the skin in children as assessmed by 20-MHz ultrasound. Dermatology, 201, 218-222.

Shah, H.S., Tojo, K., Chien, Y.W. (1992a) Transdermal controlled delivery of verapamil: Characterization of in vitro skin permeation. International Journal of Pharmaceutics, 86(2-3), 167-173.

Shah, H.S., Tojo, K., Chien, Y.W. (1992b) Development and clinical evaluation of a verapamil transdermal delivery system. Journal of Controlled Release, 22(2), 125-132.

Shah, H.S., Tojo, K., Chien, Y. (1992c) Transdermal controlled delivery of verapamil: determination of in vitro/in vivo relationship. Journal of Controlled Release, 22, 133-140.

Shah, V.P. (2003) Transdermal drug delivery, 2nd edn, Guy, R.H., J. Hadgraft, J., Eds., p.365. New York: Marcel Dekker Inc.

Shakeel, F., Baboota, S., Ahuja, A., Ali, J., Shafiq, S. (2008) Accelerated stability testing of celecoxib nanoemulsion containing cremophor-EL. African Journal of Pharmacy and Pharmacology, 2(8), 179-183.

Sherratt, J.A., Murray, J.D. (1991) Mathematical analysis of a basic model for epidermal wound healing. J. Math. Biol., 29, 389-404.

Shibata, T., Yamanaka, S., Kato, N., Kawashima, T., Nomura, M., Mineta, T., Makino, E. (2009) Fabrication of micromanipulator array for cell patterning. Microelectronic Engineering, doi:10.1016/j.mee.2009.01.046.

Shiflet, A.B., Shiflet, G.W. (2006) Introduction to computational science: modeling and simulation for the sciences. Wofford college, Princeton University Press.

Shikida, M., Odagaki, M., Todoroki, N., Ando, M., Ishihara, Y., Ando, T., Sato, K. (2004) Non-photolithographic pattern transfer for fabricating arrayed three-dimensional microstructures by chemical anisotropic etching. Sensors and Actuator, 16, 264-271.

Shikida, M., Hasada, T., Sato, K. (2006) Fabrication of a hollow needle structure by dicing wet etching and metal deposition. J. Micromech. Microeng., 16, 2230-2239.

Shirkhanzadeh, M. (2005) Microneedles coated with porous calcium phosphate ceramics: effective vehicles for transdermal delivery of solid trehalose. J. Mater. Sci. Mater. Med., 16, 37–45.

Shufelt, C.L., Braunstein, G.D. (2009) Safety of testosterone use in women. Maturitas, doi:10.1016/j.maturitas.2009.01.012.

Simon L., Weltner A.N., Wang Y., Michniak B. (2006) A parametric study of iontophoretic transdermal drug-delivery systems. Journal of Membrane Science, 278(1-2), 124-132.

Simonetti I., Trivella M. G., Michelassi C., Parodi O., De Nes D.M., L'abbate A. (1986) Dose response scrutiny of coronary vasodilation after intracoronary verapamil in man. A quantitative cineangiographic Study", European Heart Journal, 1986, 7, 10, 848-858.

Sivamani, R.K., Stoeber, B., Wu, G.C., Zhai, H., Liepmann, D., Maibach, H. (2005) Clinical microneedle injection of methyl nicotinate: stratum corneum penetration. Skin Res. Technol., 11(2), 152–156.

Shuster, S., Bottoms, E. (1963) Senile degeneration of skin collagen. Clin. Sci., 25, 487-491.

Shuster, S., Black, M.M., McVitie, E. (1975) The influence of age and sex on skin thickness, skin collagen, and density. Br. J. Dermatol., 93, 639-643.

Smith, C.R., Erickson, G.J., Neudorfer, P. O. (1992) Maximum entropy and Bayesian methods. Kluwer Academic Publishers.

Søeborg, T., Rasmussen, C.H., Mosekilde, E., Jørgensen, M.C. (2009) Absorption kinetics of insulin after subcutaneous administration. European Journal of Pharmaceutical Sciences, 36(1), 78-90.

Sonaje, K., Lin, Y.H., Juang, J.H., Wey, S.P., Chen, C.T., Sung, H.W. (2009) In vivo evaluation of safety and efficacy of self-assembled nanoparticles for oral insulin delivery. Biomaterials, 30, 2329–2339.

Southwood, W.F.W. (1955) The thickness of the skin. Plast. Reconstr. Surg., 15, 423-429.

Stachowiak, J.C., Li, T.H., Arora, A., Mitragotri, S., Fletcher, D.A. (2009) Dynamic control of needle-free jet injection. Journal of Controlled Release, 135, 104–112.

Steinstrasser, I., Merkle, H.P. (1995) Dermal metabolism of topically applied drugs: Pathways and models reconsidered. Pharmaceutica Acta Helvetiae, 70, 3-24.

Stoeber, B., Liepmann, D. (2000) Fluid injection through out-of-plane microneedles. Proceedings of the 1st Annual International IEEE-EMBS Special Topic Conference on Microtechnologies in Medicine and Biology, Lyon, France, October 12-14, pp. 224-228.

Stoeber, B., Liepmann, D. (2005) Arrays of hollow out-of-plane microneedles for drug delivery. J. Microelect. Systems, 14(3), 472-479.

Streichert, F., Ulmer, H. (2005) A java based framework for evolutionary algorithms-manual and documentation. Eberhard Karls University, Tubingen, Germany.

Stupar, P.A., Pisano, A.P. (2001) Silicon, parylene, and silicon/parylene micro-needles for strength and toughness. In Proceedings of the 11th International Conference on Solid State Sensors and Actuators (Transducers'01), Technical Digest, Munich, Germany, 10–14 June 2001, pp. 1386–1389.

Subramanian, S. (1999) Optimization models and analysis of routing, location, distribution, and design problems on networks. Virginia polytechnic institute and state university, Virginia, USA.

Sugibayashi, K., Hayashi, T., Hatanaka, T., Ogihara, M., Morimoto, Y. (1996) Analysis of simultaneous transport and metabolism of ethyl nicotinate in hairless rat skin. Pharmaceutical Research, 13(6), 855-860.

Sugibayashi K., Hayashi T., Morimoto Y. (1999) Simultaneous transport and metabolism of ethyl nicotinate in hairless rat skin after its topical application: the effect of enzyme distribution in skin. Journal of Controlled Release, 62(1-2), 201–208.

Suhonen, T.M., Bouwstra, J.A., Urtti, A. Chemical enhancement of percutaneous absorption in relation to stratum corneum structural alterations. Journal of Controlled Release, 59(2), 149-161.

Sujith, O.K., Lane, C. (2009) Therapeutic options for continuous dopaminergic stimulation in Parkinson's disease. Therapeutic Advances in Neurological Disorders, 2(2), 105–113.

Syvanen, S., Hooker, A., Rahman, O., Wilking, H., Blomquist, G., Langstrom, B., Bergstrom, M., Udenaes, M.H. Pharmacokinetics of P-Glycoprotein inhibition in the rat blood-brain barrier. Journal of Pharmaceutical Sciences, 97(12), 5386-5400.

Takema, Y., Yorimoto, Y., Kawai, M., Imokawa, G. (1994) Age-related changes in the elastic properties and thickness of human facial skin. Br. J. Dermatol., 131, 641-648.

Tan, C.Y., Statham, B., Marks, R., Payne, P.A. (1982) Skin Thickness measurement by pulsed ultrasound: its reproducibility, validation and variability. Br. J. Dermatol., 106, 657-667.

Tao, S.L., Desai, T.A. (2003) Microfabricated drug delivery systems: from particles to pores. Advanced Drug Delivery Reviews, 55(3), 315-328.

Tauber, U. (1987) Drug metabolism in the skin: Advantages and disadvantages, Transdermal Drug Deliuery, Marcel Defier, New York.

Teo, M.A., Shearwood, C., Ng, K.C., Lu, J., Moochhala, S. (2005) In vitro and in vivo characterization of MEMS microneedles. Bio. Microdevices, 7(1), 47-52.

Teo, A.L., Shearwood, C., Ng, K.C., Lu, J., Moochhala, S. (2006) Transdermal microneedles for drug delivery applications. Materials Science and Engineering, 132, 151-154.

Tobin J., Flitman S. (2008) Cluster-like headaches associated with internal carotid artery dissection responsive to verapamil headache. The Journal of Head and Face Pain, 48(3), 461–466.

Tojo, K., Valia, K.H., Chotani, G., Chien, Y.W. (1985) Long-term permeation kinetics of estradiol: (IV) a theoretical approach to the simultaneous skin permeation and bioconversion of estradiol esters. Drug development and industrial pharmacy, 11(6-7), 1175-1193.

Tojo, K. (1987) Mathematical modelling of transdermal drug delivery. Journal of Chemical Engineering of Japan, 20, 300-308.

Tojo, K, Chiang, C.C., Chien, T.W. (1987) Drug permeation across the skin: effect of penetrant hydrophilicity. J. Pharm. Sci., 76(2), 123-126.

Tojo, K. (1989) Mathematical model of iontophoretic transdermal drug delivery. Journal of Chemical Engineering in Japan, 22(5), 512–518.

Tojo, K., Yamada, K., Hikima, T. (1994) Diffusion and metabolism of prednisolone farnesylate in viable skin of the hairless mouse. Pharmaceutical Research, 11(3), 393-397.

Tojo, K. (2005) Mathematical models of transdermal and topical drug delivery, 2nd ed., Japan, Biocom Systems Inc.

Tojo, K., Hikima, T. (2007) Bioequivalence of Marketed Transdermal Delivery Systems for Tulobuterol. Biol. Pharm. Bull., 30(8), 1576-1579.

Tregear, R.T. (1966) Physical functions of skin. London, Academic Press.

Trewet, C.B., Ernst M.E. (2008) Resistant hypertension: Identifying causes and optimizing treatment regimens. Southern Medical Journal, 101(2), 166-173.

Van de Sandt, J.J.M., van Burgsteden, J.A., Cage, S., Carmichael, P.L., Dick, I., Kenyon, S., Korinth, G., Larese, F., Limasset, J.C., Maas, W.J.M., Montomoli, L., Nielsen, J.B., Payan, J.P., Robinson, E., Sartorelli, P., Schaller, K.H., Wilkinson, S.C., Williams, F.M. (2004) In vitro predictions of skin absorption of caffeine, testosterone, and benzoic acid: a multi-centre comparison study. Regulatory Toxicology and Pharmacology, 39, 271-281.

Van Rossum, J. (1977). Kinetics of Drug Action, 3rd ed., Springer-Verlag, Berlin.

Vasquez, P.A., Pelesko, J.A. (2005) A variation approach to microneedle design. Proceedings of the International Conference on MEMS, NANO and Smart Systems (ICMENS), Banff, Alberta, Canada, July 24-29, pp. 383-386.

Vecchia, B.E., Bunge, A.L. (2003) Evaluating the transdermal permeability of chemicals. In: Guy, R.H., Hadgraft, J. Editors, Transdermal Drug Delivery, Marcel Dekker, New York, pp. 25–57.

Verbaan, F.J., Bal, S.M., van den Berg, D.J., Groenink, W.H.H., Verpoorten, H., Luttge, R., Bouwstra, J.A. (2007) Assembled microneedle arrays enhance the transport of compounds varying over a large range of molecular weight across human dermatomed skin. Journal of Controlled Release, 117, 238-245.

Verbaan, F.J., Bal, S.M., van den Berg, D.J., Dijksman, J.A., van Hecke, M., Verpoorten, H., van den Berg, A., Luttge, R., Bouwstra, J.A.,. (2008) Improved piercing of microneedle arrays in dermatomed human skin by an impact insertion method. Journal of Controlled Release, 128(1), 80-88.

Wang, P.M., Cornwell, M., Hill, J., Prausnitz, M.R. (2006) Precise microinjection into skin using hollow microneedles. Journal of Investigative Dermatology, 126, 1080-1087.

Wester, R.C., Maibach, H.I. (1989) Regional variations in percutaneous absorption. In: Bronaugh RL and Maibach HI eds. percutaneous absorption, 2nd edition. New York: Marcel Dekker, 111-120.

Whitmore, S.E., Levine, M.A. (1998) Risk factors for reduced skin thickness and bone density: possible clues regarding pathophysiology, prevention, and treatment. J. Am. Acad. Dermatol., 38, 248-255.

Whitmore, S.E., Sago, N.J.G. (2000) Caliper-measured skin thickness is similar in white and black women. J. Am. Acad. Dermatol., 42(1):76-79.

Widera, G., Johnson, J., Kim, L., Libiran, L., Nyam, K., Daddona, P., Cormier, M. (2006) Effect of delivery parameters on immunization to ovalbumin following intracutaneous administration by a coated microneedle array patch system. Vaccine, 24, 1653-1664.

Wilke, N., Mulcahy, A., Ye, S.R., Morrissey, A. (2005) Process optimization and characterization of silicon microneedles fabricated by wet etch technology. Microelectronics Journal, 36, 650-656.

Wilke, N., Reed, M.L., Morrissey, A. (2006) The evolution from convex corner undercut towards microneedle formation: theory and experimental verification. Journal of Micromechanics and Microengineering, 16, 808-814.

Wilke, N., Morrissey, A. (2007) Silicon microneedle formation using modified mask designs based on convex corner undercut. J. Micromech. Microeng., 17, 238-244.

Wilkinson, S.C., Williams, F.M. (2002) Effects of experimental conditions on absorption of glycol ethers through human skin in vitro. Int. Arch. Occup. Environ. Health., 75, 519-527.

Williams, A.C., Barry, B.W. (1992). Skin absorption enhancers. Critical Review of Therapeutic Drug Carrier Systems, 9(3-4), 305–353.

Williams, A.C., Barry, B.W. (2004) Penetration enhancers. Adv. Drug Deliv. Rev., 56, 603-618.

Wilschut, A., ten Berge, W.F., Robinson, P.J., McKone, T.E. (1995) Estimating skin permeation. The validation of five mathematical skin permeation models. Chemosphere, 30(7), 1275-1296.

Wu, X. M., Todo, H., Sugibayashi, K. (2006) Effects of pretreatment of needle puncture and sandpaper abrasion on the in Vitro skin permeation of fluorescein isothiocyanate (FITC)-dextran. International Journal of Pharmaceutics, 316(1-2), 102-108.

Wu, X.M., Todo, H., Sugibayashi, K. (2007) Enhancement of skin permeation of high molecular compounds by a combination of microneedle pretreatment and iontophoresis. Journal of Controlled Release, 118, 189-195.

Wokovich, A.M., Brown, S.A., Shen, M., Doub, W.H., Cai, B., Sadrieh, N., Chen, M.L., Machado, S., Buhse, L.F. (2009) Evaluation of substrates for 90º peel adhesion-a collaborative study II. Transdermal Drug Delivery Systems. J. Biomed. Mater. Res. Part B: Appl. Biomater., 88(1), 61–65.

Xie, Y., Xu, B., Gao, Y. (2005) Controlled transdermal delivery of model drug compounds by MEMS microneedle array, Nanomedicine: Nanotechnology, Biology and Medicine, 1, 184-190.

Xu, X., Weisel, C.P. (2005) Human respiratory uptake of chloroform and haloketones during showering. Journal of Exposure analysis and Environmental Epidemiology, 15**,** 6-16.

Yahya, A., Manning, C. D. (2004) Determination of material removal rate of an electro-discharge machine using dimensional analysis. Journal of Physics D: Applied Physics, 37, 1467-1471.

Yamaguchi, K., Mitsui, T., Yamamoto, T., Shiokawa, R., Nomiyama, Y., Ohishi, N., Aso, Y., Sugibayashi, K. (2006) Analysis of in vitro skin permeation of 22-Oxacalcitriol having a complicated metabolic pathway. Pharmaceutical Research, 23(4), 680-688.

Yamaguchi, K., Mitsui, T., Aso, Y., Sugibayashi, K. (2008) Structure-permeability relationship analysis of the permeation barrier properties of the stratum coerneum and viable epidermis/dermis of rat skin. Journal of Pharmaceutical Sciences, 97(10), 4391-4403.

Yamashita, F., Bando, H., Koyama, Y., Kitagawa, S., Takakura, Y., Hashida, M. (1994) In vivo and in vitro analysis of skin penetration enhancement based on a two-layer diffusion model with polar and nonpolar routes in the stratum corneum. Pharmaceutical Research, 11, 185–191.

Yamashita F., Hashida M. (2003) Mechanistic and Empirical Modeling of Skin Permeation of Drugs. Advanced Drug Delivery Reviews, 55, 9, 1185–1199.

Yang, M., Zahn, J.D. (2004) Microneedle insertion force reduction using vibratory actuation. Biomedical Microdevices, 6(3), 177-182.

Yoshida, D., Todo, H., Hasegawa, T., Sugibayashi, K. (2008) Effect of molecular weigt on the dermatopharmacokinetics and systemic disposition of drugs after intracutaneous injection. European Journal of Pharmaceutical Sciences, 35(1-2), 5-11.

Yu, C.D., Fox, J.L., Ho, N.F., Higuchi, W.I. (1979) Physical model evaluation of topical prodrug delivery simultaneous transport and bioconversion of vidarabin-5'-valerate II: parameter determinations. Journal of Pharmaceutical Sciences, 68(11), 1341-1346.

Zahn, J.D., (2001) Microfabricated microneedles for minimally invasive drug delivery, sampling and analysis. Ph.D. thesis, University of California, USA.

Zahn, J.D., Hsieh, Y.C., Yang, M. (2005) Components of an integrated microfluidic device for continuous glucose monitoring with responsive insulin delivery. Diabetes Technology & Therapeutics, 7(3), 536–545.

Zesch, A., Schaefer, H. (1975) Penetration of radioactive hydrocortisone in human skin from various ointment bases.II. In vivo-experiments. Archiv fur Dermatologische Forschung, 252(4), 245-256.

Zhou, H., Li, G., Sun, X., Zhu, Z., Xu, B., Jin, Q., Zhao, J., Ren, Q.S. (2009) A new process for fabricating tip-shaped polymer microstructure array with patterned metallic coatings. Sensors and Actuators A: Physical, 150, 296-301.